

INAUGURAL-DISSERTATION  
zur  
Erlangung der Doktorwürde  
der  
Naturwissenschaftlich-Mathematischen Gesamtfakultät  
der  
Ruprecht-Karls-Universität Heidelberg

vorgelegt  
von  
Valeria Malieva  
geboren am 23. Mai 1986 in Lipezk, Russland

Tag der mündlichen Prüfung:



# Mathematical Modelling and Simulations of Brain Cell Swelling Under Ischaemic Conditions

Betreuer: Prof. Dr. Dr. h. c. mult. Willi Jäger



## Acknowledgements

First and foremost I would like to express my sincere gratitude to my supervisors Prof. Willi Jäger and Prof. Peter Bastian. I am especially thankful to Prof. Willi Jäger for granting me the opportunity to work on this fascinating topic, for believing in me and for his scientific as well as moral guidance. From Prof. Willi Jäger I learned not only what it takes to be an accomplished researcher, but also how important it is to stay true to oneself.

I am very thankful to Prof. Peter Bastian for supporting my research, for being understanding and for always finding time to discuss my work.

For allowing me to pursue my scientific work in an academically excellent environment, I would like to thank the Faculty of Mathematics and Computer Science of Heidelberg University.

I am very grateful to Dr. Felix Heimann for his contribution to the development of the simulation framework for my thesis and for advising me on the subject of physics. The discussions that I had with Dr. Felix Heimann and his enthusiastic participation played a great role in the development of this work.

I would also like to acknowledge the contribution of Prof. Maria Neuss-Radu to the early development of the mathematical model. I am grateful for her interest in the project and for helping in its advancement.

Being an active member of the Heidelberg Graduate School of Mathematical and Computational Methods for the Sciences (HGS MathComp) was a great experience, and I am thankful to the Graduate School for providing me with opportunities to visit exciting conferences and workshops and for encouraging me to actively participate in the life of the School. I would like to especially thank the HGS MathComp and the German Research Foundation (DFG) for the funding of my doctoral studies.

Additionally, I wish to thank the present and past members of the Scientific Computing Group and Applied Analysis Group for being genuinely friendly and helpful.

I am infinitely thankful to my kind mother for her love and for always believing in me. And most importantly, I would like to thank my husband for his loving care, invaluable support and great patience.



## Abstract

Motivated by the ischaemic brain stroke research, this work is devoted to the description of the osmotic swelling of a brain cell due to the absorption of the extracellular fluid during the formation of the cytotoxic (cellular) oedema.

A physically motivated mathematical model describing the interaction between a single swelling cell and the extracellular fluid surrounding it is developed. In particular, the dynamics of the interaction is approximated by the coupled Biot-Stokes equations, resulting in a free boundary interaction problem. The Biot equations derived using homogenization techniques are considered and it is shown, that for the relevant data range, the temporal pressure derivative term of the Biot equations is negligible. Filtering effects of the cell membrane and the driving force of the transmembrane osmotic pressure difference are reflected in the Biot-Stokes coupling condition relating the normal fluid flux to the total pressure difference across the membrane.

The analysis of the relevant experimentally obtained data for the considered biological system suggests that certain effects and processes included into the developed general coupled model can be neglected. As a result, a simpler (*reduced*) mathematical model is obtained and numerically implemented.

The *reduced* Biot-Stokes coupled problem is discretized using FEMs (in space) and the implicit Euler scheme (in time), and solved following an operator-splitting approach. The numerical implementations of the (pure) Biot problem are verified by comparing the analytic and numerical solutions, and are available for two and three dimensions. The simulation results for the *reduced* mathematical model parametrized with the estimated experimental parameters showed good agreement with the experimental observations. The sensitivity of the Biot problem solution to the variations of the key parameters and domain geometry, as well as the overall effect of the Stokes domain solution on the solution of the coupled Biot-Stokes problem are tested and analysed.





## Zusammenfassung

Diese Arbeit ist ein Beitrag zur Forschung an ischämischen Schlaganfällen und widmet sich der Beschreibung osmotisch bedingter Schwellungen von Gehirnzellen durch Absorption extrazellulärer Flüssigkeit.

Ein physikalisch motiviertes mathematisches Modell zur Beschreibung der Interaktion zwischen einer einzelnen Zelle und der sie umgebenden extra-zellulären Flüssigkeit wird präsentiert. Deren dynamischen Beziehungen werden durch eine gekoppelte Form der Biot-Stokes Gleichungen auf zeitlich veränderlichen Geometrien beschrieben. Unter Betrachtung einzelner Zwischenergebnisse der Herleitung der Biot-Gleichungen durch Homogenisierung wird gezeigt, dass die zeitlichen Ableitungen des Drucks für den problem-relevanten Parameterraum vernachlässigbar klein sind. Filtereffekte der Zellmembran sowie osmotischer Druck, werden in den Biot-Stokes Kopplungsbedingungen abgebildet, welche den transmembranen Fluss mit dem Gesamtdruckunterschied an der Zellmembran in Beziehung setzen.

Basierend auf einer Analyse relevanter Experimente zu dem betrachteten biologischen System wird eine Auswahl der wichtigsten physikalischen Prozesse getroffen, um daraus ein vereinfachtes (reduziertes) mathematisches Modell zu erhalten, welches einer numerischen Lösung zugänglich ist.

Die vereinfachten gekoppelten Biot-Stokes Gleichungen werden mit finiten Elementen im Raum und mit impliziter Euler-Integration in der Zeit diskretisiert und schließlich unter Zuhilfenahme von Operator-Splitting gelöst. Die numerische Implementierung des (reinen) Biot-Systems wird durch Vergleich mit analytischen Lösungen in zwei und drei Dimensionen verifiziert. Die Ergebnisse der Simulation des vereinfachten mathematischen Modells, welches mit experimentell bestimmten Parametern vervollständigt wurde, zeigen eine gute Übereinstimmung mit den experimentell zugänglichen Observablen des realen Systems. Die Sensitivität des Biot-Teilsystems auf einige Schlüsselparameter sowie der Einfluss der Kopplungseffekte der Lösung im Stokes-Teilsystem werden getestet und analysiert.



# Contents

<b>Introduction</b>	<b>1</b>
<b>Nomenclature</b>	<b>7</b>
<b>1 Description of the problem</b>	<b>11</b>
1.1 Problem definition	11
1.1.1 Extracellular space (ECS)	12
1.1.2 Intracellular space (ICS)	13
1.1.3 Cell membrane: mechanical properties	14
1.2 Osmosis and osmotic pressure	18
1.2.1 Membrane filtration	18
1.3 Effects of the surrounding media	20
1.4 Summary: considered domains and effects	22
1.4.1 List of assumptions	24
<b>2 Mathematical Model</b>	<b>25</b>
2.1 ICS-ECS interaction problem: Biot-Stokes model	25
2.1.1 Extracellular space: the Stokes equations	25
2.1.2 Intracellular space: the Biot poroelasticity equations	26
2.1.3 Lagrangian and ALE formulations	32
2.1.4 Initial and boundary conditions	34
2.1.5 Biot-Stokes coupling: interface conditions	35
2.2 Osmotic pressure	39
2.2.1 Osmotic pressure model	39
2.2.2 Transport equations for the molarities	40
2.2.3 Initial equilibrium relations	42
2.2.4 Fast diffusion model	43
2.2.5 Modified flux interface conditions	45
2.3 Summary: general conceptual model	46
<b>3 Data and dimensional analysis</b>	<b>51</b>
3.1 Data: parameters and characteristic values	51
3.1.1 Material properties and parameters	52
3.1.2 Biot-Stokes problem	55
3.1.3 Osmotic pressures and molar concentrations	63
3.1.4 Times and velocities	67
3.1.5 Molarity flux models	70
3.2 Dimensional equations	74
3.2.1 ALE transformation terms	76
3.2.2 Incompressible Navier-Stokes equations	76
3.2.3 Biot equations	77

3.2.4	Convection–diffusion equations . . . . .	79
3.2.5	Interface conditions . . . . .	80
3.3	Summary: data tables . . . . .	82
<b>4</b>	<b>Numerics and simulations</b>	<b>87</b>
4.1	Considered <i>reduced</i> problems . . . . .	87
4.1.1	Biot-Stokes problem . . . . .	87
4.1.2	Pure Biot problem . . . . .	90
4.1.3	Variational formulations . . . . .	92
4.2	Discretisation . . . . .	92
4.2.1	Spatial discretization . . . . .	93
4.2.2	Temporal discretization . . . . .	99
4.3	Analytic solution of the Biot problem . . . . .	100
4.3.1	2D: polar coordinates . . . . .	101
4.3.2	3D: spherical coordinates . . . . .	103
4.4	Solution approach: operator splitting . . . . .	104
4.5	Software related aspects . . . . .	106
4.6	Numerical implementation . . . . .	107
4.6.1	Verification of the Biot problem implementation . . . . .	108
4.6.2	Pure Biot problem with the <i>estimated</i> data. Parameter sensitivity . . . . .	113
4.6.3	Coupled Biot-Stokes problem with circular Biot domain . . . . .	131
4.6.4	Coupled Biot-Stokes problem with non-trivial Biot domain geometry . . . . .	137
	<b>Summary and outlook</b>	<b>147</b>
<b>A</b>	<b>Appendix</b>	<b>149</b>
A.1	Reynolds transport theorem and its applications . . . . .	149
A.2	Structure dynamics: elasticity equations . . . . .	152
A.3	Fluid Dynamics . . . . .	154
A.4	Poroelectricity equations: Mixture Theory approach . . . . .	156
A.5	Osmosis and osmotic pressure . . . . .	161
A.5.1	Virial theorem (osmotic pressure model) . . . . .	162
	<b>List of Figures</b>	<b>165</b>
	<b>List of Tables</b>	<b>167</b>
	<b>Bibliography</b>	<b>169</b>

# Introduction

## Background & motivation

Ischaemic brain stroke as well as the related processes that affect brain tissue and cells are a subject of past, recent and current studies. Occlusion of one of the cerebral arteries followed by ischaemia-induced pathological processes lead to the development of life-threatening brain oedema. On the tissue scale, brain oedema formation is characterised by substantial leakage of various substances across the blood-brain barrier. Consequent brain tissue swelling may result in the increase of intracranial pressure and in many cases leads to death.

Due to the dominant effect of hypoxia on cells, first malignant changes of the brain condition are observable at the stage of *cytotoxic (cellular) oedema*, which is characterized by swelling of different types of brain cells and consequent constriction of the extracellular space in the ischaemic areas of the brain tissue. Under the conditions of hypoxia, the energy required for the healthy functioning of the cell membrane is not available, leading to the failure of energy requiring channels (pumps). The resulting rapid accumulation of sodium ions within cells generates an *osmotic force* that drives extracellular water into the cell in order to maintain osmotic equilibrium. Cytotoxic oedema alone does not require the participation of the intravascular space constituents and does not cause the increase of the brain tissue volume. However it creates conditions for the formation and development of ionic and vasogenic oedemas, which do lead to tissue swelling.

Unless the cell membrane is compromised, cytotoxic swelling does not necessarily lead to permanent damage and may be reversed. Therefore estimating the rate of swelling and the overall condition of the brain cells is important for the treatment of the ischaemia-affected tissue.

While the original motivation of this research is related to the brain stroke and its complications, the formation of cytotoxic oedema can be observed during other malignant processes, such as traumatic or hypoxic brain injury, cancer, brain inflammation, etc. More generally, osmotic swelling of living cells can be observed in multiple other circumstances, when the energy necessary for the healthy activity of the membrane is not available.

## Goal & approach

The objective of this thesis is to develop a mathematical model describing the progression of cytotoxic oedema in damaged but not dead cells, i.e. until their rupture, such that this model satisfies the following requirements:

- it includes the description of the significant processes that affect the swelling, such that the available experimental data can be incorporated, and thus the impact of the considered effects distinguished and estimated;
- it can be implemented numerically, such that the approximation of the swelling behaviour can be evaluated by comparing the results of the numerical simulations with the available experimental observations;

- it either allows a direct up-scaling to the tissue level, or gives clear indication to a simpler cell swelling approximation that can be used as the basis for the approximation of the processes occurring on the tissue level.

In order to give a detailed description of the processes that take place during the formation of cytotoxic ischaemia, swelling of a *single brain cell surrounded by some amount of extracellular fluid* is studied. The above listed goals are approached in several steps, namely:

- The cell and extracellular fluid are approximated by physically motivated mathematical models and coupled at the interface with the help of appropriate interface conditions. The characteristics of the considered domains and materials allow the overall system to be described using *continuum mechanics* models, which for 2- or 3-dimensional problems would involve the use of *partial differential equations*. More specifically, the dynamics of the system is approximated as a *Biot-Stokes interaction free boundary problem*, and the driving force of the transmembrane osmotic pressure difference is modelled as a pure interface effect.
- The *experimental measurements* of the characteristics of the relevant biological materials and osmotic cell swelling processes available in the literature are analysed. The results of this analysis are reflected in the choice of the parameters and initial, boundary and interface conditions of the developed model and are also used to estimate the importance of some of the considered effects or subprocesses of the general problem. While some of the values can be found from experimental measurements, other quantities are estimated based on the introduced assumptions or approximated using mathematical models. Furthermore, several types of experimental settings are distinguished, and their differences are reflected in the choice of the respective characteristic values, initial, boundary or interface conditions.
- The resulting dynamical system is discretized in space and time and *simulated numerically*. The space-time discretization is realized by an operator splitting method adapted to the specific requirements of the moving meshes approximating the respective time dependent physical domains. The implemented simulations are used to demonstrate the approximation of the osmotic cell swelling behaviour by the developed model, as well as to further the analysis and estimation of the modelled effects and processes.

## State of the art

While biological cells are very complex systems, they share many characteristics with vesicles (closed lipid bilayers enclosing a liquid) that have much simpler structure. *Vesicles* and lipid membranes have been extensively studied from the experimental, theoretical and numerical perspectives, see e.g. [1], [2], [3], [4], [5], [6], [7], and certain obtained research results can be used for the development of models approximating the processes that occur to living cells. Thus the lipid bilayer membrane is commonly modelled as a two dimensional incompressible fluid, such that the fluid–structure interaction problem of the vesicle system features jump in the stress tensor at the membrane, which is determined by the properties of the bilayer. In particular, in [7], the stress discontinuity is modelled as a combination of the mechanical tension and bending, where the latter is obtained from the first variation of the Canham–Helfrich energy, [8], [9].

The intracellular space, membrane or whole living cell are often modelled as a *hydrogel* using the general equations of *mixture theory* (MT), see e.g. [10], [11], [12], [13]. Thus in [12], the cell is approximated as a fluid-filled membrane, where the membrane is described by the mixture theory equations. The MT equations are then reduced to the case of a thin membrane and compared to the classical Kedem–Katchalsky model for the solute and solvent fluxes through a semipermeable filter. Further in [11], the cell is represented as a hydrated gel surrounded by a semipermeable membrane, such that now the spherical gel is described using the mixture theory framework.

In the studies dedicated to the (experimental) estimation of some specific mechanical effects, also when the material parameters of a cell or its components are evaluated, *simplified elasticity or viscoelasticity models* relating the response of the sample to the applied deformation (stress) are often used, [14], [15], [16], [17].

The *data* related to the ischaemic (or more generally, osmotic) swelling of living cells can be found in numerous works. The experimental measurements that are relevant for the model developed in this thesis are referenced in *Section 3*. It is worth mentioning, that while most of the parameters characterising physical properties of the considered materials can be determined with some exactness, certain characteristics show strong dependence on the measurement techniques and/or conditions of the experiment. Thus the magnitudes of some material parameters are estimated within a considerably wide range, see e.g. [16], [18], [19], [20], [21].

While the *Biot type equations* were originally derived for soils, they have also been used for the modelling of biological tissues, see e.g. [22], [23], [24], [25], [26], [27], [28]. Since the appearance of the original research of Terzaghi (1925) and Biot (1941) on the consolidation of soils under loading followed by the development of the theory of Biot in 1955, there have been suggested approaches employing *homogenization* techniques, in which the macroscale poroelasticity equations are rigorously derived from the microscale equations describing each phase of the medium individually, see e.g. [29], [30], [31] and references therein.

*Analytical results* for some applications of the Biot equations are available in the existing literature. Thus in [32], the existence and uniqueness of the (two-dimensional) variational problem corresponding to an initial-boundary value problem of the Biot model for the consolidation of clays is shown and some error estimates are introduced. Further research results can be found in e.g. [33], [34], [35].

Fluid-poroelastic media interaction problems approximated by a coupled system of the Biot and Navier-Stokes equations have also been *studied and solved numerically*, see e.g. [36], [37]. Thus in [36], a semi-implicit monolithic method for the Navier–Stokes&Biot system is employed, and domain decomposition techniques are extended to the fluid-poroelastic structure interaction problem.

## Results & contributions

Based on the discussion, assumptions and conclusions drawn from the analysis of the properties of the media and processes occurring during cytotoxic swelling, a mathematical model describing osmosis-driven swelling of a brain cell is developed.

For the approximation of the intracellular space, the Biot poroelasticity equations derived from the *microscale* using homogenization techniques are chosen. As it is important to develop a

mathematical model that can be numerically simulated, such that the available experimental data can be exploited, it is shown, how the coefficients of the rigorously derived Biot equations can be related to the data obtained experimentally. It is also shown, that for the considered physical data range, the temporal pressure derivative term in the rigorously derived Biot equations can be neglected, considerably simplifying the numerical implementation of the developed model.

The Biot-Stokes coupled system is closed by the Kedem-Katchalsky type equations relating the solvent flux to the hydraulic and osmotic pressure difference across a semipermeable membrane, such that the filtering effects of the membrane are reflected in the coefficient of the interface condition.

Numerical results include the simulations of two general problems: poroelastic cell swelling (*Pure Biot*) and interaction of a swelling poroelastic cell with the extracellular fluid, i.e. poroelasticity-free fluid (*Biot-Stokes*) free boundary interaction problem. The following points deserve to be mentioned:

- The results of the numerical simulations of the Biot poroelasticity model are shown to agree with the analytic solutions for the Biot equations on spherically (3D) and rotationally (2D) symmetric domains. Furthermore, the convergence rate is optimal with regard to the approximation properties of the employed finite element spaces.
- Parametrization of the numerical models (for both the *Biot-Stokes interaction* and *Pure Biot* problems) with the relevant experimental data resulted in a good agreement with the swelling cell behaviour as observed in experimentally controlled environments.
- The sensitivity of the simulated systems to the key parameters (such as the porosity, elasticity moduli, membrane and intracellular space permeabilities) of the model is evaluated and discussed. In particular, it is shown, that the variation of the membrane filtration coefficient results in a strong response of the Biot problem solution, while the variation of the intracellular permeability parameter has almost no effect. The sensitivity of the Biot problem solution to the variations of the elasticity coefficients is shown to be relatively low.
- Analysis of the numerical solutions of the *Pure Biot* problem (where the parameters and conditions are so chosen as to correspond to the experimental observations) on the domains with different geometries indicate, that (within reasonable limits) the geometry of the cell does not have a strong influence on the character of the solution of the Biot problem.

## Outline

*Chapter 1* is devoted to the detailed description of the considered applied problem. Thus the processes occurring during cytotoxic swelling, as well as the properties of the considered media that are relevant for the purposes of this work are discussed.

In *Chapter 2*, a mathematical model for osmotic swelling of a single cell surrounded by extracellular fluid is developed. Interacting cell and extracellular space are approximated as a Biot-Stokes coupled system, where the *simplified* (as mentioned above) Biot equations are used. The Biot-Stokes coupling is complemented by the filtering effects of the separating membrane and by the influence of the transmembrane osmotic pressure difference, such that the transport



equations for the molar concentrations of the diluted osmotically active substances are included into the general interaction model.

In *Chapter 3*, the relevant physical parameters of the living cell and its extracellular environment as well as the data corresponding to various experimental settings are analysed. Using the obtained data, the importance of certain processes and effects is estimated.

*Chapter 4* is devoted to a numerical treatment of the developed mathematical model. The coupled problem is discretized using FEMs (in space) and the implicit Euler scheme (in time). A series of numerical simulations for the pure Biot and coupled Biot-Stokes problems is presented. The numerical implementation of the Biot problem is verified by comparing the analytic and numerical solutions.

A summary of the results of the thesis as well as a discussion of further research directions are offered in the *Summary and outlook*.

Additional information on the derivation of the modelling equations and the mechanisms of ischaemic brain cell swelling, as well as an explanation of the osmotic phenomenon and its modelling can be found in the *Appendix A*.



# Nomenclature

Here the notations and abbreviations introduced in *Chapters 1, 2* are listed. The description of the symbols introduced in *Chapter 3* and related to the analysis of the relevant data can be found in the tables of *Section 3.3*.

## Symbols

$d$	dimension of the problem, = $\{2, 3\}$
$(0, T)$	observation time interval
$\Omega$	overall domain
$\Omega^b$	extracellular fluid domain; bulk fluid
$\Omega^c$	cell
$\Omega^p$	poroelastic cell interior, $\subset \Omega^c$
$\Omega^{in}$	fixed inclusions of the cell, $\subset \Omega^c$
$\Omega^{fp}$	fluid part of $\Omega^p$
$\Omega^{sp}$	solid part of $\Omega^p$
$\Gamma^i$	interface between $\Omega^b$ and $\Omega^p$ , the membrane
$\Gamma^{bw}$	outer fixed walls of $\Omega^b$
$\Gamma^{b,0}$	outer impermeable fixed walls, $\subseteq \Gamma^{bw}$
$\Gamma^{b,in}$	outer inflow side fixed walls, $\subset \Gamma^{bw}$
$\Gamma^{b,out}$	outer outflow side fixed walls, $\subset \Gamma^{bw}$
$\Gamma^{pin}$	inner fixed walls of $\Omega^p$
$T_t^p$	mapping between the reference and deformed configurations of $\Omega^p$
$F^s$	deformation gradient tensor corresponding to $T_t^p$
$J^s$	determinant of $F^s$
$T_t^b$	mapping between the reference and deformed configurations of $\Omega^b$
$F^b$	deformation gradient tensor corresponding to $T_t^b$
$J^b$	determinant of $F^b$
$u^{sp}$	solid phase displacement of $\Omega^p$
$v^{fp}$	interstitial (pore) velocity of the fluid in $\Omega^p$
$v^{sp}$	solid phase velocity in $\Omega^p$
$p^p$	hydraulic (pore) pressure in $\Omega^p$
$\pi^p$	osmotic pressure in $\Omega^p$
$\sigma^p$	total stress tensor in $\Omega^p$
$\sigma^{eff}$	effective (linear elastic) stress in $\Omega^p$
$u^b$	domain displacement in $\Omega^b$
$v^b$	bulk fluid velocity in $\Omega^b$
$w^b$	velocity of the bulk fluid domain displacement
$p^b$	hydraulic bulk fluid pressure in $\Omega^b$
$\pi^b$	osmotic bulk fluid pressure in $\Omega^b$

$\sigma^b$	bulk fluid stress tensor in $\Omega^b$
$\sigma^{b,visc}$	viscous part of the fluid stress tensor $\sigma^b$
$j^p$	solvent (water) flux from the ICS side
$j^b$	solvent (water) flux from the ECS side
$n^p$	outward-pointing unit normal vector to the boundary of $\Omega^p$
$n^b$	outward-pointing unit normal vector to the boundary of $\Omega^b$
$\rho^s$	physical density of the solid phase $\Omega^{sp}$
$\rho^f$	physical density of the fluids
$\gamma^f$	porosity of $\Omega^p$
$\gamma^s$	solidity of $\Omega^p$
$\lambda^s$	Lame's first parameter (elasticity parameter)
$\mu^s$	shear modulus (elasticity parameter)
$K$	permeability tensor of a poroelastic medium
$k$	permeability function (constant) of a poroelastic medium
$\mu^f$	fluid dynamic shear viscosity
$E^f$	fluid bulk modulus
$R$	gas constant
$\Upsilon$	temperature
$C_{osm}$	osmotic pressure model coefficient (constant)
$D^p$	diffusion coefficient for the solute in the ICF
$D^b$	diffusion coefficient for the solute in the ECF
$D$	averaged diffusion coefficient for the solute in the ECS and ICS
$L^p (L)$	permeability of the membrane to water
$a^{fp}$	amount of substance of the solute in the ICF
$a^b$	amount of substance of the solute in the ECF
$c^{fp}$	osmolarity (molar concentration) in the ICF
$c^b$	osmolarity (molar concentration) in the ECF
$j^c$	flux of osmolytes
$p^\Delta$	transmembrane hydraulic pressure difference
$\pi^\Delta$	transmembrane osmotic pressure difference
$a^\Delta$	transmembrane amount of substance difference
$V$	volume of $\Omega$
$V^p$	volume of $\Omega^p$
$V^{sp}$	volume of $\Omega^{sp}$
$V^{fp}$	volume of $\Omega^{fp}$
$V^b$	volume of $\Omega^b$

### Lower indices

- "0" denotes the initial value;
- "n" denotes the normal component as defined in (2.50);
- " $\tau$ " denotes the tangential component as defined in (2.50).

### Abbreviations

ALE	Arbitrary Lagrangian-Eulerian (formulation or mapping)
CDE(s)	Convection-Diffusion Equation(s)
CSF	CerebroSpinal Fluid (also cytosol)
ECF	ExtraCellular Fluid (also <i>bulk</i> or <i>free</i> fluid)
ECS	ExtraCellular Space
FEM	Finite Element Methods
HTPD	Hydraulic Transmembrane Pressure Difference
ICF	IntraCellular Fluid (also <i>pore</i> fluid)
ICS	IntraCellular Space (also cell <i>interior</i> )
ICS-ECS	IntraCellular Space – ExtraCellular Space (interaction problem)
KK	Kedem-Katchalsky equation
OCD	One Cell Domain
OTPD	Osmotic Transmembrane Pressure Difference
2P	Two Parameter (formalism)



# 1 Description of the problem

The primary goal of this work is to derive a physically motivated mathematical model describing the formation of cytotoxic oedema. In order to approach this aim, the relevant processes occurring during the oedema formation as well as the properties of the considered medium must be well understood. Then based on the discussion, assumptions and conclusions drawn from the analysis of the related processes and of the properties of the media, the most suitable mathematical approximations can be chosen.

A number of assumptions will have to be made. There are two rather clear reasons for that: firstly, due to the complexity of the problem, certain information is not available. Secondly, the most exact representation may be not the best choice for the purposes of this work, as the idea is not only to provide a correct description, but also to derive a *mathematically feasible* model, i.e. a model which is amenable to either analysis or numerical simulations.

In this section not a single equation is derived or referenced. Instead, the modelling problem is defined, and then the domains of interest and significant processes that influence cytotoxic cell swelling (i.e. the driving forces) are described.

Descriptions of brain stroke, ischaemia, hypoxia, cytotoxic swelling and related effects can be found in e.g. [38], [39], [10], [40], [41], [42], [43], [44], [45], [46], [47], [48], [49], [50], [51], [52], [53], [54], [55]; *in vitro* tissue and cell swelling experiments descriptions can be found in e.g. [10], [41], [56].

## 1.1 Problem definition

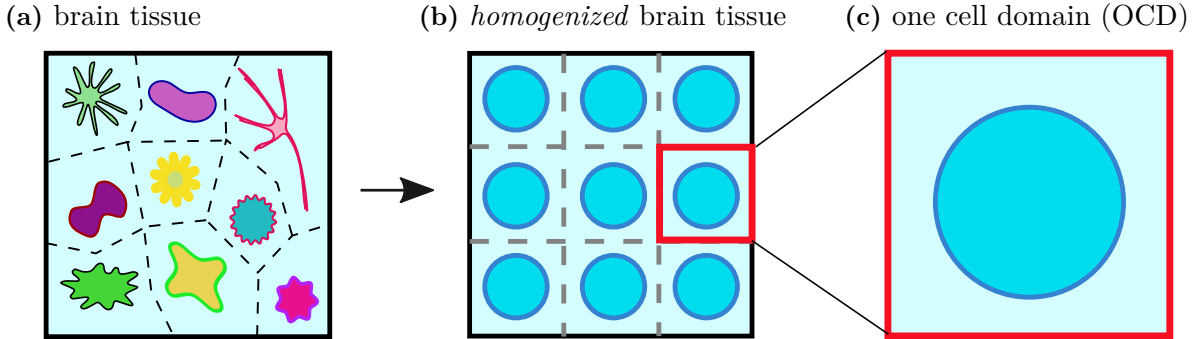
Acute cerebral ischaemia causes failure of energy requiring ion transporters leading to the rapid accumulation of sodium ions within cells and consequent inflow of water needed to maintain osmotic equilibrium. Swelling of brain cells occurs minutes after the development of hypoxia and causes a constriction of the extracellular space, since at the stage of cytotoxic oedema formation the blood-brain barrier does not yet allow penetration of substances from the surrounding tissues and vessels, and thus the overall volume of the brain is conserved.

Two classes of the human brain cells – neurons and glial cells – have in general different functions and properties. Moreover, within the same class, two different cells may differ in size and performance due to multiple factors, such as, for instance, the age, development stage or condition of the surrounding medium. Despite the differences, during cytotoxic oedema formation, as well as under artificially induced hypoxic conditions in *in vitro* studies, the cells that are situated within the oxygen-deprived area follow similar swelling patterns, [51], [43], [44], [41]. Variations in the swelling behaviour of cells are noticeably linked to the variations in the availability of oxygen within the area of observation, i.e. the position of the cell with respect to the location of the vessel blockage in *in vivo* studies and the distribution (or source) of oxygen supply within the sample in *in vitro* experiments, [55], [43], [51], [10], [48], [41], [56]. In this thesis an *average* ischaemic behaviour of an *average* brain cell is described.

Neurons and astrocytes often have singular (e.g. stellate in neurons) shapes. A brain cell can roughly be described as consisting of a *body* (soma in neurons) and narrower, possibly branching

**Figure 1.1 Localization of the problem.**

Arbitrary brain tissue sample (a) contains cells of various types and geometries, which are in general non-uniformly distributed. It can be approximated as a homogeneous brain tissue (b), i.e. a tissue consisting of identical, uniformly distributed cells. Within the homogenized tissue, one cell surrounded by an appropriate amount of extracellular fluid (c) is distinguished.



extensions (e.g. dendrites and the axon in neurons). For the modelling purposes, the cell will be assumed to have a regular, near-spherical shape.

In order to describe the process of *local* cytotoxic swelling, one cell surrounded by some amount of extracellular fluid (ECF), in particular, a *one cell domain (OCD)* comprising of a *cell* and *extracellular space (ECS)* is considered, see *Fig. 1.1*.

### 1.1.1 Extracellular space (ECS)

The cerebrospinal fluid that fills the extracellular space is a solution consisting of water, osmotically active substances (most numerous of which are sodium and potassium ions) and some other chemicals. Water is the dominant component of the ECF, [57], such that under both healthy or ischaemic conditions, the diluted substances do not influence the principal dynamic behaviour of the solution, their effects being reflected only in some slight deviations in the material parameters of the solution (e.g. viscosity, density) from the ones of water, see *Section 3.1* for details.

*Note:* The extracellular space may also contain elastic solid structures known as the extracellular matrix, and the solid-state biopolymeric scaffold to which cells adhere, [58]. In this thesis their effect is neglected.

Further in the text, the ECF is also referred to as the *bulk* or *free* fluid, since in contrast to the below defined *pore* fluid contained within the intracellular space, it occupies the ECS fully, i.e. without obstacles, and thus forms a continuous, bulk medium.



### 1.1.2 Intracellular space (ICS)

The constituents<sup>1</sup> of any brain cell can be categorized into three general parts: organelles, intracellular fluid (cytosol) and a phospholipid membrane. For the reasons given below in *Section 1.1.3*, in this work, the membrane is treated as a special, individual object. The cell without its membrane, i.e. a mixture of the organelles and intracellular fluid, constitutes the intracellular space (ICS).

The organelles of a cell split into multiple classes being diverse in shape, size, function and components from which they are made. According to their size, structure and geometry, the organelles can be subdivided into three groups:

1. *large* but few (nucleus, Golgi apparatus, rough and smooth endoplasmic reticulum);
2. *small* but many (mitochondria, ribosomes, transport vesicles, etc.);
3. thin (fine), branched, elastic, soft (cytoskeletal structures).

The *large* organelles can roughly be represented as spacious rigid objects of regular smooth shapes that are situated centrally within the cell. As suggested in *Section 3.1*, the diameter of the largest organelle is in average an order of magnitude smaller than the diameter of the cell. In order to fix the position of the cell in space, the structure formed by the large organelles is assumed to be immobile (fixed). In addition, it is assumed to be impermeable to any substances from the surrounding medium. Thus the group of large organelles can be "cut out" of the cell, defining an internal impermeable and fixed boundary of the deforming cell. Therefore in the following, when referring to the *intracellular space*, the mixture of small organelles, cytoskeleton and intracellular fluid is meant.

Most of the organelles of the second type have a spherical or oval shape and are either *vesicles*, or contain fluid and are surrounded by a lipid bilayer. The smallest organelles of this group are only nanometres in size, and the diameter of the largest of them (mitochondrion) does not normally exceed 1  $\mu\text{m}$ , which is over 50 times smaller than the diameter of an average brain cell, [60], [61], [62], [63], [64], [41].

*Note:* Similarly to the cell itself, interactions of the organelles of the first two types with different substances and objects may vary due to multiple (healthy or unhealthy) exchange processes, [61], [44]. The variations of the fluid content within the organelles and the effects on the activity of the organelles on the concentrations of osmolytes in either normal or ischaemic state are neglected in this work.

The cytoskeleton is a structure consisting of fine, long, connected filaments outstretched over the whole area of the cell. It is responsible for the shape and geometry of the cell, however while providing support to the organelles, the cytoskeleton is soft and mobile enough to allow deformations. Experiments suggest, that under moderate stresses, the brain cell demonstrates some kind of elastic behaviour, mostly due to the properties of the cytoskeleton and membrane, [56], [16], [65], [19].

Although different in size, structure and properties, cell organelles are made up from similar "building" materials (lipid bilayers, water, filaments, etc.), most of which can be assumed to be incompressible, [56], [16], [19].

---

<sup>1</sup> Some general information on the constituents of a biological cell and their physical properties can be found in e.g. [59].

The *cytosol* is a mixture of water and ions that constitutes the intracellular fluid (ICF), [66]. It may differ from the cerebrospinal (extracellular) fluid mainly in the concentrations of the diluted substances, such that the physical parameters of the intracellular fluid can be assumed to be identical to the ones of the extracellular fluid.

In contrast to the extracellular space (i.e. bulk fluid), the mathematical (physical) description of the ICS is not apparent. In particular, the inner cell geometry determined by the distribution of the organelles is very complex and is thus a great challenge for numerical simulations. In the absence of the structures, intracellular fluid, being physically almost identical to the extracellular fluid, could be described similarly. Yet the number and geometry of the organelles make them substantial obstacles to the intracellular fluid flow, therefore the overall effect of the structures should be considered.

In order to characterize the intracellular medium consisting of the *small* organelles, cytoskeleton and cytosol, and to clarify the modelling assumptions, the following properties are noted:

- more than one medium can be distinguished, i.e. *solid* and *fluid* parts;
- the fluid part (cytosol) is considered to be connected;
- the solid part, consisting of the *small* organelles and cytoskeleton, is distributed over the whole domain;
- the sizes of the solid obstacles (i.e. the diameters of the small organelles, the thickness of the cytoskeletal filaments) are small compared to the size of the mixture.

These observations suggest, that such medium can be treated as an incompressible (due to the incompressibility of the components) saturated (the two parts – solid and fluid – take up all space, i.e. there are no voids) *porous medium* that combines features of the solid and fluid components. Since the solid structures are not only deformable, but owing to the properties of the cytoskeleton can be assumed to have elastic properties, the intracellular medium can be considered to be *poroelastic*.

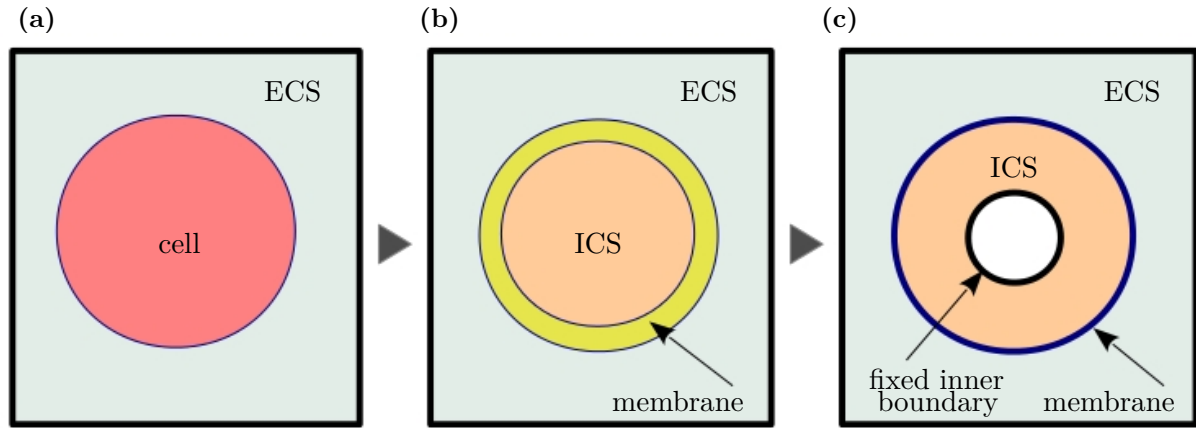
The intracellular poroelastic medium is in general anisotropic and inhomogeneous. Yet due to the mentioned above geometrical complexity of the solid skeleton, an accurate description of the material and structural singularities may be excessively complex. Thus in order to obtain a *working* (i.e. that can be solved either analytically or numerically, or mathematically analysed) model describing the dynamics of the ICS, the solid part is assumed to be isotropic, homogeneous and uniformly distributed within the cell, such that the intracellular poroelastic medium itself can be considered to be *isotropic* and *homogeneous*.

### 1.1.3 Cell membrane: mechanical properties

Consisting of similar materials, the membrane could in principle be seen as a part of the solid structures of the ICS. Yet the membrane's singular geometry, topology, filtering properties and other effects that may determine or affect some of the most important features of both normal and malignant cell behaviour suggest, that the membrane deserves an individual consideration. A biological cell membrane is a soft, curved *thin layer* separating the intracellular and extracellular spaces. Membranes of animal cells in general, and of human brain cells in particular, are attached to the cytoskeleton of the cell and are composed of a phospholipid bilayer with multiple

**Figure 1.2 Evolution of the cell representation.**

- (a) cell surrounded by extracellular fluid (ECS) is a single object;  
 (b) within the cell, the intracellular space (ICS) is distinguished from the membrane;  
 (c) large immobile organelles are excluded from the ICS, the thickness of the membrane is neglected.



types of proteins embedded in it, where the latter serve as transporters of various substances across the membrane, [56].

Membranes play a great role in the processes of living cells owing to their unique properties. In the framework of this thesis, only the filtering and mechanical features of the brain cell membrane are of interest.

One of the most prominent mechanical properties of the membrane consists in the so-called *surface incompressibility* of the cell: during a continuous swelling process and until the cell has reached a spherical shape, the membrane tends to preserve its surface area. At the same time, the rigidity of the membrane is very low, such that its flexible structure allows relatively large cell deformations without introducing any significant constraints to the movement.

*Note:* It has been shown, that under the stresses acting on the membrane of a cell swollen into a sphere, the membrane may slightly stretch, i.e. increase its surface area, [56], yet the swelling process is modelled up to the final spherical state, so this effect can be neglected.

The ability of the membrane to preserve its (and consequently the cell's) surface area relies on the mechanical properties of a *closed* phospholipid bilayer, which are clearly different from the properties of the intracellular organelles, since the latter do not in general form closed layers encompassing large areas of the cell. It means that in the absence of the membrane (assuming that the ICS "holds together" on its own), the surface area of the cell would not necessarily be preserved, but would rather continuously grow, proportionally to the rate of swelling.

It is also important to point out, that the thickness of the phospholipid membrane is only a few nanometres, [56], [62], [4], [67], and thus the membrane can not be modelled as a three dimensional domain using the equations of continuum mechanics. In addition to the scale related restrictions, the membrane thickness is several orders of magnitude smaller than the size (radius) of the ICS, and such great size difference becomes a problem for the numerical simulations of the considered problem.

Thus in this work, the membrane is treated as a *two dimensional* object (i.e. a surface), such

that its thickness is neglected on the macroscale (i.e. on the scale of the modelling). As the membrane is not mixed with the organelles, but lies strictly on the surface of the intracellular medium, it defines (coincides with) an *interface* between the intracellular and extracellular spaces.

In addition, it is assumed in this work, that the membrane is *folded on the microscopic level* as shown in Fig. 1.3b. Therefore while on the microscopic level its surface area is conserved, on the *macroscopic* level a stretching effect is observed, Fig. 1.4a, 1.4b.

**Figure 1.3 Microscopic membrane deformation types: unfolding and stretching.**

Consider a cell  $\Omega^c$  swelling from its initial configuration  $\Omega_0^c$  into a deformed (swollen) configuration  $\Omega_1^c$ , such that points  $a_0, b_0$  on the surface of the reference cell  $\Omega_0^c$  are deforming into the points  $a_T, b_T$  on the swollen cell surface. Both initially and at time  $t = 1$  the cell has a symmetric spherical shape, and thus on the macroscopic level, the increase of the surface area of the cell is observed. For an arbitrary *microscopic* surface segment  $S$  deforming from  $S_0$  into  $S_1$ , the following types of the microscale deformation can be considered: (a) the membrane contains fluid and solid parts, such that its length increases due to the increase of the pore size (i.e. fluid content); (b) the membrane is "folded", such that the lengths of the initial and deformed surface elements  $S_0, S_1$  are equal; (c) the membrane conserves its volume, such that when stretched, the surface element  $S$  becomes longer and thinner.

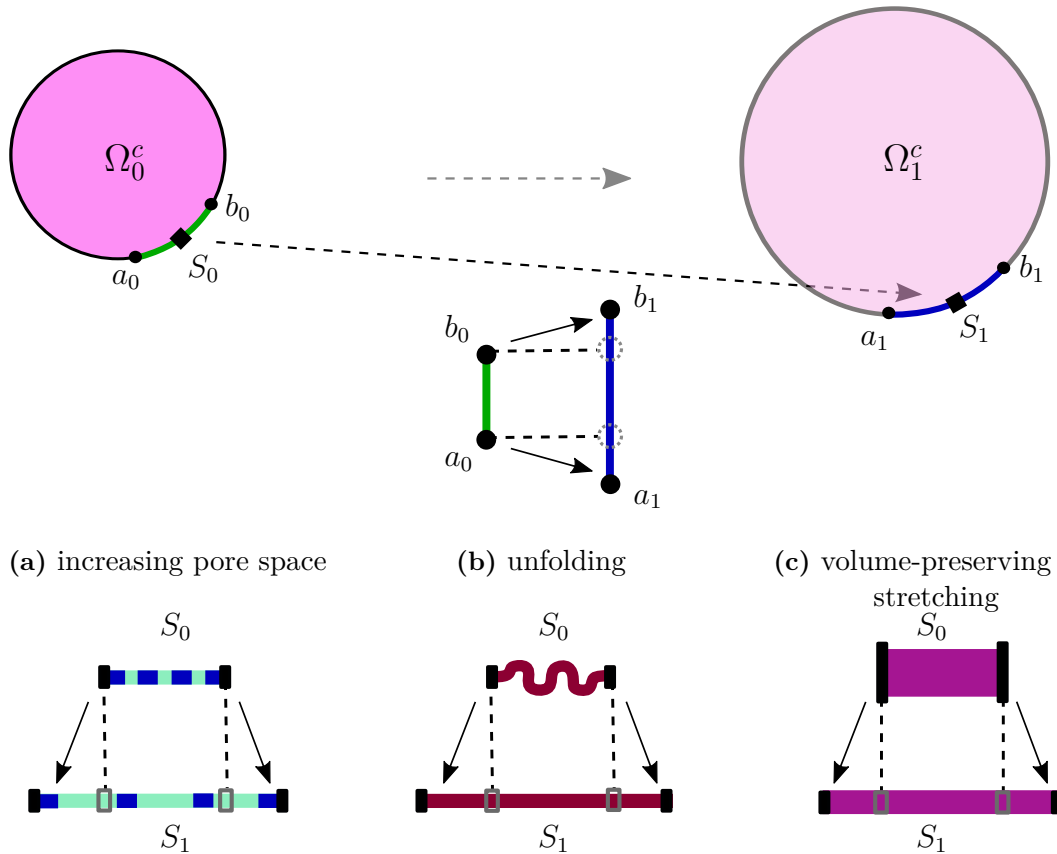
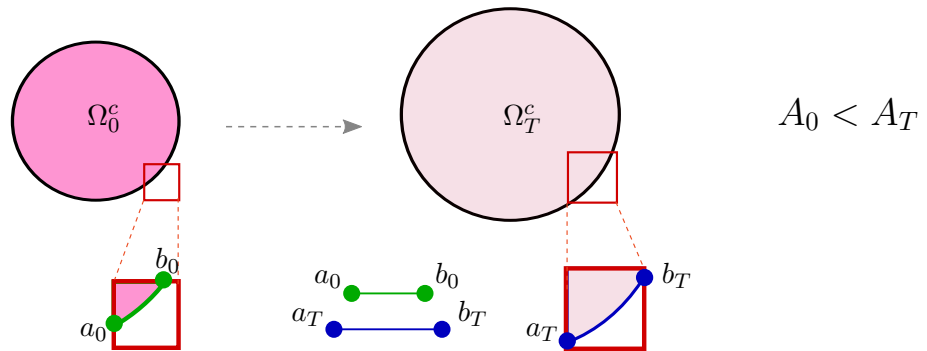


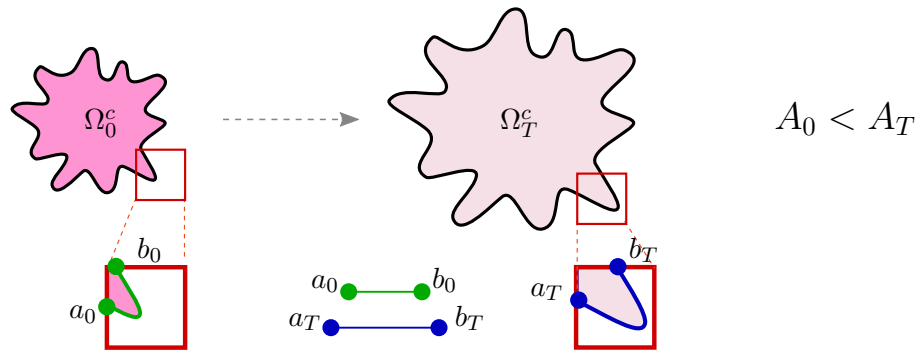
**Figure 1.4 Cell swelling with respect to the surface area conservation.**

On the pictures below, a cell  $\Omega^c$  in its initial (reference) configuration  $\Omega_0^c$  and deformed (swollen) state  $\Omega_T^c$  is shown. Points  $a_0, b_0$  on the surface of the reference cell  $\Omega_0^c$  are deforming into the points  $a_T, b_T$  on the swollen cell surface. The total initial surface area is denoted by  $A_0$ , and the surface area of the swollen cell – by  $A_T$ . The following types of cell swelling are considered:

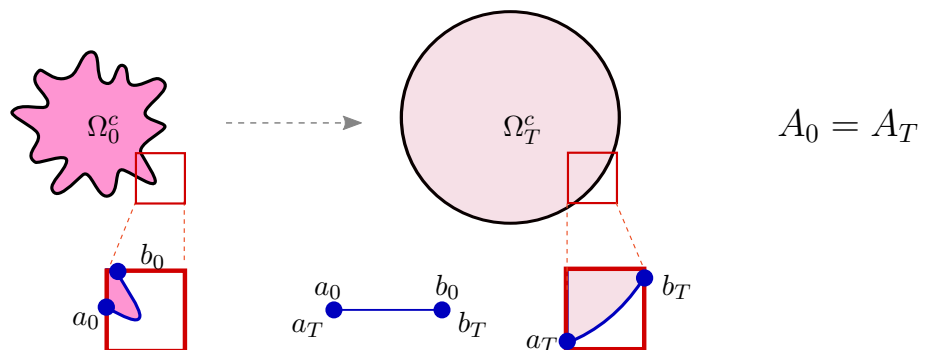
(a) Unconstrained radial swelling (deformation) of an initially spherical cell: the surface is stretching.



(b) Unconstrained swelling of a non-spherical (non-symmetric) cell: the surface is stretching.



(c) Swelling of the cell constrained by the membrane forces: the surface is unfolding, not stretching.



## 1.2 Osmosis and osmotic pressure

*Osmosis* is essential in biological systems providing the primary means by which water is transported in and out of cells, since the membranes of living cells can act as semipermeable filters. In particular, osmotic pressure gradients across the cell membranes are the **driving force** of the cytotoxic swelling of brain cells during ischaemic stroke, [51], [68], therefore osmotic pressure effects must enter the modelling equations.

*Def.:* *Osmolarity* is the molarity (molar concentration) of the substances that contribute to the osmotic pressure of the solution.

While the principles of osmotic pressure modelling and the dependence of osmotic pressure on certain factors are still disputed, it has been established, that osmosis relies on the ability of the membrane to passively transmit water while allowing only *selective* passage of osmotically active substances, such that the osmotic pressure difference at the membrane is proportional to the difference of the osmolarities of the separated solutions.

In the framework of the considered problem, the substances most significantly contributing to the magnitudes of the ICS and ECS osmotic pressures (or their differences) are the ions of sodium  $Na^+$ , potassium  $K^+$ , chloride  $Cl^-$  and the negatively charged macromolecules (amino acids in proteins, nucleic acids) which are trapped ("fixed") within the intracellular space, [69], [52], [51], [43], [10]. As osmotic pressure is a *colligative property*, which means that it depends on the osmolarity of the solution but not on the size or type of the solute particles, the osmotic pressure of a solution containing distinct osmotically active chemicals is determined by the total osmolarity of the diluted osmolytes, [70], [71].

More information on the osmotic phenomenon in general and on the role of osmosis in ischaemia can be found in *Appendix A.5*.

### 1.2.1 Membrane filtration

Intracellular and extracellular spaces contain multiple types of substances that cross the membrane of the cell during both healthy and ischaemic cell activities: biological membranes are impermeable to large molecules, such as proteins, but allow passage of non-polar hydrophobic molecules (lipids), small molecules and some ions. For the purposes of this work however, it is only relevant to consider the filtration of two classes of substances:

- **water**, i.e. the **solvent** of the extracellular and intracellular solutions that is responsible for the increase of the cell volume during swelling;
- osmotically active substances (**osmolytes**), i.e. the **solute** mixture dissolved in the extracellular and intracellular solutions.

*Def.:* *Solution* is a mixture, in which some amount of substance of a *solute* is diluted (dissolved) within much greater volume of a different substance, known as the *solvent*. For instance, in a saline water solution, the salt is the solute and the water the solvent.

Depending on the length of the chosen observation time, severity of condition and speed of swelling, the cell membrane can be *considered* to be either **strictly or leaky semipermeable**.

*Def.:* *Strictly semipermeable* membrane is the membrane, that is permeable only to the solvent and impermeable to the solute; in case the membrane is also *partially* permeable to the solute, it is called *leaky semipermeable*, see *Fig. 1.5*.

In particular, during cytotoxic swelling observations, the membrane can be assumed to be strictly semipermeable (the case denoted as *Ms*), such that the exchange of the osmolytes can be neglected, in the following cases:

- the shift in concentrations at each time step and over the observation time in total is too small to influence the magnitude of the transmembrane osmotic pressure gradient;
- most of the energy deprivation induced redistribution of the osmolytes between the ICS and ECS is achieved in the very beginning of the observation, and further osmolyte exchange is negligible;
- the transmembrane exchanges of different substances compensate one another at each time point.

In all other cases, i.e. when the membrane is clearly acting as a leaky semipermeable filter (the case denoted as *Ml*), its osmolyte transmitting properties must be considered.

Unlike in industrial filters, the distribution of channels in biological membranes is not generally uniform (periodic). In addition, with regard to the filtering properties, the complex *geometry* of the protein channels may be not as important as such factors as<sup>2</sup>:

- the electrochemical interactions between the channel proteins and transmitted substance;
- the characteristics of the chemical itself (i.e. its size, solubility, charge, etc.);
- the performance of the channels and the overall condition of the membrane;
- the availability of energy (ATP);
- the saturation of the surrounding media with other chemicals (mostly oxygen, calcium and glutamate): their concentrations or transmembrane concentration differences;
- the physical characteristics of the environment (e.g. the temperature).

Therefore in a changing environment, the membrane permeability may change correspondingly. It can then be concluded, that the ability of the membrane to transmit substances should in general depend on both space and time.

*Note:* The structure of the channels (transmitters) is such, that their geometry is not explicitly affected by the deformations caused by the swelling of the cell, thus the permeability of the membrane to water and osmolytes can be assumed not to vary with the deformation of the swelling cell.

The flow of water across the membrane is primarily realized via water channels or *aquaporins* (*AQPs*): small transporting proteins embedded in the phospholipid bilayer, which are approximately of the size of the water molecule ( $\approx 10\text{\AA}$ ). Irrespectively of the condition of the membrane and surrounding media, normally no other particles can pass through the AQPs, [73], [75].

Ionic membrane channels can be subdivided into energy requiring pumps and passive (or leaky) channels. While during a healthy brain cell activity, the pumps – and thus their transmitting properties – are of great importance, during hypoxia, the necessary energy is not available, and therefore the performance of *passive* channels becomes more significant, [51]. Different channels responsible for the passage of different types of chemicals may vary in their properties and transmitting capacities. Yet since osmotic pressure is a colligative property, such that the

<sup>2</sup> Descriptions of the membrane (water or solute) transmitting channels and their activity in either healthy or ischaemic condition, can be found in e.g. [51], [72], [43], [44], [73], [55], [74].

total concentration of the diluted osmolytes is of ultimate interest, for simplicity, the membrane permeability is chosen to reflect the characteristics of an *average* ionic channel.

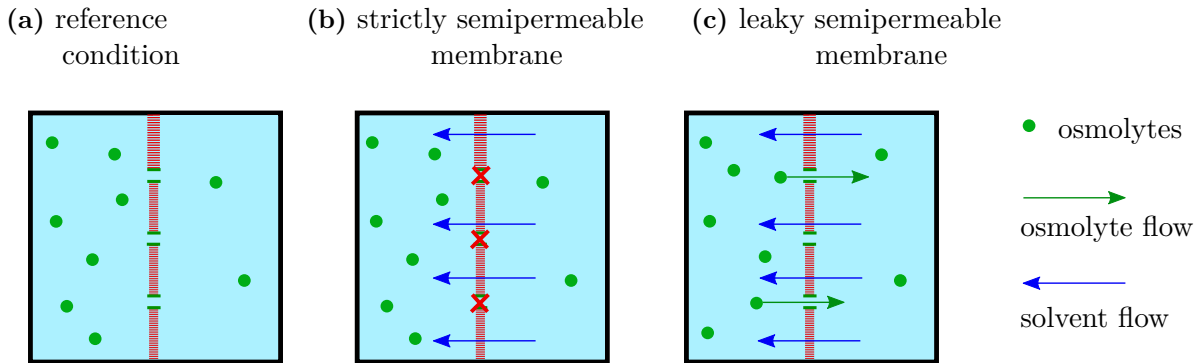
*Note:* It has been suggested (in e.g. [72], [41]), that with respect to the ionic exchange between the intra- and extracellular spaces, cytotoxic swelling of brain cells is strongly influenced by the permeability of the membrane to sodium that depends on the concentrations of oxygen and glutamate.

In this work it is assumed, that the spatial distribution of the transmitting channels is uniform, and the influence of the environmental factors on the membrane water and osmolyte permeabilities during the observed swelling is neglected, such that the water filtration and the osmolyte permeability (or solute reflection) functions can be approximated as constants.

*Note:* In some brain cells, the distribution of channels is such, that certain areas of the membrane contain significantly larger number of channels than the other areas, [76]. In order to approximate strong differences in the distribution of channels, different filtering permeabilities can be chosen for different parts of the membrane.

**Figure 1.5 Leaky and strictly semipermeable membranes.**

- (a)  $t = 0$  (reference state): there exists concentration difference between the domains separated by a semipermeable membrane;
- (b)  $t > 0$ , *strictly* semipermeable membrane: osmosis-driven solvent (water) flow through the membrane is observed;
- (c)  $t > 0$ , *leaky* semipermeable membrane: osmosis-driven solvent (water) flow and the flow of osmolytes through the membrane are observed.



### 1.3 Effects of the surrounding media

Brain cell swelling can be studied and analysed under diverse conditions. The obtained results must naturally vary depending on the settings of the experiment. In particular, the type and behaviour of the medium surrounding the One Cell Domain determines the choice of the boundary conditions at the outer walls of the OCD. In this work, the following observation types are distinguished:



- E1** *in vivo* observations of an ischaemic brain tissue area;
- E2** *in vitro* experiments on a brain tissue sample;
- E3** *in vitro* experiments on a single cell, when a brain cell is placed into a *large* tank (the boundaries of the tank are far away from the cell) filled with a fluid identical or similar to the ECF (often physiological solution);
- E4** *in vitro* experiments on a single isolated cell, when a brain cell is placed into a *small* tank filled with a fluid identical or similar to the ECF, such that the boundaries of the tank define the outer boundary of the OCD.

For simplicity, the outer boundaries of the OCD are considered to be **fixed** for all types of experiments. Then as the observed processes are such, that the matter gets neither created nor destroyed, and the materials making up the domains are assumed to be incompressible, the total volume of the OCD must be conserved over the observation time.

While the brain cells are relatively densely packed (the extracellular fluid takes only up to 20% of the total brain space), it can be assumed, that the extracellular space of the brain tissue is connected and the bodies of the cells do not touch. It then follows, that not only in the single cell experiments, but also within a tissue sample, the cells do not exert stresses on each other and can be considered to be completely surrounded by the extracellular fluid. Thus for all considered experiments, the cell can be assumed to be situated within the OCD such that it does not intersect the outer boundaries, and thus the outer boundary of the OCD coincides with the outer boundary of the ECS.

*Note:* Under the experimental *in vitro* conditions *E4*, the cell may touch the walls of the container, or it may be necessary to fix the cell along a part of its surface. Also, as mentioned earlier in *Section 1.1.1*, within the brain tissue (*E1*, *E2*), the cells may be supported by the extracellular matrix. Therefore in the general mathematical cell swelling model, the outer boundary of the overall domain should in principle be shared by the ECS and ICS walls, such that the ICS outer boundary is either empty or consists of the points that are in contact with external objects, depending on the chosen settings. In this work however, the cell is for simplicity assumed to be fixed at its inner boundary and completely surrounded by the ECF from the outside.

In the areas of the brain tissue that are affected by the cytotoxic processes, the ECS shrinks (due to the outflow of water into the cells), thus there may be created *global* ECS concentration gradients across some part of the brain tissue, which would result in the flow of water and/or osmolytes down their concentration gradients.

*Note:* In this work, the *global* processes are defined on the tissue level, in contrast to the *local* processes, that take place on the cellular level.

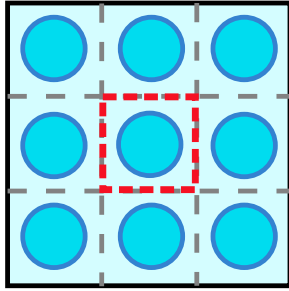
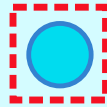
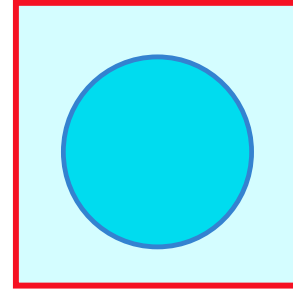
Therefore in case *E1*, apart from the processes occurring at the membrane of the cell, the movement of osmolytes and water within the extracellular fluid domain can be influenced by the *global* gradients that are reflected through the corresponding inflow-outflow boundary conditions. Depending on the severity of ischaemia and on the length of the chosen observation time, the speed of the global flow can be negligible or non-existent, allowing to assume that the OCD is surrounded by a stationary fluid. In the latter case, the flow of the fluid is caused only by the activity of the cell.

**Figure 1.6 Environment of the OCD depending on the experiment type.**

(a) In type  $E1$ ,  $E2$  experiments, the OCD is contained in a brain tissue sample, such that the outer boundaries of the OCD are defined some distance away from the cell within the extracellular space.

(b) In type  $E3$  experiments, the cell is observed in a container filled with fluid, such that it can be assumed, that the walls of the container have no influence on the boundaries of the OCD.

(c) In type  $E4$  experiments, the outer boundaries of the OCD are fixed and impermeable.

(a)  $E1$ ,  $E2$ (b)  $E3$ (c)  $E4$ 

A brain cell in the ischaemic region ( $E1$ ,  $E2$ ) is surrounded by other cells that also absorb water and exchange osmolytes with the extracellular solution. Thus throughout the observed process, the overall domain can be influenced by the swelling behaviour of the surrounding cells, which – just as the behaviour of the modelled cell – is not in general known. Therefore a simplified description of the environmental effects is used instead. In particular, considering that the cells within a small area of the given brain tissue sample do not vary in size or properties, such that their swelling behaviours are approximately identical, *periodic* boundary conditions for both water and osmolyte fluxes can be assumed. In this case, the total solute concentration is kept constant within the overall domain and the influence of the flow created by the movement of the surrounding cells is somewhat taken into account.

When only one cell is studied, and the tank containing the cell is so large, that the influence of its walls on the neighbourhood of the cell is negligible ( $E3$ ), it would be natural to define infinitely remote outer boundaries of the OCD and thus prescribe conditions on infinity. Yet as a model defined on an infinitely large domain can not be implemented numerically, in case  $E3$ , the outer boundaries of the OCD are chosen sufficiently far away from the surface of the cell, such that their influence on the cell swelling processes is negligible.

The conditions of an isolated cell experiment ( $E4$ ) require that the outer walls of the OCD must be impermeable, thus homogeneous *Dirichlet* conditions can be prescribed.

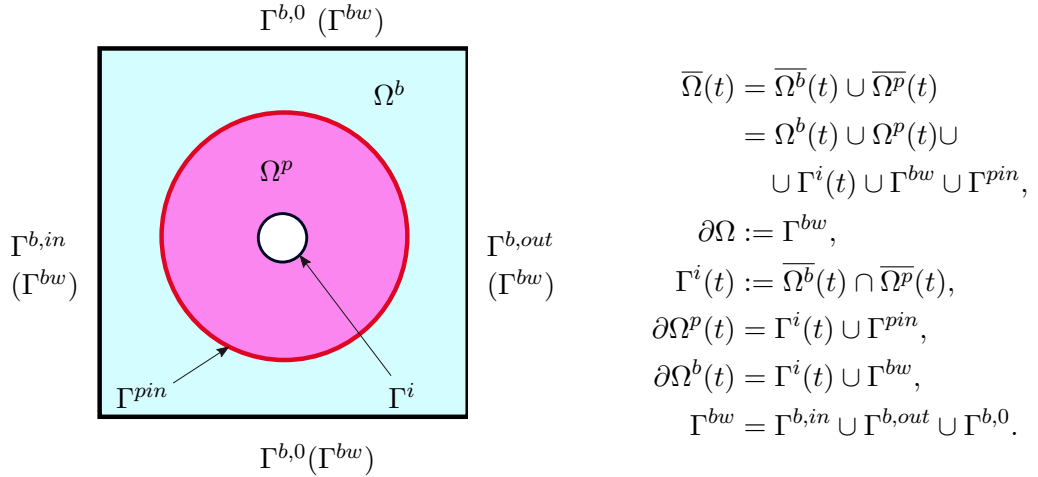
## 1.4 Summary: considered domains and effects

Here the descriptions of the considered domains and processes are summarised and complemented by the notations for the described domains. Thus over the observation time interval  $(0, T)$ , the following domains and boundaries are distinguished within the OCD (or the *overall*

domain)  $\Omega(t) \in \mathbb{R}^d \times (0, T)$ ,  $d \in \{2, 3\}$ :

- the extracellular space (ECS)  $\Omega^b(t) \in \mathbb{R}^d \times (0, T)$ : filled with an *incompressible* viscous extracellular (*bulk* or *free*) fluid (ECF) and deforming (shrinking) during the observation time;
- the intracellular space (ICS)  $\Omega^p(t) \in \mathbb{R}^d \times (0, T)$ : occupied by an incompressible saturated poroelastic medium, which is composed of the solid and fluid phases ( $\Omega^{sp}$ ,  $\Omega^{fp}$  respectively); the phases can be distinguished from one another only on the *microscale*, such that on the scale of the problem (*macroscale*) each point  $(x, t) \in \Omega^p(t) \times (0, T)$  has both the fluid and solid components. The swelling and so the deformations of the cell are caused by the inflow of the ECF;
- the cell membrane  $\Gamma^i(t) \in \mathbb{R}^{d-1} \times (0, T)$ : geometrically coincides with the interface separating the intracellular and extracellular spaces; exhibits filtering properties with respect to both water and osmolytes;
- the outer boundaries of the OCD coincide with the outer ECS boundaries  $\Gamma^{bw} \in \mathbb{R}^{d-1}$  (*bulk fluid walls*): fixed, may or may not allow fluxes of water and osmolytes depending on the chosen type of experiment (*E1–E4*); in case the flow of water and/or osmolytes is allowed, the inflow  $\Gamma^{b,in}$ , outflow  $\Gamma^{b,out}$  and impermeable  $\Gamma^{b,0}$  boundaries are distinguished within  $\Gamma^{bw}$ ;
- the inner boundary  $\Gamma^{pin} \in \mathbb{R}^{d-1}$  (*porous internal walls*): fixed and impermeable to both water and osmolytes;

**Figure 1.7 Overall domain**  $\Omega = \Omega^b(t) \cup \Omega^p(t) \in \mathbb{R}^d$ ,  $d \in \{2, 3\}$ ,  $t \in (0, T)$ .



Osmosis is the driving force of the cell swelling since the extracellular space  $\Omega^b$  and the fluid phase  $\Omega^{fp}$  of the intracellular domain  $\Omega^p$  contain osmotically active substances while the ICS and ECS are separated by an (in general leaky) semipermeable membrane.

### 1.4.1 List of assumptions

Developing a *precise* mathematical description of the behaviour of a swelling brain cell would be a great challenge as many of the processes taking place during of a living cell swelling are either not well known or very complex. Therefore in order to obtain a *working* model that can be either mathematically analysed or numerically solved (or both), a number of assumptions with regard to the characteristics of the domains and/or processes of the considered problem are made. In particular, it is assumed that at all times:

- the processes are isothermal;
- all considered materials are incompressible;
- the ECF and the fluid phase of the intracellular medium are viscous, incompressible and homogeneous;
- the solid phase of the ICS is elastic, incompressible, homogeneous and isotropic;
- the poroelastic intracellular medium is saturated, homogeneous, isotropic and has a periodic structure;
- the deformations of the swelling cell are *small* compared to its size;
- the effect of gravity (and other possible body forces) can be neglected;
- the osmolytes are contained only in the fluids and they do not react with the constituents of the solid phase of the cell;
- the total volume of the overall domain is conserved over the observation time;
- the solid and fluid phases  $\Omega^{sp}$ ,  $\Omega^{fp}$  do not exchange matter, such that the ICS is growing only due to the increase of the volume of the intracellular fluid  $\Omega^{fp}$ ;
- on the scale of the model, the thickness of the membrane can be neglected.

## 2 Mathematical Model

This chapter is organized such, that the mathematical modelling of the cell swelling problem is done *incrementally*, in the following steps:

- 1 the intracellular and extracellular spaces (ICS and ECS) are described and directly coupled through the interface conditions;
- 2 the osmotic pressure difference at the ICS-ECS interaction boundary is modelled, such that the corresponding transport equations for the molarities are added to the modelling equations; the interface conditions of the pure ICS-ECS interaction problem are modified as to include the osmotic pressure effects and cell membrane filtering properties.

### 2.1 ICS-ECS interaction problem: Biot-Stokes model

In this section, a mathematical model for the pure (i.e. not influenced by either the membrane or osmosis) intracellular-extracellular space (ICS-ECS) interaction problem is derived. First, the sets of equations describing the behaviour of the extracellular  $\Omega^b$  and intracellular  $\Omega^p$  spaces are suggested. Then the ICS and ECS interaction is coupled through the interface conditions. For each of the experimental conditions described in *Section 1.3*, corresponding boundary and initial conditions are prescribed.

#### 2.1.1 Extracellular space: the Stokes equations

Material parameters (viscosity, density) of the extracellular fluid filling the ECS  $\Omega^b$ , together with the physical and dynamical characteristics of the swelling process (i.e. the values of the velocity, temperature, pressure, etc., see *Section 3.1*) suggest, that the motion of the bulk fluid within the ECS can be described by the incompressible *Navier-Stokes* equations for an isotropic viscous *Newtonian fluid*.

The Navier-Stokes equations defined on the deforming extracellular space domain  $\Omega^b(t)$  have the following general form in the *Eulerian* coordinates:

$$\nabla \cdot \sigma^b = \rho^f \partial_t v^b + \rho^f (v^b \cdot \nabla) v^b \quad \text{in } \Omega^b(t) \times (0, T), \quad (2.1)$$

$$\sigma^b := -p^b I + \sigma^{b,visc} = -p^b I + 2\mu^f (\nabla v^b + (\nabla v^b)^T) \quad \text{in } \Omega^b(t) \times (0, T), \quad (2.2)$$

where  $\rho^f$  is the density,  $\mu^f$  – dynamic viscosity of the ECF at a given temperature,  $v^b(x, t)$  – fluid flow velocity,  $p^b(x, t)$  – hydraulic fluid pressure and  $\sigma^b$  – total stress tensor of a Newtonian fluid. Adding the *incompressibility* constraint

$$\nabla \cdot v^b = 0 \quad \text{in } \Omega^b(t) \times (0, T) \quad (2.3)$$

to the linear momentum balance (2.1), (2.2), a system of equations describing the motion of an incompressible Newtonian fluid is obtained:

$$\begin{cases} -\nabla p^b + \mu^f \Delta v^b = \rho^f (\partial_t v^b + (v^b \cdot \nabla) v^b) \\ \nabla \cdot v^b = 0 \end{cases} \quad \text{in } \Omega^b(t) \times (0, T). \quad (2.4)$$

Low value of the Reynolds number  $Re$  estimated in *Section 3.2.2* for the flow of the extracellular fluid during cytotoxic swelling indicates, that the Navier (non-linear inertial) terms can be neglected, such that the system (2.4) can be transformed into the **Stokes** equations:

$$Re \ll 1 \quad \Rightarrow \quad \begin{cases} -\nabla p^b + \mu^f \Delta v^b = \rho^f \partial_t v^b \\ \nabla \cdot v^b = 0 \end{cases} \quad \text{in } \Omega^b(t) \times (0, T). \quad (2.5)$$

*Note:* As the magnitude of the estimated *Strouhal* ( $St$ ) number is such, that the  $StRe$  product is also much smaller than 1, see (3.90), the linear inertial term in (2.5) may be dropped as well, such that the ECF flow is then approximated by the *stationary* Stokes equations. However for technical reasons, the algebraic (mass) term corresponding to the linear inertial effects is kept in the numerical implementation, therefore the Stokes equations (2.5) are not further reduced.

Some general information on the analysis, derivation and applicability of the Navier-Stokes equations can be found in e.g. [77], [78], [79], [80], [81], [82]. A derivation of the Navier-Stokes equations on the basis of the Reynolds Transport Theorem is outlined in the *Appendix* (*Sections A.1, A.3*).

### 2.1.2 Intracellular space: the Biot poroelasticity equations

As suggested in *Section 1.1.2*, the swelling interior of the cell can be approximated as a saturated, homogeneous, isotropic, deformable porous medium undergoing *small* deformations, thus the mathematical model describing the ICS  $\Omega^p$  can be based on the **Biot poroelasticity** equations. The Biot equations is a well known and widely accepted system describing the motion of slightly deforming porous media. The research on flow in deformable porous materials originates from the works of Terzaghi (1925) and Biot (1941) on the consolidation of soils under loading, such that in 1955 the theory of Biot was developed, [83]. Since then there have been suggested approaches employing *homogenization* techniques, in which the *macroscale* poroelasticity equations are rigorously derived from the *microscale* equations that describe each phase of the medium individually, see e.g. [29], [30], [31], and references therein.

*Note:* While originally derived for soils, the Biot type equations have also been used in the modelling of biological tissues, see e.g. [22], [23], [24], [25], [26], [27], [28].

In the following fragment, the description of the Biot equations according to the authors of [31], and the estimates of the coefficients of the Biot equations with respect to the data discussed in *Section 3.1* are presented. While appealing to the equations and coefficients derived in [31], for the sake of coherence, the original notations of [31] are used. Then the Biot problem on the intracellular domain (2.34) is formulated in the notations corresponding to the style of this work.

The porous medium considered in [31] consists of the connected, homogeneous, isotropic linear elastic solid phase and connected, viscous, slightly compressible fluid phase, and is assumed

to have a periodic structure (matrix). In the development of the poroelasticity equations, the inertial terms of the phase equations are dropped, the fluid-solid interaction is linearised, and the pressure is considered to be the dominant part of the fluid stress. Effective diphasic quasi-static two-scale equations for a poroelastic medium are rigorously derived from the first principles (consolidation theory). Then introducing auxiliary problems and separating the scales, the following three-dimensional Biot poroelasticity equations (more generally, an initial-boundary value problem) for  $\{\mathbf{u}, p^0\}$  on a single (slow) scale are obtained:

$$-\operatorname{div}_x \left\{ A^H e_x(\mathbf{u}) \right\} + \operatorname{div}_x \left\{ (|\mathcal{Y}_f|I - \mathcal{B}^H)p^0 \right\} = \Psi \mathbf{F}(x, t) \quad \text{in } \Omega_1 \times (0, T), \quad (2.6)$$

$$M \partial_t p^0 + \operatorname{div}_x \left\{ K(\psi_f \mathbf{F} - \nabla_x p^0) + (|\mathcal{Y}_f|I - \mathcal{B}^H) \partial_t \mathbf{u} \right\} = 0 \quad \text{in } \Omega_1 \times (0, T), \quad (2.7)$$

where  $\mathbf{u}$  is the solid phase displacement,  $p^0$  – pore pressure;  $x$  – first (or slow) scale,  $(0, T)$  – observation time interval,  $\Omega_1$  – poroelastic domain of unit size, such that  $\Omega_1$  and the given (original) poroelastic domain  $\Omega_L$  of the characteristic size  $L_{obs}$  are related as  $\Omega_L := L_{obs} \Omega_1$ ;  $|\mathcal{Y}_f|$  is the porosity,  $|\mathcal{Y}_s|$  – solidity ( $\mathcal{Y}_f$  is the open, connected, Lipschitz boundary fluid part of the unit cell  $\mathcal{Y} = [0, 1]$ ,  $\mathcal{Y}_s = \mathcal{Y} \setminus \mathcal{Y}_f$  is the solid part of the unit cell  $\mathcal{Y}$ );  $e(\mathbf{u})$  is the strain tensor for the deformation  $\mathbf{u}$ :

$$(e(\mathbf{u}))_{ij} := \frac{1}{2} \left( \frac{\partial u_i}{\partial x_j} + \frac{\partial u_j}{\partial x_i} \right), \quad i, j = 1, 2, 3, \quad (2.8)$$

such that for an isotropic linear elastic material, the stress tensor  $\sigma$  is defined as:

$$\sigma(\mathbf{u}) := A e(\mathbf{u}) = \lambda^s (\nabla \cdot \mathbf{u}) I + 2\mu^s e(\mathbf{u}), \quad (2.9)$$

where the the elasticity coefficient tensor  $A$  is determined by the Lamé coefficients  $\lambda^s, \mu^s$ ;

$\mathbf{F}$  is the forcing term, also including the contributions of the non-homogeneous non-essential boundary conditions;  $\Psi, \psi_s, \psi_f$  are the forcing terms defined as:

$$\begin{aligned} \Psi &:= |\mathcal{Y}_f| \psi_f + |\mathcal{Y}_s| \psi_s, & \psi_s &:= \rho^s \frac{F_0 L_{obs}^2}{l \Lambda}, \\ & & \psi_f &:= \rho^f \frac{F_0 L_{obs}^2}{l \Lambda}, \end{aligned} \quad (2.10)$$

where  $\rho^s, \rho^f$  are the solid and fluid phase densities respectively,  $F_0$  – characteristic value of the forcing term  $\mathbf{F}$ ,  $l$  – pore size and  $\Lambda$  is the Young's modulus of the linear elastic skeleton;  $M$  is a combined porosity and compressibility of the fluid and solid, defined as:

$$M := |\mathcal{Y}_f| \mathcal{K}_{co} + M_0, \quad (2.11)$$

$$M_0 := - \int_{\mathcal{Y}_s} \operatorname{div}_y \mathbf{w}^0(y) dy = \int_{\mathcal{Y}_s} A e_y(\mathbf{w}^0) : e_y(\mathbf{w}^0) dy > 0, \quad (2.12)$$

where  $\mathcal{K}_{co} := \frac{\Lambda}{\rho_f E_f}$ ,  $E_f$  is the fluid bulk modulus, and  $\mathbf{w}^0 \in H^1(\mathcal{Y}_s)^3$ ,  $\int_{\mathcal{Y}_s} \mathbf{w}^0(y) dy = 0$ , is a 1-periodic vector valued solution to the auxiliary problem

$$-\operatorname{div}_y \left\{ A e_y(\mathbf{w}^0) \right\} = 0 \quad \text{in } \mathcal{Y}_s, \quad (2.13)$$

$$A e_y(\mathbf{w}^0) \mathbf{n} = -\mathbf{n} \quad \text{on } \partial \mathcal{Y}_s \setminus \partial \mathcal{Y}; \quad (2.14)$$

$A^H$  – dimensionless effective coefficient tensor (Gassman’s tensor),  $\mathcal{B}^H$  – effective coefficient tensor,  $K$  – effective permeability tensor:

$$A_{kl}^H := \left( \int_{\mathcal{Y}_s} A \left( \frac{\mathbf{e}^i \otimes \mathbf{e}^j + \mathbf{e}^j \otimes \mathbf{e}^i}{2} + e_y(\mathbf{w}^{ij}) \right) dy \right)_{kl}, \quad (2.15)$$

$$\mathcal{B}^H := \int_{\mathcal{Y}_s} A e_y(\mathbf{w}^0) dy, \quad K_{ij} := \int_{\mathcal{Y}_f} q_i^j(y) dy, \quad (2.16)$$

where  $\mathbf{w}^0$  as is defined above,  $\mathbf{w}^{ij} \in H^1(\mathcal{Y}_s)^3$ ,  $\int_{\mathcal{Y}_s} \mathbf{w}^{ij}(y) dy = 0$ , is a 1-periodic vector valued solution to the auxiliary problem:

$$\begin{aligned} -\operatorname{div}_y \left\{ A \left( \frac{\mathbf{e}^i \otimes \mathbf{e}^j + \mathbf{e}^j \otimes \mathbf{e}^i}{2} + e_y(\mathbf{w}^{ij}) \right) \right\} &= 0 && \text{in } \mathcal{Y}_s, \\ A \left( \frac{\mathbf{e}^i \otimes \mathbf{e}^j + \mathbf{e}^j \otimes \mathbf{e}^i}{2} + e_y(\mathbf{w}^{ij}) \right) \mathbf{n} &= 0 && \text{on } \partial\mathcal{Y}_s \setminus \partial\mathcal{Y}; \end{aligned} \quad (2.17)$$

and  $q^i$  is a solution to the flow auxiliary problem:

$$\begin{aligned} -\Delta q^i + \nabla \pi^i &= e^i && \text{in } \mathcal{Y}_f, \\ \operatorname{div}_y q^i &= 0 && \text{in } \mathcal{Y}_f, \\ q^i &= 0 && \text{on } \partial\mathcal{Y}_f \setminus \partial\mathcal{Y}; \end{aligned} \quad (2.18)$$

such that  $\{q^i, \pi^i\}$  is 1-periodic.

*Note:* While the introduced (rigorously derived by homogenization) effective Biot equations are quasi-stationary, in some works, e.g. [84], [36], there have also been proposed and used the Biot equations including inertial effects (namely, the linear inertial term) of the elastic matrix. In particular, in [84], the Biot equations are written in the following form:

$$\begin{aligned} \nabla \cdot \{A e_x(\mathbf{u})\} - c_0 \nabla p &= \rho \partial_{tt} \mathbf{u} + \mathbf{f} \\ c_1 \partial_{tt} p - \nabla \cdot \{K \nabla p - c_0 \partial_t \mathbf{u}\} &= 0 \end{aligned} \quad \text{in } \Omega \times (0, T). \quad (2.19)$$

Within the settings of the cell model, the linear inertial term is shown to be negligible, see *Section 3.2.3*, thus in this work, the quasi-stationary Biot equations are used.

Applied to the problem considered in this work, certain estimates for the coefficients and terms of the effective Biot equations (2.6), (2.7) can be made. The parameters chosen for the cell swelling problem are discussed in *Section 3.1*, such that here only their magnitudes are used.

### **Forcing term $\mathbf{F}$**

In the formulation of the Biot problem on the intracellular space  $\Omega^p$ , it is assumed that apart from the forces produced by the interacting solid and fluid phases of the poroelastic cell interior, the effect of other body forces (such as e.g. gravity) on  $\Omega^p$  is negligible, and the boundary forces (e.g. osmotic pressure) are explicitly reflected in the boundary (interface) conditions for the Biot equations. Therefore the forcing term  $\mathbf{F}$  in the RHS of (2.6) is taken to be 0.

*Note:* With the dimensions and parameters chosen for the considered problem, in order for the forcing term coefficient  $\Psi$  to be of order  $O(1)$ , the characteristic value  $F_0$  of the



term  $\mathbf{F}$  must be large, as follows from (2.10) using the values listed in Section 3.3:

$$\Psi = \frac{F_0 L_{obs}^2}{l\Lambda} \left( |\mathcal{Y}_f| \rho^f + |\mathcal{Y}_s| \rho^s \right) < 10^{-3} F_0. \quad (2.20)$$

### Coefficient $M$

The solution (*almost* water) filling the pore space of the cell can be considered *almost* incompressible, thus its fluid bulk modulus  $E^f$  is very high (i.e. of the order  $10^9$  Pa, [85]). Therefore using the values of the porosity, elasticity coefficients and fluid density estimated in Section 3.1.1, the first component of the RHS of (2.11) is found to be negligible:

$$0 < |\mathcal{Y}_f| \mathcal{K}_{co} = \frac{|\mathcal{Y}_f| \Lambda}{\rho_f E_f} < 10^{-7} \ll 1. \quad (2.21)$$

Obtaining an estimate for the second summand of the RHS of (2.11),  $M_0$ , is slightly more challenging. First, for convenience, a bilinear form  $m(\mathbf{v}, \mathbf{w})$  is defined:

$$m(\mathbf{w}, \mathbf{v}) := \int_{\mathcal{Y}_s} A e_y(\mathbf{w}) : e_y(\mathbf{v}) dy, \quad (2.22)$$

such that  $M_0 \equiv m(\mathbf{w}^0, \mathbf{w}^0)$ . The bilinear form  $m(\mathbf{w}^0, \mathbf{w}^0)$  can be estimated as:

$$\begin{aligned} 0 < m(\mathbf{w}^0, \mathbf{w}^0) &\leq \|A \nabla \mathbf{w}^0\|_{L_2} \|\nabla \mathbf{w}^0\|_{L_2} \leq \|A\|_{op} \|\nabla \mathbf{w}^0\|_{L_2}^2 \leq \|A\|_{op} \|\nabla \mathbf{w}^0\|_{H^1}^2 \leq \\ &\leq \lambda_{max} \|\nabla \mathbf{w}^0\|_{H^1}^2, \end{aligned} \quad (2.23)$$

where  $\|A\|_{op}$  is the operator norm of  $A$  and  $\lambda_{max}$  is its largest eigenvalue. It should be noted, that from the definition of  $A$  given in (2.9) it follows, that the coefficient matrix  $A$  is diagonalizable, and its eigenvalues are of the order of the elasticity coefficients  $\lambda^s$ ,  $\mu^s$ . Since under the assumptions of the cell model  $\lambda^s$  is of the same order as  $\mu^s$  (see Section 3.1.1.2), and  $A$  describes an isotropic medium, the ratio between the largest  $\lambda_{max}$  and smallest  $\lambda_{min}$  eigenvalues of  $A$  can be estimated as:

$$\frac{\lambda_{max}}{\lambda_{min}} = O(1). \quad (2.24)$$

Since  $\mathbf{w}^0 \in H^1(\mathcal{Y}_s)^3$ , such that  $\int_{\mathcal{Y}_s} \mathbf{w}^0(y) dy = 0$ , is defined as a solution of the elliptic Neumann boundary problem (2.13), (2.14), the following estimate for the norm of its gradient applies:

$$\|\nabla \mathbf{w}^0\|_{H^1} \leq \frac{1}{c} \|g\|_{L_2}, \quad (2.25)$$

where  $c$  is a coercivity constant for  $m(\mathbf{w}^0, \mathbf{w}^0)$ :

$$c : \quad m(\mathbf{w}^0, \mathbf{w}^0) \geq c \|\mathbf{w}^0\|_{H^1}^2, \quad (2.26)$$

and  $g \in H^1(\mathcal{Y}_s)$ , such that  $g|_{\partial \mathcal{Y}_s} = -\mathbf{n}$ ,  $|g| \leq 1$ , denotes an arbitrary function which fulfils the Neumann conditions of the problem (2.13), (2.14). The proof of the estimate (2.25) can be found in e.g. [86] (Sec. 4.6).

Using the condition (2.14),  $\|g\|_{L_2}$  is estimated as:

$$\|g\|_{L_2} \leq |\mathcal{Y}_s|^{1/2} < 1. \quad (2.27)$$

Thus using (2.25), (2.27), the estimate (2.23) can be rewritten as:

$$m(\mathbf{w}^0, \mathbf{w}^0) < \frac{\lambda_{max}}{c^2}. \quad (2.28)$$

In order to determine constant  $c$ , the bilinear form  $m(\mathbf{w}^0, \mathbf{w}^0)$  is estimated from below as:

$$\begin{aligned} m(\mathbf{w}^0, \mathbf{w}^0) &\geq \lambda_{min} \|\nabla \mathbf{w}^0\|_{L_2}^2 = \lambda_{min} \left( \frac{1}{1+C_p} \|\nabla \mathbf{w}^0\|_{L_2}^2 + \frac{C_p}{1+C_p} \|\nabla \mathbf{w}^0\|_{L_2}^2 \right) \geq \\ &\geq \lambda_{min} \left( \frac{1}{1+C_p} \|\nabla \mathbf{w}^0\|_{L_2}^2 + \frac{1}{1+C_p} \|\mathbf{w}^0\|_{L_2}^2 \right) = \frac{\lambda_{min}}{1+C_p} \|\nabla \mathbf{w}^0\|_{H^1}^2, \end{aligned} \quad (2.29)$$

where  $C_p$  is the constant of the Poincaré inequality:

$$\|\mathbf{w}^0\|_{L_2}^2 \leq C_p \|\nabla \mathbf{w}^0\|_{L_2}^2.$$

As the domain  $\mathcal{Y}_s$  is considered to be regular enough, the Poincaré constant can be related to the size of the domain, such that taking into account (2.27), it can be assumed that  $C^p < 1$ , and therefore from (2.26) and (2.29) it follows that the coercivity constant can be chosen as:

$$c := \lambda_{min}. \quad (2.30)$$

Combining (2.24), (2.28) and (2.30) for the elasticity parameters of the considered problem (i.e.  $\mu^s \approx 10^4$ ), the bilinear form  $m(\mathbf{w}^0, \mathbf{w}^0)$  and thus  $M_0$  are estimated to be small:

$$M_0 \equiv |m(\mathbf{w}^0, \mathbf{w}^0)| < \frac{\lambda_{max}}{\lambda_{min}^2} \stackrel{(2.24)}{<} \frac{10}{\lambda_{min}} \approx \frac{10}{\mu^s} \ll 1. \quad (2.31)$$

Thus from (2.21), (2.31) it can be deduced, that the coefficient  $M$  is much smaller than 1:

$$0 < M := |\mathcal{Y}_f| \mathcal{K}_{co} + M_0 \ll 1, \quad (2.32)$$

and therefore the first summand of (2.7), i.e. the time derivative of the pore pressure term, can be neglected.

In a similar fashion, using the definitions (2.15), (2.16)<sub>1</sub>, and relating to the properties of the auxiliary problems (2.17), (2.13)&(2.14), the *pressure storage coupling coefficient*  $|\mathcal{Y}_f|I - \mathcal{B}^H$  (also referred to as the *Biot-Willis* constant in e.g. [84]) can be shown to be of order  $O(1)$ , and the Gassman tensor  $A^H$  can be reduced to the elasticity tensor  $A$  as defined in (2.9).

### **Permeability tensor $K$**

The elements of the permeability tensor  $K(x, t)$  depend on the local (directional) properties of the medium. Assuming that the ICS preserves its isotropy during the time of observation, tensor  $K$  can be reduced to a diagonal matrix, such that:

$$K := k(x, t)I, \quad (2.33)$$

where  $k$  is a permeability *function* and  $I$  is the identity matrix, [87], [88].

There have been derived various *heuristic* laws suggesting the dependence of the permeability function on the deformation, microscopic geometry of the porous medium and other factors, see e.g. [28], [27], [22], [88]. In slightly deforming media however, the change of the permeability

can be neglected, which is also indicated by the analysis of the permeability-displacement law considered in *Section 3.1.2.3*. Therefore as the medium is also assumed to be homogeneous, in the following, the permeability of the ICS can be assumed to be constant in both time and space, i.e. equal to the initial permeability  $k_0$ :

$$k(x, t) := k_0 \triangleq k \quad \forall (x, t) \in \Omega^p(t) \times (0, T),$$

and thus treated as a parameter.

*Note:* Flow problem (2.18) is formulated such, that tensor  $K$  in (2.7) may also include the characteristics of the pore fluid. In this work, the classical porous medium permeability  $k$  ( $[k] = [\text{m}^2]$ ), that reflects the properties of the matrix (but not the fluid) is considered, thus the fluid dynamic viscosity  $\mu^f$  appears in (2.34) explicitly.

Summarizing the above statements, the **Biot equations** describing a poroelastic behaviour of the intracellular space  $\Omega^p$  can be written (in the *Eulerian* coordinates) as:

$$\begin{cases} \nabla \cdot \sigma^p := \nabla \cdot \left( \mu^s \left( \nabla u^{sp} + (\nabla u^{sp})^T \right) + \lambda^s \nabla \cdot u^{sp} I \right) - \nabla p^p = 0 \\ \nabla \cdot \left( \partial_t u^{sp} - \frac{k}{\mu^f} \nabla p^p \right) = 0 \end{cases} \quad \text{in } \Omega^p(t) \times (0, T), \quad (2.34)$$

where  $u^{sp}$  denotes the deformation of the solid phase,  $p^p$  is the *pore* pressure exerted by the fluid,  $k$  is the permeability,  $\mu^f$  is the dynamic viscosity of the fluid and  $\sigma^p$  is the total stress within the porous medium which is determined by the pore fluid pressure tensor  $p^p I$  and the *effective* stresses  $\sigma^{eff}$  produced by the isotropic linear elastic solid skeleton, such that:

$$\begin{aligned} \sigma^p &:= \sigma^{eff} - p^p I = \\ &= \mu^s \left( \nabla u^{sp} + (\nabla u^{sp})^T \right) + \lambda^s \nabla \cdot u^{sp} I - p^p I \end{aligned} \quad \text{in } \Omega^p(t) \times (0, T), \quad (2.35)$$

where the shear modulus  $\mu^s$  and Lamé's first coefficient  $\lambda^s$  are the elastic moduli of the skeleton. The Biot poroelasticity equations (2.34) are written for the unknown displacement and pore pressure ( $u^{sp}, p^p$ ). While the behaviour of the pore fluid velocity  $v^{fp}$  may be not of any direct interest, its definition is nonetheless convenient, since the fluid velocity naturally appears in some of the physically motivated equations developed below (e.g. the boundary and interface conditions, transport equations for the molarities).

*Pore fluid velocity*  $v^{fp}$  can additionally be found from the obtained solutions for the displacement and pressure gradient using the **modified (generalized) Darcy** law, [89], [90], i.e. the Darcy law modified with respect to the displacement of the solid phase:

$$v^{fp} := \partial_t u^{sp} - \frac{k}{\gamma^f \mu^f} \nabla p^p \quad \text{in } \Omega^p(t) \times (0, T), \quad (2.36)$$

where  $\gamma^f$  is the porosity of  $\Omega^p$ . As the ICS  $\Omega^p$  is fully saturated at all times, the porosity  $\gamma^f$  and solidity  $\gamma^s$  relate to one another through the *saturation condition*:

$$\gamma^f(x, t) + \gamma^s(x, t) = 1 \quad \forall (x, t) \in \Omega^p(t) \times (0, T). \quad (2.37)$$

Porosity and solidity are generally defined with respect to the representative elementary volume (REV) of the porous medium, and are thus in general both space and time (in case of deforming

media) dependent functions (see *Appendix A.4*). Since the poroelastic ICS  $\Omega^p$  is considered to be homogeneous at all times, the solidity (and porosity) must be independent of the spatial variables. At the same time, as the intracellular medium is swelling, such that the volume of the solid skeleton is assumed to remain constant while the volume of the intracellular fluid increases, the amount (percentage) of fluid in the REV must respectively increase. Thus the porosity and solidity change in time.

Using the definition of solidity, the conservation of the total volume of the solid phase  $\Omega^{sp}$  can be written as:

$$0 = \frac{d}{dt} \int_{\Omega^{sp}(t)} dV = \frac{d}{dt} \int_{\Omega^p(t)} \gamma^s dV. \quad (2.38)$$

Then treating the solidity as a time dependent continuous function  $\gamma^s(t)$  defined over  $\Omega^p$  and applying the *Reynold's transport theorem* (see *Appendix A.1*) to the RHS of (2.38), the following conservation law is derived:

$$\partial_t \gamma^s + \nabla \cdot (\gamma^s v^s) = 0 \quad \text{in } \Omega^p(t) \times (0, T),$$

where  $v^{sp} := d_t u^{sp}$  is the velocity of the solid phase of  $\Omega^p$ . As the solidity is assumed to be spatially independent, the condition reduces to:

$$\partial_t \gamma^s + \gamma^s \nabla \cdot (\partial_t u^{sp}) = 0 \quad \text{in } \Omega^p(t) \times (0, T), \quad (2.39)$$

and the porosity can simply be found from the saturation condition (2.37).

Other porosity-displacement relations can be found in e.g. [23], [28], [26].

It is shown in *Section 3.2.3*, that in case of *small enough* deformations, the second term on the LHS of (2.39) is proportionally small, such that the porosity and solidity can be assumed to be constant, i.e. equal to their initial values. For the sake of generality however, in this chapter, the porosity equation is kept as a part of the *extended* system of the Biot equations.

### 2.1.3 Lagrangian and ALE formulations

Both the Stokes and Biot equations are derived in their original form in the Eulerian coordinates, such that the unknowns of the systems depend on the *current* coordinates, i.e. the coordinates of the deformed configurations  $\Omega^b(t)$ ,  $\Omega^p(t)$ . However due to the movement of the interface between the ECS and the ICS, the actual configurations  $\Omega^b(t)$ ,  $\Omega^p(t)$  at times  $t \in (0, T)$  are not generally known. In fact, the movement of the Biot domain is determined by the solution of the Biot problem for the deformation  $u^{sp}$ . In order to overcome this problem, the modelling equations can be rewritten with respect to some *fixed* configurations. A standard choice for the fixed frames would be the initial, undeformed configurations  $\hat{\Omega}^b$ ,  $\hat{\Omega}^p$ . Then defining mappings between the undeformed and deformed configurations, the necessary coordinate transformations can be made, [82].

Since the displacement of the elastic solid phase of the ICS defines the deformation of the entire medium, mapping  $\hat{T}_t^p$  between the reference  $\hat{\Omega}^p$  and deformed  $\Omega^p(t)$  configurations of the ICS is defined by the displacement  $u^{sp}$ :

$$\begin{aligned} \hat{T}_t^p : \hat{\Omega}^p &\rightarrow \Omega^p(t) \\ u^{sp}(x, t) &= \hat{u}^{sp}(\hat{x}(x, t), t) = x(\hat{x}, t) - \hat{x} \end{aligned} \quad \forall t \in (0, T). \quad (2.40)$$

Then with the help of the deformation gradient tensor  $\hat{F}^s$  and its determinant  $\hat{J}^s$  defined as:

$$\begin{aligned}\hat{F}^s &:= \hat{\nabla} \hat{T}^p = I + \hat{\nabla} \hat{u}^{sp}, \\ \hat{J}^s &:= \det(\hat{F}^s),\end{aligned}\tag{2.41}$$

the Eulerian formulation of the Biot equations can be transformed into the **Lagrangian** formulation, such that the poroelasticity equations would be written with respect to the reference configuration  $\hat{\Omega}^p$  (see *Appendix A.2* for further details). Since the deformations are *small*, the coordinate transformation terms can be neglected, see *Section 3.2.1*, and therefore the Lagrangian formulation of the Biot equations describing the movement of the ICS takes the following form:

$$\left\{ \begin{array}{l} \hat{\nabla} \cdot \left( \mu^s \left( \hat{\nabla} \hat{u}^{sp} + (\hat{\nabla} \hat{u}^{sp})^T \right) + \lambda^s \hat{\nabla} \cdot \hat{u}^{sp} I \right) - \hat{\nabla} \hat{p}^p = 0 \\ \hat{\nabla} \cdot \left( \partial_t \hat{u}^{sp} - \frac{k}{\mu^f} \hat{\nabla} \hat{p}^p \right) = 0 \end{array} \right. \quad \text{in } \hat{\Omega}^p \times (0, T),\tag{2.42}$$

$$\begin{aligned}\hat{v}^{fp} &= \partial_t \hat{u}^{sp} - \frac{k}{(1 - \hat{\gamma}^s) \mu^f} \hat{\nabla} \hat{p}^p \\ 0 &= \partial_t \hat{\gamma}^s + \hat{\gamma}^s \hat{\nabla} \cdot (\partial_t \hat{u}^{sp})\end{aligned}\quad \text{in } \hat{\Omega}^p \times (0, T).\tag{2.43}$$

While the Lagrangian frame is a natural choice for the elasticity or Biot equations, it would not be a valid option when describing the movement of the shrinking Stokes domain  $\Omega^b$ , as the *displacement of the points of the fluid* enclosed in the  $\Omega^b$  does not describe the *deformation of the domain*.

Thus a mapping  $\hat{T}_t^b$  between the reference  $\hat{\Omega}^b$  and deformed  $\Omega^b(t)$  Stokes domain configurations,

$$\hat{T}_t^b : \hat{\Omega}^b \rightarrow \Omega^b(t) \quad \forall t \in (0, T),\tag{2.44}$$

$$\begin{aligned}u^b(x, t) &= \hat{u}^b(\hat{x}(x, t), t) = x(\hat{x}, t) - \hat{x} \\ w^b(x, t) &:= \partial_t u^b(x, t) \neq v^b(x, t)\end{aligned}\quad \forall (x, t) \in \Omega^p(t) \times (0, T),\tag{2.45}$$

as well as the corresponding domain displacement  $u^b(x, t)$  and the velocity of the domain movement  $w^b$  functions, are in principle **arbitrary** with the only constraint that the mapping  $\hat{T}_t^b$  has to track the boundary, i.e. at the fixed walls  $\Gamma^{bw}$ , the displacement must be zero, and at the moving interface  $\Gamma^i$ , it must coincide with the displacement of the ICS:

$$\begin{aligned}\hat{u}^b &= 0 & \text{at } \hat{\Gamma}^{bw} \times (0, T), \\ \hat{u}^b &= \hat{u}^{sp} & \text{at } \hat{\Gamma}^i \times (0, T).\end{aligned}\tag{2.46}$$

The transformation  $\hat{T}_t^b$  defined in this fashion is called an **Arbitrary Lagrangian Eulerian (ALE)** transformation, and the resulting formulation – an ALE formulation.

The ALE mapping can be defined through an equation for the displacement. In order to impose some smoothness, here the displacement function is *chosen* to satisfy the Laplace equation:

$$\hat{\Delta} \hat{u}^b = 0 \quad \text{in } \hat{\Omega}^b \times (0, T).\tag{2.47}$$

*Note:* In some cases, the bi-harmonic operator would be preferable, [82]. For the purposes of this work however, the harmonic operator is sufficiently smooth.

As before, the transformation terms containing the deformation gradient tensor  $\hat{F}^b$  and its determinant  $\hat{J}^b$  are negligible under the assumption of *small* displacements, and thus the above

described ALE formulation of the Stokes equations on the reference domain  $\hat{\Omega}^b$  is in its form identical to the original Eulerian formulation on the moving domain  $\Omega^b(t)$ :

$$\begin{cases} -\hat{\nabla} \hat{p}^b + \mu^f \hat{\Delta} \hat{v}^b = \rho^f \partial_t \hat{v}^b \\ \hat{\nabla} \cdot \hat{v}^b = 0 \end{cases} \quad \text{in } \hat{\Omega}^b \times (0, T). \quad (2.48)$$

Thus the knowledge of the domain displacement  $\hat{v}^b$  is not needed in order to solve the Stokes equations on a fixed domain. Yet as the deformation of the ECS domain may still be of interest, e.g. in order to estimate volume changes or to determine the deformation of the ECS mesh in the numerical experiments, the displacement equation (2.47) is added to the system of the modelling equations.

As mentioned above, the use of the fixed frame coordinate transformations is motivated by the dependence of the coordinates of the computation domain on the solution of the considered equations. Since the use of the Lagrangian and ALE transformations solves this problem, they are often employed when fluid-structure interaction problems are studied.

However from the perspective of numerical implementation, the problem of determining the actual configuration of the deforming computational domain can be overcome by choosing an appropriate time stepping scheme. Thus the numerical solution approach described in *Section 4.4* implies that the computational domain is moved with the solution for the displacement at each time step, allowing to solve the equations on the updated meshes.

Therefore in this work, the Eulerian configurations of the modelling equations are considered for further analysis and numerical implementation. The transformations into the Lagrangian or ALE coordinates are provided only for the sake of completeness and generality.

#### 2.1.4 Initial and boundary conditions

Since the Stokes and Biot systems contain time derivatives, the corresponding initial values are prescribed:

$$\begin{aligned} v^b(x, 0) = v_0^b(x) & \quad \text{in } \Omega_0^b, & u^{sp}(x, 0) = u_0^{sp}(x), & \quad \text{in } \Omega_0^p, \\ \gamma^s(0) = \gamma_0^s & & & \end{aligned} \quad (2.49)$$

In case there assumed to exist flow through the ECF domain  $\Omega^b$  (experiment *E1*), initial velocity function  $v_0^b(x)$  is chosen as to reflect the character of the flow. Otherwise it can be assumed, that before the observation starts, the ICS-ECS system is at rest and therefore the initial velocity  $v_0^b$  and displacement  $u_0^{sp}$  are equal to zero.

*Note:* Analogously to the spatial Stokes and Biot equations, the initial, boundary and interface conditions are initially derived in the Eulerian coordinates, and can be transformed into the fixed (ALE or Lagrangian) coordinates.

The following notations for the normal and tangential components of a vector  $\mathbf{v}$  and tensor  $\sigma$  will be used:

$$\begin{aligned} \sigma_n & := \sigma \cdot \mathbf{n}^T, & \sigma_{nn} & := \sigma_n \cdot \mathbf{n}, & \sigma_\tau & := \sigma_n - \sigma_{nn} \mathbf{n}, \\ v_n & := \mathbf{v} \cdot \mathbf{n}, & v_{nn} & := v_n \mathbf{n}, & v_\tau & := \mathbf{v} - v_{nn} \mathbf{n}, \end{aligned} \quad (2.50)$$

where  $\mathbf{n} = \mathbf{n}(x, t)$  is a unit vector normal to the boundary. The outward-pointing unit normal vectors  $n^p$ ,  $n^b$  are defined at the boundaries of the respective domains  $\Omega^p$ ,  $\Omega^b$ , and for convenience, vector  $n$  is defined:

$$n(x, t) \triangleq \begin{cases} n^p (\equiv -n^b) & x \in \Gamma^i, \\ n^p & x \in \Gamma^{pin}, \\ n^b & x \in \Gamma^{bw}. \end{cases} \quad (2.51)$$

Independently of the considered cell swelling experiment<sup>1</sup>, the outer boundaries of the overall domain  $\Omega$  coincide with the outer ECS walls  $\Gamma^{bw}$  and are fixed; the internal intracellular space boundary  $\Gamma^{pin}$  is fixed and *impermeable*, and the ICS skeleton is attached to it (*clamped* boundary) at all times. From this information, the following boundary conditions are immediately available:

$$\begin{aligned} u^b &:= 0 & \text{at } \Gamma^{bw}, & & u^{sp} &:= 0 \\ v^b &:= 0 & \text{at } \Gamma^{bw}, & & v^{fp} &:= 0 & \text{at } \Gamma^{pin}. \\ \gamma^s &:= \gamma_0^s \end{aligned} \quad (2.52)$$

In case the walls  $\Gamma^{bw}$  allow flow of fluid through the extracellular fluid domain  $\Omega^b$ , velocity values at the inflow boundary  $\Gamma^{b,in}$  and the normal stresses at the outflow boundary  $\Gamma^{b,out}$  can be prescribed:

$$E1: \quad \begin{aligned} v^b &:= v_{in}^b & \text{at } \Gamma^{b,in}, \\ \sigma_n^b &:= \sigma_w^b & \text{at } \Gamma^{b,out}, \end{aligned} \quad (2.53)$$

where  $v_{in}^b$ ,  $\sigma_w^b$  are some appropriate values, and the subscript "n" denotes the normal component of the corresponding function as defined in (2.50).

As suggested in *Section 1.3*, in case the considered cell is observed *in vitro* within a tissue sample (*E2*), some appropriate periodic boundary conditions can be set.

For the experiments in which the considered domain is surrounded by a large amount of stationary fluid, such that it can be assumed that there exists no externally created convective flow through the boundaries of the ECS, normal stresses can be prescribed a constant value along the walls:

$$E3: \quad \sigma_n^b = \sigma_w^b \quad \text{at } \Gamma^{bw}. \quad (2.54)$$

Finally, if the fixed ECS walls are impermeable to water, the *no-slip* condition is applied:

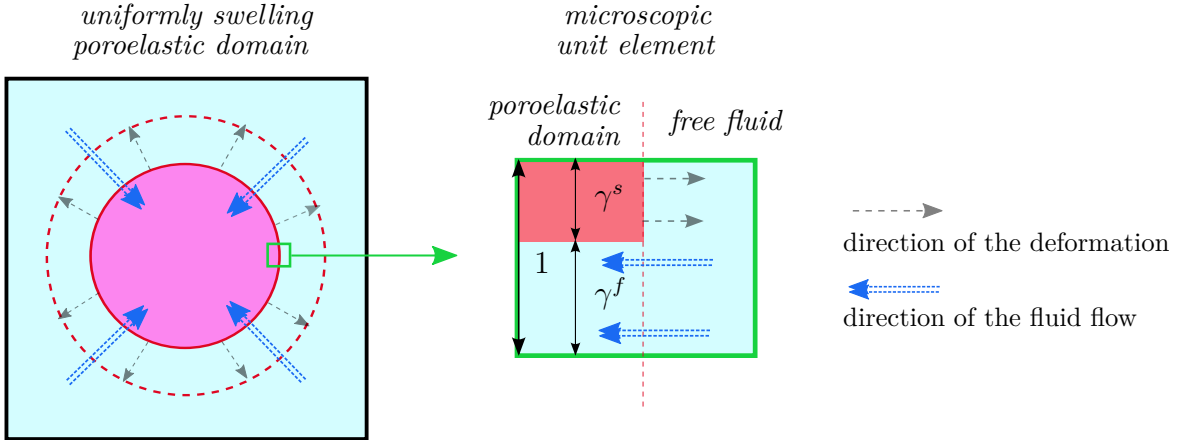
$$E4: \quad v^b = 0 \quad \text{at } \Gamma^{bw}. \quad (2.55)$$

### 2.1.5 Biot-Stokes coupling: interface conditions

In this section it is assumed, that the intracellular porous medium  $\Omega^p$  and the bulk fluid  $\Omega^b$  are directly sharing a common boundary  $\Gamma^i$ , thus a coupling between the Biot and Stokes equations is considered. Normal and tangential components, as well as the normal vector  $n$  are denoted and defined as in (2.50), (2.51).

<sup>1</sup> All experimental settings are described in *Section 1.3*.

Figure 2.1 Deformation and fluid flux on the microscopic level.



By the definition of the Stokes domain displacement (2.46), the *displacements are continuous* at the interface:

$$u^b = u^{sp} \quad \text{at } \Gamma^i. \quad (2.56)$$

Since there exist neither sinks nor sources of water at the interface, it must be required that the fluid leaving the extracellular space enters the intracellular space without any loss of its total volume, and so the normal fluxes must be continuous at the interface. As the interface is moving with the velocity  $v^{sp} := \partial_t u^{sp}$ , the (normal) fluid fluxes  $j_n^b$ ,  $j_n^p$  (leaving or entering the ECS and ICS domains respectively) can be defined as:

$$j_n^b := (v^b - \partial_t u^b)_n = (v^b - v^{sp})_n \quad \text{at } \Gamma^i, \quad (2.57)$$

$$j_n^p := \gamma^f (v^{fp} - v^{sp})_n \stackrel{(2.36)}{=} \left( -\frac{k}{\mu^f} \nabla p^p \right)_n \quad \text{at } \Gamma^i. \quad (2.58)$$

Thus the *continuity of normal fluxes* can be written as:

$$j_n^b = j_n^p \quad \Rightarrow \quad \left( \gamma^f v^{fp} + \gamma^s v^{sp} \right)_n = v_n^b \quad \text{at } \Gamma^i, \quad (2.59)$$

which naturally implies, that at the interface, the normal bulk fluid velocity  $v_n^b$  is determined by the average of the normal pore fluid and solid phase velocities  $v_n^{fp}$ ,  $v_n^{sp}$ , which are scaled with the porosity and solidity respectively, see Fig. 2.1. Using the modified Darcy equation (2.36), the flux condition (2.59) can also be written as:

$$v_n^b = \left( v^{sp} - \frac{k}{\mu^f} \nabla p^p \right)_n \quad \text{at } \Gamma^i. \quad (2.60)$$

From the momentum conservation it follows, that in the absence of forces *produced by the interface*, the total *stresses must be continuous* across the interaction boundary. Splitting for convenience the total stresses into their normal and tangential components, the stress continuity



conditions are written as:

$$\begin{aligned}\sigma_{nn}^p &= \sigma_{nn}^b, \\ \sigma_{\tau}^{eff} &= \sigma_{\tau}^{b,visc}\end{aligned}\quad \text{at } \Gamma^i(t) \times (0, T). \quad (2.61)$$

According to the *Beavers–Joseph–Saffman* (BJS) condition, [91], [92], the tangential component of the viscous stress  $\sigma^{b,visc}$  of the free (bulk) fluid is proportional to the *slip rate* (i.e. the tangential component of the total fluid flux as defined in (2.57)). In the notations of this work, the BJS condition can be written as:

$$\sigma_{\tau}^{b,visc} = \frac{\beta}{\sqrt{k}}(v_{\tau}^b - \partial_t u_{\tau}^{sp}) \quad \text{at } \Gamma^i(t) \times (0, T),$$

where  $\beta$  is the slip rate coefficient. It should be noted, that the BJS condition is normally considered when a *lateral* flow interacting with a poroelastic medium is studied. However in the absence of a constraining membrane and in case the *global* (created on the tissue scale) convective ECF fluxes are not dominant, the direction of the Stokes fluid flow in  $\Omega^b$  is primarily determined by the direction of the osmotic pressure gradient across the interface  $\Gamma^i$ , and is therefore *orthogonal* to the surface of the cell, see *Fig. 2.2a*. Thus as the cell is assumed to absorb water continuously, such that the deformations are occurring only when the external fluid flow is directed into the cell, the ***tangential velocities*** (and thus the tangential stresses) of both the free fluid and poroelastic skeleton are assumed to be negligible:

$$v_{\tau}^b = \partial_t u_{\tau}^{sp} := 0 \quad \text{at } \Gamma^i(t) \times (0, T). \quad (2.62)$$

*Note:* The cell constrained by the membrane tends to preserve its surface area, such that due to the influence of the membrane, the tangential displacements and velocities at the interface may be no longer negligible, see *Fig. 2.2b*. Yet due to the molecule-scale size of the membrane water channels (see *Section 1.2.1*), in terms of continuum mechanics, there exists no *fluid-fluid* interaction and thus no *slip* in the tangential velocities at the interface. Therefore even if the convective fluxes across the extracellular fluid domain are significant, the tangential velocity of the free fluid can be taken to be equal to the tangential solid phase velocity:

$$v_{\tau}^b = \partial_t u_{\tau}^{sp} \quad \text{at } \Gamma^i(t) \times (0, T).$$

In the existing literature, there have been suggested several ways of closing the set of coupling conditions at the interface between free fluid and poroelastic medium. Two examples of such coupling conditions are considered below.

In [84], the flow of free viscous fluid parallel to a poroelastic fully saturated medium with a flat interaction boundary is considered. It is then assumed, that the Darcy flow across the interface is proportional to the difference between the total normal stress of the free fluid and pore pressure:

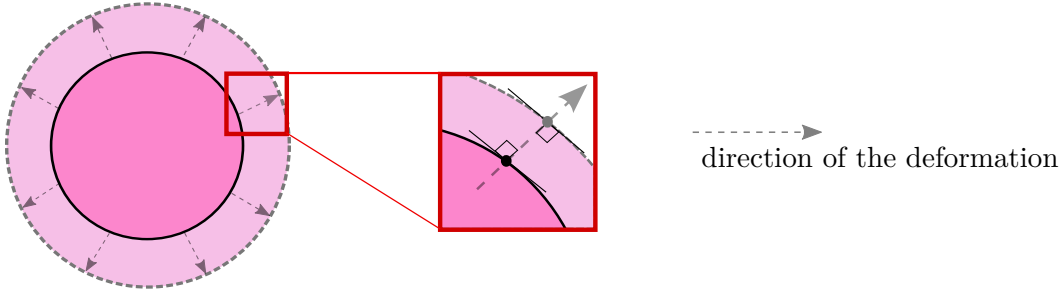
$$\sigma_{nn}^{b,visc} - p^b + p^p := \alpha \gamma^f (v^{fp} - v^{sp})_n \quad \text{at } \Gamma^i(t) \times (0, T), \quad (2.63a)$$

where  $\alpha \geq 0$  is the *fluid entry resistance* constant.

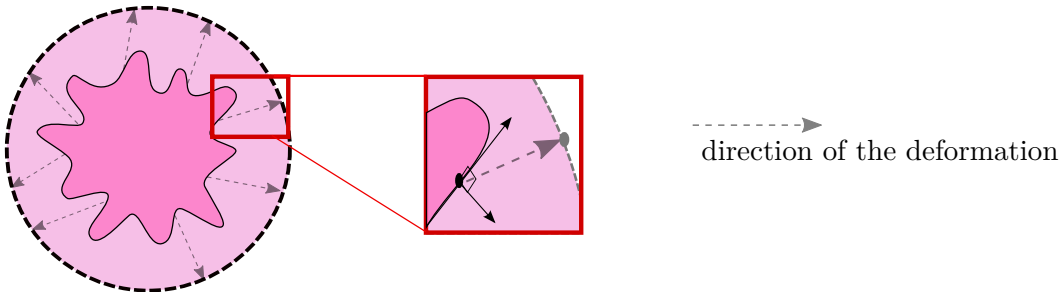
The author of [37] studies *normal* flow of a Newtonian fluid through a flat three dimensional porous layer (filter) with regular structure, such that the channels of the filter are uniformly

**Figure 2.2 Displacement of the cell surface.**

(a) Radial uniform swelling of an initially spherical cell: the displacement of the points of the surface is orthogonal to the surface of the cell.



(b) Surface area preserving swelling: the surface of the cell is unfolding, such that the displacement of a surface point is influenced by the tangential forces.



distributed and have straight flat walls. Pressure jump condition is developed considering the effects of the microscopic geometry of the porous medium on the change of the fluid pressure at the inflow and outflow interfaces, resulting in the following equations:

$$\begin{aligned}
 p^p &= p^b + \frac{\rho^f (v_x^b)^2}{2} \left( 1 - \frac{1}{\beta_{in}^2 C_c^2} \right) && \text{at inflow boundary,} \\
 p^p &= p^b - \frac{C_e \rho^f (v_x^{fp})^2}{2} (1 - \beta_{out}^2) && \text{at outflow boundary.}
 \end{aligned}
 \tag{2.63b}$$

where  $\beta_{in}$ ,  $\beta_{out}$  are the porosities of the medium at the inflow and outflow interfaces correspondingly,  $C_e$  and  $C_c$  are the geometrical parameters that relate the size of a pore at the interface to the width of the corresponding external/internal fluid "channel" determined by the streamlines of the inflow/outflow. Equations (2.63b) are briefly derived on the microscopic level for a single porous medium channel of the considered geometry and are then assumed to be valid on the macroscale as well.

In this work, a flux condition similar to the Darcy flow equation (2.63a) is considered. As the effect of the viscous stresses is shown to be small compared to the transmembrane pressure difference, see Section (3.2.5), the **normal flux condition** (2.63a) can be rewritten with respect

to the normal component of the fluid flux, such that:

$$j^b \cdot n := L(p^p - p^b) \quad \text{at } \Gamma^i(t) \times (0, T), \quad (2.64)$$

where in contrast to the fluid entry resistance  $\alpha$ , a *permeability* coefficient  $L$  is used. Further in *Section 2.2.5*, the flux condition (2.64) is modified such that the filtering properties of the membrane and osmotic pressure difference effects are taken into account, and the obtained equation can then be used as an interface condition for the full ICS-ECS interaction problem.

At last, for simplicity, the *solidity* is assumed to remain constant at the interface:

$$\gamma^s := \gamma_0^s \quad \text{at } \Gamma^i(t) \times (0, T). \quad (2.65)$$

Regarding the development and/or use of the interface conditions between a porous or poroelastic medium and free fluid, the following works can be referenced: porous medium interacting with fluid flow: [93], [94], [30], [95], [96]; poroelastic medium interacting with fluid flow: [31], [84], [36]; Beavers-Joseph-Saffman condition: [91], [92], [93], [97], [98], [84].

## 2.2 Osmotic pressure

As referenced in *Section 1.2*, osmotic pressure attributed to a solution is found to depend on the molar concentration (molarity) of the diluted osmotically active substances (osmolytes), thus a model relating osmotic pressure to the molarity, and therefore the transport (advection-diffusion) equations for the intracellular and extracellular molarities<sup>2</sup> are introduced. Osmosis is considered to be a pure boundary effect, such that the *osmotic pressure difference at the interface* between the ICS and ECS is of ultimate interest as a forcing term entering the fluid flux interface condition.

### 2.2.1 Osmotic pressure model

There exist several well-established osmotic pressure models that suggest different ways of finding the osmotic pressure of a solution through its molar concentration. The best known formula relating the osmotic pressure to the solute molar concentration was derived by Jacobus Henricus van 't Hoff in 1885 and later improved by Harmon Northrop Morse, [99]. The *Van 't Hoff* formula states that the dependence of the osmotic pressure on the osmolarity is linear, such that:

$$\begin{aligned} \pi &:= C_{osm}c, \\ C_{osm} &:= iR\Upsilon, \end{aligned} \quad (2.66)$$

where  $\pi$  is the osmotic pressure,  $R$  – Gas constant,  $\Upsilon$  – absolute temperature,  $C_{osm}$  – osmotic pressure coefficient,  $c$  – molarity and  $i$  – van 't Hoff factor of the solution. For the cell swelling model,  $i$  is taken to be equal to 1, meaning that the electrolytes of the solute neither dissociate nor associate in the solution. The derivation of the Van 't Hoff formula is based on the assumptions of the *virial theorem*, the details of which can be found in *Appendix A.5.1*.

<sup>2</sup> Unless specified otherwise, in this work, the terms *osmolarity*, *molarity* and *concentration* are used as synonyms and refer to the molar concentration of the diluted osmolytes.

Since the considered swelling processes are assumed to be isothermal (see *Section 3.1.1.1*), coefficient  $C_{osm}$  is a constant, therefore the osmotic pressures  $\pi^b$ ,  $\pi^p$  of the intracellular and extracellular solutions depend only on the behaviour of the corresponding molarities  $c^b$ ,  $c^{fp}$ .

### 2.2.2 Transport equations for the molarities

Under suitable physical conditions (which are assumed to be satisfied for all processes considered in this work), the transport of the molar concentration  $c(x, t)$  of a substance diluted in a volume  $\Psi$  can be described by the *convection-diffusion equations (CDEs)* that take the following general form in the *Eulerian* coordinates:

$$\partial_t c + \nabla \cdot (cv - D\nabla c) = 0 \quad \text{in } \Psi(t) \times (0, T), \quad (2.67a)$$

where  $v(x, t)$  is the convective velocity of the flow (i.e. solvent velocity) and  $D$  is the diffusivity coefficient that reflects the ability of the diluted chemical to diffuse within the solvent. Assuming that the domain boundary  $\partial\Psi$  splits into the *Dirichlet*  $\Gamma_D$  and *Neumann*  $\Gamma_N$  parts, such that  $\partial\Psi = \Gamma_N \cup \Gamma_D$ , the following boundary conditions can be prescribed:

$$\begin{aligned} c &:= c_D & \text{at } \Gamma_D(t) \times (0, T), \\ \nabla c \cdot n &:= f_N & \text{at } \Gamma_N(t) \times (0, T), \end{aligned} \quad (2.67b)$$

for some given values (functions)  $c_D$ ,  $f_N$ , where  $n$  denotes the outward pointing unit normal vector at the boundary.

It can be shown (see e.g. [100], [101] and [82], [102]), that with the coordinate transformation terms neglected (due to the small deformations assumption, see *Section 3.2.1*), an ALE formulation for the CDE (2.67a) defined on a domain that deforms from its reference configuration  $\hat{\Psi}$  into a current configuration  $\Psi(t)$  with a deformation velocity  $w$  takes the following form:

$$\hat{\partial}_t \hat{c} + \hat{\nabla} \cdot (\hat{c}(\hat{v} - \hat{w}) - D\hat{\nabla}\hat{c}) = 0 \quad \text{in } \hat{\Psi} \times (0, T), \quad (2.67c)$$

such that the movement of the domain is now reflected in the increment to the convective term.

The transport equations for the molarity  $c^b$  diluted in the ECF domain  $\Omega^b$  take the form of the general equations (2.67a):

$$\partial_t c^b + \nabla \cdot (c^b v^b - D^b \nabla c^b) = 0 \quad \text{in } \Omega^b(t) \times (0, T). \quad (2.68)$$

As suggested in [103], [104], [105] and related works, the terms of the transport equations for the substances that are diluted in the fluid phase of a porous medium get scaled with the porosity of the medium. thus the following equations describe the transport of the molarity  $c^p$  diluted in the intracellular fluid of  $\Omega^p$ :

$$\partial_t (\gamma^f c^{fp}) + \gamma^f \nabla \cdot (c^{fp} v^{fp} - D^p \nabla c^{fp}) = 0 \quad \text{in } \Omega^p(t) \times (0, T), \quad (2.69)$$

where the assumption on the spatial independence of the porosity  $\gamma^f$  was used. In case the porosity is also considered to be constant in time, the transport equation (2.69) takes the classical form of the CDE:

$$\partial_t c^{fp} + \nabla \cdot (c^{fp} v^{fp} - D^p \nabla c^{fp}) = 0 \quad \text{in } \Omega^p(t) \times (0, T). \quad (2.70)$$

*Note:* Although the osmotically active chemicals are assumed to be present only in the fluid part  $\Omega^{fp}$  of the intracellular space, following the porous media concept, molarity  $c^{fp}$  is defined over the whole domain  $\Omega^p$ .

As the diffusion coefficients for the osmolytes contained in the mixtures  $c^p$ ,  $c^{fp}$  are similar, see *Section 3.1.1.1*, it is possible to consider transport equations for the mixtures of substances. In addition, under the conditions of the cell swelling problem, diffusion coefficients  $D^b$ ,  $D^p$  can be assumed to be constant and taken to be equal (see *Section 3.1.1.1*):

$$D \triangleq D^p := D^b. \quad (2.71)$$

Analogously to the equations describing the dynamics of the poroelastic intracellular space  $\Omega^p$  and bulk extracellular space  $\Omega^b$ , the original transport equations (2.68), (2.70) are written in the *Eulerian* coordinates. For the reasons mentioned above, the poroelasticity and the bulk fluid systems may need to be transformed into *fixed* configurations. As the transport equations must be solved simultaneously with the flow equations, the CDEs (2.68),(2.70) should then also be transformed into the Lagrangian (on  $\Omega^p$ ) and ALE (on  $\Omega^b$ ) frames. Thus according to (2.67c), under the assumptions of small deformations, the ALE formulation of (2.68) and the Lagrangian formulation of (2.69) on the corresponding reference domains  $\hat{\Omega}^b$ ,  $\hat{\Omega}^p$  read:

$$\hat{\partial}_t \hat{c}^b + \hat{\nabla} \cdot (\hat{c}^b(\hat{v}^b - \hat{\partial}_t \hat{u}^b) - D \hat{\nabla} \hat{c}^b) = 0 \quad \text{in } \hat{\Omega}^b \times (0, T), \quad (2.72)$$

$$\hat{\partial}_t(\hat{\gamma}^f \hat{c}^{fp}) + \hat{\gamma}^f \hat{\nabla} \cdot (\hat{c}^{fp}(\hat{v}^{fp} - \hat{v}^{sp}) - D \hat{\nabla} \hat{c}^{fp}) = 0 \quad \text{in } \hat{\Omega}^p \times (0, T). \quad (2.73)$$

### **Boundary, interface and initial conditions**

Since the fixed ICS walls  $\Gamma^{pin}$  are assumed to be fully (to both solvent and solute) impermeable, the total normal fluxes must be zero at this boundary:

$$(c^{fp} v^{fp} - D \nabla c^{fp}) \cdot n = 0 \quad \text{at } \Gamma^{pin}(t) \times (0, T). \quad (2.74)$$

The type of the ECF domain boundary  $\Gamma^{bw}$  as well as the prescribed boundary values depend on the considered experimental settings described in *Section 1.3*. The *in vivo* cell swelling may be influenced by the *global* convective flow of fluid through  $\Omega^b$ , thus a *Dirichlet* value at the inflow boundary  $\Gamma^{b,in}$  and homogeneous *Neumann* condition at the outflow  $\Gamma^{b,out}$  and impermeable  $\Gamma^{b,0}$  boundaries are prescribed:

$$E1: \quad \begin{aligned} c^b &= c_D^b & \text{at } \Gamma^{b,in}(t) \times (0, T), \\ \nabla c^b \cdot n &= 0 & \text{at } (\Gamma^{b,out}(t) \cup \Gamma^{b,0}(t)) \times (0, T). \end{aligned} \quad (2.75a)$$

When the cell is studied in a tissue sample, such that the influence of the global extracellular fluid fluxes can be neglected (case *E2*), periodic boundary conditions are set.

For the experiments in which the cell is placed into a comparatively large fluid tank, a constant *Dirichlet* condition is chosen:

$$E3: \quad c^b = c_D^b \quad \text{at } \Gamma^{bw}(t) \times (0, T). \quad (2.75b)$$

For the experiments in which the walls  $\Gamma^{bw}$  are assumed to be impermeable, the total fluxes are

set to zero:

$$E4: \quad (c^b v^b - D \nabla c^b) \cdot n = 0 \quad \text{at } \Gamma^{bw}(t) \times (0, T). \quad (2.75c)$$

*Note:* Conditions (2.75a), (2.75b) are physically justified if the boundary  $\Gamma^{bw}$  is defined *far enough* from the ICS-ECS interface.

As the substances leaving or entering the ICS do not get suspended, accumulated, created or destroyed while passing the membrane, the osmolyte fluxes must be continuous across the common interface:

$$\gamma^f (c^{fp} v^{fp} - D \nabla c^{fp}) \cdot n = (c^b v^b - D \nabla c^b) \cdot n := j^c \quad \text{at } \Gamma^i(t) \times (0, T), \quad (2.76)$$

where  $j^c$  is the flux function that needs to be prescribed in order to formulate a well-posed coupled transport problem. Some ideas for the transmembrane osmolyte flux modelling are suggested in *Section 3.1.5*.

Finally, the initial values are prescribed:

$$\begin{aligned} c^b &:= c_0^b & \text{in } \Omega^b(0), \\ c^{fp} &:= c_0^{fp} & \text{in } \Omega^p(0). \end{aligned} \quad (2.77)$$

The choices for the boundary and initial values  $c_D^b$ ,  $c_0^b$ ,  $c_0^{fp}$  are discussed in *Section 3.1.3*.

In *Section 3.2.4* it is shown, that the Peclet numbers  $Pe^b$ ,  $Pe^p$  estimated over the ECS and ICS domains are much smaller than 1. Thus the convective terms in the above derived convection-diffusion equations can be dropped, such that the **diffusion equations** are assumed to approximate the transport of the diluted osmolytes:

$$\begin{aligned} \partial_t c^b - D \Delta c^b &= 0 & \text{in } \Omega^b(t) \times (0, T), \\ \partial_t (\gamma^f c^{fp}) - \gamma^f D \Delta c^{fp} &= 0 & \text{in } \Omega^p(t) \times (0, T), \\ \gamma^f (c^{fp} v^{fp} - D \nabla c^{fp}) \cdot n &= (c^b v^b - D \nabla c^b) \cdot n := j^c & \text{at } \Gamma^i(t) \times (0, T), \\ \nabla c^{fp} \cdot n &= 0 & \text{at } \Gamma^{pin}(t) \times (0, T); \end{aligned} \quad (2.78a)$$

$$E1: \quad \begin{aligned} c^b &= c_D^b & \text{at } \Gamma^{b,in} \times (0, T), \\ \nabla c^b \cdot n &= 0 & \text{at } (\Gamma^{b,out} \cup \Gamma^{b,0}) \times (0, T), \end{aligned} \quad (2.78b)$$

$$E2: \quad c^b \text{ is periodic} \quad \text{at } \Gamma^{bw} \times (0, T), \quad (2.78c)$$

$$E3: \quad c^b = c_D^b \quad \text{at } \Gamma^{bw} \times (0, T), \quad (2.78d)$$

$$E4: \quad \nabla c^b \cdot n = 0 \quad \text{at } \Gamma^{bw} \times (0, T), \quad (2.78e)$$

with the initial conditions (2.77).

### 2.2.3 Initial equilibrium relations

Assuming that the initial conditions of the considered cell swelling experiment correspond to the settings of a healthy brain tissue, the requirements that insure the electrochemical balance

between the intracellular and extracellular solutions must be fulfilled. These requirements consist in two conditions specifying the relations between the positively and negatively charged substances, [106], [107], [108], [109].

The *electro-neutrality* condition states that positively and negatively charged particles of the intracellular and extracellular spaces are balanced within their corresponding domains:

$$\begin{aligned} c_{0,+}^b - c_{0,-}^b &= 0 & \text{in } \Omega_0^b, \\ c_{0,+}^{fp} - c_{0,-}^{fp} - c_{fc}^{fp} &= 0 & \text{in } \Omega_0^{fp}, \end{aligned} \quad (2.79)$$

where  $c_+$ ,  $c_-$  denote the sums of concentrations of positively (index " + ") and negatively (index " - ") charged osmolytes that are able to travel through the membrane and  $c_{fc}^{fp}$  is the molarity of the fixed charges trapped within the intracellular fluid. Since the fixed charges are known to bear a negative charge, the molarity  $c_{fc}^{fp}$  enters the balance equation (2.79)<sub>2</sub> with a negative sign.

*Note:* The electro-neutrality of the ICS and ECS is only an approximation, which is however suitable when considering the magnitudes of the osmolarities of the intracellular and extracellular spaces.

Knowing the concentration of the fixed charges, the overall osmolarities of the intracellular and extracellular solutes can then be expressed through the concentrations of either of the charges:

$$\begin{aligned} c_0^b &= 2c_{0,+}^b = 2c_{0,-}^b & \text{in } \Omega_0^b, \\ c_0^{fp} &= 2c_{0,+}^{fp} - c_{fc}^{fp} = 2c_{0,-}^{fp} + 2c_{fc}^{fp} & \text{in } \Omega_0^{fp}. \end{aligned} \quad (2.80)$$

The second, *Donnan equilibrium* condition requires that the osmolarities of the free charges must be proportional:

$$c_{0,+}^b c_{0,-}^b = c_{0,+}^{fp} c_{0,-}^{fp}. \quad (2.81)$$

Thus from (2.80) and (2.81) it follows, that the initial concentrations are coupled in the following way:

$$c_{0,+}^b = \sqrt{c_{0,+}^{fp}{}^2 - c_{0,+}^{fp} c_{fc}^{fp}}, \quad (2.82)$$

such that given the osmolarities of the fixed charges and positively charged substances, the total initial osmolarities  $c_0^b$ ,  $c_0^{fp}$  can be found.

### 2.2.4 Fast diffusion model

In case the diffusion of the solutes is so fast, that at each  $t \in (0, T)$  it can be assumed that the osmolytes are in spatial equilibrium within their respective domains, i.e.

$$\begin{aligned} c^b(x, t) &= c^b(t) & \forall (x, t) \in \Omega^b(t) \times (0, T), \\ c^{fp}(x, t) &= c^{fp}(t) & \forall (x, t) \in \Omega^{fp}(t) \times (0, T), \end{aligned}$$

the spatially independent osmolarities  $c^b$ ,  $c^{fp}$  can be found through algebraic relations:

$$c^b(t) = \frac{a^b(t)}{V^b(t)}, \quad c^{fp}(t) = \frac{a^{fp}(t)}{V^{fp}(t)} \quad \forall t \in (0, T), \quad (2.83)$$

where  $V^b(t)$ ,  $V^{fp}(t)$  are the extracellular and intracellular fluid volumes respectively:

$$V^b(t) = \int_{\Omega^b(t)} dV, \quad V^{fp}(t) = \int_{\Omega^{fp}(t)} \gamma^f(t) dV,$$

and  $a^b(t)$ ,  $a^{fp}(t)$  are the corresponding amounts of substance of the diluted osmolytes.

Since the outer and inner boundaries  $\Gamma^{bw}$ ,  $\Gamma^{pin}$  are assumed to be fixed, and the constituents of  $\Omega$  are incompressible, the volume  $V$  of the overall domain  $\Omega$  remains constant, such that the variations in the volumes  $V^b(t)$ ,  $V^{fp}(t)$  are caused exclusively by the transmembrane solvent exchange between the ICS and ECS:

$$\int_{\Omega(t)} dV = V = \int_{\hat{\Omega}} d\hat{V} \quad \forall t \in (0, T), \quad (2.84)$$

$$V^b(t) + V^p(t) = V$$

such that since the amounts of substance are constant, the extracellular fluid gets more concentrated proportionally to the dilution of the intracellular solution.

Within the settings of the considered problem, the volume of the skeleton  $V^{sp}(t)$  is assumed to be constant at all times. It can be shown (see e.g. [28]), that if the volume of the solid phase of a deforming swelling porous medium remains constant, the volume of the overall medium can be found as an integral of the determinant  $\hat{J}^s$  of the domain deformation gradient tensor  $\hat{F}^s$  in the Lagrangian coordinates:

$$V^{sp}(t) = V_0^{sp} \quad \Rightarrow \quad V^p(t) = \int_{\hat{\Omega}^p} \hat{J}^s(t) d\hat{V} \quad \forall t \in (0, T). \quad (2.85)$$

The time dependent fluid volumes  $V^b(t)$ ,  $V^{fp}(t)$  can then be found through the cell volume  $V^p(t)$  as:

$$V^b(t) = V - V^p(t) = - \int_{\hat{\Omega}^p} \hat{J}^s d\hat{V} + V \quad \forall t \in (0, T). \quad (2.86)$$

$$V^{fp}(t) = V^p(t) - V_0^{sp} = \int_{\hat{\Omega}^p} \hat{J}^s d\hat{V} - \gamma_0^s V_0^p$$

Another way of finding the ECF and ICF volumes is to use the concept of porosity and solidity:

$$V^b(t) = V - V^p(t) = V - \frac{1}{\gamma^s(t)} V_0^{sp} \quad \forall t \in (0, T). \quad (2.87)$$

$$V^{fp}(t) = \gamma^f(t) V^p(t) = \frac{\gamma^f(t)}{\gamma^s(t)} V_0^{sp} = \left( \frac{1}{\gamma^s(t)} - 1 \right) V_0^{sp}$$

In the preceding sections, based on the *small* deformation assumption, the determinant of the deformation gradient  $J^s$  is approximated by 1 and the solidity  $\gamma^s(t)$  of the ICS domain  $\Omega^p(t)$  is approximated by its initial constant value. Such approximations used in either (2.85) or (2.87) would imply that the volumes  $V^b(t)$ ,  $V^{fp}(t)$  remain constant during the entire swelling time, therefore (as follows from (2.66), (2.83)) the effect of solvent exchange between the ICS



and ECS on the osmotic pressure difference across the membrane is not considered. Thus in order to include the effect of the osmotic pressure difference change over time into the modelling equations, either the dependence of  $J^s$  on the displacement  $u^{sp}$ , (2.41), or the conservation law for the solidity  $\gamma^s(t)$ , (2.39), must be used. Alternatively, the change in the fluid volume can be computed numerically, e.g. as suggested in Section 4.6.

In case the membrane can be assumed to be *strictly* semipermeable, and either the extracellular fluid walls  $\Gamma^{bw}$  are impermeable (E4) or the net inflow/outflow of the substances  $a^b$  through the walls  $\Gamma^{bw}$  can be neglected (E2), the amounts of substance  $a^b(t)$ ,  $a^{fp}(t)$  can be assumed to remain equal to their initial values. Otherwise, given the initial and terminal values  $a_0^b$ ,  $a_0^{fp}$ ,  $a_T^b$ ,  $a_T^{fp}$ , see Section 3.1.3, the dependence of functions  $a^b(t)$ ,  $a^{fp}(t)$  on time can be approximated as suggested in Section 3.1.5.

### 2.2.5 Modified flux interface conditions

It is rather natural to assume, that if two domains containing fluids are separated by a filtering membrane, the magnitude of the normal fluid flux at the membrane is proportional not only to the pressure gradient across the membrane, but also to the permeability of the interface which is determined by the characteristics of the water transmitting channels. In fact, the poroelasticity-fluid flux interface condition (2.64), in which the poroelastic boundary filtration is reflected in the permeability coefficient  $L$  (or fluid entry resistance  $\alpha$ ), clearly follows this principle.

The well-known **Kedem-Katchalsky** (KK) equation for the solvent volume flux  $j^w$  through an in general *leaky* selectively permeable membrane reflects the dependence of the fluid normal flux across the membrane on the hydraulic ( $p^\Delta$ ) and osmotic ( $\pi^\Delta$ ) pressure differences across the membrane, [110], [111], [112], [12], [113]. The condition reads:

$$j^w \cdot n = L^p \left( p^\Delta + \sigma \pi^\Delta \right), \quad (2.88)$$

where  $L^p$  is the water filtration coefficient and  $\sigma$  is the solute reflection coefficient of the membrane. Coefficient  $L^p$  characterizes the ability of the membrane to transmit the solvent. Reflection coefficient  $\sigma$  is determined by the solute transmitting properties of the membrane. It varies between 0 and 1, such that if the membrane is strictly semipermeable (i.e. there is no leakage of the solute across the interface), coefficient  $\sigma$  must be equal to 1. In this case, as it follows from equation (2.88), the osmotic pressure difference contributes to the value of the flux *at the same rate* as the hydraulic pressure. If the passage of the osmolytes through the membrane is free,  $\sigma$  equals 0, and consequently osmosis is not participating in the fluid exchange between the domains.

It has been shown, that for the bilipid membranes that transport solvent and solute *through distinct channels*, the KK formalism can be simplified by eliminating the solute reflection coefficient  $\sigma$  – the approach known as the *two parameter (2P) formalism*, [113], [114]. Since the aquaporins can be assumed to transmit only water molecules (see Section 1.2.1), the KK solvent flux condition transforms into:

$$j^w \cdot n = L^p \left( (p^b - p^p) + (\pi^b - \pi^p) \right). \quad (2.89)$$

*Note:* A concept similar to the above described ones is also employed on the scale of the brain tissue oedema formation and is known as the *Starling's principle*. According to the principle, under normal and pathological conditions, the flow of fluid through the capillary

endothelial cells depends on the hydraulic and osmotic pressure differences scaled with the filtering permeabilities of the blood-brain barrier, [51].

The 2P equations are derived for a system comprising of two domains filled with bulk solutions and separated by a (leaky) semipermeable membrane. In this work it is assumed, that compared to the filtering effect of the membrane, the transition effect induced by the porous medium is negligible, such that the permeability coefficient of the membrane alone accounts for the filtering of the fluid flux. Thus the ICS-ECS interaction is approximated by the 2P equation, such that:

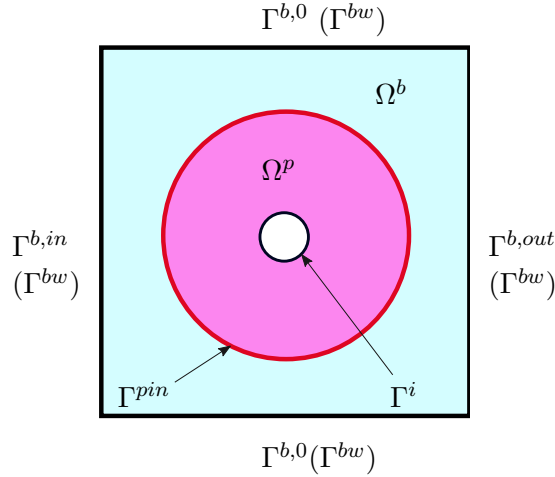
$$j^b \cdot n \stackrel{(2.59)}{=} j^p \cdot n := L^p \left( (p^b - p^p) + (\pi^b - \pi^p) \right) \quad \text{at } \Gamma^i(t) \times (0, T). \quad (2.90)$$

### 2.3 Summary: general conceptual model

The mathematical description of the considered problem developed in this chapter is shortly summarized below. Following the arguments given in the end of *Section 2.1.3*, the modelling equations are written in the *Eulerian* coordinates, e.g. with respect to the deformed configurations  $\Omega^p(t)$  or  $\Omega^b(t)$  respectively.

**Figure 2.3 Overall domain**  $\Omega = \Omega^b(t) \cup \Omega^p(t) \in \mathbb{R}^d$ ,  $d \in \{2, 3\}$ ,  $t \in (0, T)$ .

$\Omega^p(t)$  – deforming poroelastic intracellular space,  $\Omega^b(t)$  – deforming bulk (free) extracellular fluid,  $\Gamma^i(t) := \partial\Omega^b(t) \cap \partial\Omega^p(t)$  – moving interface,  $\Gamma^{pin}$  – fixed impermeable inner wall,  $\Gamma^{bw} := \Gamma^{b,0} \cup \Gamma^{b,in} \cup \Gamma^{b,out}$  – fixed outer (extracellular fluid) walls, where the inflow  $\Gamma^{b,in}$ , outflow  $\Gamma^{b,out}$  and impermeable  $\Gamma^{b,0}$  boundaries can be distinguished.



**Extracellular fluid: Stokes domain**  $\Omega^b$

$$\text{Stokes eq.:} \quad \nabla \cdot \sigma^b = \rho^f \partial_t v^b \quad \text{in } \Omega^b(t) \times (0, T), \quad (2.91a)$$

$$\nabla \cdot v^b = 0 \quad \text{in } \Omega^b(t) \times (0, T), \quad (2.91b)$$

$$\text{Transport eq.:} \quad \partial_t c^b - D \Delta c^b = 0 \quad \text{in } \Omega^b(t) \times (0, T), \quad (2.91c)$$

$$\text{Domain displacement eq.:} \quad \Delta u^b = 0 \quad \text{in } \Omega^b(t) \times (0, T), \quad (2.91d)$$

where  $v^b$  is the fluid velocity,  $p^b$  – hydraulic fluid pressure,  $u^b$  – domain displacement,  $\rho^f$  – fluid density,  $c^b$  – molar concentration of the diluted osmolytes,  $D$  – diffusion coefficient for  $c^b$  in  $\Omega^b$ , and  $\sigma^b$  is the fluid stress tensor consisting of the pressure term and purely viscous stress  $\sigma^{b,visc}$ :

$$\sigma^b := -p^b I + \sigma^{b,visc} = -p^b I + 2\mu^f \left( \nabla v^b + (\nabla v^b)^T \right), \quad (2.91e)$$

where  $\mu^f$  is the dynamic fluid viscosity. The deformed configuration coordinates  $x(t) \in \Omega^b(t)$  are related to the reference state coordinates  $\hat{x} \in \hat{\Omega}^b$  through the artificially constructed ALE displacement  $u^b$ :

$$\begin{aligned} x(\hat{x}, t) &:= u^b(x, t) + \hat{x} & \forall x \in \Omega^b(t) \times (0, T), \\ \partial_t u^b(x, t) &\neq v^b(x, t). \end{aligned} \quad (2.91f)$$

### Intracellular space: Biot domain $\Omega^p$

$$\text{Biot eq.:} \quad \nabla \cdot \sigma^p = 0 \quad \text{in } \Omega^p(t) \times (0, T), \quad (2.92a)$$

$$\nabla \cdot \left( \partial_t u^{sp} - \frac{k}{\mu^f} \nabla p^p \right) = 0 \quad \text{in } \Omega^p(t) \times (0, T), \quad (2.92b)$$

$$\text{Transport eq.:} \quad \partial_t (\gamma^f c^{fp}) - \gamma^f D^p \Delta c^{fp} = 0 \quad \text{in } \Omega^p(t) \times (0, T), \quad (2.92c)$$

where  $u^{sp}$  is the domain displacement,  $p^p$  – hydraulic pore pressure,  $k$  – Darcy fluid permeability,  $\mu^f$  – dynamic fluid viscosity,  $c^{fp}$  – molar concentration of the diluted osmolytes,  $D$  – diffusion coefficient for  $c^{fp}$  in  $\Omega^p$  and  $\sigma^p$  is the poroelasticity stress tensor consisting of the pore fluid term and effective stress tensor  $\sigma^{eff}$ :

$$\sigma^p := -p^p I + \sigma^{eff} = -p^p I + \mu^s \left( \nabla u^{sp} + (\nabla u^{sp})^T \right) + \lambda^s \nabla \cdot u^{sp} I, \quad (2.92d)$$

where the shear modulus  $\mu^s$  and Lamé's first coefficient  $\lambda^s$  are the elastic moduli of the skeleton. The coordinates of the deformed configuration  $\Omega^p$  are related to the coordinates of the reference configuration  $\hat{\Omega}^p$  through the displacement  $u^{sp}$ :

$$x(\hat{x}, t) := u^{sp}(x, t) + \hat{x} \quad \forall x \in \Omega^p(t) \times (0, T).$$

The pore fluid velocity  $v^{fp}$  and solidity  $\gamma^s := \gamma^s(t)$  can additionally be found as:

$$\text{Modified Darcy law:} \quad v^{fp} = \partial_t u^{sp} - \frac{k}{(1 - \gamma^s)\mu^f} \nabla p^p \quad \text{in } \Omega^p(t) \times (0, T), \quad (2.92e)$$

$$\text{Solidity eq.:} \quad \partial_t \gamma^s + \gamma^s \nabla \cdot (\partial_t u^{sp}) = 0 \quad \text{in } \Omega^p(t) \times (0, T). \quad (2.92f)$$

### Initial conditions

$$v^b(x, 0) = v_0^b(x) \quad \text{in } \Omega^b(0), \quad (2.93a) \quad u^{sp}(x, 0) = 0 \quad \text{in } \Omega^p(0), \quad (2.93c)$$

$$c^b(x, 0) = c_0^b \quad \text{in } \Omega^b(0), \quad (2.93b) \quad \gamma^s(0) = \gamma_0^s \quad \text{in } \Omega^p(0), \quad (2.93d)$$

$$c^{fp}(x, 0) = c_0^{fp} \quad \text{in } \Omega^p(0), \quad (2.93e)$$

where  $v_0^b$ ,  $c_0^b$ ,  $c_0^{fp}$ ,  $\gamma_0^s$  are some given values.

**Boundary conditions (fixed walls)**

The internal cell boundary  $\Gamma^{pin}$  is assumed to be fixed and impermeable:

$$\begin{aligned} u^{sp} &= 0, \\ v^{fp} &= 0, \\ \gamma^s &= \gamma_0^s, \\ \nabla c^{fp} \cdot n &= 0 \end{aligned} \quad \text{at } \Gamma^{pin} \times (0, T). \quad (2.94a)$$

The conditions at the external Stokes domain boundaries  $\Gamma^{bw} := \Gamma^{b,0} \cup \Gamma^{b,in} \cup \Gamma^{b,out}$  depend on the type of the considered experimental settings *E1–E4*:

$$\begin{aligned} E1: \quad u^b &= 0 & \text{at } \Gamma^{bw} \times (0, T), & \quad v^b = 0 & \text{at } \Gamma^{b,0} \times (0, T), \\ c^b &= c_D^b & \text{at } \Gamma^{b,in} \times (0, T), & \quad v^b = v_{in}^b & \text{at } \Gamma^{b,in} \times (0, T), \\ \nabla c^b \cdot n &= 0 & \text{at } (\Gamma^{b,out} \cup \Gamma^{b,0}) \times (0, T), & \quad \sigma_n^b = \sigma_w^b & \text{at } \Gamma^{b,out} \times (0, T); \end{aligned} \quad (2.94b)$$

$$E2: \quad u^b = 0, \quad v^b, c^b \text{ are periodic} \quad \text{at } \Gamma^{bw} \times (0, T), \quad (2.94c)$$

$$E3: \quad u^b = 0, \quad \sigma_n^b = \sigma_w^b, \quad c^b = c_D^b \quad \text{at } \Gamma^{bw} \times (0, T), \quad (2.94d)$$

$$E4: \quad u^b = 0, \quad v^b = 0, \quad \nabla c^b \cdot n = 0 \quad \text{at } \Gamma^{bw} \times (0, T), \quad (2.94e)$$

where  $v_{in}^b, c_D^b, \sigma_w^b$ , are some given values.

Boundaries  $\Gamma^{bw}, \Gamma^{pin}$  are fixed, thus at any  $t \in (0, T)$  they coincide with their reference configurations.

**Interface conditions**

$$u^b = u^{sp} \quad \text{at } \Gamma^i(t) \times (0, T), \quad (2.95a)$$

$$\gamma^s = \gamma_0^s \quad \text{at } \Gamma^i(t) \times (0, T), \quad (2.95b)$$

$$v_n^b = \left( v^{sp} - \frac{k}{\mu^f} \nabla p^p \right)_n \quad \text{at } \Gamma^i(t) \times (0, T), \quad (2.95c)$$

$$\sigma_{nn}^p = \sigma_{nn}^b \quad \text{at } \Gamma^i(t) \times (0, T), \quad (2.95d)$$

$$v_\tau^b = \partial_t u_\tau^{sp} \quad \text{at } \Gamma^i(t) \times (0, T), \quad (2.95e)$$

$$j^p \cdot n = j^b \cdot n = L^p (p^\Delta + \pi^\Delta) \quad \text{at } \Gamma^i(t) \times (0, T), \quad (2.95f)$$

$$\nabla c^b \cdot n = (1 - \gamma^s) \nabla c^{fp} \cdot n = j^c(x, t) \quad \text{at } \Gamma^i(t) \times (0, T), \quad (2.95g)$$

where  $j^b, j^p$  are the fluid fluxes defined at the boundaries of the Stokes and Biot domains respectively:

$$j^b \cdot n := (v^b - \partial_t u^b) \cdot n \stackrel{(2.95a)}{=} (v^b - v^{sp}) \cdot n \quad \text{at } \partial\Omega^b(t) \times (0, T), \quad (2.95h)$$

$$j^p \cdot n := (1 - \gamma^s)(v^{fp} - v^{sp}) \cdot n \stackrel{(2.92e)}{=} \left( -\frac{k}{\mu^f} \nabla p^p \right) \cdot n \quad \text{at } \partial\Omega^p(t) \times (0, T), \quad (2.95i)$$

$j^c(x, t)$  is the solute flux function modelled in *Section 3.1.5*,  $L^p$  is the membrane permeability

to water,  $p^\Delta$ ,  $\pi^\Delta$  are respectively the hydraulic and osmotic pressure differences across the interface:

$$\begin{aligned} p^\Delta &:= p^p - p^b && \text{at } \Gamma^i(t) \times (0, T), \\ \pi^\Delta &:= C_{osm} c^\Delta = C_{osm} (c^b - c^{fp}) && \text{at } \Gamma^i(t) \times (0, T), \end{aligned} \tag{2.95j}$$

and  $C_{osm}$  is the osmotic pressure coefficient. Due to the continuity of the displacements (2.95a), the configuration of the deforming interface  $\Gamma^i(t)$  can be found through either of the solutions  $u^{sp}$ ,  $u^b$ .

The parameters  $\mu^f$ ,  $D$ ,  $\gamma^s$ ,  $k$ ,  $\mu^s$ ,  $\lambda^s$ ,  $L^p$ ,  $C_{osm}$ , initial values  $v_0^b(x)$ ,  $c_0^b$ ,  $c_0^{fp}$ ,  $\gamma_0^s$ , and boundary values  $v_{in}^b$ ,  $\sigma_w^b$ ,  $c_D^b$ , are discussed and specified in *Chapter 3*.

It should be noted, that the above presented equations constitute a *general* derived model describing an interaction between a swelling poroelastic cell and extracellular fluid, while for numerical implementation and simulations, a *reduced* model described in *Section 4.1* is considered. Thus under the assumptions of *fast diffusion*, neither of the transport equations 2.91c, 2.92c is implemented in *Chapter 4*.



## 3 Data and dimensional analysis

In this chapter, the values of the parameters as well as the initial, boundary and characteristic values of the variables entering the modelling equations developed in the previous chapter are estimated. The obtained data is used to estimate the coefficients of the non-dimensionalized modelling equations, such that the dominating effects and the relative relevance of the terms of the equations can be determined.

Some of the values may vary depending on the set of the chosen modelling assumptions. In particular, different results may be obtained depending on:

- the experimental settings  $E1-E4$ ;
- the membrane permeability: membrane is assumed to be either strictly ( $Ms$ ) or leaky ( $Ml$ ) semipermeable;

Thus where necessary, different values of the same parameter or function corresponding to different settings are specified.

### 3.1 Data: parameters and characteristic values

For a given function  $f$ , the following lower index notations will be used:

- subscript " $t$ " indicates, that the function is assumed to be only time (and not space) dependent, such that subscripts " $0$ ", " $T$ " are used to denote the initial and final (terminal) values:

$$f_t \triangleq f(t), \quad t \in (0, T); \quad \begin{array}{l} f_0 \triangleq f(t), \quad t = 0, \\ f_T \triangleq f(t), \quad t = T; \end{array}$$

- characteristic values are denoted by lower index " $c$ ", i.e.  $f_c$  is the characteristic value of the variable  $f$ .
- when it is necessary to distinguish the *healthy* and *reference* ( $t = 0$ ) states of the system, the values that correspond to the healthy state are denoted by an  $H$ , i.e.  $f_H$  is the value of the variable  $f$  in the healthy state of the system.

The parameters, initial, terminal and characteristic values of the variables that are chosen for the considered cell swelling problem split into the *primary* and *secondary* values. When determining the primary values, only the experimental settings and physical characteristics of the considered physical problem are relevant. The secondary values depend not only on the problem settings, but also on the primary values.

In particular, the primary values are the temperature, dynamic fluid viscosity, diffusivity coefficient, mass densities, elasticity coefficients, lengths (sizes) of the domains and initial transmembrane hydraulic pressure difference:

$$\Upsilon, \mu^f, D, \rho^s, \rho^f, \mu^s, \lambda^s, l_0^p, l_0^b, l_T^p, p_0^\Delta. \quad (3.1a)$$

The secondary values are the permeability coefficients, characteristic and terminal hydraulic pressure jumps, characteristic porosity (solidity), initial, terminal and characteristic osmotic pressure and molarity jumps, characteristic velocities, observation and diffusion times.

The choices for the primary values as well as actual dependences of the secondary values on the primary values and problem settings are motivated and developed below. Thus the following dependences are either considered or derived in this chapter:

$$\gamma_c^s := \gamma_c^s(l_0^p), \quad (3.1b) \quad L^p := L^p(\Upsilon), \quad (3.1g)$$

$$u_c^{sp} := u_c^{sp}(l_0^p, l_T^p), \quad (3.1c) \quad k_0 := k_0(\gamma_c^s) = k_0(l_0^p), \quad (3.1h)$$

$$l_c^p := l_c^p(l_0^p, l_T^p), \quad (3.1d) \quad \pi_H^\Delta := \pi_H^\Delta(p_0^\Delta), \quad (3.1i)$$

$$l_T^b := l_T^b(l_0^b, u_c^{sp}) = l_T^b(l_0^b, l_0^p, l_T^p), \quad (3.1e) \quad p_T^\Delta := p_T^\Delta(l_0^p, l_T^p, \mu^s, \lambda^s), \quad (3.1j)$$

$$l_c^b := l_c^b(l_0^b, l_T^b) = l_c^b(l_0^b, l_0^p, l_T^p), \quad (3.1f) \quad p_c^\Delta := p_c^\Delta(l_0^p, l_T^p, \mu^s, \lambda^s), \quad (3.1k)$$

$$t_c^{D,b} := t_c^{D,b}(l_c^b, D) \stackrel{(3.1f)}{=} t_c^{D,b}(l_0^b, l_T^b, D), \quad t_c^{D,p} := t_c^{D,p}(l_c^p, D) \stackrel{(3.1d)}{=} t_c^{D,p}(l_0^p, l_T^p, D), \quad (3.1l)$$

$$c_H^\Delta := c_H^\Delta(\Upsilon, \pi_H^\Delta) \stackrel{(3.1i)}{=} c_H^\Delta(\Upsilon, p_0^\Delta), \quad (3.1m)$$

$$\pi_T^\Delta := \pi_T^\Delta(p_T^\Delta) \stackrel{(3.1j)}{=} \pi_T^\Delta(l_0^p, l_T^p, \mu^s, \lambda^s), \quad (3.1n)$$

$$c_T^\Delta := c_T^\Delta(\Upsilon, \pi_T^\Delta) \stackrel{(3.1n)}{=} c_T^\Delta(\Upsilon, l_0^p, l_T^p, l_0^b, \mu^s, \lambda^s), \quad (3.1o)$$

$$c_0^\Delta := c_0^\Delta(c_T^\Delta, c_H^\Delta, l_0^b, l_0^p, l_T^p) \stackrel{(3.1m), (3.1o)}{=} c_0^\Delta(\Upsilon, \mu^s, \lambda^s, p_0^\Delta, l_0^b, l_0^p, l_T^p), \quad (3.1p)$$

$$c_c^\Delta := c_c^\Delta(c_T^\Delta, c_H^\Delta, l_0^b, l_0^p, l_T^p) \stackrel{(3.1m), (3.1o)}{=} c_c^\Delta(\Upsilon, \mu^s, \lambda^s, p_0^\Delta, l_0^b, l_0^p, l_T^p), \quad (3.1q)$$

$$\pi_c^\Delta := \pi_c^\Delta(\Upsilon, c_c^\Delta) \stackrel{(3.1p)}{=} \pi_c^\Delta(\Upsilon, \mu^s, \lambda^s, p_0^\Delta, l_0^b, l_0^p, l_T^p), \quad (3.1r)$$

$$v_c^{sp} := v_c^{sp}(L^p, p_c^\Delta, \pi_c^\Delta) \stackrel{(3.1g), (3.1k), (3.1r)}{=} v_c^{sp}(\Upsilon, \mu^s, \lambda^s, p_0^\Delta, l_0^b, l_0^p, l_T^p), \quad (3.1s)$$

$$v_c^b := v_c^b(\gamma_c^s, v_c^{sp}) \stackrel{(3.1s)}{=} v_c^b(\Upsilon, \mu^s, \lambda^s, p_0^\Delta, l_0^b, l_0^p, l_T^p), \quad (3.1t)$$

$$t_c := t_c(u_c^{sp}, v_c^{sp}) \stackrel{(3.1c), (3.1s)}{=} t_c(\Upsilon, \mu^s, \lambda^s, p_0^\Delta, l_0^b, l_0^p, l_T^p). \quad (3.1u)$$

While the parameters, characteristic and some initial values are of direct interest for either the actual numerical simulations or estimation of the terms of the modelling equations, the terminal, healthy state or initial values of some of the variables need to be considered in order to determine the respective values that are of direct interest.

### 3.1.1 Material properties and parameters

#### 3.1.1.1 Temperature, viscosities, diffusion coefficients, densities

For the *in vitro* experiments on osmotic swelling of living cells (e.g. swelling of endothelial cells, [115], brain tissue swelling, [10], glial cell swelling, [41]), the temperature is commonly maintained



at 37 °C, that corresponds to the normal brain temperature, [116]. The temperature of the *living* mammalian brain may drop (spontaneously or externally induced) by several degrees following ischaemia, [44], [117], and is measured to be slightly elevated in acutely ischaemic human brain, [116], [40]. Since for the purposes of this work the magnitude of those measured temperature variations is not significant, it is assumed that all considered experiments  $E1-E4$  are isothermal throughout the entire observation time, and are conducted at the normal brain *temperature*  $\Upsilon = 37\text{ °C} \approx 310\text{ K}$ .

*Note:* experiments aimed at measuring certain material properties of the cells may be conducted at lower temperatures (e.g. permeability measurements in [118], [119]). Yet the temperature related variations in the measured coefficients appear to be insignificant regarding the purposes of this work.

The mass density of the cerebrospinal fluid, [120], as well as the densities of soft living cell structures (such as lipid membranes, [121], and actin layers, [122]), are found to be approximately the same as of pure water. Thus the *densities*  $\rho^f$ ,  $\rho^s$  of the fluid and solid parts composing the OCD are assumed to be equal, such that  $\rho^f \approx \rho^s \approx 10^3\text{ kg/m}^3$ .

At the considered temperature  $\Upsilon = 37\text{ °C}$ , the dynamic (apparent) viscosity of the cytoplasm (cerebrospinal fluid) is measured to be similar (slightly higher) to the viscosity of water at the same temperature, [123], [124], [125], [126], [66], [127]. In this work the fluid *viscosity* is chosen as  $\mu^f \approx 10^{-3}\text{ kg/m s}$ .

Sodium and potassium (as well as many other ions or small molecules) diluted in pure water at temperatures close to 37 °C have diffusion coefficients of order  $10^{-9}\text{ m}^2/\text{s}$ , [128]. Due to the presence of multiple macromolecules, the diffusion of osmolytes in the cerebrospinal fluid is somewhat slower than in pure water, yet generally not more than by an order of magnitude, [129], [125]. Inside the cell, the diffusion of ions may be additionally impeded by the large number of organelles, yet their influence on the magnitude of the diffusion coefficient is also relatively benign, [130]. Therefore the *diffusion coefficients*  $D^p$ ,  $D^b$  of the intracellular and extracellular fluids are taken to be equal, such that  $D \triangleq D^p \approx D^b \approx 10^{-10}\text{ m}^2/\text{s}$ .

### 3.1.1.2 Elasticity coefficients

Solid phase  $\Omega^{sp}$  of the poroelastic cell interior  $\Omega^p$  consists of the membrane bound organelles and cytoskeleton – an elastic deformable network composed of various types of filamentous proteins, [20], [21]. Owing to the distribution of the constituents and to the structure of the cytoskeletal networks, the elastic medium  $\Omega^{sp}$  is in general non-homogeneous and anisotropic. Additionally, advanced studies of the cytoskeletal filament networks suggest, that with the increase of applied stresses, the response of the cytoskeletal structures can be highly non-linear, with some networks exhibiting stress-stiffening and some – stress-softening behaviour, [20], [65].

While the non-linearity, inhomogeneity and anisotropy effects may influence the response of the cell to the applied stresses, these, as well as other effects that may affect the mechanics and dynamics of the swelling cell (e.g. some chemicals can influence stiffening or softening of the cytoskeleton, [21]) will not be considered in this work due to the excessive complexity of the implied modelling. Instead, the material is considered to be homogeneous and isotropic, such that under the stresses induced by swelling, its response is linear elastic. Then the shear modulus  $\mu^s$  and Lamé's first parameter  $\lambda^s$  of the cell skeleton can be found through any pair of elasticity coefficients using the well known conversion formulae (e.g. (3.2)), see e.g. [131].

Owing to the above mentioned factors, elasticity coefficients (Young's, shear, bulk moduli, etc.) of the cytoplasmic structures may not be related to one another according to the standard conversion formulæ, such that measured individually, they may differ from one another by orders of magnitude, [16], [20], [21]. Considering the type of deformation the cell undergoes and the physical meanings of the elasticity coefficients for which experimental measurements are available, Young's modulus and Poisson's ratio appear to be most suited for the description of the material response of the intracellular structures.

In literature, experimental estimates for the elastic coefficients of the cytoskeletal filaments, bilipid membranes and hydrogels vary significantly, such that depending on the particular type of material, measurement type and experimental conditions, the values of the shear and Young's moduli are estimated to be in the range of  $10^3$ – $10^6$  Pa, [16],[18], [19], [20], [21].

*Note:* In addition, cytoskeletal filaments are often treated as *viscoelastic* objects, thus the moduli of *viscoelasticity* are evaluated as in e.g. [21], [20].

Following [16], where the total elasticity (elastic properties of the cell cortex and cytoplasmic structures) of the cell is estimated, Young's modulus  $E$  is chosen to be of order  $10^4$  Pa.

The values of the Poisson's ratio  $\nu$  for gels, hydrogels, lipid membranes and cellular constituents are considered to be in the range of 0.3–0.5, [58], [132], [133], [18], [16]. While when considering the components of the cell to be perfectly incompressible, Poisson's ratio is taken to be 0.5, [18], [16], in order to allow certain material flexibility (as in [16]) and avoid numerical complications, here Poisson's ratio is chosen as  $\nu = 0.4$ .

Then using conversion formulae for elastic moduli of homogeneous isotropic linear elastic materials, the *shear modulus*  $\mu^s$  and *Lame's first parameter*  $\lambda^s$  of the cell skeleton are found as:

$$\begin{aligned} E &:= 10^4 \text{ Pa}, & \mu^s &= \frac{E}{2(1+\nu)} \approx 3.6 \cdot 10^3 \text{ Pa}, & \frac{\lambda^s}{\mu^s} &= \frac{2\nu}{(1-2\nu)} = 4. \\ \nu &:= 0.4, & \lambda^s &= \frac{E\nu}{(1+\nu)(1-2\nu)} \approx 1.4 \cdot 10^4 \text{ Pa}, & & \end{aligned} \quad (3.2)$$

### 3.1.1.3 Membrane filtration coefficient

Numerous experimental measurements of various water permeability coefficients for lipid (phospholipid) membranes taken under diverse conditions (including living cell settings) are available in literature. The transport of water molecules is *passive*, and is either purely diffusive, or is driven by osmotic pressure gradients [43], [55], [134], [135]. Correspondingly, the diffusional and osmotic filtering properties of the water channels are distinguished. Osmotic and diffusional water permeabilities  $P_f$ ,  $P_d$  are found to be in the range of  $10^{-6}$ – $10^{-4}$  m/s, [134], [136], [118], [75], [113], [135], [137], [119].

*Note:* During cytotoxic cell swelling, the transport of water across the membrane is primarily driven by osmosis, and since the diffusional permeability quantifies the exchange of water molecules irrespectively of the transmembrane osmotic pressure gradients, it is not of interest in this work. The membrane permeability to water is therefore characterised by only the osmotic transmitting properties of the aquaporins.

Mechanical filtration coefficient (i.e. membrane water permeability in the context of this work)  $L_p$  that enters the flux condition (2.89) is related to the osmotic water permeability  $P_f$  through

the following formula, [134], [113]:

$$L_p := P_f \frac{V_w}{R\Upsilon}, \quad (3.3)$$

where  $V_w$  is the partial molar volume of water,  $V_w = 1.8 \cdot 10^{-5} \text{ m}^3/\text{mol}$ , [138],  $R$  – the Gas constant,  $R \approx 8.3 \text{ J/K mol}$ , and  $\Upsilon$  – the temperature of the medium. Taking an average value for the osmotic water permeability, e.g.  $P_f := 10^{-5}$ , the filtration coefficient  $L_p$  is found from (3.3) to be around  $10^{-13} \text{ m}^2\text{s/kg}$ . This magnitude agrees with the values suggested in [113], [137], [114].

Water (as well as solute) permeability coefficients show dependence on such factors as the temperature and some of the concentrations of the solutions, [118], [75], [113], [137], [139]. The variations in the obtained values are however very small compared to the magnitudes of the coefficients, and are therefore not considered, such that  $L_p$  is assumed to be constant and to have the same value regardless of the considered experimental conditions.

### 3.1.2 Biot-Stokes problem

#### 3.1.2.1 Lengths and displacements

The nucleus of a biological cell is centrally located and has a smooth, rounded shape, [63]. Thus for simplicity, the cell is approximated as either a spherical *nearly*-spherical object, within which the *immobile structures* (see Section 1.1.2) are assumed to form a continuous sphere and are centrally located.

*Note:* Brain cells are generally diverse in shapes and sizes, and may have very complex geometries due to their branching extensions (e.g. stellate cells and astrocytes), [140], [141], [59]. Here only the central, rounded *cell bodies* (*soma* for a neuron) are considered.

The shape of the overall domain  $\Omega$  can be chosen arbitrarily. For convenience, domain  $\Omega$  is taken to be either a cube or a sphere, such that the cell is situated in the center of the overall domain, see Pic.1.7. As the ICS and ECS domains  $\Omega^p$ ,  $\Omega^b$  are chosen to be (*approximately*) axially symmetric, the characteristic lengths  $l_{c,i}^p$ ,  $l_{c,i}^b$ ,  $i \in \{1 \dots \text{dim}\}$  of those domains can be assumed to be equal in all directions:

$$\begin{aligned} l_{c,i}^p &= l_{c,j}^p =: l_c^p \\ l_{c,i}^b &= l_{c,j}^b =: l_c^b \end{aligned} \quad \forall i, j \in \{1 \dots \text{dim}\}.$$

The modelled swelling processes influence the entire volumes of the domains (and not only some local parts), therefore the characteristic lengths  $l_c^b$ ,  $l_c^p$  will be defined with respect to the diameters (lengths) of the corresponding domains.

The body of a *healthy brain cell* ranges from less than  $10^{-5} \text{ m}$  to over  $10^{-4} \text{ m}$  in diameter, [140], [141], [142], [143], [59], [62]. The sizes of the centrally located organelles are normally proportional to the size of the cell, [63], such that the diameter of the largest organelle – the nucleus – is roughly an order of magnitude smaller than the diameter of the cell, [62], [144]. Thus the radius  $r_0^c$  of the reference (not swollen) cell  $\Omega_0^c$  and the radius  $r^{in}$  of the fixed, constant

in size inclusion are chosen as:

$$r_0^c \approx 5 \cdot 10^{-5} \text{ m}, \quad (3.4)$$

$$r^{in} \approx 0.5 \cdot 10^{-5} \text{ m}. \quad (3.5)$$

The characteristic length  $l_c^p$  of the poroelastic domain (ring)  $\Omega^p$  is chosen to correspond to the initial size  $r_0^p$  of  $\Omega^p$ , and is thus equal to the difference between the initial radius of the whole cell and the radius of the inclusion:

$$l_c^p := l_0^p = r_0^c - r^{in} \approx 4.5 \cdot 10^{-5} \text{ m}. \quad (3.6)$$

The maximum size that a swelling cell can achieve is restricted by the volume of the available extracellular fluid. In a healthy brain, extracellular fluid is estimated to occupy from 12–19%, [51], to 20%, [55], [43], of the total brain tissue volume. It has been observed, that cytotoxic swelling causes an average reduction of the extracellular space from the physiological  $\sim 20\%$  to 5–10% of the brain volume, [55], [43]. Therefore assuming that the extracellular space shrinks to the average 7%, such that the cells in a tissue sample grow from 80% to 93%, the average cell growth ratio  $g^c$  is found as:

$$g^c := \frac{V_T^c}{V_0^c} = \frac{93}{80} \approx 1.16, \quad (3.7)$$

where  $V_0^c$  is the initial and  $V_T^c$  is the final (total) cell volume.

*Note:* The swollen cell may in principle become *considerably* larger than the healthy one. For instance astrocytes, being more prone to pathological swelling than neurons, [43], are able to swell several times their size, [55]. Also in some *in vitro* experiments, where the ratio between the extracellular and total volumes is greater, larger swelling rates may be observed for some hypotonic baths, [41], [56]. However larger deformations (i.e. the deformations comparable to the size of the domain) would require modifications to the modelling equations in the ALE coordinates (see *Section 2.1.3*), introducing non-linearities. Therefore for all considered experiments, irrespective of the size of the extracellular domain, the growth ratio (3.7) is taken.

Assuming that the final shape of the cell  $\Omega^c$  is a sphere, the terminal cell radius  $r_T^c$  and the characteristic (total) displacement  $u_c^{sp} := u_T^{sp}$ , defined as the difference between the terminal  $r_T^c$  and the initial  $r_0^c$  cell radii, are found as:

$$r_T^c = \sqrt[3]{\frac{3}{4\pi} V_T^c} \stackrel{(3.7)}{=} \sqrt[3]{\frac{3}{4\pi} g^c V_0^c} = \sqrt[3]{g^c} r_0^c \approx 5.25 \cdot 10^{-5} \text{ m}, \quad (3.8)$$

$$u_c^{sp} := u_T^{sp} = r_T^c - r_0^c = (\sqrt[3]{g^c} - 1) r_0^c \approx 2.53 \cdot 10^{-6} \text{ m}. \quad (3.9)$$

As the displacements are continuous at the interface (2.46), the characteristic displacement  $u_c^b$  of the bulk fluid domain  $\Omega^b$  is considered to be equal to  $u_c^{sp}$ :

$$u_c^b = u_c^{sp} =: u_c. \quad (3.10)$$

The sizes and shapes of the total  $\Omega$  and extracellular  $\Omega^b$  domains can be estimated with regard to the considered experiment:

- Brain tissue experiments *E1*, *E2*.

As mentioned above, initially (in a healthy tissue) the extracellular fluid takes around 20% of the total domain volume  $V$ . Therefore in case the modelled cell is assumed to be surrounded by other cells (i.e. in brain tissue experiments  $E1$ ,  $E2$ ), the total volume  $V$  and the reference volume  $V_0^b$  of the domain  $\Omega^b$  can be found through the reference cell volume  $V_0^c$  as:

$$f_0^c := \frac{V_0^c}{V} = 0.8 \quad \Rightarrow \quad V = \frac{V_0^c}{f_0^c}; \quad V_0^b = V - V_0^c.$$

In such case, the overall domain  $\Omega$  can not be defined as a cube, as even the initial cell  $\Omega_0^c$  would not fit into it:

$$5 \cdot 10^{-5} = r_0^c > r^{cube} = \frac{1}{2} \sqrt[3]{V} \approx 4.34 \cdot 10^{-5}.$$

Instead, the overall domain  $\Omega$  can be defined as a sphere of radius  $r^\Omega$ :

$$E1, E2: \quad r^\Omega := \sqrt[3]{\frac{3}{4\pi} V} = \frac{r_0^c}{\sqrt[3]{f_0^c}} \approx 5.38 \cdot 10^{-5} \text{ m.}$$

- Single cell experiments  $E3$ ,  $E4$ .

In the single cell experiments, the extracellular fluid to the cell proportions can be chosen arbitrarily, however with the restriction that the domain  $\Omega$  is large enough to allow uncompromised swelling (and can be defined as a cube for convenience), yet not so large that the difference between the sizes of the cell and the overall domain would involve numerical complications. Here the half-size (i.e. half of the length of the edge)  $r^\Omega$  of the one cell domain  $\Omega$  will be taken 3 times larger than the radius of the cell:

$$E3, E4: \quad r^\Omega := 3r_0^c \approx 1.5 \cdot 10^{-4} \text{ m.}$$

Characteristic length  $l_c^b$  of the bulk fluid domain  $\Omega^b$ , chosen as the initial size  $r_0^b$  of  $\Omega^b$ , can be found as the difference between the half-size (or radius) of the overall domain  $r^\Omega$  and the reference cell radius  $r_0^c$ :

$$l_c^b := r_0^b = r^\Omega - r_0^c,$$

$$E1, E2: \quad l_c^b = \left( \frac{1}{\sqrt[3]{f_0^c}} - 1 \right) r_0^c \approx 3.8 \cdot 10^{-6} \text{ m,}$$

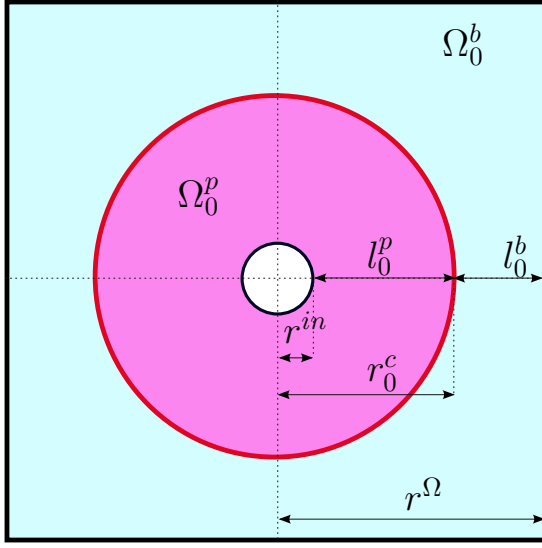
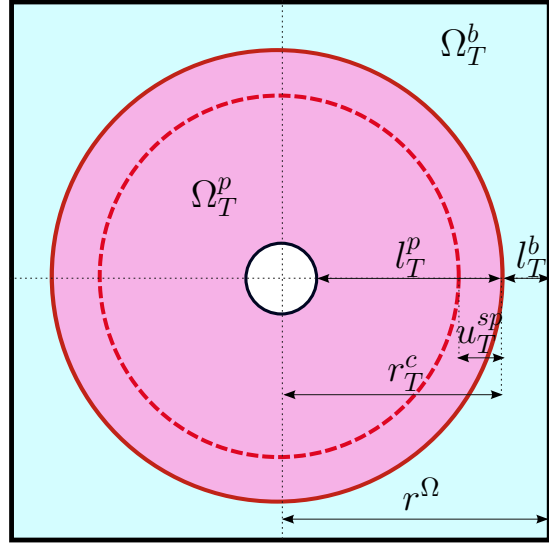
$$E3, E4: \quad l_c^b = 2r_0^c \approx 10^{-4} \text{ m.}$$

*Note:* The thickness  $h^m$  of the phospholipid cell membrane is estimated to be around  $5 \cdot 10^{-9}$  m, [62], [121], which is much smaller than the size of either of the domains  $\Omega^b$ ,  $\Omega^p$ :

$$\frac{h^m}{l_c^p} < \frac{h^m}{l_c^b} < 10^{-2} \text{ (} E1, E2 \text{),} \quad \frac{h^m}{l_c^b} < \frac{h^m}{l_c^p} < 10^{-3} \text{ (} E3, E4 \text{),}$$

therefore it appears to be reasonable to neglect the thickness of the membrane and to approximate it as a two dimensional surface.

Figure 3.1 Lengths of the domains.

 (a) Initial configuration,  $t = 0$ .

 (b) Final (terminal) configuration,  $t = T$ .


The ratios  $\mathcal{R}_c^b, \mathcal{R}_c^p$  between the characteristic displacements in the extracellular and intracellular domains  $\Omega^b, \Omega^p$  and their respective lengths are then estimated as:

$$\mathcal{R}_c^p \triangleq \frac{u_c^{sp}}{l_0^p} \approx 0.056, \quad \mathcal{R}_c^b \triangleq \frac{u_c^b}{l_0^b} \approx 0.66 \quad (E1, E2), \quad (3.11)$$

$$\mathcal{R}_c^b \triangleq \frac{u_c^b}{l_0^b} \approx 0.025 \quad (E3, E4).$$

As follows from (3.11), for the choice of the extracellular domain size corresponding to the brain tissue settings  $E1, E2$ , the domain deformation  $u_c^b = u_c$  is large compared to the size of the domain, therefore the *small deformation* assumptions would no longer be valid in such case. Thus in this work, the cell to the extracellular space proportions are chosen to correspond to the ones of the single cell experiments  $E3, E4$ :

$$r^\Omega := 3r_0^c = 1.5 \cdot 10^{-4} \text{ m}, \quad (3.12)$$

$$l_c^b := r_0^b = r^\Omega - r_0^c = 2r_0^c \approx 10^{-4} \text{ m}. \quad (3.13)$$

### 3.1.2.2 Cell porosity

Water is measured to account for around 70% of the total living cell volume, [145], [124], yet the proportion of the unbound fluid is found to be somewhat lower, [146], such that depending on the cell type, the cytosol (i.e. intracellular unbound fluid) occupies 20% to 55% of the total cell volume, [147], [148]. In this work, the intracellular fluid is assumed to occupy 50% of the total healthy cell volume  $V_0^c$ , thus:

$$\phi_0^{fc} \triangleq \frac{V_0^{fp}}{V_0^c} := 0.5,$$

where  $V_0^{fp}$  is the reference volume of the intracellular fluid  $\Omega^{fp}$ . As the volume of the membrane is neglected, the remaining part must be shared by the organelles  $\Omega^{sp}$  that form the skeleton of the porous medium  $\Omega_0^p$ , and the immobile organelles. Assuming that the cytosol is uniformly distributed within the cell, the initial porosity  $\gamma_0^f$  can be found as the fraction of the cytosol  $\Omega_0^{fp}$  within the reference poroelastic space  $\Omega_0^p$ :

$$\gamma_0^f := \frac{V_0^{fp}}{V_0^p} = \frac{\phi_0^{fc} V_0^c}{V_0^c - V^{in}} = \frac{\phi_0^{fc} (r_0^c)^3}{(r_0^c)^3 - (r^{in})^3} \approx 0.50, \quad (3.14)$$

where  $V_0^p$  is the initial volume of the ICS  $\Omega_0^p$ , and  $V^{in}$  is the volume of the inclusions. From the saturation condition (2.37) it follows that the initial porosity  $\gamma_0^f$  and solidity  $\gamma_0^s$  are approximately equal:

$$\frac{V^{sp}}{V_0^p} =: \gamma_0^s \stackrel{(2.37)}{=} 1 - \gamma_0^f \approx 0.50 \quad \stackrel{(3.14)}{\Rightarrow} \quad \gamma_0^f \approx \gamma_0^s =: \gamma_0, \quad (3.15)$$

where  $V^{sp}$  is the (constant) volume of the solid phase of  $\Omega^p$ .

The terminal porosity and solidity are found to deviate from their initial values by only around 13.3%:

$$\begin{aligned} \gamma_T^s := \frac{V_T^{sp}}{V_T^p} &= \frac{V_0^{sp}}{V_T^p} = \frac{\gamma_0^s V_0^p}{V_T^p} \approx 0.867 \gamma_0^s \approx 0.433, \\ \gamma_T^f &\approx 0.567, \end{aligned} \quad (3.16)$$

thus the characteristic porosity and solidity are chosen to be equal to their initial values:

$$\gamma_c^s = \gamma_c^f := \gamma_c := \gamma_0. \quad (3.17)$$

In the *reduced* model considered for the numerical simulations, the change in the porosity is neglected, such that  $\gamma^f(t)$ ,  $\gamma^s(t)$  are considered to be constant and are denoted by  $\gamma$ :

$$\gamma^f(t) := \gamma^s(t) := \gamma_0 \triangleq \gamma \quad \forall t \in (0, T). \quad (3.18)$$

### 3.1.2.3 Intracellular (Darcy) permeability to water

Estimating the permeability of the interior of a biological cell experimentally, or verifying modelling approximations of the permeability coefficient is a challenging task. As the constituents of the cell do not hold together in the absence of the membrane, it would be very hard to conduct experiments aiming at the estimation of the permeability of the intracellular medium. In the experiments on the membrane-bound cells, the permeability of the membrane can strongly influence the fluid flow and therefore the experimental measurements. At the same time the significant differences between the microscopic geometries of the membrane and ICS do not allow to *simply assume* that their permeabilities are equal. Additionally, unlike the membrane, a swelling cell increases its porosity during the observation, and the deformations may introduce changes to the microscopic geometry of the skeleton, and thus influence the permeating properties of the medium.

As an alternative to experimental data, mathematical (heuristic) models will be employed in order to estimate the permeability  $k_0$  of the reference configuration of the intracellular space

$\Omega_0^p$ , and the dependence of the permeability  $k(t)$  on the porosity  $\gamma(t)$  or displacement  $u^{sp}(x, t)$  of the intracellular space.

There exist several ways of estimating the permeability of a porous medium from the information on its microscopic structure (some of the models are listed in e.g. [149], [150], [151]). One of the most widely used formulae is the **Kozeny-Carman (KC)** equation, various forms of which are described in e.g. [152], [149], [153], [154]. The KC equation can be used to model the permeability of a *fixed* porous medium if the processes and geometry of the medium satisfy the following requirements:

- the medium is homogeneous and isotropic with *regular* structure;
- the flow of the fluid is laminar; the pore velocity can be found from an equation of Hagen-Poiseuille type, and the Darcy equations hold on the domain.

The first condition is fulfilled due to the assumptions made on the geometry of the cell. Assuming also, that until the beginning of the swelling the structure of the cell is fixed, the KC equation can be used to determine the reference (initial) permeability  $k_0$  of the ICS.

***Derivation of the Kozeny-Carman equation for  $\Omega_0^p$ .***

Combining the Hagen-Poiseuille and the Darcy equations on a fixed porous domain, the permeability  $k_0$  can be expressed through the microstructural tortuosity  $\tau$ , hydraulic diameter  $d_h$  and dimensionless shape factor  $s$ :

$$-\frac{d_h^2}{16s\mu^f\tau} = \frac{v^{fp}}{\nabla p^p} = -\frac{k_0\tau}{\mu^f\gamma^f} \quad \Rightarrow \quad k_0 = \frac{\gamma^f d_h^2}{16s\tau^2}. \quad (3.19)$$

In order to simplify the computations of the geometric characteristics, it is further assumed that the reference porous medium  $\Omega_0^p$  is composed of  $N^\epsilon$  identical elementary volumes  $V^\epsilon$  that are cubes with side length  $\epsilon$ , such that in each elementary volume the solid phase (grain) is surrounded by the fluid and defines a sphere of radius  $r^{\epsilon s}$ , surface area  $A^{\epsilon s}$  and volume  $V^{\epsilon s}$ . Then the necessary coefficients are found as described below.

- Dimensionless shape factor  $s$  is estimated to be of order  $O(1)$  for various grain shapes (around 2 for spherical grains), see e.g. [155], [156], [37].
- Tortuosity  $\tau$ , which in this context is understood as a ratio between the length of the path that a fluid particle travels from one point to another in a porous medium and the length of a straight line connecting these two points. For the type of the considered porous medium,  $\tau$  can be assumed to be of order  $O(1)$ , [157], [158].
- Hydraulic diameter  $d_h$  is defined through the porosity  $\gamma^f$ , solidity  $\gamma^s$  and the ratio  $R$  between the total solid-fluid phase interface area  $A^{sf}$  and the total solid grain volume  $V^s$  as:

$$d_h := \frac{4\gamma_0^f}{R\gamma_0^s}, \quad R := \frac{A^{sf}}{V^s}.$$



The solid grains do not touch and are all equivalent, therefore the ratio  $R$  can be found through the microscale quantities:

$$R := \frac{A^{sf}}{V^s} = \frac{\sum_{N^\epsilon} A^{\epsilon s}}{\sum_{N^\epsilon} V^{\epsilon s}} = \frac{N^\epsilon A^{\epsilon s}}{N^\epsilon V^{\epsilon s}} = \frac{A^{\epsilon s}}{V^{\epsilon s}} = \frac{4\pi(r^{\epsilon s})^2}{\frac{4}{3}\pi(r^{\epsilon s})^3} = \frac{3}{r^{\epsilon s}}.$$

The diameter of the largest among the small organelles (i.e. the ones that are assumed to constitute the skeleton) does not normally exceed  $1\mu\text{m}$ , [60], [63], thus the radius of the  $\epsilon$ -grain is chosen as  $r^{\epsilon s} := 5 \cdot 10^{-7}$  m.

Putting the obtained expressions into (3.19), the permeability  $k_0$  is found to be proportional to the square of the solid grain size  $r^{\epsilon s}$ , such that the proportionality coefficient  $C^{\epsilon s}$  reflects the structural characteristics of the porous medium  $\Omega_0^p$ :

$$C^{\epsilon s} := \frac{(\gamma_0^f)^3}{9s\tau^2 (1 - \gamma_0^f)^2} \stackrel{\substack{s:=2 \\ \tau:=1.5}}{\approx} \frac{(\gamma_0^f)^3}{40 (1 - \gamma_0^f)^2} \approx 0.01, \quad (3.20)$$

$$k_0 = C^{\epsilon s} (r^{\epsilon s})^2 \approx 2.5 \cdot 10^{-15} \text{ m}^2.$$

Since the swelling cell deforms, growing due to the inflow of water, the permeability of the porous medium  $\Omega^p$  may change. In a series of works (e.g. [28], [23], [27], [26] [88]) an exponential dependence of the permeability function on the spatial deformation derivatives has been suggested and tested. Following [23], for the given initial permeability  $k_0$  and material parameter  $m$ , the permeability of a deforming medium can be expressed as:

$$k(x, t) = k_0 \exp(m \nabla \cdot u^{sp}(x, t)). \quad (3.21)$$

Material parameter  $m$  is found to be in the range of 0 to 10, [28], [23], and the displacement gradients are estimated to be small (see Section 3.2), therefore  $k(x, t)$  is expected to be of the order of the initial permeability  $k_0$ ,

$$\frac{k(x, t)}{k_0} = \exp(m \nabla \cdot u^{sp}(x, t)) \sim O(1),$$

and thus the permeability of the intracellular porous medium  $\Omega_t^p$  is assumed to be constant:

$$k(x, t) = k_0 \triangleq k.$$

It should be noted, that permeability models are normally developed and used regarding the specific type of the considered porous medium and are not in general universal. Thus the exponential model (3.21) is used in [28], [23], [27], [26], where biological tissues are considered.

### 3.1.2.4 Hydraulic pressures

Normal intracranial pressure (ICP) is measured to be in average  $\pm 1300$  Pa for an adult in the supine ("+") or vertical ("-") position respectively, with the critical value of normal ICP considered to be around 3300 Pa (25 mmHg), [53], [159]. ICP strongly depends on the volume of intracranial liquids and tissues (the relationship being described by the Monro-Kellie hypothesis, [160], [161]), such that the accumulation of fluid within brain tissue may lead to significant

increases in ICP, [159], [42]. During normal brain activity, also for some moderate increases in the intracranial volume, the ICP remains low and stable, [53]. Therefore as it is assumed that within the chosen observation time the effects of vasogenic processes are either negligible or non-existent, the extracellular fluid pressure  $p^b(x, t)$  and its gradients in the *in vivo* experiments can be considered to depend only on the processes taking place within the one cell domain  $\Omega$ . Then if there (pre)exists flow through the extracellular domain  $\Omega^b$ , pressure gradient across the domain, and so the inflow and outflow pressure values, are considered to preserve their initial values. Thus when considering the experiments *E1*, the normal stresses at the outflow boundary are assumed to be constant:

$$E1: \quad \sigma_n^b(x, t) := \sigma_w^b = \text{const} \quad (x, t) \in \Gamma^{b, \text{out}}. \quad (3.22)$$

The considered *in vitro* experiments are such, that the pressures in the domain  $\Omega$  can also be assumed to take no influence from the environment, thus:

$$E3: \quad \sigma_n^b(x, t) := \sigma_w^b = \text{const} \quad (x, t) \in \Gamma^{bw}. \quad (3.23)$$

Intracellular pressure  $p_0^p$  of a healthy living cell is in general not equal to the pressure  $p_0^b$  of the surrounding fluid, such that the initial hydraulic pressure difference  $p_0^\Delta$  can be computed through Laplace's law:

$$p_0^\Delta := p_0^p - p_0^b = 2 \frac{\tau_0}{r_0^c} \approx 5 \text{ Pa}, \quad (3.24)$$

where  $\tau_0 \approx 10^{-4}$  N/m is the reference cell cortex tension, [16]. Values obtained using Laplace's law show agreement with measurements, see e.g. [162], [163].

The cell swells until the material resistance forces created by the solid components of the cell are balanced by the driving forces of the swelling. In order to estimate the terminal pressure difference across the membrane, a simplified stress-pressure jump relation is considered. Namely, with the viscous stresses neglected<sup>1</sup>, the continuity of normal stresses interface condition (2.61) written in polar ( $r, \theta$ ) or spherical ( $r, \theta, \phi$ ) coordinates, where for simplicity it is assumed that the domain is symmetric and the stresses are uniform, becomes (see *Section 4.3*):

$$2D: \quad (2\mu^s + \lambda^s) \partial_r u_r^{sp} + \lambda^s \frac{u_r^{sp}}{r} - p^p = -p^b, \quad (3.25)$$

$$3D: \quad (2\mu^s + \lambda^s) \partial_r u_r^{sp} + 2\lambda^s \frac{u_r^{sp}}{r} - p^p = -p^b, \quad (3.26)$$

where  $u_r^{sp}$  is the  $r$ -coordinate of the displacement  $u^{sp}$  and  $\partial_r$  is the partial  $r$ -derivative. Assuming further that the equilibrium ( $t = T$ ) solution is spatially linear,

$$u_r^{sp} := \alpha r = \frac{l_T^p - l_0^p}{l_T^p} r = \frac{u_T^{sp}}{l_T^p} r, \quad (3.27)$$

where  $u_T^{sp} = u_c^{sp}$  is the final displacement and  $l_0^p, l_T^p$  are the initial and terminal lengths of the porous domain  $\Omega^p$ , then substituting relation (3.27) into (3.25) and (3.26), the following estimate

---

<sup>1</sup> It is in fact suggested in *Section 3.2*, (3.121), that with the chosen characteristic and parametric values, the viscous stress contribution to the continuity of normal stresses is negligible.

for the terminal hydraulic pressure difference  $p_T^\Delta$  is obtained:

$$p_T^\Delta := p_T^p - p_T^b = \mathcal{M} \frac{u_c^{sp}}{l_T^p}, \quad (3.28)$$

$$\mathcal{M} := \begin{cases} 2(\lambda^s + \mu^s) & \text{in } 2D, \\ (3\lambda^s + 2\mu^s) & \text{in } 3D. \end{cases} \quad (3.29)$$

Substituting the values for  $\lambda^s$ ,  $\mu^s$ ,  $u_c^{sp}$ ,  $l_T^p$  into (3.28), the pressure difference  $p_T^\Delta$  is estimated as:

$$p_T^\Delta \approx \begin{cases} 1.87 \cdot 10^3 & \text{in } 2D, \\ 2.62 \cdot 10^3 & \text{in } 3D. \end{cases} \quad (3.30)$$

*Note:* Here and in the following, the default pressure units are  $[\text{kg/m s}^2] \equiv [\text{Pa}]$  in 3D and  $[\text{kg/s}^2]$  in 2D.

The characteristic transmembrane pressure difference  $p_c^\Delta$  is estimated through the scaling of the dimensionalized *continuity of normal stresses* interface condition (3.120), and as expected (from the nature of the cell deformation and the approach chosen for the evaluation of the terminal pressure), is similar to the average in time value:

$$0.2 \cdot 10^3 \text{ Pa} \stackrel{(3.122)}{\approx} p_c^\Delta \approx p_{avg}^\Delta := \frac{1}{2} (p_T^\Delta - p_0^\Delta) \approx \begin{cases} 0.94 \cdot 10^3 & \text{in } 2D, \\ 1.31 \cdot 10^3 & \text{in } 3D. \end{cases} \quad (3.31)$$

### 3.1.3 Osmotic pressures and molar concentrations

As discussed in *Section 2.2.1*, for isothermal processes, osmotic pressure difference  $\pi^\Delta$  across the semipermeable membrane separating solutions  $\Omega^\alpha$ ,  $\Omega^\beta$  depends on the concentration difference  $c^\Delta := c^\alpha - c^\beta$  at the interface:

$$\begin{aligned} \pi &:= C^{osm} c, \\ \pi^\Delta &:= \pi^\alpha - \pi^\beta = C^{osm} c^\Delta, \end{aligned} \quad C^{osm} := R\Upsilon \approx 2.58 \cdot 10^3 \text{ kg m}^2/\text{s}^2 \text{ mol}, \quad (3.32)$$

where the proportionality coefficient  $C_{osm}$  is computed for the chosen domain temperature  $\Upsilon = 310 \text{ K}$ . In order to estimate healthy, initial and terminal osmotic pressure (and therefore concentration) jump across the interface, the flux condition (2.89) is employed.

*Note:* When discussing concentrations and osmotic pressures, healthy conditions do not necessarily correspond to the reference state: in case the membrane is assumed to be strictly semipermeable (i.e. if the osmolytes can not cross the membrane during the observed process), the *unhealthy* osmotic pressure jump that would lead to cell swelling must be a pre-existing (therefore initial) condition.

In particular, assuming that at the healthy state there exists no water flux through the membrane, i.e.  $j_H^p \cdot n = j_H^b \cdot n =: j_H \cdot n = 0$ , the healthy state osmotic pressure jump across the interface can be found as:

$$0 = j_H \cdot n = L^p (p_H^\Delta + \pi_H^\Delta) \quad \Rightarrow \quad \pi_H^\Delta = p_H^\Delta \quad \text{at } \Gamma^i(0), \quad (3.33)$$

where the healthy state hydraulic pressure difference  $p_H^\Delta$  is equivalent to the initial pressure difference, i.e.  $p_H^\Delta = p_0^\Delta$ . Also, since it is assumed, that at the end of the observation time the cell achieves its maximum (or near maximum) volume, such that the inflow of water reduces to zero, from the flux condition (2.89) it follows, that at  $t = T$  the hydraulic and osmotic pressures are again in equilibrium:

$$0 = j_T \cdot n = L^p \left( p_T^\Delta + \pi_T^\Delta \right) \quad \Rightarrow \quad \pi_T^\Delta = p_T^\Delta \quad \text{at } \Gamma_T^i. \quad (3.34)$$

Thus since  $p_T^\Delta \neq 0$ , while in the end of the observation there still exists osmotic pressure jump across the interface of the cell, the elastic stress of the membrane and cytoskeleton would not allow further cell expansion.

From (3.32), (3.33) and (3.34), using the initial and terminal hydraulic pressure difference values (3.24), (3.30), the osmotic pressure  $\pi_H^\Delta$ ,  $\pi_T^\Delta$  and concentration  $c_H^\Delta$ ,  $c_T^\Delta$  differences are found as:

$$\pi_H^\Delta = p_0^\Delta \stackrel{(3.24)}{\approx} 5, \quad c_H^\Delta := c_H^{fp} - c_H^b = \frac{\pi_H^\Delta}{C_{osm}} \approx 1.9 \cdot 10^{-3}, \quad (3.35)$$

$$\pi_T^\Delta = p_T^\Delta \stackrel{(3.30)}{\approx} \begin{cases} 1.87 \cdot 10^3 & (2D), \\ 2.62 \cdot 10^3 & (3D), \end{cases} \quad c_T^\Delta := c_T^{fp} - c_T^b = \frac{\pi_T^\Delta}{C_{osm}} \approx \begin{cases} 0.73 & (2D), \\ 1.01 & (3D). \end{cases} \quad (3.36)$$

*Note:* Here and in the following, the default concentration units are  $[\text{mol}/\text{m}^d]$  for  $d = \{2, 3\}$ .

Molar concentrations of osmotically active substances diluted in the cytosol of a cell and cerebrospinal fluid of a *healthy* brain tissue are found to be around 290–300 mol/m<sup>3</sup>, [56], [41], [164]. As the healthy state transmembrane concentration difference (3.35) is found to be small, the intracellular and extracellular concentrations  $c_H^{fp}$ ,  $c_H^b$  in a healthy state are taken to be approximately equal (for  $d = \{2, 3\}$ ):

$$\begin{aligned} c_H^b &:= 300, & c_H^{fp} &:= c_H^\Delta + c_H^b \approx 300.002 & \Rightarrow \\ c_H^{fp} &\approx c_H^b =: c_H \approx 300, \end{aligned}$$

such that using (as in (2.2.4)) the algebraic relations for the spatially constant concentrations,

$$c_t^{fp} = \frac{a_t^{fp}}{V_t^{fp}}, \quad c_t^b = \frac{a_t^b}{V_t^b},$$

the amounts of substance  $a_H^{fp}$ ,  $a_H^b$  corresponding to the healthy concentrations  $c_H^{fp}$ ,  $c_H^b$  respectively can be found as:

$$a_H^{fp} := c_H^{fp} V_0^{fp} = c_H \gamma_0 V_0^p, \quad a_H^b := c_H^b V_0^b = c_H V_0^b. \quad (3.37)$$

Under ischaemic conditions, the distribution of substances between the intracellular and extracellular spaces changes due to the accumulation of the osmolytes within the cell. Thus if the total amount of substance  $a^\Omega$  diluted in the fluid parts of  $\Omega$  can be assumed to be *conserved over time*, e.g. if the external walls  $\Gamma^{bw}$  of the overall domain  $\Omega$  are impermeable to the osmolytes (case *E4*), or if the outer boundaries are periodic (case *E2*), the amounts of substance in the ICF ( $a_t^{fp}$ ) and ECF ( $a_t^b$ ) can be related to each other and to the healthy state values  $a_H^{fp}$ ,  $a_H^b$  in

the following way:

$$\begin{aligned}
 E2, E4: \quad a_t^{fp} &= a_H^{fp} + a_t^{sh} & a^\Omega &:= a_t^{fp} + a_t^b = \text{const} \\
 a_t^b &= a_H^b - a_t^{sh} & a_t^{sh} &:= a_t^{fp} - a_H^{fp} \equiv a_H^b - a_t^b
 \end{aligned} \quad t \in (0, T),$$

where  $a_t^{sh}$  is the increase (shift) of the intracellular amount of substance. The total amount of substance  $a^{SH}$  that is needed to realize the osmosis driven swelling and the terminal concentrations  $c_T^{fp}$ ,  $c_T^b$  can be found through (3.36) as:

$$\begin{aligned}
 E2, E4: \quad c_T^\Delta &= c_T^{fp} - c_T^b = \frac{a_H^{fp} + a^{SH}}{V_T^{fp}} - \frac{a_H^b - a^{SH}}{V_T^b} \Rightarrow \\
 a^{SH} &= \frac{c_T^\Delta V_T^{fp} V_T^b + a_H^b V_T^{fp} - a_H^{fp} V_T^b}{V_T^b + V_T^{fp}},
 \end{aligned}$$

$$\begin{aligned}
 E2, E4: \quad c_T^{fp} &= \frac{a_H^{fp} + a^{SH}}{V_T^{fp}} \approx \begin{cases} 300.101 & (2D), \\ 301.015 & (3D), \end{cases} \\
 c_T^b &= \frac{a_H^b - a^{SH}}{V_T^b} \approx \begin{cases} 299.375 & (2D), \\ 300.000 & (3D). \end{cases}
 \end{aligned}$$

Further on, in case the membrane is assumed to be impermeable to the solutes during swelling, i.e. the membrane is *strictly* semipermeable (assumption  $M_s$ ), the shift  $a^{SH}$  in the amounts of substance leading to the osmotic inflow of water and consequent increase of intracellular fluid volume to  $V_T^{fp}$  must pre-exist, such that the intracellular amount of substance  $a_t^{fp}$  is constant at all times:

$$\begin{aligned}
 (E2, E4) M_s: \quad a_t^{fp} &= a_0^{fp} = a_H^{fp} + a^{SH} \\
 a_t^b &= a_0^b = a_H^b - a^{SH}
 \end{aligned} \quad \forall t \in (0, T). \quad (3.38)$$

It follows that the concentration jump  $c_t^\Delta$  has its maximum value in the beginning of the observation,

$$\begin{aligned}
 (E2, E4) M_s (2D): \quad c_0^{fp} &= \frac{a_0^{fp}}{V_0^{fp}} \approx 375.982, & c_0^\Delta &:= c_0^{fp} - c_0^b \approx 79.58, \\
 c_0^b &= \frac{a_0^b}{V_0^b} \approx 296.408, & \pi_0^\Delta &:= C_{osm} c_0^\Delta \approx 2.05 \cdot 10^5,
 \end{aligned} \quad (3.39)$$

$$\begin{aligned}
 (E2, E4) M_s (3D): \quad c_0^{fp} &= \frac{a_0^{fp}}{V_0^{fp}} \approx 395.889, & c_0^\Delta &:= c_0^{fp} - c_0^b \approx 96.84, \\
 c_0^b &= \frac{a_0^b}{V_0^b} \approx 299.053, & \pi_0^\Delta &:= C_{osm} c_0^\Delta \approx 2.50 \cdot 10^5,
 \end{aligned} \quad (3.40)$$

such that the concentration  $c_t^{fp}$  decreases in time only due to the inflow of water. Then the

characteristic concentration and osmotic pressure jumps are chosen as average in time values:

$$\begin{aligned}
 (E2, E4) \text{ Ms:} \quad c_c^\Delta &:= \frac{1}{2}(c_0^\Delta + c_T^\Delta) \approx \frac{1}{2}c_0^\Delta \approx \begin{cases} 40.15 & (2D), \\ 48.93 & (3D), \end{cases} \\
 \pi_c^\Delta &:= C_{osm}c_c^\Delta \approx \begin{cases} 1.036 \cdot 10^5 & (2D), \\ 1.262 \cdot 10^5 & (3D). \end{cases}
 \end{aligned} \tag{3.41}$$

*Note:* In the above considered case, the initial osmotic pressure difference  $\pi_0^\Delta$  is not equal to the healthy osmotic pressure difference  $\pi_H^\Delta$ , thus as follows from (3.35), the osmotic and hydraulic pressure differences are not equal at the beginning of observation:

$$(E2, E4) \text{ Ms:} \quad \pi_0^\Delta \neq \pi_H^\Delta \stackrel{(3.35)}{=} p_0^\Delta. \tag{3.42}$$

which is reflected in the non-zero initial values of the corresponding velocities (3.54).

In case the substances move through the membrane during the swelling process, i.e. the membrane is *leaky* semipermeable (assumption *Ml*), it can be assumed that the intracellular concentration  $c_t^{fp}$  and amount of substance  $a_t^{fp}$  initially correspond to their healthy state values, such that the total shift  $a^{SH}$  is achieved only after some time  $T_j \leq T$  (or at the end of the observation):

$$(E2, E4) \text{ Ml:} \quad a_t^{sh} = \begin{cases} 0 & t = 0, t > T_j, \\ a^{SH} & t = T; \end{cases} \tag{3.43}$$

$$c_0^{fp} = c_H^{fp} \approx 300, \quad c_0^b = c_H^b \approx 300. \tag{3.44}$$

The characteristic values  $c_c^\Delta$ ,  $\pi_c^\Delta$  are then found as:

$$\begin{aligned}
 (E2, E4) \text{ Ml:} \quad c_c^\Delta &:= \frac{1}{2}(c_0^\Delta + c_T^\Delta) \approx \frac{1}{2}c_T^\Delta \approx \begin{cases} 0.36 & (2D), \\ 0.51 & (3D), \end{cases} \\
 \pi_c^\Delta &:= C_{osm}c_c^\Delta \approx \pi_T^\Delta \approx \begin{cases} 0.936 \cdot 10^3 & (2D), \\ 1.311 \cdot 10^3 & (3D). \end{cases}
 \end{aligned} \tag{3.45}$$

Exchange of the osmolytes across the membrane (i.e. osmolyte flux function  $j^c$ ) for a leaky membrane is modelled below in *Section 3.1.5*.

*Note:* It is assumed here, that changes in the molarities (and thus osmotic pressures) over time are not strongly deviating from linear behaviour, thus average values are chosen for the characteristic values of the molar concentrations.

In case the outer walls  $\Gamma^{bw}$  are considered to be *permeable to the osmolytes*, such that it can be assumed that an average in space value of the extracellular molarity  $\tilde{c}^b(t)$  is constant in time and is equal to the healthy initial ECF concentration (cases *E1*, *E3*),

$$\begin{aligned}
 E1, E3: \quad \tilde{c}_t^b &= c_0^b = c_T^b := c_H \approx 300, \\
 c_T^{fp} &:= c_T^\Delta + c_T^b \stackrel{(3.36)}{\approx} 301,
 \end{aligned}$$

similar results can be obtained in 2D and 3D. Thus for both the strictly semipermeable membranes:

$$\begin{aligned}
 (E1, E3) \text{ Ms (3D):} \quad a_0^{fp} = a_T^{fp} \quad \Rightarrow \quad c_0^{fp} &= \frac{a_0^{fp}}{V_0^{fp}} = \frac{a_T^{fp}}{V_0^{fp}} = \frac{c_T^{fp} V_T^{fp}}{V_0^{fp}} \approx 393.85, \\
 c_0^\Delta &:= c_0^{fp} - c_0^b \approx 93.85, \\
 \pi_0^\Delta &:= C_{osm} c_0^\Delta \approx 2.42 \cdot 10^5,
 \end{aligned}$$

$$\begin{aligned}
 (E1, E3) \text{ Ms (3D):} \quad c_c^\Delta &:= \frac{1}{2}(c_0^\Delta + c_T^\Delta) \approx \frac{1}{2}c_0^\Delta \approx 47, \\
 \pi_c^\Delta &:= C_{osm} c_c^\Delta \approx \pi_0^\Delta \approx 1.21 \cdot 10^5,
 \end{aligned} \tag{3.46}$$

and leaky semipermeable membranes,

$$\begin{aligned}
 (E1, E3) \text{ Ml (3D):} \quad c_0^{fp} &= c_H^{fp} \approx 300, \\
 c_0^\Delta &= c_0^{fp} - c_0^b \approx 0,
 \end{aligned}$$

$$\begin{aligned}
 (E1, E3) \text{ Ml (3D):} \quad c_c^\Delta &:= \frac{1}{2}(c_0^\Delta + c_T^\Delta) \approx \frac{1}{2}c_T^\Delta \approx 0.5, \\
 \pi_c^\Delta &:= C_{osm} c_c^\Delta \approx \pi_T^\Delta \approx 1.29 \cdot 10^3,
 \end{aligned} \tag{3.47}$$

the transmembrane osmotic pressure jumps (3.47), (3.47) are found to be almost identical to the values (3.41), (3.45) obtained for the experiments *E2*, *E4*.

### 3.1.4 Times and velocities

#### 3.1.4.1 Velocities and their relations

In the considered cell swelling problem, the fluid flowing into the cell is not leaving the domain  $\Omega^p$ , i.e. there exists no flow *through* the porous medium. Instead, the inflow of fluid causes the growth of the intracellular space  $\Omega^p$ , such that the movement of the fluid phase is volumetrically compensated by the movement of the solid phase, i.e.

$$A^{fp\epsilon} v_c^{fp} \cdot n^\epsilon = -A^{sp\epsilon} v_c^{sp} \cdot n^\epsilon, \tag{3.48}$$

where  $A^{fp\epsilon}$ ,  $A^{sp\epsilon}$  are the cross-sectional areas of the fluid and solid phases within an elementary volume  $V^\epsilon$  and  $n^\epsilon$  is a unit vector normal to the surface. Dividing both sides of the equation by the total area  $A^\epsilon = A^{sp\epsilon} \cup A_c^{sp\epsilon}$  and assuming that the phase to the total area ratios  $A^{sp\epsilon}/A^\epsilon$ ,  $A^{fp\epsilon}/A^\epsilon$  are equal to the corresponding volumetric ratios, i.e.

$$\begin{aligned}
 \frac{A^{sp\epsilon}}{A^\epsilon} &\triangleq \frac{V^{sp\epsilon}}{V^\epsilon} =: \gamma_c^s, \\
 \frac{A^{fp\epsilon}}{A^\epsilon} &\triangleq \frac{V^{fp\epsilon}}{V^\epsilon} =: \gamma_c^f,
 \end{aligned}$$

the characteristic (average) fluid phase velocity  $v_c^{fp}$  is found to relate to the solid phase velocity

$v_c^{sp}$  in the following way:

$$\begin{aligned} \gamma_c^f v_c^{fp} \cdot n &= -\gamma_c^s v_c^{sp} \cdot n & \Rightarrow \\ v_c^{fp} \cdot n &= -\frac{\gamma_c^s}{\gamma_c^f} v_c^{sp} \cdot n \stackrel{(3.17)}{=} -v_c^{sp} \cdot n. \end{aligned} \quad (3.49)$$

In case the outer walls of the overall domain  $\Omega$  are impermeable (experiments  $E4$ ) or the influence of the surrounding media on the fluid flow is assumed to be negligible ( $E2$ ,  $E3$ ), the fluid velocity  $v^b$  within the extracellular domain  $\Omega^b$  exists only due to the outflow of the fluid and the corresponding movement of the interaction interface  $\Gamma^i$ . Due to the incompressibility of the fluid and continuity of fluxes at the interface (2.59), the bulk fluid velocity created by the outflow and interface deformation is *in average* zero (see Fig. 2.1):

$$v_{avg}^b := \gamma_c^s v_c^{sp} + \gamma_c^f v_c^{fp} = 0,$$

which does not however reflect the *pointwise* behaviour of the moving bulk fluid, unless dictated by the symmetry arguments. Instead, the characteristic bulk fluid velocity is chosen to correspond to the pore fluid velocity  $v_c^{fp}$ :

$$v_c^b := v_c^{fp} = -v_c^{sp} \triangleq v_c. \quad (3.50)$$

*Note:* For the *in-vivo* brain tissue experiments ( $E1$ ), if the velocity  $v_c^{global}$  of the *global* extracellular fluid flow through the one cell domain is either much smaller, or of the order of the velocity associated with the interface movement, the characteristic velocity  $v_c^b$  can be chosen as in (3.50). Otherwise, the bulk fluid flow velocity would be dominated by the *global* flow, and thus  $v_c^b$  is chosen such that  $v_c^b := v_c^{global}$ . In the absence of global ECF velocity measurements, it is assumed in this work that an average magnitude of the global flow velocity is approximately equal to the value of the bulk fluid velocity created by the activity at the interface, thus (3.50) is assumed to hold in all experiments.

Using the definition of the characteristic normal interface flux  $j_c^b \cdot n$ , the characteristic normal velocity values can be estimated from the flux interface condition (2.89):

$$\begin{aligned} j_c^b \cdot n &\stackrel{(2.57)}{:=} (v^b - v^{sp}) \cdot n \stackrel{(3.50)}{\Rightarrow} j_c^b \cdot n = 2v_c \cdot n & \Rightarrow \\ v_c \cdot n &= \frac{1}{2} j_c^b \cdot n \stackrel{(2.89)}{=} \frac{1}{2} L^p (p_c^\Delta + \pi_c^\Delta), \end{aligned} \quad (3.51)$$

$$v_c \cdot n \approx \begin{cases} \left[ \begin{array}{ll} L^p \pi_c^\Delta \approx 5 \cdot 10^{-9} \text{ m/s} & Ms \\ 9 \cdot 10^{-11} \text{ m/s} & Ml \end{array} \right] & (2D), \\ \left[ \begin{array}{ll} L^p \pi_c^\Delta \approx 6 \cdot 10^{-9} \text{ m/s} & Ms \\ 7 \cdot 10^{-11} \text{ m/s} & Ml \end{array} \right] & (3D), \end{cases} \quad (3.52)$$

where the values of  $p_c^\Delta$  and  $\pi_c^\Delta$  for assumptions  $Ms$ ,  $Ml$  can be found in (3.122) and (3.41), (3.45) correspondingly.

It should be stressed, that the characteristic velocity values can be estimated through the values of the velocities at the moving interface  $\Gamma^i$ , since there assumed to exist no other (external)



effects that may significantly contribute to the magnitudes of the velocities.

In case the membrane is considered to be leaky semipermeable (assumption *Ml*), the initial condition of the cell is assumed to correspond to the healthy state in all aspects. As the healthy cell is assumed to be in a stable equilibrium, the initial velocities in such settings are taken to be zero:

$$Ml: \quad v_0^b = 0 \quad \Rightarrow \quad v_0^{fp} = v_0^{sp} = 0. \quad (3.53)$$

When the membrane is assumed to be strictly semipermeable (assumption *Ms*), the initial velocities can be estimated through the flux condition (2.89):

$$Ms: \quad (v_0^b - v_0^{sp}) \cdot n = j_0^b \cdot n = L^p(p_0^\Delta + \pi_0^\Delta) \approx L^p\pi_0^\Delta \approx \begin{cases} 20 \cdot 10^{-9} \text{ m/s} & (2D), \\ 25 \cdot 10^{-9} \text{ m/s} & (3D), \end{cases} \quad (3.54)$$

where  $p_0^\Delta, \pi_0^\Delta$  for the case *Ms* are given in (3.24), (3.40). Thus for the assumption *Ms*, the initial normal velocities are found to correspond to the characteristic values (3.51)<sub>1</sub>.

### 3.1.4.2 Observation time

Cytotoxic oedema develops several minutes after the onset of ischaemia in the living brain and persists for *hours*, [47], [45], [43]. During this period, living ischaemic brain is normally also affected by other processes that contribute to the swelling behaviour of the cells, [51]. In particular, in most cases, cytotoxic and vasogenic oedemas occur (almost) simultaneously, [38], [47], [48], such that cytotoxic processes are influenced by the inflow of substances from the adjacent tissues into the brain tissue, [48], [50], [51]. It has however been noticed, that cytotoxic oedema dominates in the *early* phase of ischaemic stroke, [45], [47], [48], [55], therefore for *sufficiently short* observation times (i.e. minutes rather than hours), it can be assumed that living cell swelling is close enough to pure cytotoxic swelling and the other effects can be neglected.

The *in vitro* experiments on cytotoxic osmotic swelling of mammalian cells suggest, that after exposure to hypotonic (i.e. of lower concentration) solutions, cells swell either immediately or over a short time (seconds to minutes), such that the speed and the rate of swelling naturally depend on the tonicity (i.e. relative concentration) of the extracellular solution, as well as on the amount of oxygen and certain other substances diluted in the solution, [10], [41], [56].

Since the characteristic value of the solid phase velocity  $v^{sp} := \partial_t u^s$  can naturally be defined as a ratio between the characteristic displacement  $u_c$  and time  $t_c$ :

$$v_c^{sp} := \frac{u_c}{t_c}, \quad (3.55)$$

using the values (3.10), (3.51) estimated for  $u_c^{sp}, v_c^{sp}$ , the characteristic observation time  $t_c$  is found as:

$$Ms: \quad t_c := \frac{u_c}{v_c^{sp}} \approx \begin{cases} 4.8 \cdot 10^2 \text{ s} & (2D), \\ 4.0 \cdot 10^4 \text{ s} & (3D), \end{cases} \quad (3.56)$$

$$Ml: \quad t_c := \frac{u_c}{v_c^{sp}} \approx \begin{cases} 2.7 \cdot 10^2 \text{ s} & (2D), \\ 3.4 \cdot 10^4 \text{ s} & (3D). \end{cases} \quad (3.57)$$

Thus the observation time (3.56) for assumption *Ms* agrees with the above mentioned experimental time estimates. The leaky membrane time estimate (3.57) is although significantly larger, yet still within the acceptable limits. Moreover, osmotic pressure jump (3.45) and time (3.57) are estimated for the osmolyte exchange that takes place during the entire observation time, e.g.  $T_j = T$  in (3.43). Choosing a shorter time interval  $(0, T_j)$  would lead to shorter time estimates, such that it can be easily shown that in the limit  $T_j \rightarrow 0$ , observation time shortens to (3.56).

### 3.1.4.3 Diffusion time

Diffusion time  $t_c^D$  defined as an approximate time required for solute particles to diffuse within certain volume, can be estimated as:

$$t_c^D := \frac{l_c^2}{2D},$$

where  $l_c$  is the characteristic length of the domain and  $D$  is the diffusivity of the solute diluted in the given solvent. Using this definition, the diffusion times  $t_c^{D,p}$ ,  $t_c^{D,b}$  for the intracellular and extracellular solutes respectively,

$$t_c^{D,b} = \frac{(l_c^b)^2}{2D} \approx 50 \text{ s}, \quad (3.58)$$

$$t_c^{D,p} = \frac{(l_c^p)^2}{2D} \approx 10 \text{ s}, \quad (3.59)$$

are found to be comparable to the observation time (3.56) estimated with the assumption that the membrane is strictly semipermeable (*Ms*), but significantly smaller than the time (3.57) estimated for the leaky semipermeable membrane assumption (*Ml*). The relations between the diffusion and observation times are further discussed in *Section 3.2.4*.

### 3.1.5 Molarity flux models

Solute (substance) flux  $j^{c,i}$  through a leaky semipermeable membrane can be described by the equations of the 2P (two parameter) or KK (Kedem-Katchalsky) formalism:

$$j^{c,i} = w^i RT c^{\Delta,i} = P_s^i c^{\Delta,i}, \quad (3.60)$$

where  $w^i$ ,  $P_s^i := w^i RT$  are the membrane permeability coefficients for the substance  $i$ , and  $c^{\Delta,i}$  is the transmembrane concentration difference of the chemical, [113], [134]. In living cells, equation (3.60) can be used to describe equilibration of concentrations across the membrane or the movement of chemicals down their concentration gradients for each substance type (e.g. potassium, sodium, chloride ions) individually. However if a mixture  $c := \sum_i c^i$  of  $i$  chemicals is considered, flux equation (3.60) may be no longer suitable in case it is not possible to determine an (averaged) permeability coefficient  $P_s$  for the mixture. Moreover, even if the concentrations of principle osmolytes are treated individually, depending on the experimental conditions, membrane thickness and type of the considered cell,  $P_s^i$  are estimated to range from  $10^{-14}$  to  $10^{-7}$  [m/s] for the sodium and potassium ions, [165], [166], [167], [168], and it is not exactly clear how the permeability coefficient should be chosen, such that it reflects the substance exchange during abnormal ischaemic processes when some of the transporters are not able to function properly.

In addition, at some point (at the end of experiment or at time  $T_j < T$ , see *Section 3.1.3*), the exchange of substances must stop, which in case equation (3.60) is used (assuming that the permeabilities  $P_s^i$  are constant), would be possible only if the concentration difference is zero. Yet as shown in *Section 3.1.3*, due to the elastic stresses of the membrane and cell skeleton, transmembrane molarity difference does not vanish at the end of observation.

Therefore here an alternative approach to the derivation of the flux function  $j^c(x, t)$  will be taken.

Molarity (concentration) flux  $j^c(x, t)$  defined at an interface  $\Gamma(t)$  separating two solutions is a measure of how much substance passes through the interface at each  $(x, t) \in \Gamma(t) \times (0, T_j)$ , where  $(0, T_j)$  is the time interval within which molarity flux exists, i.e.  $j^c \neq 0$ . In particular,  $j^c(x, t)$  can be expressed in the following way:

$$\int_0^t j^c(x, t) A(t) dt = a^{sh}(x, t) \quad \text{at } \Gamma(t),$$

where  $A(t)$  is the area of the interface and  $a^{sh}(x, t)$  is the amount of substance that has crossed the interface in the time interval  $(0, t)$ . Since the cell is assumed to be able to exchange the osmolytes only at the membrane  $\Gamma^i$ , and assuming for simplicity that the flux  $j^c$  is spatially uniform at all times, i.e.,  $j^c(x, t) = j^c(t)$ , the molar flux integral equation for the one cell problem reads:

$$\int_0^t j_t^c A_t^c dt = a_0^{fp} - a_t^{fp} \quad \text{at } \Gamma^i(t), \quad (3.61)$$

where  $A_t^c$  is the surface area of the cell (i.e. the area of the membrane) and  $a^{fp}$  is the amount of substance of the osmolytes diluted in the intracellular fluid  $\Omega^{fp}$ . Applying partial time derivative to both sides of (3.61), an ordinary differential equation for  $a^{fp}$  is obtained:

$$j_t^c A_t^c = -\partial_t a_t^{fp} \quad \text{at } \Gamma^i(t). \quad (3.62)$$

In case the membrane is assumed to stretch during cell swelling (assumption **Ag**), the cell surface area  $A_t^c$  must depend on time through the deformation  $u^{sp}(x, t)$  of the domain  $\Omega^p(t)$ . In order to avoid the use of the primary variables of the Biot-Stokes system in the modelling of the flux functions, some assumptions on the surface area growth need to be made. For instance, one of the following possibilities can be considered:

- linear growth of the cell radius  $r_t^c$ :

$$r_t^c = \frac{r_T^c - r_0^c}{T} t + r_0^c \quad \Rightarrow \quad \begin{aligned} 2D: \quad A_t^c &= 2\pi r^c = 2\pi \left( \frac{r_T^c - r_0^c}{T} t + r_0^c \right), \\ 3D: \quad A_t^c &= 4\pi (r_t^c)^2 = 4\pi \left( \frac{r_T^c - r_0^c}{T} t + r_0^c \right)^2; \end{aligned} \quad (3.63)$$

- linear growth of the cell area  $A_t^c$ :

$$A_t^c = \frac{A_T^c - A_0^c}{T} t + A_0^c; \quad (3.64)$$

- linear growth of the cell volume  $V_t^c$ :

$$V_t^c = \frac{V_T^c - V_0^c}{T}t + V_0^c \quad \Rightarrow \quad \begin{aligned} 2D: \quad A_t^c &= 2\sqrt{\pi}\sqrt{V_t^c} = 2\sqrt{\pi}\left(\frac{V_T^c - V_0^c}{T}t + V_0^c\right)^{1/2}, \\ 3D: \quad A_t^c &= 36\pi(V_t^c)^{2/3} = 36\pi\left(\frac{V_T^c - V_0^c}{T}t + V_0^c\right)^{2/3}. \end{aligned} \quad (3.65)$$

As the amount of substance function  $a_t^{fp}$  is in general not known, in order to find the molar flux  $j_t^c$  from (3.62), either  $a_t^{fp}$  or the dependence of  $j_t^c$  on  $a_t^{fp}$  can be modelled, such that in the latter case, the flux is found through the solution of an ODE. Thus based on the assumptions made with regard to the dynamics of the substance exchange, several models are suggested below.

**Flux model 1 (F1):** assume that the flow of the osmolytes through the membrane is uniform during the entire observation. Then the extracellular amount of substance function  $a_t^{fp}$  must change linearly in time:

$$a_t^{fp} := \frac{a_T^{fp} - a_0^{fp}}{T}t + a_0^{fp}, \quad (3.66)$$

where  $a_0^{fp}$ ,  $a_T^{fp}$  are the initial and terminal values of  $a_t^{fp}$ . Substituting (3.66) into (3.62) and differentiating  $a_t^{fp}$ , the flux is found as:

$$j_t^c = \frac{\partial_t a^{fp}}{A_t^c} = \frac{a_T^{fp} - a_0^{fp}}{TA_t^c}, \quad (3.67)$$

where it is assumed that either the surface area is constant (as on Fig. 2.2b):

$$F1-Ac: \quad j_t^c = \frac{a_T^{fp} - a_0^{fp}}{TA_0^c}, \quad (3.68)$$

or the membrane stretches following the growth of the cell (as on Fig. 2.2a), such that the dependence of  $A_t^c$  on time can be expressed through one of the suggested approximations (3.63)–(3.65). Thus for the linear in time area growth (3.64):

$$F1-Ag: \quad j_t^c = \frac{a_T^{fp} - a_0^{fp}}{(A_T^c - A_0^c)t + A_0^c T}. \quad (3.69)$$

**Flux model 2 (F2):** assume that the flux function  $j_t$  depends (linearly) on the transmembrane concentration difference of osmolytes:

$$j_t^c = \alpha (c_t^{fp} - c_t^b), \quad (3.70)$$

where  $\alpha$  is a proportionality coefficient that has to be determined using the available information.

*Note:* Equation (3.70) is in its form identical to the 2P (or KK) flux equation (3.60) written for the mixture of osmolytes. Thus the coefficient  $\alpha$  can be regarded as the osmolyte permeability coefficient of the membrane.

Considering that the extracellular molarity  $c_t^b$  remains constant, i.e.  $c_t^b := c_0^b \forall t \in (0, T)$  (experiments E1, E3), and substituting the flux model (3.70) into (3.62), the following ODE for the

amount of substance  $a_t^{fp}$  is obtained:

$$E1, E3: \quad \partial_t a^{fp} = -\alpha A_t^c \left( \frac{a_t^{fp}}{V_t^{fp}} - c_0^b \right). \quad (3.71)$$

The explicit dependence of the fluid phase volume  $V_t^{fp}$  on time can be approximated analogously to the modelling of the surface area growth (3.63)–(3.65). Assuming for simplicity that the surface area is conserved, i.e.  $A_t^c := A_0^c \forall t \in (0, T)$  (assumption **A**c), and that the intracellular fluid volume  $V_t^{fp}$  increases uniformly in time, i.e.

$$V_t^{fp} := \frac{V_T^{fp} - V_0^{fp}}{T} t + V_0^{fp} := C_2 t + C_3, \quad \begin{aligned} C_2 &:= \frac{V_T^{fp} - V_0^{fp}}{T}, \\ C_3 &:= V_0^{fp}, \end{aligned} \quad (3.72)$$

where the initial  $V_0^{fp}$  and final  $V_T^{fp}$  volumes are given in *Tables 3.3*, the solution of the differential equation (3.71) is found as:

$$F2-Ac (E1, E3): \quad \begin{aligned} \partial_t a_t^{fp} &\stackrel{(3.62)}{=} -j_t^c A_0^c \stackrel{(3.70)}{=} -\alpha A_0^c \left( \frac{a_t^{fp}}{C_2 t + C_3} - c_0^b \right), \\ a_t^{fp} &= c_1 (C_2 t + C_3)^{-A_0^c \alpha / C_2} + \alpha A_0^c c_0^b \frac{C_2 t + C_3}{\alpha A_0^c + C_2}, \end{aligned} \quad (3.73)$$

where  $c_1$  is the integration constant. Then substituting the obtained solution for the amount of substance function  $a_t^{fp}$  back into (3.62) and differentiating it, the solute flux function is found:

$$F2-Ac (E1, E3): \quad j_t^c \stackrel{(3.62)}{=} -\frac{1}{A_0^c} \partial_t a_t^{fp} \stackrel{(3.73)}{=} \alpha c_1 (C_2 t + C_3)^{-A_0^c \alpha / C_2 - 1} - \frac{\alpha c_0^b C_2}{\alpha A_0^c + C_2},$$

such that using the initial and terminal values  $a_0^{fp}$ ,  $a_T^{fp}$  estimated in *Section 3.1.3*, the integration constant  $c_1$  and the coefficient  $\alpha$  can be determined:

$$F2-Ac (E1, E3): \quad \begin{aligned} (t = 0) \quad a_0^{fp} &= c_1 C_3^{-A_0^c \alpha / C_2} + \frac{\alpha A_0^c c_0^b C_3}{\alpha A_0^c + C_2}, \\ (t = T) \quad a_T^{fp} &= c_1 (C_2 T + C_3)^{-A_0^c \alpha / C_2} + \alpha A_0^c c_0^b \frac{C_2 T + C_3}{\alpha A_0^c + C_2}. \end{aligned} \quad (3.74)$$

In case the interface stretches following the growth of the cell,  $A_t^c$  must be growing as the area of a sphere (in 3D) or the circumference of a circle (in 2D), thus the surface area and the total volume  $V_t^c$  of the cell are related in the following way:

$$Ag: \quad \begin{aligned} 3D: \quad A_t^c &= \sqrt[3]{36\pi} (V_t^c)^{2/3}, \\ 2D: \quad A_t^c &= 2\sqrt{\pi} (V_t^c)^{1/2}, \end{aligned} \quad (3.75)$$

where the total cell volume  $V_t^c$  consists of the fluid phase volume  $V_t^{fp}$  and constant volume  $\tilde{V}^p$ :

$$V_t^c = V_t^{fp} + \tilde{V}^p.$$

Assuming as in (3.72) that the fluid phase volume grows linearly in time and considering the

relations (3.75), the surface area to fluid phase volume ratio is then found as:

$$\begin{aligned}
 3D : \quad & \frac{A_t^c}{V_t^{fP}} = \frac{\sqrt[3]{36\pi} (V_t^{fP} + \tilde{V}^p)^{2/3}}{V_t^{fP}} = \frac{\sqrt[3]{36\pi} (C_2t + C_4)^{2/3}}{C_2t + C_3}, \\
 Ag: \quad & \\
 2D : \quad & \frac{A_t^c}{V_t^{fP}} = \frac{2\sqrt{\pi} (V_t^{fP} + \tilde{V}^p)^{1/2}}{V_t^{fP}} = \frac{2\sqrt{\pi} (C_2t + C_4)^{1/2}}{C_2t + C_3},
 \end{aligned}
 \quad C_4 := \tilde{V}^p + C_3.$$

Then substituting the obtained relations into (3.71), solving the resulting ODE and determining the integration constant and  $\alpha$  through the initial and final values  $a_0^{fP}$ ,  $a_T^{fP}$  (as is done above), the amount of substance  $a_t^{fP}$  and then molar flux  $j_t^c$  can be found for the assumption set *F2-Ag* (*E1*, *E3*).

Assuming that the total amount of substance  $a^\Omega$  diluted in the extracellular and intracellular fluids of the overall domain  $\Omega$  is conserved (*E2*, *E4*), and using the total volume conservation assumption, the flux equation (3.70) can be written as:

$$E2, E4: \quad \partial_t a^{fP} = -\alpha A_t^c \left( \frac{a_t^{fP}}{V_t^{fP}} - \frac{a_t^b}{V_t^b} \right) = -\alpha A_t^c \left( \frac{a_t^{fP}}{V_t^{fP}} - \frac{a^\Omega - a_t^{fP}}{V - \tilde{V}^p - V_t^{fP}} \right),$$

where  $V$ ,  $V_t^b$  are respectively the volumes of the domains  $\Omega$ ,  $\Omega^b(t)$ , and  $\tilde{V}^p$  is the volume of the solid components of the cell, which (the volume) remains constant during the entire observed process.

*Note:* Coefficient  $\alpha$  in (3.74) can not be expressed as an algebraic function, and also for some of the above considered assumption sets, the solutions of the corresponding ODEs do not have closed forms. In those cases, numerical approximations of the corresponding coefficients or functions can be used.

As mentioned above in *Section 1.2.1*, the membrane (osmolyte) permeability may depend on multiple factors, which are however a challenge to account for in the modelling of the filtration parameters. In this work, the construction of the osmolyte flux function models is such, that the averaged transmitting properties of the membrane are implicitly reflected in the choice of:

- the duration of the substance exchange,
- (the change of) the surface area of the cell,
- the initial and terminal values of the intracellular and extracellular molarities or amounts of substance.

## 3.2 Dimensional equations

Now when the parameters and characteristic values are determined, the model equations can be written in a dimensionless form. For an *original* quantity  $z$  having the *characteristic* value  $z_c$ , the corresponding *dimensionless* coordinate  $[z]$  and its partial time derivative  $[\partial_t z]$  are defined as:

$$[z] := \frac{z}{z_c}, \quad [\partial_t z] = \frac{t_c}{z_c} \partial_t z, \quad (3.76)$$

where  $t_c$  is the characteristic time of the considered problem. Assuming that the characteristic lengths  $l_{c,i}^b, l_{c,i}^p$  of the domains  $\Omega^b, \Omega^p$  are equal in all directions  $i \in \{1, \dots, dim\}$ , the original coordinates of the domains  $x_i$  relate to the dimensionless coordinates  $[x_i]$  as:

$$\begin{aligned} x_i &= l_c^b [x_i], & x_i &\in \Omega^b, & [\Omega^b] &= \{ \{ [x_i] \} : 0 < [x_i] < 1 \} \\ x_i &= l_c^p [x_i], & x_i &\in \Omega^p, & [\Omega^p] &= \{ \{ [x_i] \} : 0 < [x_i] < 1 \} \end{aligned} \quad i = \{1, \dots, dim\}. \quad (3.77)$$

Then the partial spatial derivatives of a variable  $z$  transform into dimensionless coordinates, such that:

$$\partial_i z := \frac{\partial z}{\partial x_i} = \frac{z_c}{l_c} [\partial_i z], \quad \partial_{ij}^2 z := \frac{\partial^2 z}{\partial x_i^2} = \frac{z_c}{l_c^2} [\partial_{ij}^2 z] \quad i, j \in \{1 \dots dim\}. \quad (3.78)$$

Problem variables, their dimensionless counterparts and characteristic values are related in the following way:

$$\begin{aligned} u^b &= u_c^b [u^b], & v^b &= v_c^b [v^b], & \gamma^f &= \gamma_c^f [\gamma^f], & c^b &= c_c^b [c^b], & \pi^b &= \pi_c^b [\pi^b], \\ u^{sp} &= u_c^{sp} [u^{sp}], & v^{fp} &= v_c^{fp} [v^{fp}], & \gamma^s &= \gamma_c^s [\gamma^s], & c^{fp} &= c_c^{fp} [c^{fp}], & \pi^p &= \pi_c^p [\pi^p]. \end{aligned} \quad (3.79)$$

Since the spatial modelling equations include pressure gradients, the characteristic *pressure gradients*  $p_\Delta^b, p_\Delta^p$  reflecting the characteristic pressure *difference* across the domain<sup>2</sup> are considered:

$$\nabla p^b = \frac{p_\Delta^b}{l_c^b} [\nabla p^b], \quad \nabla p^p = \frac{p_\Delta^p}{l_c^p} [\nabla p^p]. \quad (3.80)$$

When considering interface conditions (2.61), (2.89), pressure difference across the interface is estimated as a whole, and the notion of the characteristic transmembrane pressure difference  $p_c^\Delta$  is employed:

$$p^\Delta := p^p - p^b, \quad (3.81)$$

$$p^\Delta = p_c^\Delta [p^\Delta]. \quad (3.82)$$

For the one cell problem, the characteristic pressure gradients  $p_\Delta^b, p_\Delta^p$  and pressure difference  $p_c^\Delta$  will be determined with the help of dimensional analysis.

Other quantities, such as the temperature  $\Upsilon$ , dynamic fluid viscosity  $\mu^f$ , fluid and solid densities  $\rho^f, \rho^s$ , diffusion coefficient  $D$ , elasticity coefficients  $\mu^s, \lambda^s$ , water filtration coefficient  $L^p$ , porosity and solidity  $\gamma^f, \gamma^s$  and Darcy permeability  $k$  are assumed to be constant. As suggested in *Section 3.1*, the following relations hold:

$$\begin{aligned} \lambda^s &= 4\mu^s, & \gamma_c^f &= \gamma_c^s =: \gamma_0, & u_c^b &= u_c^{sp} =: u_c, \\ \rho^s &= \rho^f =: \rho, & v_c^b &= v_c^{fp} = -\frac{\gamma^s}{\gamma^f} v_c^{sp} = -v_c^{sp} = -\frac{u_c}{t_c}. \end{aligned} \quad (3.83)$$

<sup>2</sup> For instance in a pipe flow experiment, where constant pressures applied at the inflow and outflow boundaries  $a$  and  $b$  are driving the flow, characteristic pressure gradient  $p_\Delta$  can be chosen as the difference between the pressure boundary values,  $p_\Delta := p(a) - p(b)$ .

In this section some of the well known dimensional coefficients (numbers) will be used, namely:

$$\begin{aligned} \text{Strouhal Number } (St) &= \frac{l_c}{t_c v_c}, & \text{Euler Number } (Eu) &= \frac{p_c}{\rho v_c^2}, \\ \text{Reynolds Number } (Re) &= \frac{\rho l_c v_c}{\mu}, & \text{Peclet Number } (Pe) &= \frac{l_c v_c}{D}. \end{aligned}$$

Reynolds and Strouhal numbers are used to determine the relative magnitudes of inertial terms in the Navier-Stokes equations. With the help of Reynolds number, the dominating effects (viscous, inertial or both) can be identified. Low Reynolds numbers indicate that the pressure gradients are primarily caused by the dominant viscous effects, and at high Reynolds numbers the inertial effects become crucial instead. The Peclet number determines the ratio of convection to diffusion in transport equations: in case the Peclet number is much smaller than 1, transport may be modelled considering diffusion only. The other way around, at high value of  $Pe$ , the transport is considered to be driven mainly by convection (which does not however mean that diffusion can be neglected). More details on the dimensionalization approaches and above mentioned dimensionless numbers can be found in, e.g. [169], [97], [170].

### 3.2.1 ALE transformation terms

Deformation gradients defined on the poroelastic and bulk fluid domains  $\Omega^p$ ,  $\Omega^b$  ( $\hat{\Omega}^p$ ,  $\hat{\Omega}^b$ ) are estimated to be *considerably* smaller than unity:

$$\begin{aligned} \hat{\nabla} \hat{u}^{sp} &= \frac{u_c}{l_c^p} [\hat{\nabla} \hat{u}^{sp}], & \frac{u_c}{l_c^p} &\approx 0.056, & [\hat{\nabla} \hat{u}^{sp}] &\sim O(1), \\ \hat{\nabla} \hat{u}^b &= \frac{u_c}{l_c^b} [\hat{\nabla} \hat{u}^b], & \frac{u_c}{l_c^b} &\approx 0.025, & [\hat{\nabla} \hat{u}^b] &\sim O(1), \end{aligned} \quad (3.84)$$

therefore in this work the transformation tensors  $\hat{F}^{sp}$ ,  $\hat{F}^b$  are reduced to the identity matrix and their determinants – to 1:

$$\hat{F}^{sp} := I + \hat{\nabla} \hat{u}^{sp} \approx I, \quad \hat{J}^{sp} := \det(\hat{F}^{sp}) \approx 1, \quad (3.85)$$

$$\hat{F}^b := I + \hat{\nabla} \hat{u}^b \approx I, \quad \hat{J}^b := \det(\hat{F}^b) \approx 1. \quad (3.86)$$

It then follows, that the ALE formulations of the modelling equations can be significantly simplified, see *Section 2.1.3*.

### 3.2.2 Incompressible Navier-Stokes equations

In order to justify the choice of the Stokes equations for the modelling of the bulk fluid motion in  $\Omega^b$ , the Navier-Stokes equations as a general description for an incompressible flow of a Newtonian fluid are considered:

$$\mu^f \Delta v^b - \nabla p^b = \rho^f \partial_t v^b + \rho^f (v^b, \nabla) v^b \quad \text{in } \Omega^b(t) \times (0, T), \quad (3.87)$$

$$\nabla \cdot v^b = 0 \quad \text{in } \Omega^b(t) \times (0, T). \quad (3.88)$$



Writing the momentum balance equation (3.87) in a dimensionless form,

$$\frac{\mu^f v_c^b}{(l_c^b)^2} [\Delta v^b] - \frac{p_\Delta^b}{l_c^b} [\nabla p^b] = \frac{\rho^f v_c^b}{t_c} [\partial_t v^b] + \frac{\rho^f (v_c^b)^2}{l_c^b} [(v^b, \nabla) v^b] \quad \text{in } [\Omega^b],$$

and then dividing the obtained equation by the coefficient that appears at the viscous term, gives the following result:

$$[\Delta v^b] - Eu^b Re^b [\nabla p^b] = St^b Re^b [\partial_t v^b] + Re^b [(v^b, \nabla) v^b] \quad \text{in } [\Omega^b], \quad (3.89)$$

where the Euler  $Eu^b$ , Strouhal  $St^b$  and Reynolds  $Re^b$  numbers for the fluid flow in  $\Omega^b$  are defined as:

$$\begin{aligned} St^b &:= \frac{l_c^b}{t_c v_c^b} = -\frac{l_c^b}{u_c}, & Eu^b &:= \frac{p_\Delta^b}{\rho^f (v_c^b)^2}, \\ Re^b &:= \frac{\rho^f v_c^b l_c^b}{\mu^f} = -\frac{\rho u_c l_c^b}{\mu^f t_c}, & Eu^b Re^b &:= \frac{p_\Delta^b l_c^b}{\mu^f v_c^b} = \frac{p_\Delta^b l_c^b t_c}{\mu^f u_c}, \\ St^b Re^b &= \frac{\rho (l_c^b)^2}{\mu^f t_c}. \end{aligned}$$

Both  $St^b$  and  $St^b Re^b$  are found to be very small for either of the time scales ( $Ms$ ,  $Ml$ ):

$$Re^b < 10^{-6} \ll 1, \quad St^b Re^b < 10^{-4} \ll 1, \quad (3.90)$$

therefore the inertial terms are negligible due to the dominance of the viscous effects, and so the Navier-Stokes equations in  $\Omega^b$  can be reduced to the stationary Stokes equations.

Choosing the characteristic pressure difference  $p_\Delta^b$  such that the coefficient at the dimensionless pressure gradient  $[\nabla p^b]$  is equal to unity (i.e. viscous scaling):

$$Eu^b Re^b = \frac{p_\Delta^b l_c^b t_c}{\mu^f u_c} \triangleq 1 \quad \Rightarrow \quad p_\Delta^b := \frac{\mu^f u_c}{l_c^b t_c} \approx \begin{cases} 10^{-6} \text{ Pa} & (Ms), \\ 10^{-8} \text{ Pa} & (Ml), \end{cases}$$

the following dimensionless bulk fluid flow equations are obtained:

$$[\Delta v^b] - [\nabla p^b] = St^b Re^b [\partial_t v^b] \quad \text{in } [\Omega^b], \quad (3.91)$$

$$[\nabla \cdot v^b] = 0 \quad \text{in } [\Omega^b], \quad (3.92)$$

where for the reasons mentioned in *Section 2.1.1*, the linear inertial term on the RHS of (3.91) is kept.

### 3.2.3 Biot equations

The extended set of the Biot equations on the poroelastic intracellular domain  $\Omega^p$  including the solidity equation and the modified Darcy law describing the dependence of the relative (to the movement of the skeleton) fluid flow velocity on the pressure gradient take the following form in dimensionless coordinates:

$$\frac{\mu^s u_c^{sp}}{(l_c^p)^2} [\nabla] \cdot \left[ \nabla u^{sp} + (\nabla u^{sp})^T + \frac{\lambda^s}{\mu^s} \nabla \cdot u^{sp} I \right] - \frac{p_\Delta^p}{l_c^p} [\nabla p^p] = \frac{\rho^s \gamma_c^s u_c^{sp}}{(t_c)^2} [\gamma^s \partial_{tt} u^{sp}] \quad \text{in } [\Omega^p], \quad (3.93)$$

$$\frac{u_c^{sp}}{l_c^p t_c} [\nabla \cdot \partial_t u^{sp}] - \frac{k p_\Delta^p}{\mu^f (l^p)^2} [\Delta p^p] = 0 \quad \text{in } [\Omega^p], \quad (3.94)$$

$$\frac{\gamma_c^s}{t_c} [\partial_t \gamma^s] + \frac{\gamma_c^s u_c^{sp}}{t_c l_c^p} [\gamma^s \nabla \cdot (\partial_t u^{sp})] = 0 \quad \text{in } [\Omega^p], \quad (3.95)$$

$$v_c^{fp} [v^{fp}] - \frac{u_c^{sp}}{t_c} [\partial_t u^{sp}] = -\frac{k^p p_\Delta^p}{\gamma_c^f \mu^f l_c^p} [\gamma^f \nabla p^p] \quad \text{in } [\Omega^p], \quad (3.96)$$

where following (2.19), the linear inertial term enters the RHS of the momentum balance equation (3.93). Using the relations (3.83), the dimensionalized equations (3.93)-(3.96) can be simplified to:

$$\frac{\mu^s u_c^{sp}}{(l_c^p)^2} \left( 5 [\nabla \cdot (\nabla u^{sp})^T] + [\Delta u^{sp}] \right) - \frac{p_\Delta^p}{l_c^p} [\nabla p^p] = \frac{\rho \gamma_0 u_c^{sp}}{(t_c)^2} [\gamma^s \partial_{tt} u^{sp}] \quad \text{in } [\Omega^p], \quad (3.97)$$

$$\frac{u_c^{sp}}{t_c} [\nabla \cdot \partial_t u^{sp}] = \frac{k p_\Delta^p}{\mu^f l_c^p} [\Delta p^p] \quad \text{in } [\Omega^p], \quad (3.98)$$

$$[\partial_t \gamma^s] + \frac{u_c^{sp}}{l_c^p} [\gamma^s \nabla \cdot (\partial_t u^{sp})] = 0 \quad \text{in } [\Omega^p], \quad (3.99)$$

$$\frac{u_c^{sp}}{t_c} \left( [v^{fp}] + [\partial_t u^{sp}] \right) = \frac{k^p p_\Delta^p}{\gamma_0 \mu^f l_c^p} [\gamma^f \nabla p^p] \quad \text{in } [\Omega^p]. \quad (3.100)$$

The second term of the porosity equation (3.99) is scaled with the *displacement to the domain length ratio*, which in this work is assumed to be *sufficiently small*, therefore (3.99) can be reduced to:

$$[\partial_t \gamma^s] = 0 \quad \text{in } [\Omega^p], \quad (3.101)$$

and so the solidity can be considered to be constant and equal to its initial value:

$$\begin{aligned} \gamma^f(x, t) = \gamma^s(x, t) &:= \gamma_0, \\ [\gamma^s] &:= 1. \end{aligned} \quad (3.102)$$

Assuming that the dimensionless sum of velocities  $[v^{fp}] + [\partial_t u^{sp}]$  in the Darcy equation (3.100) is still of order  $O(1)$ , the characteristic pressure gradient  $p_\Delta^p$  is chosen such that the coefficients on the LHS and RHS of (3.100) are equal:

$$\frac{u_c}{t_c} \triangleq \frac{k^p p_\Delta^p}{\gamma_0 \mu^f l_c^p} \Rightarrow p_\Delta^p := \frac{\gamma_0 \mu^f l_c^p u_c}{k^p t_c} \approx \begin{cases} 10^{-1} \text{ Pa} & (Ms), \\ 10^{-3} \text{ Pa} & (Ml). \end{cases} \quad (3.103)$$

In order to determine the relations between the elastic and inertial effects, the momentum balance equation (3.97) is divided by the dimensionless elasticity coefficient  $\mu^s u_c / (l_c^p)^2$  resulting in:

$$\left( 5 [\nabla \cdot (\nabla u^{sp})^T] + [\Delta u^{sp}] \right) - \mathcal{P} [\nabla p^p] = \frac{\rho \gamma_0 (l_c^p)^2}{\mu^s (t_c)^2} [\partial_{tt} u^{sp}] \quad \text{in } [\Omega^p], \quad (3.104)$$

where  $\mathcal{P}^p$  is the dimensionless pressure gradient coefficient,

$$\mathcal{P}^p := \frac{p_{\Delta}^p l_c^p}{\mu^s u_c}, \quad (3.105)$$

which for the chosen pressure scaling (3.103) is found as:

$$\mathcal{P}^p := \frac{p_{\Delta}^p l_c^p}{\mu^s u_c} \approx \begin{cases} 10^{-3} \text{ Pa} & (Ms), \\ 10^{-5} \text{ Pa} & (Ml). \end{cases} \quad (3.106)$$

The magnitude of the dimensionless coefficient on the RHS of (3.104) is very low, also compared to the pressure coefficient  $\mathcal{P}^p$ :

$$\frac{\rho \gamma_0 (l_c^p)^2}{\mu^s t_c^2} < 10^{-14} \ll 1, \quad (3.107)$$

and therefore the linear inertial effects of the considered type can be neglected. Eventually, the dimensionalized extended Biot system reduces to:

$$\left( 5 \left[ \nabla \cdot (\nabla u^{sp})^T \right] + [\Delta u^{sp}] \right) - \mathcal{P}^p [\nabla p^p] = 0 \quad \text{in } [\Omega^p], \quad (3.108)$$

$$[\nabla \cdot \partial_t u^{sp}] = \gamma_0 [\Delta p^p] \quad \text{in } [\Omega^p], \quad (3.109)$$

$$[v^{fp}] + [\partial_t u^{sp}] = [\nabla p^p] \quad \text{in } [\Omega^p]. \quad (3.110)$$

### 3.2.4 Convection–diffusion equations

The convection-diffusion equations (2.68), (2.70) for the molar concentrations  $c^b$ ,  $c^{fp}$  of osmotically active substances diluted in the bulk fluid  $\Omega^b$  and in the fluid phase of the poroelastic domain  $\Omega^p$  take the following forms in dimensionless coordinates:

$$\frac{c_c^b}{t_c} [\partial_t c^b] - \frac{D c_c^b}{(l_c^b)^2} [\Delta c^b] + \frac{v_c^b c_c^b}{l_c^b} [\nabla \cdot (v^b c^b)] = 0 \quad \text{in } [\Omega^b], \quad (3.111)$$

$$\frac{c_c^{fp}}{t_c} [\partial_t c^{fp}] - \frac{D c_c^{fp}}{(l_c^p)^2} [\Delta c^{fp}] + \frac{v_c^{sp} c_c^{fp}}{l_c^p} [\nabla \cdot (v^{fp} c^{fp})] = 0 \quad \text{in } [\Omega^p]. \quad (3.112)$$

Each of the equations (3.111), (3.112) is divided by the coefficient standing at the corresponding diffusion term:

$$\begin{aligned} \mathcal{T}^b [\partial_t c^b] - [\Delta c^b] + Pe^b [\nabla \cdot (v^b c^b)] &= 0 \quad \text{in } [\Omega^b], \\ \mathcal{T}^p [\partial_t c^{fp}] - [\Delta c^{fp}] + Pe^p [\nabla \cdot (v^{fp} c^{fp})] &= 0 \quad \text{in } [\Omega^p], \end{aligned} \quad (3.113)$$

such that coefficients  $\mathcal{T}^b$ ,  $\mathcal{T}^p$  and Peclet numbers  $Pe^b$ ,  $Pe^p$  are defined:

$$\mathcal{T}^b := \frac{(l_c^b)^2}{Dt_c} \stackrel{(3.58)}{=} \frac{2t_c^{D,b}}{t_c}, \quad \mathcal{T}^p := \frac{(l_c^p)^2}{Dt_c} \stackrel{(3.59)}{=} \frac{2t_c^{D,p}}{t_c}, \quad (3.114)$$

$$Pe^b := \frac{v_c^b l_c^b}{D} = -\frac{u_c l_c^b}{t_c D}, \quad Pe^p := \frac{v_c^{fp} l_c^p}{D} = -\frac{u_c l_c^p}{t_c D}, \quad (3.115)$$

where  $t_c^{D,b}$ ,  $t_c^{D,p}$  are the diffusion times estimated in *Section 3.1.4.3*. For either of the assumptions on the membrane permeability to the osmolytes ( $Ms$  or  $Ml$ ), the Peclet numbers are found to be much smaller than 1:

$$Pe^b < 10^{-2} \ll 1, \quad Pe^p < 10^{-2} \ll 1, \quad (3.116)$$

and so as noted above, the convective terms of the ICS and ECS equations (3.113) can be neglected:

$$\begin{aligned} \mathcal{T}^b[\partial_t c^b] - [\Delta c^b] &= 0 & \text{in } [\Omega^b], \\ \mathcal{T}^p[\partial_t c^{fp}] - [\Delta c^{fp}] &= 0 & \text{in } [\Omega^p]. \end{aligned} \quad (3.117)$$

*Note:* Since the velocity of the convective flux and the deformations are closely related, also on the scale of the diffusion time (i.e. setting  $t_c := t_c^{D,b}$  in  $\Omega^b$ ,  $t_c := t_c^{D,p}$  in  $\Omega^p$ ), the Peclet number is found to be of the order of the deformation to the domain length ratio ( $u^{sp}/l_c^p$  or  $u^{sp}/l_c^b$ ), which is assumed to be small.

As observed in *Section 3.1.4.3*, the diffusion and total observation times for the strictly semipermeable membrane experiments are comparable, thus in case  $Ms$ , the time derivative is an important term in each of the diffusion equations (3.117).

On the scale of the leaky semipermeable membrane ( $Ml$ ) observation time (3.57), coefficients  $\mathcal{T}^b$ ,  $\mathcal{T}^p$  are found to be very small, thus diffusion can be assumed to be instantaneous, and so the molarities  $c^{fp}$ ,  $c^b$  – spatially constant at each time step (point). Then instead of solving the diffusion equations (3.117), the molar concentrations  $c^{fp}(t) \in \Omega^p$ ,  $c^b(t) \in \Omega^b$ , changing in time due to the flow of water and osmolytes across the interface  $\Gamma^i$  (and if applicable, other boundaries) can be found through the fast diffusion model described in *Section 2.2.4*.

### 3.2.5 Interface conditions

*Continuity of normal fluxes* condition (2.60) takes the following form in dimensionless coordinates,

$$v_c^b[v^b]_n = \frac{u_c^{sp}}{t_c} [\partial_t u^{sp}]_n - \frac{kp^p \Delta}{\mu^f l_c^p} [\Delta p^p]_n \quad \text{at } [\Gamma^i],$$

such that owing to the choice of the pressure gradient scaling (3.103) and relations between the fluid phase, solid phase, bulk fluid velocities (3.83), it reduces to:

$$[v^b]_n + [\partial_t u^{sp}]_n = \gamma_0 [\Delta p^p]_n \quad \text{at } [\Gamma^i]. \quad (3.118)$$

In the *continuity of normal stresses* condition (2.61) written with respect to the dimensionless coordinates, the pressure difference across the interface is treated as a single variable as suggested in (3.81):

$$\begin{aligned} \frac{\mu^s u_c^{sp}}{l_c^p} \left( [\nabla u^{sp}] + [(\nabla u^{sp})^T] + \frac{\lambda^s}{\mu^s} [\nabla \cdot u^{sp}] I \right)_n &= \\ \frac{2\mu^f v_c^b}{l_c^b} \left( \nabla v^b + (\nabla v^b)^T \right)_n + p_c^\Delta [p^p - p^b] \cdot n & \quad \text{at } [\Gamma^i]. \end{aligned} \quad (3.119)$$

Dividing (3.119) by the elasticity coefficient  $\mu^s u_c^{sp}/l_c^p$  and employing (3.83),

$$\left( [\nabla u^{sp}] + [(\nabla u^{sp})^T] + 4[\nabla \cdot u^{sp}]I - \frac{2\mu^f l_c^p}{\mu^s t_c l_c^b} (\nabla v^b + (\nabla v^b)^T) \right)_n = \frac{l_c^p p_c^\Delta}{\mu^s u_c} [p^p - p^b] \cdot n \quad \text{at } [\Gamma^i], \quad (3.120)$$

it can be shown, that the viscous stress term is negligible compared to the elasticity terms:

$$\frac{2\mu^f l_c^p}{\mu^s t_c l_c^b} < 10^{-8}. \quad (3.121)$$

It then follows, that the transmembrane pressure difference is almost entirely balanced by the increase of the elastic stresses following the growth of the cell, and thus the characteristic pressure difference value  $p_c^\Delta$  is chosen such that the RHS of (3.120) is of the same order as its LHS,

$$\frac{l_c^p p_c^\Delta}{\mu^s u_c} := 1 \quad \Rightarrow \quad p_c^\Delta := \frac{\mu^s u_c}{l_c^p} \approx 0.2 \cdot 10^3 \text{ Pa}. \quad (3.122)$$

The obtained value shows agreement with the average transmembrane pressure difference  $p_{avg}^\Delta$  (3.31) estimated in Section (3.1.2.4).

Using (3.50), the *normal flux* interface condition (2.89) in dimensionless coordinates can be written in the following way:

$$\begin{aligned} v_c^{sp} ([v^b]_n + [v^{sp}]_n) &= j_c^b [j^b]_n = L^p (p_c^\Delta [p^\Delta] + \pi_c^\Delta [\pi^\Delta]) \quad \Rightarrow \\ [v^b]_n + [v^{sp}]_n &= \frac{L^p \pi_c^\Delta}{v_c^{sp}} \left( \frac{p_c^\Delta}{\pi_c^\Delta} [p^\Delta] + [\pi^\Delta] \right) \quad \text{at } [\Gamma^i]. \end{aligned} \quad (3.123)$$

Since the characteristic bulk fluid flow velocity  $v_c^b$  was chosen through the flux condition for the characteristic transmembrane pressure differences  $p_c^\Delta$ ,  $\pi_c^\Delta$ , see Section 3.1.4.1, the dimensionless coefficient on the RHS of (3.123) reduces to unity for either of the assumptions *Ms*, *ML*:

$$\frac{L^p \pi_c^\Delta}{v_c^{sp}} \approx 1 \quad (Ms, ML), \quad (3.124)$$

and the dimensionless flux condition (3.123) takes form:

$$[v^b]_n = (\Pi_c [p^\Delta] + [\pi^\Delta]) \quad \text{at } [\Gamma^i], \quad (3.125)$$

where coefficient  $\Pi_c$  is defined and estimated as:

$$\Pi_c := \frac{p_c^\Delta}{\pi_c^\Delta} \approx \begin{cases} 10^{-2}, & Ms, \\ 1, & ML. \end{cases} \quad (3.126)$$

It then follows, that in case the membrane is assumed to be *strictly* semipermeable, i.e. impermeable to the osmolytes, the hydraulic pressure difference at the interface is in average dominated by the osmotic pressure differences. For the leaky permeable membranes however, the effects of the osmotic and hydraulic transmembrane pressure differences are (in average) comparable.

### 3.3 Summary: data tables

The values given below are introduced and discussed in *Sections 3.1, 3.2*, and in columns "Ref.", the (sub)sections (or equations) in which the meaning, derivation or choice of the values is explained, are referenced.

**Table 3.1 Parameters (in SI units).**

		Unit	Value	Ref.
Temperature	$\Upsilon$	K	$3.1 \cdot 10^2$	3.1.1.1
Density of the fluid	$\rho^f$	kg/m <sup>d</sup>	$1.0 \cdot 10^3$	3.1.1.1
Density of the solid	$\rho^s$	kg/m <sup>d</sup>	$1.0 \cdot 10^3$	3.1.1.1
Dynamic viscosity of the fluid	$\mu^f$	kg/m <sup>d-2</sup> s	$1.0 \cdot 10^{-3}$	3.1.1.1
Diffusivity in $\Omega^b, \Omega^p$	$D$	m <sup>2</sup> /s	$1.0 \cdot 10^{-10}$	3.1.1.1
Shear modulus of $\Omega^{sp}$	$\mu^s$	kg/m <sup>d-2</sup> s <sup>2</sup>	$3.6 \cdot 10^3$	3.1.1.2
Lame's 1st parameter of $\Omega^{sp}$	$\lambda^s$	kg/m <sup>d-2</sup> s <sup>2</sup>	$1.4 \cdot 10^4$	3.1.1.2
Ratio $\lambda^s/\mu^s$	$\lambda^\mu$	–	4.0	3.1.1.2
Membrane permeability to water	$L^p$	m <sup>d-1</sup> s/kg	$1.0 \cdot 10^{-13}$	3.1.1.3
Permeability of $\Omega^p$ to water	$k$	m <sup>2</sup>	$2.5 \cdot 10^{-15}$	(3.20)
Osmotic pressure coefficient	$C_{osm}$	kg m <sup>2</sup> /s <sup>2</sup> mol	$2.58 \cdot 10^3$	(3.32)

**Table 3.2 Domain dimensions (in SI units).**

The measured lengths of the domains are depicted on *Fig. 3.1*.

		Unit	Value	Ref.
Size (half side length) of $\Omega$	$r^\Omega$	m	$15 \cdot 10^{-5}$	(3.12)
Initial outer radius of the cell	$r_0^c$	m	$5 \cdot 10^{-5}$	(3.4)
Constant inner radius of the cell	$r^{in}$	m	$0.50 \cdot 10^{-5}$	(3.5)
Initial size of $\Omega^p$	$l_0^p$	m	$4.5 \cdot 10^{-5}$	(3.6)
Initial min. size of $\Omega^b$	$l_0^b$	m	$10 \cdot 10^{-5}$	(3.13)
Initial porosity of $\Omega^p$	$\gamma_0^f$	–	0.5	(3.15)
Initial solidity of $\Omega^p$	$\gamma_0^s$	–	0.5	(3.15)
Terminal outer radius of $\Omega^p$	$r_T^c$	m	$5.25 \cdot 10^{-5}$	(3.8)
Total displacement in $\Omega^p$	$u_T^{sp}$	m	$0.253 \cdot 10^{-5}$	(3.9)
Total displacement in $\Omega^b$	$u_T^b$	m	$0.253 \cdot 10^{-5}$	(3.10)
Terminal solidity of $\Omega^p$	$\gamma_T^s$	–	0.433	(3.16)
Terminal porosity of $\Omega^p$	$\gamma_T^f$	–	0.567	(3.16)
Characteristic length of $\Omega^p$	$l_c^p$	m	$4.5 \cdot 10^{-5}$	(3.6)
Characteristic length of $\Omega^b$	$l_c^b$	m	$10 \cdot 10^{-5}$	(3.13)
Characteristic displacements	$u_c$	m	$0.253 \cdot 10^{-5}$	(3.10)
Diffusion time in $\Omega_t^b$	$t_c^{D,b}$	s	50	(3.58)
Diffusion time in $\Omega_t^p$	$t_c^{D,p}$	s	12	(3.59)
Ratio $u_c/l_c^p$	$\mathcal{R}_c^p$	–	0.056	(3.11)
Ratio $u_c/l_c^b$	$\mathcal{R}_c^b$	–	0.025	(3.11)

**Table 3.3 Description of further symbols.**

The following abbreviations are used below: HTPD – hydraulic transmembrane pressure difference, OTPD – osmotic transmembrane pressure difference, V. – volume, C. concentration, AoS – amount of substance. ch. – characteristic.

Time of observation	$t_c$	V. of $\Omega$	$V$
Ch. velocities in $\Omega_t^b, \Omega_t^p$	$v_c$	V. of $\Omega_0^c$	$V_0^c$
Initial velocities in $\Omega_0^b, \Omega_0^p$	$v_0$	V. of $\Omega_T^c$	$V_T^c$
		V. of $\Omega^{in}$	$V^{in}$
Ch. HTPD at $\Gamma_t^i$	$p_c^\Delta$	V. of $\Omega_0^p$	$V_0^p$
Initial HTPD at $\Gamma_0^i$	$p_0^\Delta$	V. of $\Omega_T^p$	$V_T^p$
Terminal HTPD at $\Gamma_T^i$	$p_T^\Delta$	V. of $\Omega_0^{fp}$	$V_0^{fp}$
		V. of $\Omega_T^{fp}$	$V_T^{fp}$
Ch. OTPD at $\Gamma_t^i$	$\pi_c^\Delta$	V. of $\Omega_0^b$	$V_0^b$
Initial OTPD at $\Gamma_0^i$	$\pi_0^\Delta$	V. of $\Omega_T^b$	$V_T^b$
Terminal OTPD at $\Gamma_T^i$	$\pi_T^\Delta$		
		C. in $\Omega_0^p$	$c_0^{fp}$
		C. in $\Omega_T^p$	$c_T^{fp}$
AoS in $\Omega_0^p$	$a_0^{fp}$	C. in $\Omega_0^b$	$c_0^b$
AoS in $\Omega_T^p$	$a_T^{fp}$	C. in $\Omega_T^b$	$c_T^b$
AoS in $\Omega_0^b$	$a_0^b$	Ch. C. difference at $\Gamma^i$	$c_c^\Delta$
AoS in $\Omega_T^b$	$a_T^b$	C. difference at $\Gamma_0^i$	$c_0^\Delta$
AoS shift at $\Gamma^i$	$a^{SH}$	C. difference at $\Gamma_T^i$	$c_T^\Delta$

**Table 3.4 Times, velocities and pressures (in SI units).**

The descriptions of the symbols are given in *Table 3.3*. Where necessary, the values estimated with the *strictly semipermeable* ("Ms") and *leaky semipermeable* membrane ("Ml") assumptions are distinguished and listed in respectively denoted columns.

Unit		$d = 3$		$d = 2$		Ref.
$p_c^\Delta$	kg/m <sup>d-2</sup> s <sup>2</sup>	0.2 · 10 <sup>3</sup>		0.939 · 10 <sup>3</sup>		(3.122)
$p_0^\Delta$	kg/m <sup>d-2</sup> s <sup>2</sup>	5.0		5.0		(3.24)
$p_T^\Delta$	kg/m <sup>d-2</sup> s <sup>2</sup>	2.618 · 10 <sup>3</sup>		1.873 · 10 <sup>3</sup>		(3.30)
$\pi_T^\Delta$	kg/m <sup>d-2</sup> s <sup>2</sup>	2.618 · 10 <sup>3</sup>		1.873 · 10 <sup>3</sup>		(3.36)
		<i>Ms</i>	<i>Ml</i>	<i>Ms</i>	<i>Ml</i>	
$t_c$	s	4.00 · 10 <sup>2</sup>	3.35 · 10 <sup>4</sup>	4.84 · 10 <sup>2</sup>	2.69 · 10 <sup>4</sup>	(3.56)/(3.57)
$v_c$	m/s	6.32 · 10 <sup>-9</sup>	7.55 · 10 <sup>-11</sup>	5.22 · 10 <sup>-9</sup>	9.34 · 10 <sup>-11</sup>	(3.51)
$v_0$	m/s	25 · 10 <sup>-9</sup>	0.0	20 · 10 <sup>-9</sup>	0.0	(3.54)/(3.53)
$\pi_c^\Delta$	kg/m <sup>d-2</sup> s <sup>2</sup>	1.26228 · 10 <sup>5</sup>	1.311 · 10 <sup>3</sup>	1.036 · 10 <sup>5</sup>	0.936 · 10 <sup>3</sup>	(3.41)/(3.45)
$\pi_0^\Delta$	kg/m <sup>d-2</sup> s <sup>2</sup>	2.49836 · 10 <sup>5</sup>	5.0	2.053 · 10 <sup>5</sup>	5.0	(3.40)/(3.24)

**Table 3.5 Volumes, amounts of substance and concentrations (in SI units).**

The values of the volumes of the domains are computed according to the relations (3.127); concentration and amount of substance values are discussed in Section 3.1.3. Where necessary, the values estimated with the *strictly semipermeable* ("Ms") and *leaky semipermeable* membrane ("Ml") assumptions are distinguished and listed in respectively denoted columns.

Volume units: [m<sup>d</sup>], concentration units: [mol/m<sup>d</sup>], amount of substance units: [mol].

The descriptions of the symbols are given in Table 3.3.

	$d = 3$		$d = 2$	
$V$	$27 \cdot 10^{-12}$		$90 \cdot 10^{-9}$	
$V_0^c$	$5.23599 \cdot 10^{-13}$		$7.8539 \cdot 10^{-9}$	
$V_T^c$	$6.07171 \cdot 10^{-13}$		$8.6689 \cdot 10^{-9}$	
$V^{in}$	$5.23599 \cdot 10^{-16}$		$7.8539 \cdot 10^{-11}$	
$V_0^p$	$5.23075 \cdot 10^{-13}$		$7.7754 \cdot 10^{-9}$	
$V_T^p$	$6.06647 \cdot 10^{-13}$		$8.5903 \cdot 10^{-9}$	
$V_0^{fp}$	$2.61538 \cdot 10^{-13}$		$3.8877 \cdot 10^{-9}$	
$V_T^{fp}$	$3.43969 \cdot 10^{-13}$		$4.8707 \cdot 10^{-9}$	
$V_0^b$	$264.769 \cdot 10^{-13}$		$82.2246 \cdot 10^{-9}$	
$V_T^b$	$263.934 \cdot 10^{-13}$		$81.4096 \cdot 10^{-9}$	
$a_T^{fp}$	$1.0354 \cdot 10^{-10}$		$1.46171 \cdot 10^{-6}$	
$a_T^b$	$7.918 \cdot 10^{-9}$		$24.372 \cdot 10^{-6}$	
$a^{SH}$	$2.50785 \cdot 10^{-11}$		$0.2954 \cdot 10^{-6}$	
$c_T^{fp}$	301.015		300.101	
$c_T^b$	300		299.375	
$c_T^\Delta$	1.01507		0.726232	
	<i>Ms</i>	<i>Ml</i>	<i>Ms</i>	<i>Ml</i>
$a_0^{fp}$	$1.0354 \cdot 10^{-10}$	$7.84613 \cdot 10^{-11}$	$1.46171 \cdot 10^{-6}$	$1.16632 \cdot 10^{-6}$
$a_0^b$	$7.918 \cdot 10^{-9}$	$7.94308 \cdot 10^{-09}$	$24.3772 \cdot 10^{-6}$	$24.6674 \cdot 10^{-6}$
$c_0^{fp}$	395.889	300.002	375.982	300.002
$c_0^b$	299.053	300	296.408	300.000
$c_0^\Delta$	96.8357	0.002	79.5747	0.002
$c_c^\Delta$	48.9254	0.508506	40.1505	0.364085

$$\begin{array}{l}
 V_0^p = V_0^c - V^{in} \\
 V_0^b = V - V_0^p \\
 V_T^p = V_T^c - V^{in} \\
 V_T^b = V - V_T^p \\
 V_0^{fp} = \gamma_0^f V_0^p \\
 V_T^{fp} = \gamma_T^f V_T^p
 \end{array}
 \quad
 \begin{array}{l}
 3D : \\
 V = (2r^\Omega)^3 \\
 V^{in} = \frac{4\pi}{3} (r^{in})^3 \\
 V_0^c = \frac{4\pi}{3} (r_0^c)^3 \\
 V_T^c = \frac{4\pi}{3} (r_T^c)^3
 \end{array}
 \quad
 \begin{array}{l}
 2D : \\
 V = (2r^\Omega)^2 \\
 V^{in} = \pi (r^{in})^2 \\
 V_0^c = \pi (r_0^c)^2 \\
 V_T^c = \pi (r_T^c)^2
 \end{array}
 \quad
 (3.127)$$



**Table 3.6 Data in the units of the numerical implementation.**

Below the parameters, characteristic (ch.), initial and terminal values that are used in the numerical implementations of the considered problems are listed. The data is translated from the SI units [m, kg, s, mol] into [ $\mu\text{m}$ , mg, min, mol] units as indicated in (3.128). Where necessary, the values estimated with the *strictly semipermeable* ("Ms") and *leaky semipermeable* membrane ("Ml") assumptions are distinguished and listed in respectively denoted columns. The descriptions of the symbols are given in Tables 3.1, 3.3.

	Unit				
$r^\Omega$	$\mu\text{m}$	150			
$r_0^c$	$\mu\text{m}$	50			
$r^{in}$	$\mu\text{m}$	5			
$r_T^c$	$\mu\text{m}$	52.5			
$u_c$	$\mu\text{m}$	2.53			
$C_{osm}$	mg $\mu\text{m}^2/\text{min}^2\text{mol}$	$9.288 \cdot 10^{24}$			
$\gamma^f$	–	0.5			
$k$	$\mu\text{m}^2$	$2.5 \cdot 10^{-3}$			
		$d = 3$		$d = 2$	
$L^p$	$\mu\text{m}^{d-1}\text{min}/\text{mg}$	$1.67 \cdot 10^{-9}$		$1.67 \cdot 10^{-15}$	
$\mu^f$	mg/ $\mu\text{m}^{d-2}$ min	$6 \cdot 10^{-2}$		$6 \cdot 10^4$	
$\mu^s$	mg/ $\mu\text{m}^{d-2}$ min <sup>2</sup>	$1.3 \cdot 10^7$		$1.3 \cdot 10^{13}$	
$\lambda^s$	mg/ $\mu\text{m}^{d-2}$ min <sup>2</sup>	$5.1 \cdot 10^7$		$5.1 \cdot 10^{13}$	
$p_0^\Delta$	mg/ $\mu\text{m}^{d-2}$ min <sup>2</sup>	$1.8 \cdot 10^4$		$1.8 \cdot 10^{10}$	
$p_T^\Delta$	mg/ $\mu\text{m}^{d-2}$ min <sup>2</sup>	$9.43 \cdot 10^6$		$6.745 \cdot 10^{12}$	
$\pi_T^\Delta$	mg/ $\mu\text{m}^{d-2}$ min <sup>2</sup>	$9.43 \cdot 10^6$		$6.745 \cdot 10^{12}$	
		<i>Ms</i>	<i>Ml</i>	<i>Ms</i>	<i>Ml</i>
$\pi_0^\Delta$	mg/ $\mu\text{m}^{d-2}$ min <sup>2</sup>	$8.994 \cdot 10^8$	$1.8 \cdot 10^4$	$7.391 \cdot 10^{14}$	$1.8 \cdot 10^{10}$
$t_c$	min	6.67	557.78	8.13	740.2
$v_c$	$\mu\text{m}/\text{min}$	0.38	$4.53 \cdot 10^{-3}$	0.31	$3.42 \cdot 10^{-3}$

$$1[\text{m}] = 10^6[\mu\text{m}], \quad 1[\text{kg}] = 10^6[\text{mg}], \quad 1[\text{s}] = 1/60[\text{min}] \approx 1.67 \cdot 10^{-2}[\text{min}] \quad (3.128)$$



## 4 Numerics and simulations

This chapter is devoted to a numerical treatment of the mathematical model for osmotic swelling of a brain cell. In the first section of the chapter, the *reduced* mathematical models, in particular, the coupled Biot-Stokes and pure Biot problems that are considered for the numerical simulations are formulated. The summary of the considered reduced problems is followed by the variational formulations for the Stokes and Biot problems.

The discretizations of the Biot and Stokes problems in space and time are described in *Section 4.2*. In particular, following the method of lines, both problems are spatially discretized using FEMs, and for the temporal discretization, the implicit Euler scheme is chosen.

An analytic solution of the stationary Biot problem defined on a rotationally or spherically symmetric domain is derived in *Section 4.3*, such that it can be later used in *Section 4.6* in order to verify the obtained numerical results.

*Section 4.4* summarizes the considered problems, outlines the time stepping scheme and the operator splitting approach implemented in the following section.

Some of the software related implementation aspects are mentioned in *Section 4.5*.

*Section 4.6* contains the results of numerical simulations for the Biot and Biot-Stokes problems.

### 4.1 Considered *reduced* problems

While certain assumptions allowing to derive a comprehensive model for the osmosis driven swelling of a brain cell have been made, the resulting mathematical model summarized in *Section 2.3* is still very complex. Therefore certain further assumptions are made, such that less elaborated problems can be formulated for numerical implementation.

In particular, the change of porosity and permeability, as well as the mechanical constraints introduced by the membrane are neglected. Also, it is assumed here, that the diffusion of the osmolytes is very fast compared to the transmembrane water flow; then as suggested in *Section 2.2.4*, the modelling of the osmotic pressure difference across the membrane can be simplified, and the transport equations can be dropped. These assumptions result in the reduction of the full One Cell Model formulated in the previous chapter to a quasi-stationary Biot-Stokes coupled problem influenced by osmotic pressure, where the latter one is modelled as a boundary force.

In addition to the *coupled system* describing the behaviour of both the cell and the extracellular space, an isolated or *pure Biot problem* describing the movement of the poroelastic cell interior is also formulated below.

#### 4.1.1 Biot-Stokes problem

The coupled Biot-Stokes problem is formulated on a bounded domain  $\Omega \in \mathbb{R}^d$ ,  $d \in \{2, 3\}$ , consisting of subdomains  $\Omega^b(t)$ ,  $\Omega^p(t)$  deforming over time  $t \in (0, T)$ , which are separated by a common interface  $\Gamma^i(t) := \partial\Omega^b(t) \cap \partial\Omega^p(t)$ . Domain  $\Omega^b(t)$  is filled with an incompressible Newtonian fluid described by the Stokes equations, and is bounded by the interface  $\Gamma^i(t)$  and

the fixed walls  $\Gamma^{bw}$ . Depending on the chosen set up,  $\Omega$  is either surrounded by stationary bulk fluid, or there can be distinguished impermeable  $\Gamma^{b,0}$ , inflow  $\Gamma^{b,in}$  and outflow  $\Gamma^{b,out}$  boundaries, such that  $\Gamma^{bw} := \Gamma^{b,0} \cup \Gamma^{b,in} \cup \Gamma^{b,out}$ . Domain  $\Omega^p(t)$  is occupied by a fully-saturated poroelastic matrix described by the Biot equations, and is bounded by the interface  $\Gamma^i(t)$  and the fixed impermeable inner boundary  $\Gamma^{pin}$ , see *Fig. 4.1*.

**Stokes domain**  $\Omega^b(t)$ ,  $t \in (0, T)$  (*extracellular fluid*):

$$\nabla \cdot \left\{ -p^b I + \mu^f \left( \nabla v^b + (\nabla v^b)^T \right) \right\} = 0, \quad (4.1)$$

$$\nabla \cdot v^b = 0, \quad (4.2)$$

$$\Delta u^b = 0, \quad (4.3)$$

where  $v^b$  – fluid velocity,  $\rho^f$  – fluid density,  $u^b$  – fluid domain displacement,  $\mu^f$  – dynamic fluid viscosity,  $p^b$  – fluid pressure.

**Biot domain**  $\Omega^p(t)$ ,  $t \in (0, T)$  (*cell interior*):

$$\nabla \cdot \left\{ -p^p I + \mu^s \left( \nabla u^{sp} + (\nabla u^{sp})^T \right) + \lambda^s \nabla \cdot u^{sp} I \right\} = 0, \quad (4.4)$$

$$\nabla \cdot \left( v^{sp} - \frac{k}{\mu^f} \nabla p^p \right) = 0, \quad (4.5)$$

$$v^{sp} - \partial_t u^{sp} = 0, \quad (4.6)$$

where  $u^{sp}$  – solid phase displacement,  $v^{sp}$  – solid phase velocity,  $p^p$  – pore fluid pressure,  $\rho^s$  ( $\rho^f$ ) – solid (fluid) density,  $\gamma^s$  ( $\gamma^f$ ) – solidity (porosity),  $\mu^f$  – dynamic fluid viscosity,  $k$  – permeability. Pore fluid velocity  $v^{fp}$  can be found from the solution of (4.4)-(4.6) through the modified Darcy law:

$$v^{fp} = v^{sp} - \frac{k}{\gamma^f \mu^f} \nabla p^p \stackrel{(4.6)}{=} \partial_t u^{sp} - \frac{k}{\gamma^f \mu^f} \nabla p^p. \quad (4.7)$$

Assuming that before the beginning of the observation there exists no movement of the solid phase, the *initial conditions* can be written as:

$$u^{sp} = 0 \quad \text{in } \Omega^p(0). \quad (4.8)$$

The inner *boundary*  $\Gamma^{pin}$  of the porous intracellular space  $\Omega^p(t)$  is assumed to be impermeable to the intracellular fluid and fixed, i.e.  $\Gamma^{pin}(t) \equiv \Gamma^{pin}(0)$ ,  $\forall t \in (0, T)$ , such that the solid matrix of the medium is attached to it:

$$u^{sp} = 0 \quad \text{at } \Gamma^{pin} \times (0, T), \quad (4.9)$$

$$v^{fp} = 0 \quad \text{at } \Gamma^{pin} \times (0, T). \quad (4.10)$$

While the condition (4.10) reflects the physical impermeability constraint, the intracellular velocity does not enter the Biot system (4.4)-(4.6), thus for the numerical implementation of either the Biot-Stokes or pure Biot problems, the condition on the flow velocity is equivalent to the pressure gradient condition:

$$\nabla p^p = 0 \quad \text{at } \Gamma^{pin} \times (0, T), \quad (4.11)$$

as follows from:

$$-\frac{k}{\gamma^f \mu^f} \nabla p^p \stackrel{(4.9)}{=} \partial_t u^{sp} - \frac{k}{\gamma^f \mu^f} \nabla p^p \stackrel{(4.7)}{=} v^{fp} \stackrel{(4.10)}{=} 0 \quad \text{at } \Gamma^{pin} \times (0, T).$$

External extracellular fluid boundary  $\Gamma^{bw}$  is also fixed, thus:

$$u^b = 0 \quad \text{at } \Gamma^{bw} \times (0, T). \quad (4.12)$$

Depending on the chosen experimental set up,  $\Gamma^{bw}$  can be split into impermeable  $\Gamma^{b,0}$ , inflow  $\Gamma^{b,in}$  and outflow  $\Gamma^{b,out}$  boundaries, such that:

$$\begin{aligned} v^b &= 0 & \text{at } \Gamma^{b,0} \times (0, T), \\ v^b &= v_{in}^b & \text{at } \Gamma^{b,in} \times (0, T), \\ \sigma_n^b &= p_{out}^b & \text{at } \Gamma^{b,out} \times (0, T). \end{aligned} \quad (4.13)$$

For all implemented problems (as presented in *Section 4.6*), the normal fluid stress is set to zero along the entire  $\Gamma^{bw}$ :

$$\sigma_n^b = 0 \quad \text{at } \Gamma^{bw} \times (0, T), \quad (4.14)$$

thus corresponding to the conditions of the experimental settings **E3**.

As suggested in the previous chapter, the Biot and Stokes domains are coupled at the *interface*  $\Gamma^i(t)$ ,  $t \in (0, T)$ , according to the following laws:

$$j_n^b = j_n^p \Rightarrow v_n^b = \left( v^{sp} - \frac{k}{\mu^f} \nabla p^p \right)_n, \quad (4.15)$$

$$v_\tau^b = 0, \quad (4.16)$$

$$u^b = u^{sp}, \quad (4.17)$$

$$\sigma^p \cdot n = \sigma^b \cdot n, \quad (4.18)$$

$$j^p \cdot n = L^p \left( p^b - p^p + \pi^\Delta \right), \quad (4.19)$$

where  $\sigma^b$ ,  $\sigma^p$  are the fluid and poroelastic stress tensors correspondingly:

$$\begin{aligned} \sigma^b &:= -p^b I + \mu^f \left( \nabla v^b + (\nabla v^b)^T \right), \\ \sigma^p &:= -p^p I + \mu^s \left( \nabla u^{sp} + (\nabla u^{sp})^T \right) + \lambda^s \nabla \cdot u^{sp} I, \end{aligned} \quad (4.20)$$

$j_n^b$ ,  $j_n^p$  are the normal fluid fluxes defined at the boundaries of the Stokes and Biot domains respectively:

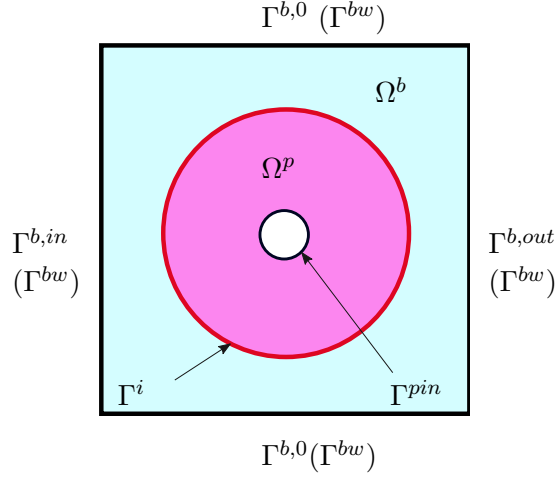
$$j_n^b := (j^b \cdot n)n, \quad j^b \cdot n := (v^b - \partial_t u^b) \cdot n \quad \text{at } \partial\Omega^b(t) \times (0, T), \quad (4.21)$$

$$j_n^p := (j^p \cdot n)n, \quad j^p \cdot n := \gamma^f (v^{fp} - v^{sp}) \cdot n \stackrel{(4.7)}{=} -\frac{k}{\mu^f} \nabla p^p \quad \text{at } \partial\Omega^p(t) \times (0, T), \quad (4.22)$$

$L^p$  is the membrane water permeability and  $\pi^\Delta$  in (4.19) is the osmotic pressure difference across the interface. Some ways of modelling (approximating) the transmembrane osmotic pressure difference  $\pi^\Delta$  without solving transport equations for the solute concentrations are suggested in

## Section 4.6.

**Figure 4.1 Overall domain**  $\Omega = \Omega^b(t) \cup \Omega^p(t) \in \mathbb{R}^d$ ,  $d \in \{2, 3\}$ ,  $t \in (0, T)$ .  
 $\Omega^p(t)$  – poroelastic Biot domain,  $\Omega^b(t)$  – Stokes fluid domain,  
 $\Gamma^i(t) := \partial\Omega^b(t) \cap \partial\Omega^p(t)$  – moving interface,  $\Gamma^{pin}$  – fixed impermeable inner wall,  
 $\Gamma^{bw} (:= \Gamma^{b,0} \cup \Gamma^{b,in} \cup \Gamma^{b,out})$  – fixed extracellular fluid walls.



#### 4.1.2 Pure Biot problem

The pure Biot problem is formulated on a domain  $\Omega^p(t) \in \mathbb{R}^d$ ,  $d \in \{2, 3\}$ , deforming over time  $t \in (0, T)$  and occupied by a fully-saturated poroelastic medium bounded by a moving (free) boundary  $\Gamma^i(t)$  and fixed impermeable inner wall  $\Gamma^{pin}$ , see *Figure 4.2*.

$$\nabla \cdot \left\{ -p^p I + \mu^s \left( \nabla u^{sp} + (\nabla u^{sp})^T \right) + \lambda^s \nabla \cdot u^{sp} I \right\} = 0 \quad \text{in } \Omega^p(t) \times (0, T), \quad (4.23)$$

$$\nabla \cdot \left( v^{sp} - \frac{k}{\mu^f} \nabla p^p \right) = 0 \quad \text{in } \Omega^p(t) \times (0, T), \quad (4.24)$$

$$v^{sp} - \partial_t u^{sp} = 0 \quad \text{in } \Omega^p(t) \times (0, T), \quad (4.25)$$

where  $u^{sp}$  – solid phase displacement,  $v^{sp}$  – solid phase velocity,  $p^p$  – pore fluid pressure,  $\rho^s$  ( $\rho^f$ ) – solid (fluid) density,  $\gamma^s$  ( $\gamma^f$ ) – solidity (porosity),  $\mu^f$  – dynamic fluid viscosity,  $k$  – permeability. Pore fluid velocity  $v^{fp}$  can be additionally found from the solution of (4.23)-(4.25) through the modified Darcy law:

$$v^{fp} = v^{sp} - \frac{k}{\gamma^f \mu^f} \nabla p^p \quad \text{in } \Omega^p(t) \times (0, T). \quad (4.26)$$

**Inner boundary**  $\Gamma^{pin}$  is assumed to be fixed and impermeable:

$$\nabla p^p = 0 \quad \text{at } \Gamma^{pin} \times (0, T) \quad (4.27)$$

$$u^{sp} = 0 \quad \text{at } \Gamma^{pin} \times (0, T) \quad (4.28)$$

where the pressure gradient boundary condition is derived in (4.11).

As in the coupled Biot-Stokes system, the *Pure Biot* problem is supposed to approximate movement of a swelling cell, therefore the conditions at the **outer moving boundary**  $\Gamma^i(t)$  would be chosen such as to mimic the influence of the extracellular fluid. Thus choosing to prescribe the normal flux  $j_n^p$  and normal stresses  $\sigma_n^p$ , and then selecting the corresponding equations from the coupling interface conditions (4.15)-(4.19), the conditions for the pure Biot problem at the outer boundary read:

$$\begin{aligned} j_n^p &:= L^p \left( p^b - p^p + \pi^\Delta \right) & \text{at } \Gamma^i(t) \times (0, T), \\ \sigma^p \cdot n &:= \sigma^b \cdot n \end{aligned}$$

which (using the definition of flux (4.22) and estimate (3.121) allowing to neglect the viscous fluid stress) can be rewritten as:

$$\frac{k}{\mu^f} \nabla p^p \cdot n = L^p \left( p^p - p^b - \pi^\Delta \right) \quad \text{at } \Gamma^i(t) \times (0, T), \quad (4.29)$$

$$\left\{ \mu^s \left( \nabla u^{sp} + (\nabla u^{sp})^T \right) + \lambda^s \nabla \cdot u^{sp} I \right\} \cdot n = (p^p - p^b) \cdot n \quad \text{at } \Gamma^i(t) \times (0, T), \quad (4.30)$$

where  $\pi^\Delta$  is the osmotic pressure difference across  $\Gamma^i(t)$ , and  $p^b$  is a given function reflecting the extracellular hydraulic pressure. Assuming that the extracellular pressure remains constant,  $p^b$  can be chosen as:

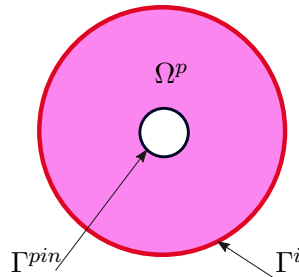
$$p^b := p_0^b \quad (\text{or } p_c^b) \quad (4.31)$$

where  $p_0^b$ ,  $p_c^b$  are the initial and characteristic bulk fluid pressure values estimated in *Section 3.1.2.4* and listed in *Tables 3.3*.

Assuming that before the beginning of the observation, the intracellular domain is at rest, the **initial conditions** can be written as:

$$u^{sp} = 0 \quad \text{in } \Omega_0^p. \quad (4.32)$$

**Figure 4.2 Pure Biot domain**  $\Omega^p(t) \in \mathbb{R}^d$ ,  $d \in \{2, 3\}$ ,  $t \in (0, T)$ .  
 $\Gamma^i(t)$  – moving boundary,  $\Gamma^{pin}$  – fixed impermeable inner wall.



### 4.1.3 Variational formulations

The variational formulation of the Stokes problem formulated on the extracellular bulk fluid domain  $\Omega^b(t)$  bounded by  $\Gamma^b(t) := \partial\Omega^b(t)$ ,  $t \in (O, T)$ , consists of finding  $(v^b, p^b, u^b) \in V^b \times Q^b \times V^b$ , such that for all  $(\phi^b, \psi^b, \eta^b) \in V^b \times Q^b \times V^b$  the following equalities hold:

$$\begin{aligned} \left( \mu^f \left( \nabla v^b + (\nabla v^b)^T \right) - p^b I, \nabla \phi^b \right)_{\Omega^b(t)} &= \left\langle \left( \mu^f \left( \nabla v^b + (\nabla v^b)^T \right) - p^b I \right) \cdot n^b, \phi^b \right\rangle_{\Gamma^b(t)}, \\ \left( \nabla \cdot v^b, \psi^b \right)_{\Omega^b(t)} &= 0, \\ \left( \nabla u^b, \nabla \eta^b \right)_{\Omega^b(t)} &= \left\langle \nabla u^b n^b, \eta^b \right\rangle_{\Gamma^b(t)}, \end{aligned} \quad (4.33)$$

where for the mapping  $\hat{T}_t^b : \hat{\Omega}^b \rightarrow \Omega^b(t)$ , see (2.44), the corresponding functional spaces are defined as:

$$\begin{aligned} V^b(t) &:= \{v : \Omega^b(t) \rightarrow \mathbb{R}^d, v(x, t) = \hat{T}_t^b(\hat{v}), \hat{v} \in H^1(\hat{\Omega}^b)^d\} \subset H^1(\Omega^b(t))^d, \\ Q^b(t) &:= \{q : \Omega^b(t) \rightarrow \mathbb{R}, q(x, t) = \hat{T}_t^b(\hat{q}), \hat{q} \in L^2(\hat{\Omega}^b)\} \subset L^2(\Omega^b(t)), \end{aligned} \quad d = \{2, 3\}.$$

The variational formulation of the Biot problem formulated on the deformable porous medium  $\Omega^p(t)$  bounded by  $\Gamma^p(t) := \partial\Omega^p(t)$ ,  $t \in (O, T)$ , consists of finding  $(u^{sp}, p^p, v^{sp}) \in U^p \times Q^p \times U^p$ , such that for all  $(\xi^p, \psi^p, \eta^p) \in U^p \times Q^p \times U^p$  the following equations hold:

$$\begin{aligned} \left( \mu^s \left( \nabla u^{sp} + (\nabla u^{sp})^T \right) + \lambda^s \nabla \cdot u^{sp} I, \nabla \xi^p \right)_{\Omega^p(t)} - \left( p^p, \nabla \cdot \xi^p \right)_{\Omega^p(t)} &= \\ \left\langle \left( \mu^s \left( \nabla u^{sp} + (\nabla u^{sp})^T \right) + (\lambda^s \nabla \cdot u^{sp} - p^p) I \right) \cdot n, \xi^p \right\rangle_{\partial\Omega^p(t)}, \\ \left( \nabla \cdot v^{sp}, \psi^p \right)_{\Omega^p(t)} + \frac{k}{\mu^f} \left( \nabla p^p, \nabla \psi^p \right)_{\Omega^p(t)} &= \\ \frac{k}{\mu^f} \left\langle \nabla p^p \cdot n, \psi^p \right\rangle_{\partial\Omega^p(t)}, \\ \left( v^{sp}, \eta^p \right)_{\Omega^p(t)} &= \left( \partial_t u^{sp}, \eta^p \right)_{\Omega^p(t)}, \end{aligned} \quad (4.34)$$

where for the mapping  $\hat{T}_t^p$ , see (2.40), the corresponding functional spaces are defined as:

$$\begin{aligned} U^p(t) &= \{w : \Omega^p(t) \rightarrow \mathbb{R}^d, w(x, t) = \hat{T}_t^p(\hat{w}), \hat{w} \in H^1(\hat{\Omega}^p)^d\} \subset H^1(\Omega^p(t))^d, \\ Q^p(t) &= \{q : \Omega^p(t) \rightarrow \mathbb{R}, q(x, t) = \hat{T}_t^p(\hat{q}), \hat{q} \in H^1(\hat{\Omega}^p)\} \subset H^1(\Omega^p(t)), \end{aligned} \quad d = \{2, 3\}.$$

## 4.2 Discretisation

In this chapter, the Biot and Stokes problems are numerically discretized in space and time following the *method of lines*. For the spatial discretization, the **Finite Element Method (FEM)** techniques – in particular, the standard Galerkin method – are chosen. The time discretization is done using the  $\theta$ -scheme approach, namely, the **implicit backward Euler** method.



### 4.2.1 Spatial discretization

In order to outline the finite element discretization scheme and to introduce the general concepts that are repeatedly addressed, first a general time dependent system of equations is considered. In particular, for a variable  $v(x, t)$  defined on a moving domain  $\Omega(t) \in \mathbb{R}^d \times (0, T)$ ,  $d \in \{1, 2, 3\}$  being the dimension of the problem, with boundary  $\Gamma(t) := \partial\Omega(t)$ , consider the following boundary value problem:

$$O(v(x, t)) = f(x, t), \quad x \in \Omega(t) \times (0, T), \quad (4.35)$$

$$(4.36)$$

where  $O$  is a first or second order partial differential operator and  $f(x, t)$  is some algebraic function. Multiplying equation (4.35) by weighting (test) functions  $w \in (W(t))^d$ , where  $(W(t))^d$  is some suitable continuous trial function space (as a rule chosen such that the Dirichlet values are zero), then integrating the equation over the domain  $\Omega(t)$  and applying integration by parts to the terms containing second order derivatives, the following variational formulation of the original equation (4.35) is obtained:

$$o(v, w)_{\Omega(t)} = - (f, w)_{\Omega(t)} + o^s \langle v, w \rangle_{\Gamma(t)} \quad \forall w \in (W(t))^d, \quad (4.37)$$

where  $o, o^s$  are spatial and boundary operators resulting from applying integration by parts to the higher order terms of the operator  $O$ , i.e.:

$$(O(v), w)_{\Omega(t)} := o^s \langle v, w \rangle_{\Gamma(t)} - o(v, w)_{\Omega(t)} \quad \forall w \in (W(t))^d.$$

Thus the original problem reduces to finding a solution  $v \in (V(t))^d$  that satisfies (4.37), where  $(V(t))^d$  is a space of lower (than the original) differential order due to the reduction of the order of the operator  $O$ .

For the problem (4.37) to be solved numerically, the infinite dimensional *trial* (or *admissible*)  $(V(t))^d$  and test  $(W(t))^d$  function spaces are approximated by appropriate **finite** dimensional subspaces  $(V_h(t))^d, (W_h(t))^d$  (with  $(V_h(t))^d \subset (V(t))^d$  corresponding to a *conforming* finite element method), such that the continuous problem (4.37) is reformulated into finding an **approximate solution**  $v_h(x, t) \in (V_h(t))^d$  tested against a finite number of test functions  $w_h \in (W_h(t))^d$ .

In case variable  $v$  is a **scalar** function, the finite subspaces  $V_h(t), W_h(t)$  can be defined through some basis (nodal) functions  $\{\nu_h^i(x, t)\}_{i=1}^N, \{\omega_h^i(x, t)\}_{i=1}^N$  in the following way:

$$V_h(t) = \text{span}\{\nu_h^i(x, t)\}_{i=1}^N, \quad W_h(t) = \text{span}\{\omega_h^i(x, t)\}_{i=1}^N,$$

where  $N$  is the dimension of the finite subspaces or the number of the degrees of freedom. Then the approximate solution  $v_h(x, t)$  can be represented through the basis of the finite trial space  $\{\nu_h^i(x, t)\}_{i=1}^N$  with some coefficients  $\{v^i(t)\}_{i=1}^N$ :

$$v_h(x, t) = \sum_{i=1}^N v^i(t) \nu_h^i(x, t). \quad (4.38)$$

It should be noted, that while it is convenient to choose the coefficients  $v^i$  and the basis functions  $\nu_h^i$  according to the principle of *variable separation* (i.e. such that  $\nu_h^i := \nu_h^i(x), v^i := v^i(t)$ ), such approach is not acceptable for problems defined on moving domains, since the basis functions

must reflect temporal changes. The coefficients  $v^i$  however can be chosen to depend only on time, in which case spatial derivatives applied to  $v_h(x, t)$  would relate only to the basis functions  $\nu_h^i$ :

$$\nabla v_h(x, t) := \sum_{i=1}^N v_i(t) \nabla \nu_h^i(x, t).$$

For a **vector** function  $\mathbf{v}$ , vector trial space  $(V_h(t))^d$ ,  $d = \{2, 3\}$ ,  $t \in (0, T)$ , can be defined through the corresponding vector basis functions  $\{\nu_h^n(x, t)\}_{n=1}^{d \times N}$ :

$$\nu_h^n(x, t) = [\nu_{h,1}^n(x, t), \dots, \nu_{h,d}^n(x, t)], \quad n = 1 \dots d \times N,$$

such that

$$(V_h(t))^d = V_h(t) \times (V_h(t))^{d-1}, \quad (V_h(t))^d = \text{span}\{\nu_h^n(x)\}_{n=1}^{d \times N}.$$

The components of the vector valued function  $\mathbf{v}_h \in (V_h(t))^d$  are scalar functions  $v_{h,k} \in V_h(t)$ ,  $k = 1 \dots d$ , that as described above, can be represented by the basis functions  $\{\nu_h^i\}_{i=1}^N \in V_h(t)$  with coefficients  $\{v_k^i\}_{i=1}^N$ :

$$v_{h,k}(x, t) = \sum_{i=1}^N v_k^i(t) \nu_h^i(x, t), \quad k = 1 \dots d, \quad (4.39)$$

and therefore the vector valued function  $\mathbf{v}_h$  can be written as:

$$\mathbf{v}_h(x, t) = \sum_{k=1}^d \sum_{i=1}^N v_k^i(t) \nu_h^i(x, t) \mathbf{e}_k, \quad (4.40)$$

where  $\{\mathbf{e}_k\}_{k=1}^d$  are  $d$ -dimensional Cartesian unit vectors. Thus for  $N$  nodal basis functions  $\{\nu_h^i\}_{i=1}^N$ , the set of basis vector functions is defined as:

$$\nu_h^n(x, t) = \nu_h^m(x, t) \mathbf{e}_\alpha, \quad \begin{aligned} m &= [(n-1) \bmod N] + 1, \\ \alpha &:= [(n-1)/N] + 1. \end{aligned} \quad (4.41)$$

Choosing the basis  $\{\omega_h^i\}_{i=1}^N$  for the test space  $(W_h(t))^d$  to correspond to the trial basis  $\{\nu_h^i\}_{i=1}^N$ , such that:

$$\omega_h^i \equiv \nu_h^i \quad \forall i = 1 \dots N \quad \Rightarrow \quad (W_h(t))^d \equiv (V_h(t))^d,$$

corresponds to the so-called (Bubnov-)Galerkin method or classical **Galerkin method**.

Thus eventually the original problem (4.35) reduces to finding a weak approximate solution  $\mathbf{v}_h \in (V_h(t))^d$  tested against a finite number of basis (vector) functions  $\nu_h^i \in (V_h(t))^d$ :

$$o(\mathbf{v}_h, \nu_h^i)_{\Omega(t)} = - (f_h, \nu_h^i)_{\Omega(t)} + o^s \langle \mathbf{v}_h, \nu_h^i \rangle_{\Gamma(t)} \quad \forall \nu_h^i \in (V_h(t))^d, \quad i = 1 \dots N. \quad (4.42)$$

In order to define the trial and test **spaces**  $(V_h(t))^d$ ,  $(W_h(t))^d$ , a triangulation of the domain  $\Omega$

into  $N_e$  open non-overlapping subregions (also called *elements* or *cells*)  $\Omega_{h,e}$  is introduced:

$$\begin{aligned}\Omega_h &:= \bigcup_{e=1}^{N_e} \Omega_{h,e}, & \Omega_{h,i} \cap \Omega_{h,j} &= \emptyset, \quad i \neq j. \\ \bar{\Omega} &= \Omega_h \subseteq \Omega,\end{aligned}\tag{4.43}$$

The **mesh**  $\Omega_h$  is said to be *structurally regular*, if the closures of two distinct elements  $\Omega_{h,i}$ ,  $\Omega_{h,j}$  can either have no intersections, or share a common vertex, edge or face, and *shape regular*, if its geometry does not degenerate. In this work, the meshes are constructed such that these regularity conditions are fulfilled. In particular, the computational domain is approximated by a mesh consisting of simplexes (triangles in 2D and tetrahedra in 3D).

On the mesh  $\Omega_h$ , a space of **continuous piecewise polynomial functions** is defined:

$$P_r(\Omega_h) := \left\{ \phi : \Omega_h \rightarrow \mathbb{R} \mid \phi \in C(\Omega_h), \quad \phi|_{\Omega_{h,e}} \in P^r(\Omega_{h,e}) \right\},\tag{4.44}$$

where on each element  $\Omega_{h,e}$ ,  $e = 1 \dots N_e$ , space  $P_r^e(\Omega_{h,e})$  is defined as a space of polynomials of **maximum order**  $r$ :

$$P_r^e(\Omega_{h,e}) := \text{span} \left\{ (x_1^{\gamma_1}, \dots, x_d^{\gamma_d}) \mid 0 \leq \sum_{k=1}^d \gamma_k \leq r, \quad x := (x_1, \dots, x_d) \in \Omega_{h,e} \right\}.$$

Choosing a set of  $N_o$  Lagrangian nodal points  $x_j$  (or simply *nodes*; not to be confused with the mesh vertices, see *Figure 4.3*) on each element  $\Omega_{h,e}$  that sum up to  $N$  nodes  $x_j$ ,  $j = 1 \dots N$ , over the entire mesh  $\Omega_h$ , a continuous **Lagrangian nodal basis**  $\{\nu_h^i\}_{i=1}^{d \times N}$  is defined as:

$$\begin{aligned}P_r(\Omega_h) &:= \text{span} \left\{ \nu_h^i \right\}_{i=1}^{d \times N}, \\ \nu_h^n(x) &:= \nu_h^m(x) \mathbf{e}_\alpha, \quad \forall n = 1 \dots d \times N, \quad m = [(n-1) \bmod N] + 1, \quad \alpha := [(n-1)/N] + 1,\end{aligned}$$

such that on each nodal point  $x_j$ ,  $j = 1 \dots N$ , exactly one basis function is non-zero and is equal to 1, and the set of functions  $\{\nu_h^i\}_{i=1}^N$  defines a partition of unity:

$$\begin{aligned}\nu_h^i(x_j) &= \delta_{ij} & \forall i, j = 1 \dots N, \\ \sum_{i=1}^N \nu_h^i(x) &= 1 & \forall x \in \Omega_h,\end{aligned}$$

where  $\delta_{ij}$  is the Kronecker delta function.

Then the scalar basis functions  $\{\nu_h^i\}$ ,  $i = 1 \dots N$ , can be used to interpolate the approximate solution  $\mathbf{v}_h$  over the entire domain:

$$\mathbf{v}_h(x, t) = \sum_{k=1}^d \sum_{i=1}^N v_k^i(t) \nu_h^i(x, t) \mathbf{e}_k \quad \forall x \in \Omega_h, \quad d = \{1, 2, 3\},\tag{4.45}$$

where  $v_k^i(t)$  are the nodal coefficients:

$$v_k^i(t) := v_{h,k}(x_i, t), \quad i = 1 \dots N, \quad k = 1 \dots d.$$

The simplest examples for the choice of space (4.44) include  $P_1$  – **piecewise linear** functions,

and  $P_2$  – *piecewise quadratic* functions. Thus in order to define a linear basis over a triangular element, the nodal points  $N_o$  can be chosen to coincide with the vertices of the element, i.e. in two dimensions each element contains 3 nodal points, and in three dimensions – 4 points. For the definition of a quadratic basis,  $N_o := 6$  is chosen for  $d = 2$  and  $N_o := 10$  – for  $d = 3$ , see *Figure 4.3*.

*Note:* The (initially regular) mesh is *moving*, thus its regularity must be ensured at all times. Yet the deformations considered in this work are sufficiently small, thus no special measures in order to preserve shape regularity of the moving mesh are needed to be applied.

Regarding the operators that are relevant for the Biot-Stokes problem, the following bilinear forms on vectors  $\mathbf{v}$ ,  $\mathbf{w}$  or/and scalars  $p$ ,  $q$  are defined:

$$m(\mathbf{v}, \mathbf{w})_\Omega := (\mathbf{v}, \mathbf{w})_{\Omega(t)}, \tag{4.46}$$

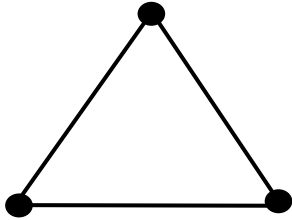
$$\begin{aligned} a(\mathbf{v}, \mathbf{w})_\Omega &:= (\nabla \mathbf{v}, \nabla \mathbf{w})_{\Omega(t)}, & \widehat{a}(\mathbf{v}, \mathbf{w})_\Gamma &:= (\nabla \mathbf{v}, \mathbf{n}\mathbf{w})_{\Gamma(t)}, \\ a'(\mathbf{v}, \mathbf{w})_\Omega &:= ((\nabla \mathbf{v})^T, \nabla \mathbf{w})_{\Omega(t)}, & \widehat{a}'(\mathbf{v}, \mathbf{w})_\Gamma &:= ((\nabla \mathbf{v})^T, \mathbf{n}\mathbf{w})_{\Gamma(t)} \\ a''(\mathbf{v}, \mathbf{w})_\Omega &:= ((\nabla \cdot \mathbf{v})I, \nabla \mathbf{w})_{\Omega(t)}, & \widehat{a}''(\mathbf{v}, \mathbf{w})_\Gamma &:= ((\nabla \cdot \mathbf{v})I, \mathbf{n}\mathbf{w})_{\Gamma(t)}, \end{aligned} \tag{4.47}$$

$$b(\mathbf{v}, p)_\Omega := (\nabla \cdot \mathbf{v}, p)_{\Omega(t)}, \quad b(p, \mathbf{v})_\Omega := (\nabla p, \mathbf{v})_{\Omega(t)}, \quad \widehat{b}(\mathbf{v}, p)_\Gamma := (\mathbf{n} \cdot \mathbf{v}, p)_{\Gamma(t)}, \tag{4.48}$$

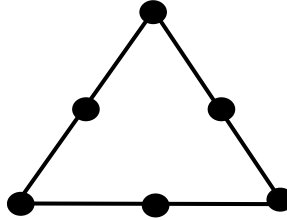
where  $\mathbf{n}$  is the unit normal vector to the boundary  $\Gamma(t)$ ,  $I$  is the identity matrix and  $A^T$  denotes the transposed matrix  $A$ .

**Figure 4.3 Nodal points of  $P_1$ ,  $P_2$  simplex elements in dimensions  $d = \{2, 3\}$ .**

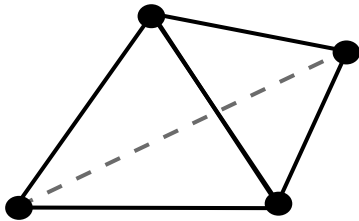
(a)  $P_1$ ,  $d = 2$ ,  $N_o = 3$ :



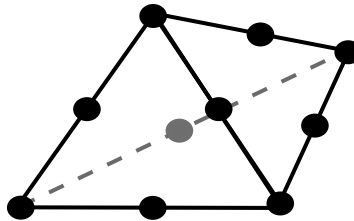
(b)  $P_2$ ,  $d = 2$ ,  $N_o = 6$ :



(c)  $P_1$ ,  $d = 3$ ,  $N_o = 4$ :



(d)  $P_2$ ,  $d = 3$ ,  $N_o = 10$ :



### 4.2.1.1 Stokes problem

Following the construction of the Lagrangian nodal basis described in the previous section, a triangulation  $\Omega_h^b$  of the domain  $\Omega^b(t)$  into  $N_e^b$  elements  $\Omega_{h,e}^b$  is introduced:

$$\begin{aligned}\Omega_h^b &:= \bigcup_{e=1}^{N_e^b} \Omega_{h,e}^b, & \Omega_{h,i}^b \cap \Omega_{h,j}^b &= \emptyset, \quad i \neq j, \\ \overline{\Omega^b} &= \overline{\Omega_h^b} \subseteq \overline{\Omega^b},\end{aligned}\tag{4.49}$$

For each of the variables, on the Stokes domain mesh  $\Omega_h^b$ , a number of Lagrangian points is chosen, i.e.,  $N^{b,v}$  nodes for  $v^b$ ,  $N^{b,p}$  nodes for  $p^b$ ,  $N^{b,u}$  nodes for  $u^b$ , and thus corresponding vector or scalar finite dimensional Lagrangian nodal bases are defined:

$$\begin{aligned}\left\{ \phi_h^{b,n}(x, t) \right\}_{n=1}^{d \times N^{b,v}}, & \quad \phi_h^{b,n}(x, t) = \phi_h^{b,m}(x, t) \mathbf{e}_\alpha, \\ & \quad m := [(n-1) \bmod N^{b,v}] + 1, \quad \alpha := [(n-1)/N^{b,v}] + 1, \\ \left\{ \psi_h^{b,i}(x, t) \right\}_{i=1}^{N^{b,p}}, & \\ \left\{ \xi_h^{b,n}(x, t) \right\}_{n=1}^{d \times N^{b,u}}, & \quad \xi_h^{b,n}(x, t) = \xi_h^{b,m}(x, t) \mathbf{e}_\alpha, \\ & \quad m := [(n-1) \bmod N^{b,u}] + 1, \quad \alpha := [(n-1)/N^{b,u}] + 1,\end{aligned}$$

where  $\left\{ \phi_h^{b,i} \right\}_{i=1}^{N^{b,v}}$ ,  $\left\{ \xi_h^{b,i} \right\}_{i=1}^{N^{b,u}}$  are scalar basis functions used to define the corresponding vector basis functions. Then the approximate solution  $\left\{ \mathbf{v}_h^b(x, t), p_h^b(x, t), \mathbf{u}_h^b(x, t) \right\}$  can be represented through the basis functions  $\left\{ \phi_h^{b,i}(x, t), \psi_h^{b,i}(x, t), \xi_h^{b,i}(x, t) \right\}$  as:

$$\begin{aligned}\mathbf{v}_h^b(x, t) &= \sum_{k=1}^d \sum_{i=1}^{N^{b,v}} v_k^{b,i}(t) \phi_h^{b,i}(x, t) \mathbf{e}_k, & p_h^b(x, t) &= \sum_{i=1}^{N^{b,p}} p^{b,i}(t) \psi_h^{b,i}(x, t), \\ \mathbf{u}_h^b(x, t) &= \sum_{k=1}^d \sum_{i=1}^{N^{b,u}} u_k^{b,i}(t) \xi_h^{b,i}(x, t) \mathbf{e}_k,\end{aligned}\tag{4.50}$$

where  $\left\{ v_k^{b,i}(t), p^{b,i}(t), u_k^{b,i}(t) \right\}$  are the nodal coefficients for the corresponding functions.

Using the bilinear forms notations (4.46)-(4.48), the continuous variational formulation (4.33) for the Stokes problem on  $\Omega^b(t)$  can be rewritten in finite dimensions in the following way:

find  $(\mathbf{v}_h^b, p_h^b, \mathbf{u}_h^b) \in V_h^b(t) \times Q_h^b(t) \times V_h^b(t)$  such that for all  $(\phi^b, \psi^b, \xi^b) \in V_h^b(t) \times Q_h^b(t) \times V_h^b(t)$ :

$$\begin{aligned}\mu^f a(\mathbf{v}_h^b, \phi_h^{b,n})_{\Omega_h^b} + \mu^f a'(\mathbf{v}_h^b, \phi_h^{b,n})_{\Omega_h^b} - b(\phi_h^{b,n}, p_h^b)_{\Omega_h^b} - \\ \mu^f \hat{a}(\mathbf{v}_h^b, \phi_h^{b,n})_{\Gamma_h^b} + \mu^f \hat{a}'(\mathbf{v}_h^b, \phi_h^{b,n})_{\Gamma_h^b} - \hat{b}(\phi_h^{b,n}, p_h^b)_{\Gamma_h^b} = 0 & \quad \forall \phi_h^{b,n} \in V_h^b(t), \\ b(\mathbf{v}_h^b, \psi_h^{b,i})_{\Omega_h^b} = 0 & \quad \forall \psi_h^{b,i} \in Q_h^b(t), \\ a(\mathbf{u}_h^b, \xi_h^{b,n})_{\Omega_h^b} - \hat{a}(\mathbf{u}_h^b, \xi_h^{b,n})_{\Gamma_h^b} = 0 & \quad \forall \xi_h^{b,n} \in V_h^b(t)\end{aligned}\tag{4.51}$$

for some finite element spaces  $V_h^b(t), Q_h^b(t)$ .

There exist some well-known stable element pairs for the approximation of the Stokes solution.

In particular, the Stokes velocity can be approximated by piecewise quadratic, and the Stokes pressure – by piecewise linear functions, i.e.  $V_h^b := P_2(\Omega_h^b)$ ,  $Q_h^b := P_1(\Omega_h^b)$ .

#### 4.2.1.2 Biot problem

In much the same way as for the Stokes problem, a triangulation  $\Omega_h^p$  of the Biot domain  $\Omega^p(t)$  into  $N_e^p$  elements  $\Omega_{h,e}^p$  is introduced:

$$\begin{aligned} \Omega_h^p &:= \bigcup_{e=1}^{N_e^p} \Omega_{h,e}^p, & \Omega_{h,i}^p \cap \Omega_{h,j}^p &= \emptyset, \quad i \neq j. \\ \overline{\Omega^p} &= \overline{\Omega_h^p} \subseteq \Omega^p, \end{aligned} \quad (4.52)$$

On the Biot domain mesh  $\Omega_h^p$ ,  $N^{p,u}$  local nodes for the displacement  $u^{sp}$ ,  $N^{p,p}$  local nodes for the pressure  $p^p$  and  $N^{p,w}$  local nodes for the solid phase velocity  $v^{sp}$  are chosen, and the following vector and scalar finite dimensional Lagrangian nodal bases are correspondingly defined:

$$\begin{aligned} \left\{ \xi_h^{p,n}(x, t) \right\}_{n=1}^{d \times N^{p,u}}, & \quad \xi_h^{p,n}(x, t) = \phi_h^{p,m}(x, t) \mathbf{e}_\alpha, \\ & \quad m := [(n-1) \bmod N^{p,u}] + 1, \quad \alpha := [(n-1)/N^{p,u}] + 1, \\ \left\{ \psi_h^{p,i}(x, t) \right\}_{i=1}^{N^{p,p}}, & \\ \left\{ \eta_h^{p,n}(x, t) \right\}_{n=1}^{d \times N^{p,w}}, & \quad \eta_h^{p,n}(x, t) = \eta_h^{p,m}(x, t) \mathbf{e}_\alpha, \\ & \quad m := [(n-1) \bmod N^{p,w}] + 1, \quad \alpha := [(n-1)/N^{p,w}] + 1, \end{aligned}$$

where  $\left\{ \xi_h^{p,i} \right\}_{i=1}^{N^{p,u}}$ ,  $\left\{ \eta_h^{p,i} \right\}_{i=1}^{N^{p,w}}$  are scalar basis functions used to define the corresponding vector basis functions. Then the approximate solution  $\left\{ \mathbf{u}_h^{sp}(x, t), p_h^p(x, t), \mathbf{v}_h^{sp}(x, t) \right\}$  can be represented through the basis functions  $\left\{ \xi_h^{p,i}(x, t), \psi_h^{p,i}(x, t), \eta_h^{p,i}(x, t) \right\}$  as:

$$\begin{aligned} \mathbf{u}_h^{sp}(x, t) &= \sum_{k=1}^d \sum_{i=1}^{N^{p,u}} \mathbf{u}_k^{sp,i}(t) \xi_h^{p,i}(x, t) \mathbf{e}_k, & p_h^b(x, t) &= \sum_{i=1}^{N^{p,p}} p^{b,i}(t) \psi_h^{b,i}(x, t), \\ \mathbf{v}_h^{sp}(x, t) &= \sum_{k=1}^d \sum_{i=1}^{N^{p,w}} \mathbf{v}_k^{sp,i}(t) \eta_h^{p,i}(x, t) \mathbf{e}_k, \end{aligned} \quad (4.53)$$

where  $\left\{ \mathbf{u}_k^{sp,i}(t) \right\}$ ,  $\left\{ p^{b,i}(t) \right\}$ ,  $\left\{ \mathbf{v}_k^{sp,i}(t) \right\}$  are the nodal coefficients for the corresponding functions.

Using the notations (4.46)-(4.48), the continuous variational formulation (4.34) for the Biot problem on  $\Omega^p(t)$  can be rewritten in finite dimensions in the following way:

find  $(\mathbf{u}_h^{sp}, p_h^p, \mathbf{v}_h^{sp}) \in U_h^p(t) \times Q_h^p(t) \times U_h^p(t)$ , such that for all  $(\boldsymbol{\xi}^p, \psi^p, \boldsymbol{\eta}^p) \in U_h^p(t) \times Q_h^p(t) \times U_h^p(t)$ :

$$\begin{aligned} \mu^s a(\mathbf{u}_h^{sp}, \boldsymbol{\xi}_h^{p,n})_{\Omega_h^p} + \mu^s a'(\mathbf{u}_h^{sp}, \boldsymbol{\xi}_h^{p,n})_{\Omega_h^p} + \lambda^s a''(\mathbf{u}_h^{sp}, \boldsymbol{\xi}_h^{p,n})_{\Omega_h^p} - b(\boldsymbol{\xi}_h^{p,n}, p_h^p)_{\Omega_h^p} = \\ \mu^s \hat{a}\langle \mathbf{u}_h^{sp}, \boldsymbol{\xi}_h^{p,n} \rangle_{\Gamma_h^p} + \mu^s \hat{a}'\langle \mathbf{u}_h^{sp}, \boldsymbol{\xi}_h^{p,n} \rangle_{\Gamma_h^p} + \lambda^s \hat{a}''\langle \mathbf{u}_h^{sp}, \boldsymbol{\xi}_h^{p,n} \rangle_{\Gamma_h^p} - \hat{b}\langle \boldsymbol{\xi}_h^{p,n}, p_h^p \rangle_{\Gamma_h^p}, \quad \forall \boldsymbol{\xi}_h^{p,n} \in U_h^p(t), \\ b(\mathbf{v}_h^{sp}, \psi_h^{p,n})_{\Omega_h^p} + \frac{k}{\mu^f} a(p_h^p, \psi_h^{p,n})_{\Omega_h^p} = \\ \frac{k}{\mu^f} \hat{a}\langle p_h^p, \psi_h^{p,n} \rangle_{\Gamma_h^p}, \quad \forall \psi_h^{p,n} \in Q_h^p(t), \\ m(\mathbf{v}_h^{sp}, \boldsymbol{\eta}_h^{p,n})_{\Omega_h^p} = m(\partial_t \mathbf{u}_h^{sp}, \boldsymbol{\eta}_h^{p,n})_{\Omega_h^p}, \quad \forall \boldsymbol{\eta}_h^{p,n} \in U_h^p(t) \end{aligned} \quad (4.54)$$

for some finite element spaces  $U_h^p(t), Q_h^p(t)$ . The Biot displacement and pore pressure are chosen to be approximated by piecewise linear functions, i.e.  $U_h^p := P_1(\Omega_h^p), Q_h^p := P_1(\Omega_h^p)$ .

### 4.2.2 Temporal discretization

As the problems of interest contain time derivatives of maximum first order, for the purpose of introducing the chosen time discretization method, the following general initial value problem for a function  $u(t) \in \Omega \times [0, T]$  is considered:

$$\begin{aligned} \partial_t u(t) &= f(u(t), t) \quad t \in (0, T), \\ u(x, 0) &= u_0, \end{aligned} \quad (4.55)$$

where  $f$  is some (sufficiently smooth) function.

In order to discretise any given time dependent problem in time, a subdivision of the total time interval  $[0, T]$  into  $\mathcal{I}$  discrete time-steps  $(t_i, t_{i+1}]$  of sizes  $t_i^\Delta$  is introduced:

$$\begin{aligned} 0 = t_0 < t_1 < \dots < t_i < t_{i+1} < \dots < t_{\mathcal{I}} = T, \quad t_{i+1}^\Delta := t_{i+1} - t_i, \\ (0, T] &= \bigcup_{i=0}^{\mathcal{I}-1} (t_i, t_{i+1}], \quad t^\Delta := \max_{i \in \{0, \dots, \mathcal{I}-1\}} t_i^\Delta. \end{aligned} \quad (4.56)$$

When using the basic  $\theta$ -scheme method, the value of  $u$  at time point  $t_{i+1}$  (denoted as  $u_{i+1}$ ) is expressed through the value of the operator at the previous time step, i.e.  $u_i$ , in the following way:

$$u_{i+1} = u_i + t_{i+1}^\Delta (\theta f(u_{i+1}, t_{i+1}) + (1 - \theta) f(u_i, t_i)), \quad (4.57)$$

where  $\theta \in [0, 1]$  is a fixed parameter of the method. For instance, some of the well-known  $\theta$  schemes include implicit (backward) Euler scheme for  $\theta := 1$ , explicit Euler scheme for  $\theta := 0$  and trapezoidal rule for  $\theta = 0.5$ . Thus from (4.57) it follows, that an implicit scheme reads:

$$u_{i+1} - u_i = t_{i+1}^\Delta f(u_{i+1}, t_{i+1}). \quad (4.58)$$

The discretizations of the common time interval  $(0, T)$  into sets of subintervals for the Stokes and Biot problems are chosen to be identical and in form equivalent to (4.56). Then the **implicit Euler** time discretizations of the Biot and Stokes spatially discretized problems (4.51), (4.54) on the time interval  $(t_{i-1}, t_i)$  read:

**Stokes problem:**

$$\begin{aligned}
 \mu^f a(\mathbf{v}_{h,i}^b, \phi_{h,i}^{b,n})_{\Omega_{h,i}^b} + \mu^f a'(\mathbf{v}_{h,i}^b, \phi_{h,i}^{b,n})_{\Omega_{h,i}^b} - b(\phi_{h,i}^{b,n}, p_{h,i}^b)_{\Omega_{h,i}^b} = \\
 \mu^f \hat{a}\langle \mathbf{v}_{h,i}^b, \phi_{h,i}^{b,n} \rangle_{\Gamma_{h,i}^b} + \mu^f \hat{a}'\langle \mathbf{v}_{h,i}^b, \phi_{h,i}^{b,n} \rangle_{\Gamma_{h,i}^b} - \hat{b}\langle \phi_{h,i}^{b,n}, p_{h,i}^b \rangle_{\Gamma_{h,i}^b} & \quad \forall \phi_{h,i}^{b,n} \in V_{h,i}^b, \\
 b(\mathbf{v}_{h,i}^b, \psi_{h,i}^{b,i})_{\Omega_{h,i}^b} = 0 & \quad \forall \psi_{h,i}^{b,i} \in Q_{h,i}^b, \\
 a(\mathbf{u}_{h,i}^b, \boldsymbol{\xi}_{h,i}^{b,n})_{\Omega_{h,i}^b} - \hat{a}\langle \mathbf{u}_{h,i}^b, \boldsymbol{\xi}_{h,i}^{b,n} \rangle_{\Gamma_{h,i}^b} = 0 & \quad \forall \boldsymbol{\xi}_{h,i}^{b,n} \in V_{h,i}^b.
 \end{aligned} \tag{4.59}$$

**Biot problem:**

$$\begin{aligned}
 \mu^s a(\mathbf{u}_{h,i}^{sp}, \boldsymbol{\xi}_{h,i}^{p,n})_{\Omega_{h,i}^p} + \mu^s a'(\mathbf{u}_{h,i}^{sp}, \boldsymbol{\xi}_{h,i}^{p,n})_{\Omega_{h,i}^p} + \lambda^s a''(\mathbf{u}_{h,i}^{sp}, \boldsymbol{\xi}_{h,i}^{p,n})_{\Omega_{h,i}^p} - b(\boldsymbol{\xi}_{h,i}^{p,n}, p_{h,i}^p)_{\Omega_{h,i}^p} = \\
 \mu^s \hat{a}\langle \mathbf{u}_{h,i}^{sp}, \boldsymbol{\xi}_{h,i}^{p,n} \rangle_{\Gamma_{h,i}^p} + \mu^s \hat{a}'\langle \mathbf{u}_{h,i}^{sp}, \boldsymbol{\xi}_{h,i}^{p,n} \rangle_{\Gamma_{h,i}^p} - \lambda^s \hat{a}''\langle \mathbf{u}_{h,i}^{sp}, \boldsymbol{\xi}_{h,i}^{p,n} \rangle_{\Gamma_{h,i}^p} - \hat{b}\langle \boldsymbol{\xi}_{h,i}^{p,n}, p_{h,i}^p \rangle_{\Gamma_{h,i}^p} & \quad \forall \boldsymbol{\xi}_{h,i}^{p,n} \in U_{h,i}^p, \\
 b(\mathbf{v}_{h,i}^{sp}, \psi_{h,i}^{p,n})_{\Omega_{h,i}^p} + \frac{k}{\mu^f} a(p_{h,i}^p, \psi_{h,i}^{p,n})_{\Omega_{h,i}^p} = \\
 \frac{k}{\mu^f} \hat{a}\langle p_{h,i}^p, \psi_{h,i}^{p,n} \rangle_{\Gamma_{h,i}^p} & \quad \forall \psi_{h,i}^{p,n} \in Q_{h,i}^p, \\
 t_i^\Delta m(\mathbf{v}_{h,i}^{sp}, \boldsymbol{\eta}_{h,i}^{p,n})_{\Omega_{h,i}^p} = \\
 m(\mathbf{u}_{h,i}^{sp}, \boldsymbol{\eta}_{h,i}^{p,n})_{\Omega_{h,i}^p} - m(\mathbf{u}_{h,i-1}^{sp}, \boldsymbol{\eta}_{h,i}^{p,n})_{\Omega_{h,i}^p} & \quad \forall \boldsymbol{\eta}_{h,i}^{p,n} \in U_{h,i}^p,
 \end{aligned} \tag{4.60}$$

where the second lower index ( $i-1$  or  $i$ ) denotes the corresponding time step, e.g.  $u_{h,i}^{sp} := u_h^{sp}(t_i)$ ,  $\boldsymbol{\xi}_{h,i}^{p,n} := \boldsymbol{\xi}_h^{p,n}(t_i)$ ,  $U_{h,i}^p := U_h^p(t_i)$ , etc.

It should be noted, that as the Stokes problem is quasi stationary on the given domain, its solution adapts instantaneously to the change of the domain geometry. However, the stationary problem must still be solved in each time step to account for the change in the domain geometry. This idea becomes more illustrative when the time stepping scheme is developed, see [Section 4.4](#).

### 4.3 Analytic solution of the Biot problem

The best way to verify a numerical implementation of a problem is to compare it with an analytic solution. While it would be quite a challenge to attempt to find an analytic solution of the strongly coupled Biot-Stokes problem, under certain assumptions, an analytic solution to the pure Biot problem is possible to obtain. Thus in this section, a solution to the stationary Biot problem defined on a spherically or rotationally symmetric domain is derived.

In particular, the mathematical problem is formulated as follows: find an analytic solution to the stationary Biot problem (obtained from (4.23), (4.24), (4.26) by dropping the time derivatives):

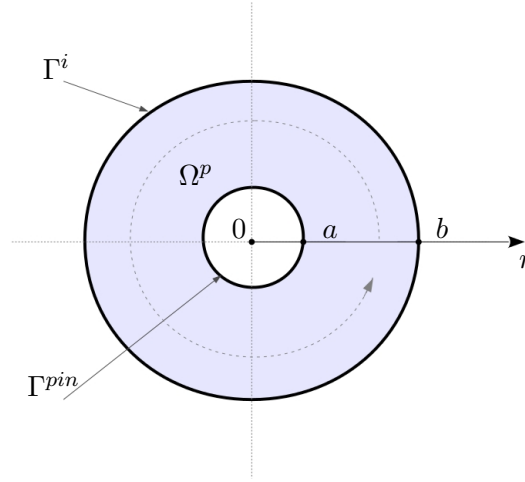
$$\nabla \cdot \left\{ -p^p I + \mu^s \left( \nabla u^{sp} + (\nabla u^{sp})^T \right) + \lambda^s \nabla \cdot u^{sp} I \right\} = 0 \quad \text{in } \Omega^p, \tag{4.61}$$

$$\Delta p^p = 0 \quad \text{in } \Omega^p, \tag{4.62}$$

$$v^{fp} = -\frac{k}{\gamma^f \mu^f} \nabla p^p \quad \text{in } \Omega^p, \tag{4.63}$$

with boundary conditions:



Figure 4.4 Rotationally symmetric Biot domain  $\Omega^p$ .


$$\begin{aligned} u^{sp} &:= u_a^{sp} & \text{at } \Gamma^{pin}, \\ p^p &:= p_a^p & \text{at } \Gamma^{pin}, \end{aligned} \quad (4.64)$$

$$\begin{aligned} u^{sp} &:= u_b^{sp} & \text{at } \Gamma^i, \\ p^p &:= p_b^p & \text{at } \Gamma^i, \end{aligned} \quad (4.65)$$

where the domain  $\Omega^p$  is rotationally (in 2D) or spherically (in 3D) symmetric with inner radius  $a$  and outer radius  $b$ , see *Fig. 4.4*.

The idea behind finding a solution to (4.61)-(4.63) consists in transforming the equations into polar/spherical coordinates, reducing the multidimensional system of equations to a one dimensional problem depending on the radius  $r$  (which is possible due to the symmetry of the domain), and then integrating the resulting ODEs. Further details on the solution of the stationary and instationary Biot consolidation equations can be found in e.g. [171], [23].

### 4.3.1 2D: polar coordinates

In two dimensions, the rectangular  $(x_1, x_2)$  and polar  $(r, \theta)$  coordinates are related to one another in the following way:

$$\begin{aligned} x_1 &= r \cos \theta, \\ x_2 &= r \sin \theta. \end{aligned}$$

In the case of rotational symmetry, the gradient of a scalar function  $q$ , the divergence and Laplace operators of a vector function  $\mathbf{q} = (q_r, q_\theta)$  reduce to:

$$\begin{aligned} \nabla q &= \partial_r q, & \nabla \cdot \mathbf{q} &= \frac{1}{r} \partial_r (r \mathbf{q}_r), \\ \Delta q &= \frac{1}{r} \partial_r (r \partial_r q) = \frac{1}{r} \partial_r q + \partial_{rr} q, & \Delta \mathbf{q} &= \partial_r^2 \mathbf{q}_r + \frac{1}{r} \partial_r \mathbf{q}_r - \frac{\mathbf{q}_r}{r^2}. \end{aligned} \quad (4.66)$$

Then the stationary Biot equations in polar coordinates reduce to a system of one dimensional

equations:

$$(\lambda^s + 2\mu^s)\partial_r \left( \frac{1}{r} \partial_r (ru_r^{sp}) \right) - \partial_r p^p = 0, \quad (4.67)$$

$$\partial_r (r \partial_r p^p) = 0, \quad (4.68)$$

$$v_r^{fp} = -\frac{k}{\gamma^f \mu^f} \partial_r p^p. \quad (4.69)$$

Pressure  $p^p$  and its derivative  $\partial_r p^p$  can be directly found from (4.68) by integrating the equation over  $r$ :

$$\partial_r p^p = \frac{C_1^p}{r}, \quad (4.70)$$

$$p^p = C_1^p \ln(r) + C_2^p, \quad (4.71)$$

where  $C_1^p, C_2^p$  are integration constants. Substituting (4.70) into (4.69), the fluid velocity  $v_r^{fp}$  is found as:

$$v_r^{fp} = -\frac{k}{\gamma^f \mu^f} \frac{C_1^p}{r}. \quad (4.72)$$

Integrating (4.67), then substituting the solution for pressure (4.71) into the obtained relation,

$$(\lambda^s + 2\mu^s) \frac{1}{r} \partial_r (ru_r^{sp}) = p^p + C_{01}^u \stackrel{(4.71)}{=} C_1^p \ln(r) + C_{02}^u,$$

and solving the resulting differential equation for  $u_r^{sp}$ , gives a general solution for the displacement:

$$\begin{aligned} u_r^{sp} &= \frac{C_1^p}{2(\lambda^s + 2\mu^s)} r \ln(r) + \frac{2C_{01}^u - C_1^p}{4(\lambda^s + 2\mu^s)} r + \frac{C_2^u}{r} = \\ &= \frac{C_1^p}{2(\lambda^s + 2\mu^s)} r \ln(r) + C_1^u r + \frac{C_2^u}{r}, \end{aligned} \quad (4.73)$$

where  $C_1^u, C_2^u$  are some integration coefficients.

The four integration coefficients  $C_1^p, C_2^p, C_1^u, C_2^u$  are evaluated through the boundary conditions:

$$\begin{cases} u_a^{sp} =: u^{sp}(a) = \frac{a \ln(a)}{2(\lambda^s + 2\mu^s)} C_1^p + a C_1^u + \frac{C_2^u}{a}, \\ p_a^p =: p^p(a) = C_1^p \ln(a) + C_2^p, \\ u_b^{sp} =: u^{sp}(b) = \frac{b \ln(b)}{2(\lambda^s + 2\mu^s)} C_1^p + b C_1^u + \frac{C_2^u}{b}, \\ p_b^p =: p^p(b) = C_1^p \ln(b) + C_2^p, \end{cases} \quad (4.74)$$

$$\begin{aligned} C_1^p &= \frac{p_a^p - p_b^p}{\ln(a/b)}, & C_1^u &= \frac{(au_a^{sp} - bu_b^{sp})}{a^2 - b^2} - \frac{(a^2 \ln(a) - b^2 \ln(b))}{2(\lambda^s + 2\mu^s)(a^2 - b^2)} \frac{(p_a^p - p_b^p)}{\ln(a/b)}, \\ C_2^p &= \frac{\ln(a)p_b^p - \ln(b)p_a^p}{\ln(a/b)}, & C_2^u &= \frac{(bu_a^{sp} - au_b^{sp})ab}{b^2 - a^2} - \frac{a^2 b^2 (p_a^p - p_b^p)}{2(\lambda^s + 2\mu^s)(b^2 - a^2)}. \end{aligned} \quad (4.75)$$

### 4.3.2 3D: spherical coordinates

In three dimensions, the rectangular  $(x_1, x_2, x_3)$  and spherical  $(r, \phi, \theta)$  coordinates are related to one another in the following way:

$$\begin{aligned}x_1 &= r \cos \phi \sin \theta, \\x_2 &= r \sin \phi \sin \theta, \\x_3 &= r \cos \theta.\end{aligned}$$

In the case of spherical symmetry, the gradient of a scalar function  $q$ , the divergence and Laplace operators of a vector function  $\mathbf{q} = (q_r, q_\phi, q_\theta)$  reduce to:

$$\begin{aligned}\nabla q &:= \partial_r q, & \nabla \cdot \mathbf{q} &:= \frac{1}{r^2} \partial_r (r^2 \mathbf{q}_r), \\ \Delta q &:= \frac{1}{r^2} \partial_r (r^2 \partial_r q), & \Delta \mathbf{q} &= \frac{1}{r} \partial_{rr} (r \mathbf{q}_r) - \frac{2}{r^2} \mathbf{q}_r.\end{aligned}\tag{4.76}$$

Then the stationary Biot equations in spherical coordinates reduce to a system of one dimensional equations:

$$(\lambda^s + 2\mu^s) \partial_r \left( \frac{1}{r^2} \partial_r (r^2 u_r^{sp}) \right) - \partial_r p^p = 0,\tag{4.77}$$

$$\partial_r (r^2 \partial_r p^p) = 0,\tag{4.78}$$

$$v_r^{fp} = -\frac{k}{\gamma^f \mu^f} \partial_r p^p.\tag{4.79}$$

As in the case of rotational symmetry, general solutions for the pressure  $p^p$  can be directly found from the continuity equation (4.78), for the velocity  $v_r^{fp}$  – from (4.79) using the obtained pressure solution:

$$\partial_r p^p = \frac{C_1^p}{r^2},\tag{4.80}$$

$$p^p = -\frac{C_1^p}{r} + C_2^p,\tag{4.81}$$

$$v_r^{fp} = -\frac{k}{\gamma^f \mu^f} \frac{C_1^p}{r^2},\tag{4.82}$$

where  $C_1^p, C_2^p$  are integration constants. Substituting (4.81) into the integrated momentum balance (4.77),

$$(\lambda^s + 2\mu^s) \frac{1}{r^2} \partial_r (r^2 u_r^{sp}) = p^p + C_{01}^u = -\frac{C_1^p}{r} + C_1^u,$$

a general solution for the displacement  $u_r^{sp}$  is obtained:

$$u_r^{sp} = -\frac{C_1^p}{2(\lambda^s + 2\mu^s)} + C_1^u r + \frac{C_2^u}{r^2},\tag{4.83}$$

where  $C_1^u, C_2^u$  are integration constants.

Using the boundary conditions (4.64), (4.65), the integration coefficients  $C_1^p, C_2^p, C_1^u, C_2^u$  are

determined:

$$\begin{cases} u_a^{sp} =: u^{sp}(a) = -\frac{C_1^p}{2(\lambda^s + 2\mu^s)} + C_1^u a + \frac{C_2^u}{a^2}, \\ p_a^p =: p^p(a) = -\frac{C_1^p}{a} + C_2^p, \\ u_b^{sp} =: u^{sp}(b) = -\frac{C_1^p}{2(\lambda^s + 2\mu^s)} + C_1^u b + \frac{C_2^u}{b^2}, \\ p_b^p =: p^p(b) = -\frac{C_1^p}{b} + C_2^p, \end{cases} \quad (4.84)$$

$$\begin{aligned} C_1^p &= \frac{(p_a^p - p_b^p)ab}{(a-b)}, & C_1^u &= \frac{a^2 u_a^{sp} - b^2 u_b^{sp}}{a^3 - b^3} + \frac{ab(a+b)(p_a^p - p_b^p)}{2(\lambda^s + 2\mu^s)(a^3 - b^3)}, \\ C_2^p &= \frac{p_a^p a - p_b^p b}{(a-b)}, & C_2^u &= \frac{a^2 b^2}{(b^3 - a^3)} \left( b u_a^{sp} - a u_b^{sp} - \frac{(p_a^p - p_b^p)ab}{2(\lambda^s + 2\mu^s)} \right). \end{aligned} \quad (4.85)$$

#### 4.4 Solution approach: operator splitting

There can generally be distinguished two approaches to solving coupled interaction problems: a monolithic approach, i.e. when all equations of the system are solved simultaneously, and a partitioned approach, when the sub-problems of the coupled problem are treated individually. There exist advantages and disadvantages to both approaches. Monolithic approach is often used for solving strongly coupled problems, for which operator splitting may entail minuscule time steps. However, if coupling is weak enough, the application of operator splitting is advantageous, since it results in two smaller algebraic systems for each time step. Thus in this work, the coupled Biot-Stokes problem is solved in a partitioned (or operator splitting) way.

Subdividing the total observation time interval  $[0, T]$  into  $\mathcal{I}$  time steps as in (4.56), namely:

$$(0, T] = (0, t_1] \cup (t_1, t_2] \cup \dots \cup (t_i, t_{i+1}] \cup \dots \cup (t_{\mathcal{I}-1}, T] \quad (4.86)$$

for each time step  $i \in \{1, \dots, \mathcal{I}\}$ ,  $t \in (t_{i-1}, t_i]$ , the corresponding reference mesh configurations  $\Omega_{h,i-1}^b$ ,  $\Omega_{h,i-1}^p$  and deformed mesh configurations  $\Omega_{h,i}^b$ ,  $\Omega_{h,i}^p$  are defined. Then within each time step  $i \in \{1, \dots, \mathcal{I}\}$ , the coupled one cell problem is solved in the following *operator splitting* way:

1. Solve the Biot poroelasticity problem (4.4)–(4.6) on  $\Omega_{h,i-1}^p$  with the initial, interface and boundary conditions (4.28)–(4.32) for the the displacement, pore pressure and solid phase velocity  $(u^{sp}, p^p, v^{sp})$ :

$$\nabla \cdot \left\{ \mu^s \left( \nabla u^{sp} + (\nabla u^{sp})^T \right) + \lambda^s \nabla \cdot u^{sp} I - p^p I \right\} = 0 \quad \text{in } \Omega_{h,i-1}^p, \quad (4.87)$$

$$\nabla \cdot \left( v^{sp} - \frac{k}{\mu^f} \nabla p^p \right) = 0 \quad \text{in } \Omega_{h,i-1}^p, \quad (4.88)$$

$$v^{sp} - \partial_t u^{sp} = 0 \quad \text{in } \Omega_{h,i-1}^p, \quad (4.89)$$

$$u^{sp} := 0 \quad \text{in } \Omega_{h,0}^p, \quad (4.90)$$

$$\frac{k}{\mu^f} \nabla p^p \cdot n := L^p (p^p - p^b - \pi^\Delta) \quad \text{at } \Gamma_{h,i-1}^i, \quad (4.91)$$

$$\left\{ \mu^s (\nabla u^{sp} + (\nabla u^{sp})^T) + \lambda^s \nabla \cdot u^{sp} I \right\} \cdot n := (p^p - p^b) \cdot n \quad \text{at } \Gamma_{h,i-1}^i, \quad (4.92)$$

$$u^{sp} := 0 \quad \text{at } \Gamma_{h,i-1}^{pin}, \quad (4.93)$$

$$\nabla p^p := 0 \quad \text{at } \Gamma_{h,i-1}^{pin}, \quad (4.94)$$

where  $\Gamma_{h,j}^{pin} \equiv \Gamma_{h,0}^{pin}$  for all  $j \in \{1, \dots, \mathcal{I}\}$  is the *fixed* inner boundary. The values of the parameters ( $\mu^s$ ,  $\lambda^s$ ,  $k$ ,  $\mu^f$ ,  $L^p$ ) are listed in *Table 3.1*, the value of the extracellular pressure  $p^b$  on the RHSs of (4.91), (4.92) is taken from the Stokes solution for time step  $t_{i-1}$ :

$$p^b := p^b(t_{i-1}),$$

which is available from step 4 of the previous cycle. The transmembrane osmotic pressure difference  $\pi^\Delta$  on the RHS of (4.91) is approximated as specified in (4.108).

If necessary, the intracellular fluid velocity  $v^{fp}$  at the time step  $t_i$  can be evaluated from the solution of the Biot problem (4.87)-(4.94) using the relation (4.7):

$$v^{fp} = v^{sp} - \frac{k}{\gamma^f \mu^f} \nabla p^p \quad \text{in } \Omega_{h,i-1}^p. \quad (4.95)$$

2. Solve the Stokes domain deformation equation (4.3) with the interface and boundary conditions (4.17), (4.12):

$$\Delta u^b = 0 \quad \text{in } \Omega_{h,i-1}^b, \quad (4.96)$$

$$u^b := u^{sp} \quad \text{at } \Gamma_{h,i-1}^i, \quad (4.97)$$

$$u^b := 0 \quad \text{at } \Gamma_{h,0}^{bw}, \quad (4.98)$$

where  $u^{sp}$  on the RHS of (4.97) is the solution of (4.87)-(4.94) for the displacement obtained in step 1:

$$u^{sp} := u^{sp}(t_{i-1}). \quad (4.99)$$

3. Update (move) the interface and the nodes (coordinates) of the grids (meshes)  $\Omega_h^p$ ,  $\Omega_h^b$  of the Biot and Stokes domains with the corresponding displacements  $u^{sp}$ ,  $u^b$ :

$$\begin{aligned} \Omega_{h,i}^p &:= \left\{ x_i^p = x_{i-1}^p + u^{sp}(x_{i-1}^p, t_{i-1}) \mid x_{i-1}^p \in \Omega_{h,i-1}^p \right\}, \\ \Omega_{h,i}^b &:= \left\{ x_i^b = x_{i-1}^b + u^b(x_{i-1}^b, t_{i-1}) \mid x_{i-1}^b \in \Omega_{h,i-1}^b \right\}. \end{aligned} \quad (4.100)$$

4. Solve the Stokes equations (4.1)-(4.2) with the boundary and interface conditions (4.14),

(4.15) for the fluid velocity and hydraulic pressure  $(v^b, p^b)$ :

$$\nabla \cdot \left\{ -p^b I + \mu^f \left( \nabla v^b + (\nabla v^b)^T \right) \right\} = 0 \quad \text{in } \Omega_{h,i}^b, \quad (4.101)$$

$$\nabla \cdot v^b = 0 \quad \text{in } \Omega_{h,i}^b, \quad (4.102)$$

$$v_n^b := \left( v^{sp} - \frac{k}{\mu^f} \nabla p^p \right)_n \quad \text{at } \Gamma_{h,i}^i, \quad (4.103)$$

$$\sigma_n^b = \left( -p^b I + \mu^f \left( \nabla v^b + (\nabla v^b)^T \right) \right)_n := 0 \quad \text{at } \Gamma_{h,i}^{bw}, \quad (4.104)$$

where  $\Gamma_{h,j}^{bw} \equiv \Gamma_{h,0}^{bw}$ ,  $\forall j \in \{1, \dots, \mathcal{I}\}$ , are the external *fixed* extracellular walls. In the RHS of (4.103),  $v^{sp}$ ,  $p^p$  are the solid phase velocity and pore fluid pressure solutions of the Biot problem that were obtained in step 1:

$$\begin{aligned} v^{sp} &:= v^{sp}(t_{i-1}), \\ p^p &:= p^p(t_{i-1}). \end{aligned}$$

Notice that (4.104) is a homogeneous Neumann boundary condition. If the derivatives of the bulk fluid velocity  $v^b$  disappear in the vicinity of  $\Gamma^{bw}$ , then this condition corresponds to a pressure boundary condition, i.e.

$$(4.104) \quad \Leftrightarrow \quad p^b := 0 \quad \text{at } \Gamma_{h,i}^{bw}.$$

## 4.5 Software related aspects

All simulations presented in this thesis were implemented based on the Distributed and Unified Numerics Environment (DUNE), [172], a powerful C++ library for the solution of PDEs in the context of high-performance computing. In particular, the external discretisation module `dune-pdelab`, [173], was used for the implementation of both the Stokes and Biot equations; `dune-multidomaingrid` module developed by Steffen Müthing, [174], was used as the foundation for the multi-domain coupling. Significant parts of the technically challenging aspects of the coupling terms and local operators of the coupled Biot-Stokes problem simulations were implemented by Dr. Felix Heimann (former researcher at the IWR, Heidelberg University), who also assisted in conducting and evaluating these simulations.

The algebraic systems which resulted from the discretisation of the weak problem formulation were solved with the direct solver `SuperLU`, [175]. For the rather simple and restricted geometries considered in this thesis, this approach provided acceptable run-times. On the platform *Intel(R) i3-3217U CPU 1.80GHz*, none of the presented simulations required more than 8 hours for the 3D-simulations and 1 hour for the 2D-simulations of the coupled problem. It should be noted, that there are various ways in which the run-time of the numerical solution of the presented Biot-Stokes problem could be improved, and that simulations with significantly higher numbers of degrees of freedom are certainly feasible.

## 4.6 Numerical implementation

The implemented problems and corresponding numerical simulation results presented in this work can be subdivided into four general groups and are thus discussed in detail in their respective sections. In order to verify the numerical implementation of the Biot problem, the analytic and numerical solutions of the *Pure Biot* problem are compared in [Section 4.6.1](#). In [Section 4.6.2](#), the swelling of a spherically ( $d = 3$ ) and rotationally ( $d = 2$ ) symmetric ICS (*Pure Biot* problem) with the *estimated* parameters, initial and boundary values is simulated. Then the sensitivity of the *Pure Biot* problem solution to the variations of some of the physical parameters is tested and analysed. In [Section 4.6.3](#), the swelling of a rotationally symmetric (i.e. circular for  $d = 2$ ) poroelastic cell surrounded by extracellular bulk fluid (*Coupled Biot-Stokes* problem) is simulated. The obtained solution for the Biot sub-problem is compared with the solution for the *Pure Biot* problem described in [Section 4.6.2](#). In [Section 4.6.4](#), the *Coupled Biot-Stokes* problem, where the geometry of the Biot domain is *non-trivial*, is simulated and the effect of the Biot domain geometry on the solution of the *Coupled Biot-Stokes* problem is analysed.

In the simulations that are described in [Sections 4.6.2, 4.6.3, 4.6.4](#), the parameters characterising the physical living cell and extracellular environment, as well the data corresponding to the experimental settings are used. The values discussed in [Section 3.1](#) (further referred to as the *estimated* values) are obtained in the SI units. In order to equilibrate the numerical residual and achieve a numerically stable computation of the residual Jacobian matrix using the method of numerical differentiation, alternative units were employed. In particular, the SI units [m, kg, s, mol] are translated into the units [ $\mu\text{m}$ , mg, min, mol]<sup>1</sup> and are listed in [Table 3.6](#).

Some of the values estimated in [Section 3.1](#) (i.e. osmotic pressures, velocities, times) vary depending on the assumption on the osmolyte permeability of the membrane. In particular, the membrane is assumed to be either strictly (not permeable to the osmolytes) or leaky (permeable to the osmolytes) semipermeable, thus the *strict* and *leaky* membrane assumptions are distinguished. Simulation results shown in [Section 4.6.2](#) are available for both assumptions; in [Sections 4.6.3, 4.6.4](#), the membrane is assumed to be strictly semipermeable.

### Volumes

At each  $t \in (0, T)$ , the ICS volume  $V^p$  is computed through the sum of the volume integrals over the mesh cells; the intracellular fluid volume  $V^{fp}(t)$  is then evaluated using the porosity concept, i.e.  $V^{fp} := \gamma^f V^p$ . As the total volume  $V$  is constant, the extracellular fluid volume  $V^b(t)$  can be found as the difference:  $V^b := V - V^p$ .

Volumetric transmembrane fluid flux  $j^\Sigma$  is defined as the surface integral of the transmembrane Neumann flux ([4.91](#)). Then the volume  $V^\Sigma(t)$  of the transmembrane fluid that has crossed the interface of the ICS  $\Omega^p$  by the time  $t$  is computed as:

$$V^\Sigma(t) := \sum_{t \in (0, T)} j^\Sigma(t). \quad (4.105)$$

### Osmotic transmembrane pressure difference (OTPD)

As mentioned above, the intracellular and extracellular concentrations  $c^{fp}$ ,  $c^b$  are assumed to be

<sup>1</sup> In this thesis, these units are referred to as the *numerics* units.

spatially constant at all times. Thus at each time step  $t$ , the OTPD is computed as:

$$\pi^\Delta(t) := C_{osm} c^\Delta(t) = C_{osm} \left( c^{fp}(t) - c^b(t) \right) = C_{osm} \left( \frac{a^{fp}(t)}{V^{fp}(t)} - \frac{a^b(t)}{V^b(t)} \right), \quad (4.106)$$

where  $C_{osm}$  is the osmotic pressure model coefficient,  $a^{fp}$ ,  $a^b$  are the intracellular and extracellular amounts of substance and  $V^{fp}$ ,  $V^b$  are the intracellular and extracellular fluid volumes respectively. In the *strict membrane* case, the amounts of substance  $a^{fp}$ ,  $a^b$  are constant and equal to their initial values. For the *leaky membrane* assumption, the transmembrane exchange of osmolytes is assumed to be linear in time, such that:

$$\begin{aligned} a^{fp}(t) &= a_0^{fp} + a^\Delta(t), & a^\Delta(t) &:= \frac{a_T^\Delta - a_0^\Delta}{T} t + a_0^\Delta, \\ a^b(t) &= a_0^b - a^\Delta(t), \end{aligned} \quad (4.107)$$

where the initial and terminal values  $a_0^\Delta$ ,  $a_T^\Delta$  as well as the swelling time  $T$  correspond to their *estimated* values discussed in [Section 3.1](#), in particular,  $T := 558$  min for  $d = 3$ ,  $T := 740$  min for  $d = 2$ . The implications of such choice of the amount of substance exchange function are discussed in the context of the analysis of the *Pure Biot with leaky semipermeable membrane problem* implementation results in [Section 4.6.2](#).

Using [\(4.107\)](#) and the above described volume relations, [\(4.106\)](#) can be found as:

$$\pi^\Delta(t) := C_{osm} \left( \frac{a^{fp}(t)}{\gamma^f V^{fp}(t)} - \frac{a^b(t)}{V - V^p(t)} \right). \quad (4.108)$$

#### 4.6.1 Verification of the Biot problem implementation

*Problem:* Pure Biot problem [\(4.23\)](#)-[\(4.25\)](#) (or [\(4.60\)](#)) for the solid phase displacement, pore pressure and solid phase velocity  $(u^{sp}, p^p, v^{sp})$ . At the inner and outer boundaries  $\Gamma^{pin}$ ,  $\Gamma^i(t)$ , pure Dirichlet conditions [\(4.64\)](#), [\(4.65\)](#) for the displacement  $u^{sp}$  and pressure  $p^p$  are prescribed.

*Domain:*  $\Omega^p(t) \in \mathbb{R}^d$ ,  $d = \{2, 3\}$ , – spherically ( $d = 3$ ) or rotationally ( $d = 2$ ) symmetric with the inner radius  $r = a$  at  $\Gamma^{pin}$  and outer radius  $r = b$  at  $\Gamma^i(t)$ , see [Fig. 4.4](#). The 2- and 3-dimensional meshes approximating the Pure Biot domain are shown in [Fig. 4.5](#).

The dimensions of the domain, parameters, initial and boundary conditions are chosen as:

$$\begin{aligned} a &:= 0.5, & b &:= 1; \\ \lambda^s &:= 573, & \mu^s &:= 230, & \mu^f &:= 0.02, & k &:= 10^{-6}; \\ u^{sp}(x, 0) &:= 0 & \forall x &\in \Omega_0^p; \end{aligned}$$

$$d = 2 : \quad u^{sp}(a) := 0.01, \quad u^{sp}(b) := 0.02, \quad p^p(a) := 100, \quad p^p(b) := 200 \quad \forall t \in (0, T),$$

$$d = 3 : \quad u^{sp}(a) := 0.1, \quad u^{sp}(b) := 0.2, \quad p^p(a) := 10, \quad p^p(b) := 100 \quad \forall t \in (0, T).$$

The above described *instationary* Pure Biot problem is solved on *coarse* and *refined* (finer) fixed<sup>2</sup> meshes for a number of time steps until it reaches a stationary equilibrium. In [Fig. 4.6](#), the

<sup>2</sup> In this context, the term "fixed" means that the reference mesh is not updated (i.e. moved with the computed displacement) after each time step.



equilibrium numerical solution for the displacement  $u^{sp}$  (Fig. 4.6a, 4.6b) and hydraulic pressure  $p^p$  (Fig. 4.6c, 4.6d) obtained on the coarsest mesh level (Fig. 4.5) is compared to the analytic solution of the stationary Biot problem derived in Section 4.3 (i.e. (4.71), (4.73) for  $d = 2$ , (4.81), (4.83) for  $d = 3$ ). In Table 4.1, an  $L^2$ -convergence is shown by computing  $L^2$ -errors ( $Err_2$ ) between the analytic solution and numerical solutions computed on a series of refined meshes. Thus for a quantity  $q$  defined over  $\Omega^p$ , such that  $q_a, q_n$  are the analytic and numerical solutions of the Biot problem respectively,  $Err_2$  is defined as:

$$Err_2(q) := \left( \int_{\Omega} (q_a(x) - q_n(x))^2 dx \right)^{1/2}. \quad (4.109)$$

**Figure 4.5 Pure Biot problem meshes.**

On the pictures below, computation meshes for the 2- and 3-dimensional Pure Stokes problem considered in *Section 4.6.1* are shown on the coarsest mesh level.

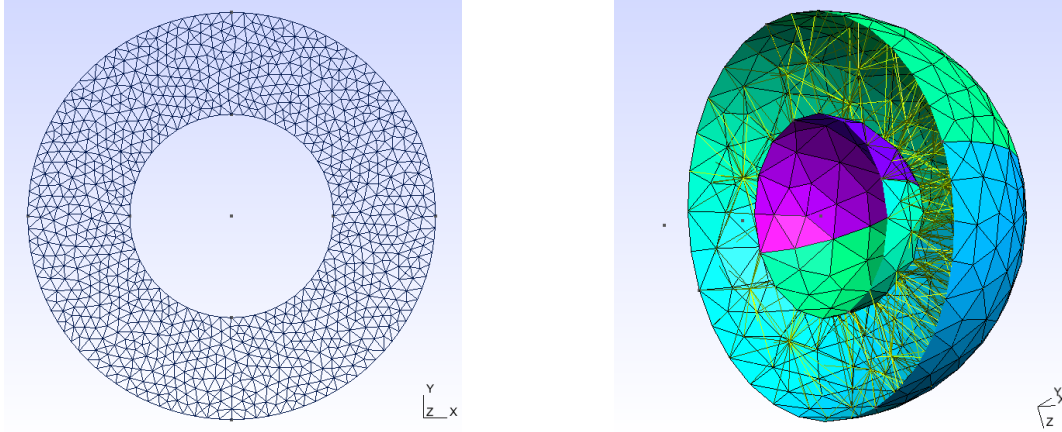


**Table 4.1 Comparison between numerical and analytic Biot problem solutions.**

The tables below show convergence behaviour of the discrete 2- and 3-dimensional Biot problem solution for the deformation  $u_h^{sp}$  and hydraulic pressure  $p_h^p$  on a sequence of refined meshes. For each refinement level, the numbers of nodes, cells, degrees of freedom (DOF), as well as the  $L^2$ -errors ( $Err_2$  defined in 4.109) between the analytic and numerical solutions are given.

$d = 2$

Level	Nodes	Cells	DOF	$Err_2$	
				$u^{sp}$	$p^p$
0	1000	1840	5000	6.25e-05	7.15e-02
1	3840	7360	19200	1.61e-05	1.80e-02
2	15040	29440	75200	4.11e-06	4.52e-03
3	59520	117760	297600	1.03e-06	1.13e-03
4	238800	471040	1184000	2.60e-07	2.83e-04

$d = 3$

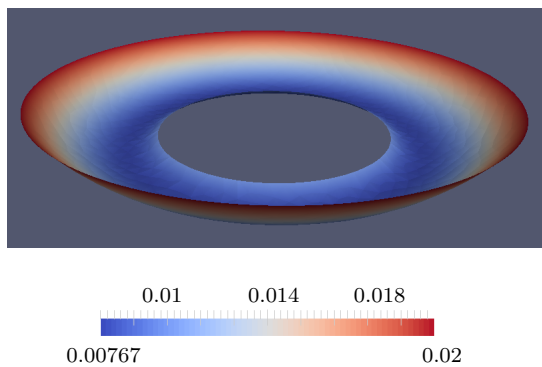
Level	Nodes	Cells	DOF	$Err_2$	
				$u^{sp}$	$p^p$
0	552	1777	13980	4.08e-03	1.49e+01
1	3372	14216	92394	1.09e-03	4.76e+00
2	22930	113728	662932	2.91e-04	1.37e+00

**Figure 4.6 Numerical vs analytic Biot problem solution.**

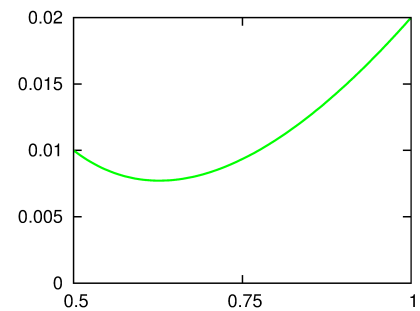
On the pictures below, the numerical equilibrium solutions of the 2- and 3-dimensional Biot problem (described above in *Section 4.6.1*) for the deformation  $u_h^{sp}$  and hydraulic pressure  $p_h^p$  on the coarsest mesh level are compared to the analytic solutions  $u^{sp}$ ,  $p^p$  of a stationary Biot problem. Finer level solutions look very much the same and are thus not shown.

(a) Displacement,  $d = 2$ :

$u_h^{sp}$  (numerical solution)

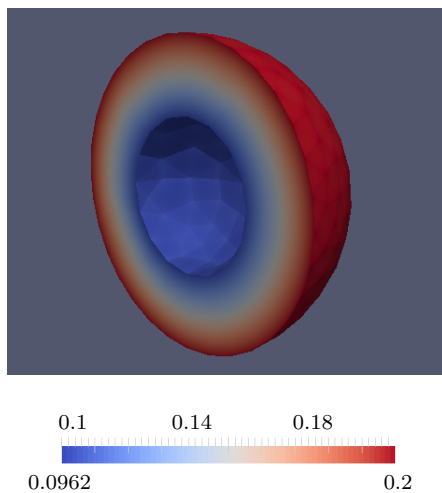


$u^{sp}$  (analytic solution)



(b) Displacement,  $d = 3$ :

$u_h^{sp}$  (numerical solution)



$u^{sp}$  (analytic solution)

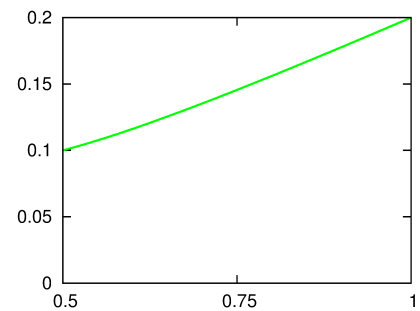
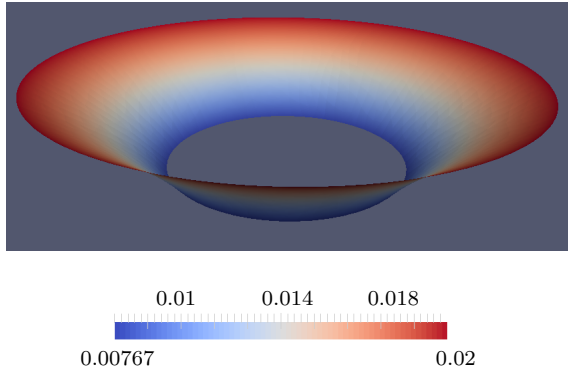


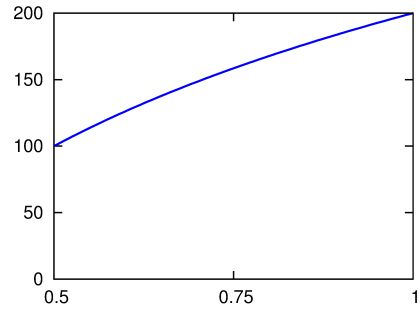
**Figure 4.6**

(c) Hydraulic pressure,  $d = 2$ :

$p_h^p$  (numerical solution)

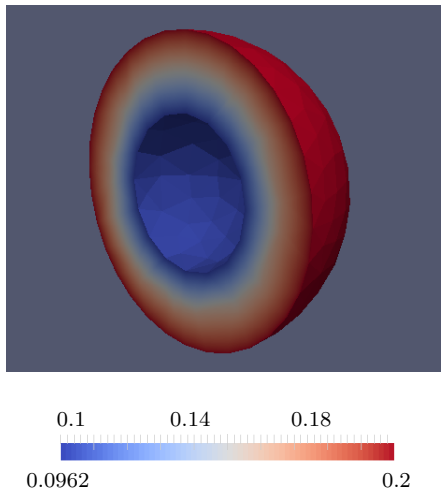


$p^p$  (analytic solution)

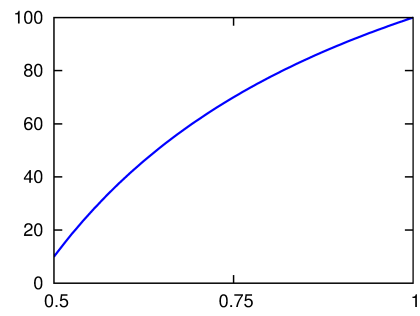


(d) Hydraulic pressure,  $d = 3$ :

$u_h^{sp}$  (numerical solution)



$u^{sp}$  (analytic solution)



### 4.6.2 Pure Biot problem with the *estimated* data. Parameter sensitivity

*Problem:* pure Biot problem (4.23)-(4.25) (or (4.60)) for the solid phase displacement, pore pressure and solid phase velocity  $(u^{sp}, p^p, v^{sp})$ . At the boundaries, Dirichlet and Neumann conditions (4.28), (4.30) for the displacement  $u^{sp}$  and Neumann conditions (4.27), (4.29) for the pore pressure  $p^p$  are prescribed. The parameters, initial and boundary conditions correspond to the *estimated* data written in the *numerics units*, see Section 3.3.

*Domain:*  $\Omega^p(t) \in \mathbb{R}^d$ ,  $d = \{2, 3\}$ , – spherically ( $d = 3$ ) or rotationally ( $d = 2$ ) symmetric with the inner radius  $r = a$  at  $\Gamma^{pin}$  and outer radius  $r = b$  at  $\Gamma^i(t)$ , see Fig. 4.4.

It should be noted, that while in this section only the Biot problem is simulated, the conditions at the outer boundary of the Biot domain are chosen as to mimic the most significant effects of the extracellular Stokes domain. In particular, at  $\Gamma^i$ , the hydraulic extracellular pressure  $p^b$  is assumed to remain constant, i.e.  $p^b := 0$ , and the osmotic pressure difference  $\pi^\Delta$  is computed according to (4.108), (4.107).

#### 4.6.2.1 Simulations with the *estimated* data

The equilibrium (terminal swollen state) is assumed to be achieved, when the fluid flow and solid phase velocities, as well as the deformation and volume growth (change) are zero. As can be seen on Fig. 4.7, the cell approaches its equilibrium state at times  $t \approx 10$  min ( $d = 3$ ),  $t \approx 15$  min ( $d = 2$ ) for the strict membrane assumption, and  $t \approx 585$  min ( $d = 3$ ),  $t \approx 780$  min ( $d = 2$ ) for the leaky membrane assumption. In order to demonstrate the behaviour of the numerical solution, the simulation times are terminated at  $t = 30$  min and  $t \approx 590$  min ( $d = 3$ ),  $t \approx 785$  min ( $d = 2$ ) for the strict and leaky membrane assumptions respectively.

*The results of the simulations show good agreement with the estimates made in Section 3.1.* In particular, using the physical parameters, initial domain dimensions, initial and terminal amounts of substance from the Tables 3.5, 3.6 as the *input* values for the numerical implementation, the *obtained* growth characteristics (i.e. deformations, volumes, etc.), average (characteristic) velocities and equilibration times are found to be reasonably close to the corresponding *estimated* values, see Table 4.2. It is also shown (see Table 4.2, Fig. 4.7) that with mesh refinement, the simulation results get (slightly) closer to the *estimated* values. The general improvement of the numerical solution to the Biot problem with mesh refinement is shown in Section 4.6.1, where the numerical and analytic Biot problem solutions are compared.

As shown in Fig. 4.8, the numerical solution of the Biot problem with the *estimated* data for the displacement  $u^{sp}$  is smooth and radially monotonous.

As described in Section 3.1, in case the membrane is assumed to be strictly semipermeable, the initial transmembrane concentration (and thus osmotic pressure) difference is highest in the beginning of the observation and falls to its estimated terminal (equilibrium) value due to the outflow of water from the extracellular into the intracellular space. Thus on the strict membrane assumption plots (Fig. 4.7a, 4.7b), the transmembrane fluid flux  $j^\Sigma$  and solid velocity  $v^{sp}$  gradually decrease to zero, while the deformation  $u^{sp}$  and ICS volume  $V^p$  smoothly converge to their equilibrium values.

In case the membrane is assumed to be *leaky* semipermeable, the transmembrane osmotic pressure difference is initially much lower, yet over time it changes not only due to the flow of water, but also because of the ICS-ECS exchange of the osmolytes, as prescribed in (4.107). Due to

the choice of the amount of substance exchange function  $a^\Delta$ , the magnitudes of the OTPD at each time step are so small, that the Biot system is *close* to its equilibrium at each  $t \in (0, T)$ . Therefore as soon as  $a^\Delta$  reaches its terminal value (at a pre-determined time  $T$ ), the ultimate equilibrium state of the Biot system is rapidly achieved. Thus as shown in *Fig. 4.7c, 4.7d*, under the leaky membrane assumption, abrupt transitions of the measured quantities from  $t = 0$  to  $t > 0$  and then from  $t \approx T$  into their equilibrium values for  $t > T$  are observed. For the approximation of  $a^\Delta$  by a function that smoothly decreases to zero, the evolution of the numerical solution into its equilibrium can naturally be expected to be smoother.

The algorithm that realises the movement of the mesh nodes is verified through the computation of the numerical volume growth error  $V_{err}^p$ , which is defined as the absolute value of the relative difference between the cell volume growth  $V_\Delta^p := V_T^p - V_0^p$  and the volume  $V^\Sigma$  of the fluid crossing the interface of the cell:

$$V_{err}^p := \left| \frac{V_\Delta^p - V^\Sigma}{V_\Delta^p} \right| = \left| \frac{V_T^p - V_0^p - V^\Sigma}{V_\Delta^p} \right|. \quad (4.110)$$

The magnitude of  $V_{err}^p$  is found to be small, which is demonstrated in *Table 4.2*.

**Table 4.2 Pure Biot problem simulations with the *estimated* data.**

The data given below was obtained for the 2- and 3-dimensional Biot problem simulations with the (*estimated*) parameters and initial values (from table 3.6) for the strict and leaky membrane assumptions on mesh refinement levels 0, 1 (denoted as L0, L1). The following quantities are evaluated:  $u_T$  – final (terminal) displacement,  $A_0^p$  – initial surface area of in the ICS  $\Omega^p$ ,  $A_T^p$  – final surface area of the ICS  $\Omega^p$ ,  $\pi_0^\Delta$  – initial transmembrane osmotic pressure difference,  $\pi_T^\Delta$  – final transmembrane osmotic pressure difference,  $V_0^p$  – initial volume of the ICS  $\Omega^p$ ,  $V_T^p$  – final volume of the ICS  $\Omega^p$ ,  $V_\Delta^p := V_T^p - V_0^p$  – increase (growth) of the ICS volume,  $V_{err}^p$  – numerical volume growth error defined in (4.110). As discussed above in Section 4.6.2, the simulations are terminated at  $T := 30$  min for the strict membrane assumption and at  $T := 780$  min ( $d = 2$ ),  $T := 585$  min ( $d = 3$ ) for the leaky membrane assumption. All initial values are computed (given) at  $t = 0$ , final values – at  $t = T$ .

**Strictly semipermeable membrane assumption**

Unit		$d = 2$		$d = 3$	
		L0	L1	L0	L1
$T$	min	30.0	30.0	30.0	30.0
$u_T$	$\mu\text{m}$	5.475	5.490	4.626	4.667
$V_0^p$	$\mu\text{m}^d$	7732	7770	4952e2	5151e2
$V_T^p$	$\mu\text{m}^d$	9543	9588	6471e2	6731e2
$V_\Delta^p$	$\mu\text{m}^d$	1810	1818	1519e2	1579e2
$V_{err}^p$	–	2.51e-3	1.13e-3	7.15e-3	3.00e-3
$A_0^p$	$\mu\text{m}^{d-1}$	344.27	344.65	307.55e2	314.13e2
$A_T^p$	$\mu\text{m}^{d-1}$	378.766	379.161	367.06e2	374.88e2
$\pi_0^\Delta$	$\text{mg}/\mu\text{m}^{d-2}\text{min}^2$	7.425e14	7.389e14	9.436e8	9.070e8
$\pi_T^\Delta$	$\text{mg}/\mu\text{m}^{d-2}\text{min}^2$	1.357e13	1.397e13	1.531e7	1.536e7

**Leaky semipermeable membrane assumption**

Unit		$d = 2$		$d = 3$	
		L0	L1	L0	L1
$T$	min	780.0	780.0	585.0	585.0
$u_T$	$\mu\text{m}$	5.487	5.505	4.627	4.668
$V_0^p$	$\mu\text{m}^d$	7732	7770	4952e2	5151e2
$V_T^p$	$\mu\text{m}^d$	9547	9594	6471e2	6731e2
$V_\Delta^p$	$\mu\text{m}^d$	1815	1823	1519e2	1579e2
$V_{err}^p$	–	7.16e-5	3.29e-5	1.57e-4	8.23e-5
$A_0^p$	$\mu\text{m}^{d-1}$	344.27	344.65	307.55e2	314.13e2
$A_T^p$	$\mu\text{m}^{d-1}$	378.841	379.259	367.06e2	374.89e2
$\pi_0^\Delta$	$\text{mg}/\mu\text{m}^{d-2}\text{min}^2$	3.044e10	3.029e10	1.051e4	1.010e4
$\pi_T^\Delta$	$\text{mg}/\mu\text{m}^{d-2}\text{min}^2$	1.283e13	1.284e13	1.529e7	1.528e7

**Figure 4.7 Pure Biot problem simulations with the *estimated* data.**

The plots below show the 2- and 3-dimensional Pure Biot problem simulation results on mesh refinement levels 0, 1, for such quantities as the ICS volume  $V^p$  (*Volume*, [ $\mu\text{m}^d$ ]), volumetric transmembrane fluid flux  $j^\Sigma$  (*Water flux*, [ $\mu\text{m}^d/\text{min}$ ]), maximum value (over mesh cells) of the ICS deformation  $u^{sp}$  (*Max. Deformation*, [ $\mu\text{m}$ ]), max. value of the ICS deformation velocity  $v^{sp}(t) := \partial_t u^{sp}(t)$  (*Max. Solid velocity*, [ $\mu\text{m}/\text{min}$ ]). All quantities are shown to develop over time  $t \in (0, T)$ , [min], where  $T := 30$  min for the strict membrane assumption and  $T := 585$  min ( $d = 3$ ),  $T := 780$  min ( $d = 2$ ) for the leaky membrane assumption.

(a) Strictly semipermeable membrane assumption,  $\mathbf{d} = \mathbf{3}$ :

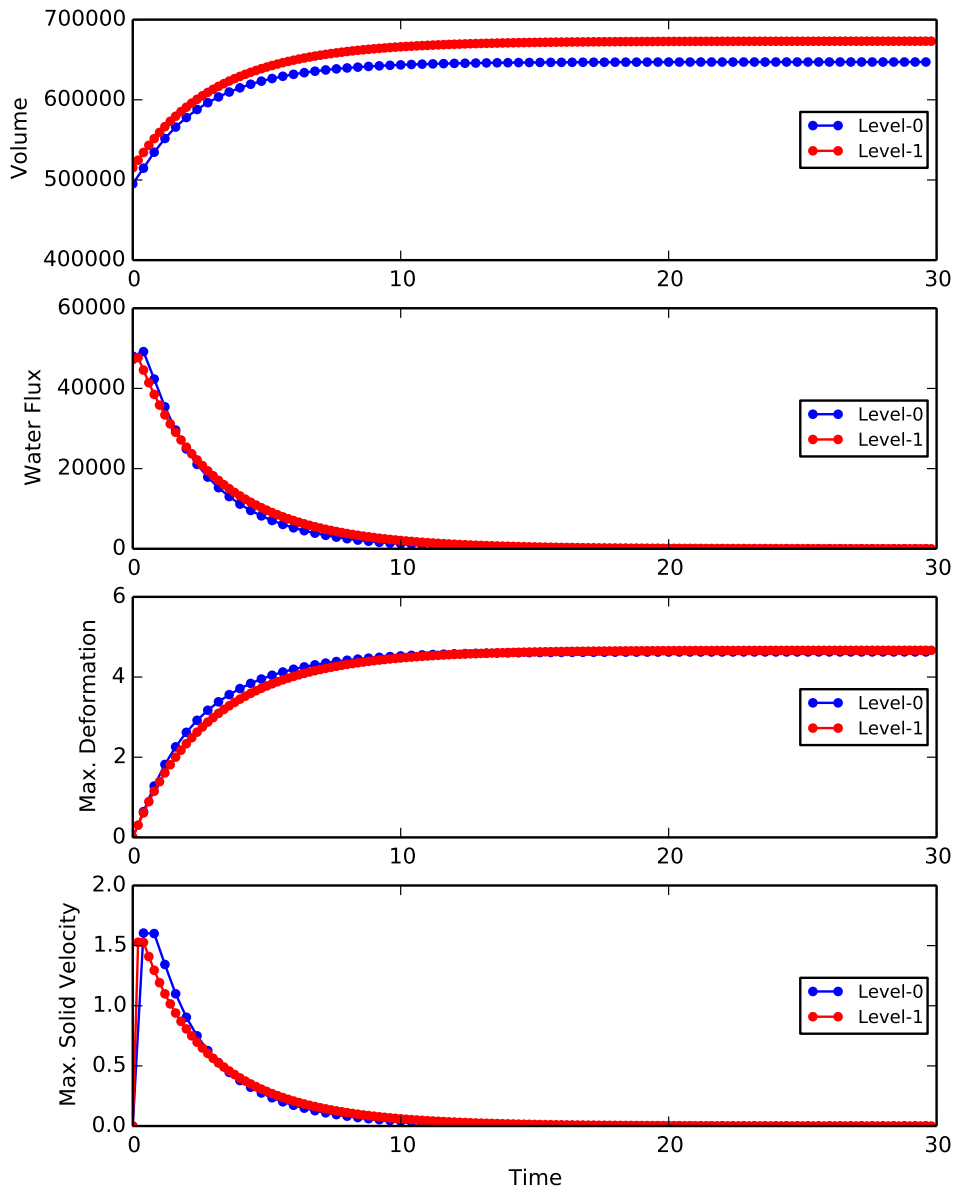




Figure 4.7

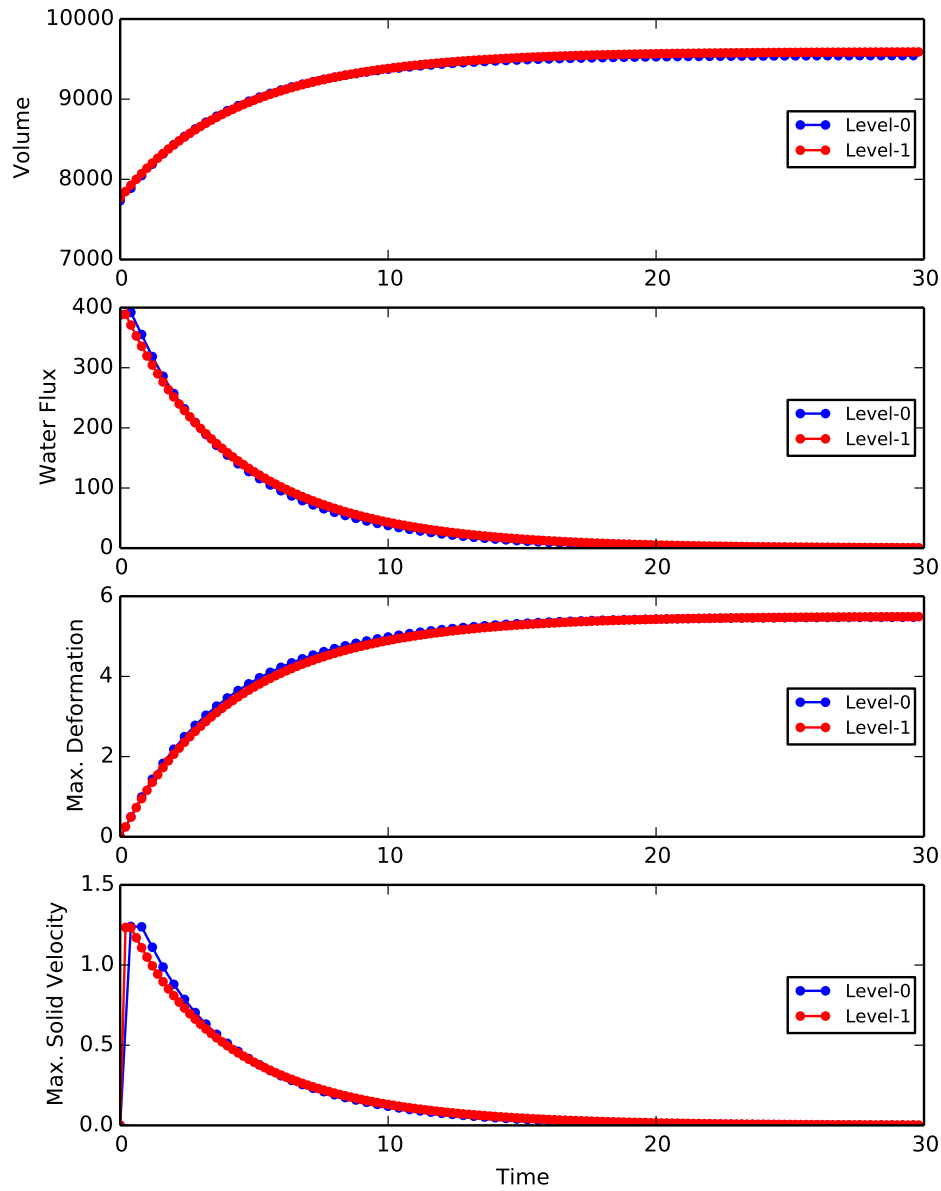
(b) Strictly semipermeable membrane assumption,  $d = 2$ :

Figure 4.7

(c) Leaky semipermeable membrane assumption,  $d = 3$ :

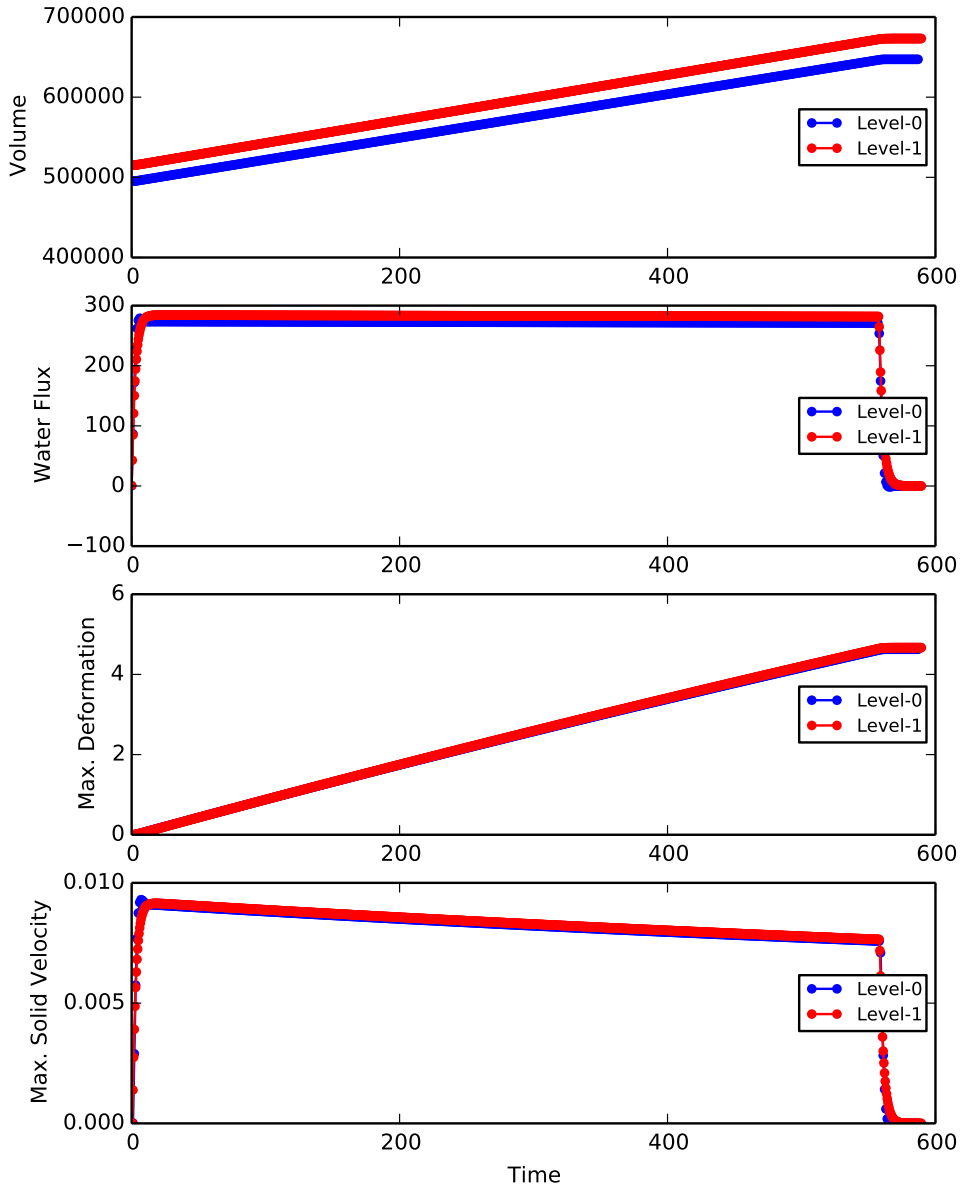
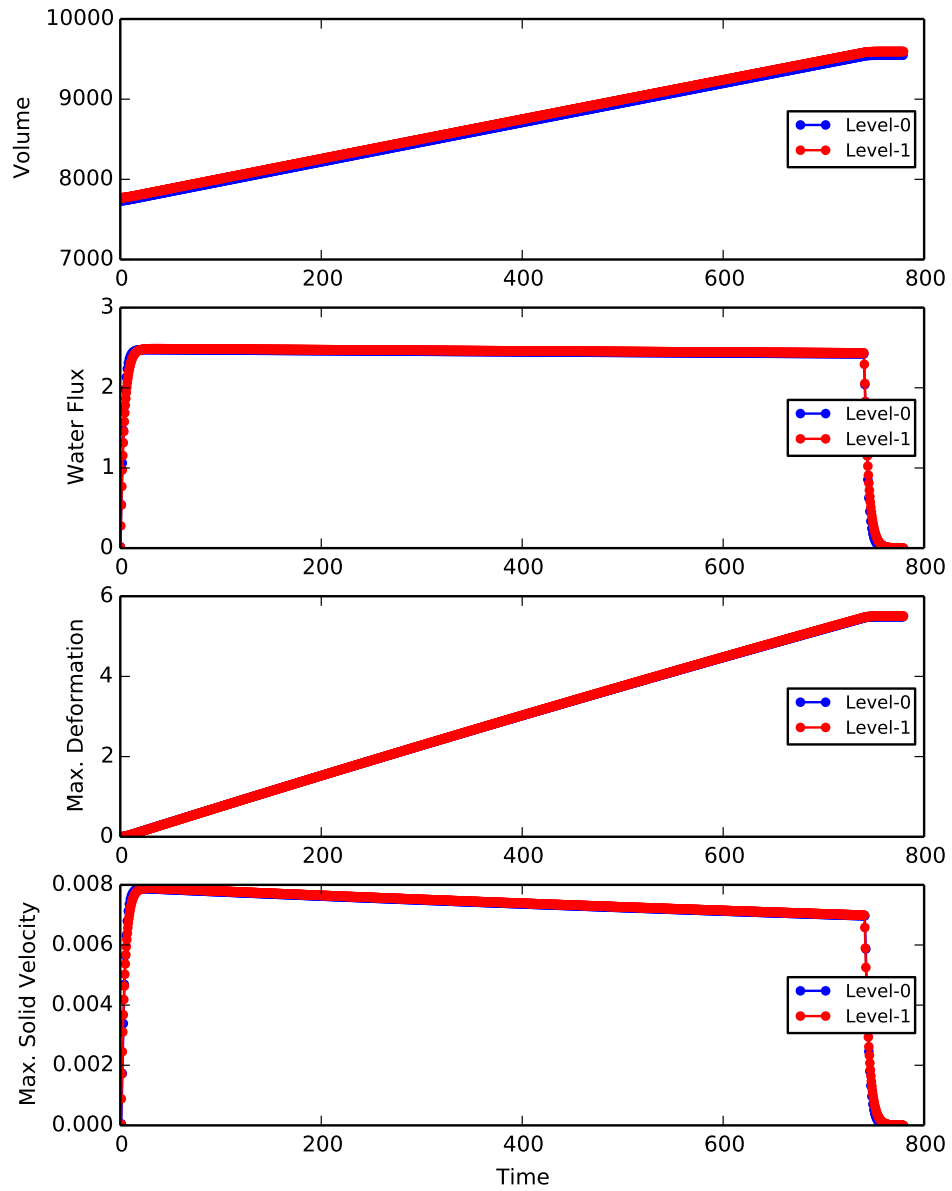


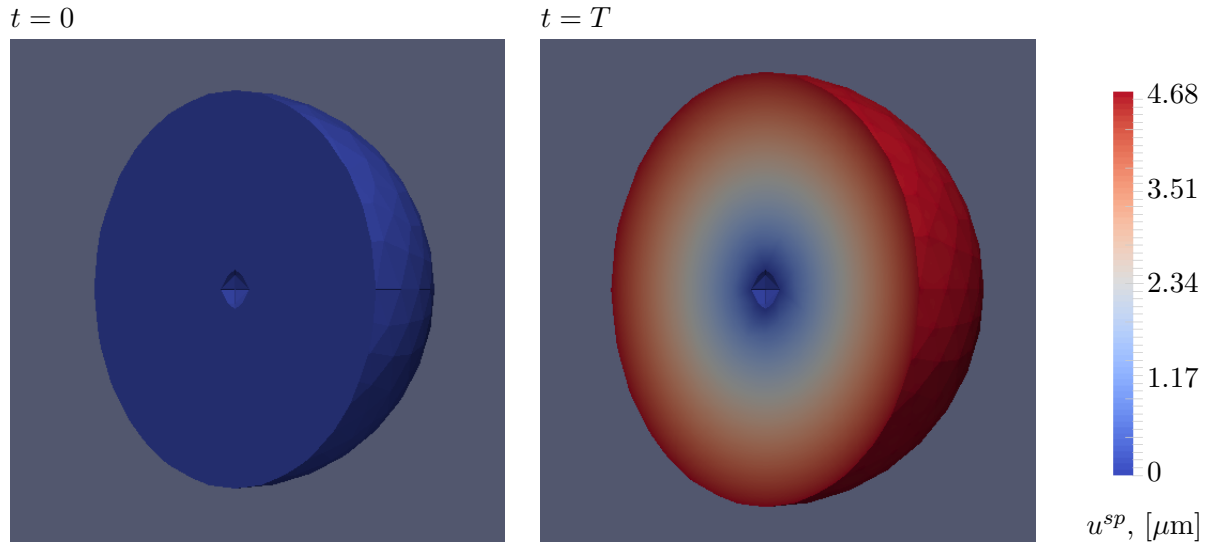
Figure 4.7

(d) Leaky semipermeable membrane assumption,  $d = 2$ :

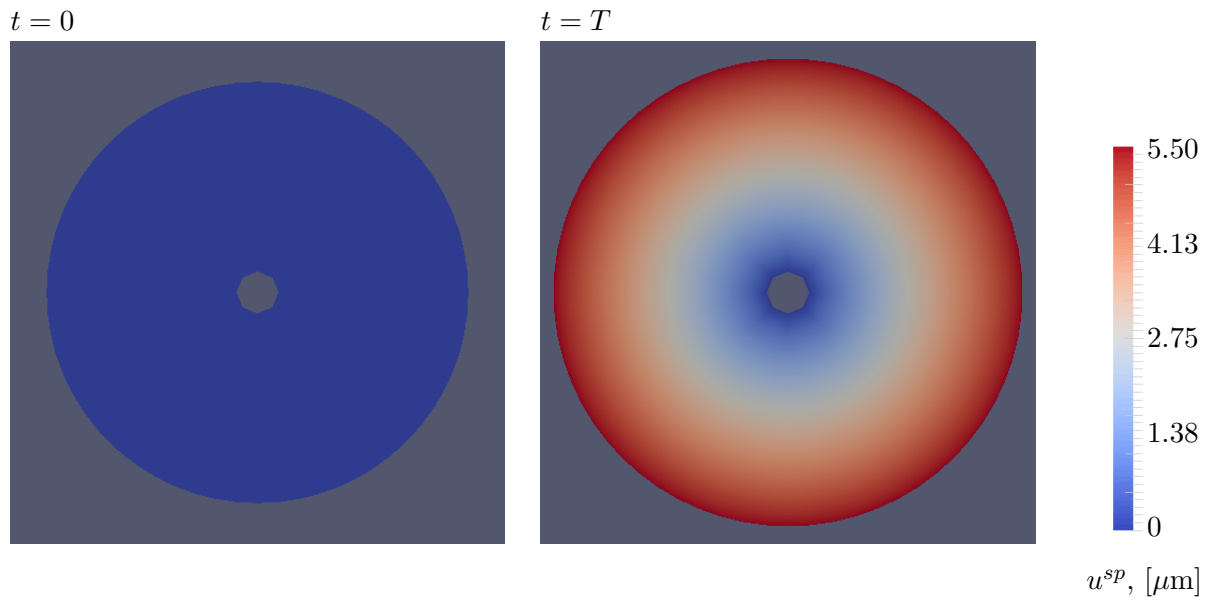
**Figure 4.8 Pure Biot problem simulations with the *estimated* data: deformation solution.**

On the pictures below, the initial and terminal magnitudes of the deformation function  $u^{sp}$  over the ICS  $\Omega^p$  are shown for the 2- and 3-dimensional Pure Biot problem simulations with the *estimated* parameters (from *Table 3.6*, strict membrane assumption) on mesh refinement level 1.

**d = 3**



**d = 2**



### 4.6.2.2 Parameter sensitivity

The parameters chosen for the sensitivity analysis are the porosity (solidity)  $\gamma^f$  ( $\gamma^s$ ), elasticity coefficients  $\lambda^s$ ,  $\mu^s$ , membrane water permeability  $L^p$  and ICS (Biot domain) permeability  $k$ .

The *reference parameters* correspond to the *estimated* (physical living cell) parameter values that are listed in the *numerics* units in *Table 3.6*, namely:

$$d = 3: \quad \gamma^f := 0.5, \quad L^p := 1.67 \cdot 10^{-9}, \quad \lambda^s := 51.0 \cdot 10^6, \quad \mu^s := 13.0 \cdot 10^6; \quad (4.111)$$

$$d = 2: \quad \gamma^f := 0.5, \quad L^p := 1.67 \cdot 10^{-15}, \quad \lambda^s := 51.0 \cdot 10^{12}, \quad \mu^s := 13.0 \cdot 10^{12}, \quad (4.112)$$

where the parameter units are:

$$[\gamma^f] = [-], \quad [L^p] = [\mu\text{m}^{d-1}\text{min}/\text{mg}], \quad [\lambda^s], [\mu^s] = [\text{mg}/\mu\text{m}^{d-2}\text{min}^2], \quad d = \{2, 3\}. \quad (4.113)$$

For each parameter, the results of the simulations obtained for the reference parameter set are compared to the simulation results in which the chosen parameter is varied, while the other parameters preserve their reference values.

The simulation results given in this section are obtained for the 2- and 3-dimensional Biot problem under the strict membrane assumption. In order to compare the equilibration times, the characteristic growth time  $t_{gc}$ , i.e. the time by which approximately  $(1 - 1/e) \cdot 100\%$  ( $\approx 63\%$ ) of the total ICS volume growth is reached, is defined:

$$t_{gc}: \quad V_{t_{gc}}^p - V_0^p := (1 - 1/e) \cdot (V_T^p - V_0^p). \quad (4.114)$$

The interdependence of the Biot problem quantities can be reflected through the following general laws and conditions:

- Normal flux interface (boundary) condition (4.91),

$$\gamma^f (v_n^{fp} - v_n^{sp}) \cdot n =: j_n^p \cdot n = L^p (p^\Delta + \pi^\Delta) \quad \text{at } \Gamma^i(t) \times (0, T), \quad (4.115)$$

relates the normal flux  $j_n^p$  (and so the permeability  $\gamma^f$ , normal fluid and solid phase velocities  $v_n^{fp}$ ,  $v_n^{sp}$ ), membrane permeability  $L^p$ , osmotic and hydraulic transmembrane pressure differences  $\pi^\Delta$ ,  $p^\Delta$ . From this condition it follows, that at the equilibrium state, the osmotic and hydraulic pressure differences must be equal.

- Continuity of normal stresses condition (4.30), that following (3.28), at the equilibrium state can be approximated as:

$$p_T^\Delta = \mathcal{M} \frac{u_T^{sp}}{l^p}, \quad \mathcal{M} := \begin{cases} 2(\lambda^s + \mu^s) & d = 2, \\ (3\lambda^s + 2\mu^s) & d = 3, \end{cases} \quad (4.116)$$

relates the equilibrium deformation  $u_T^{sp}$ , domain size  $l^p$ , elasticity coefficients  $\mu^s$ ,  $\lambda^s$  and equilibrium hydraulic transmembrane pressure difference  $p_T^\Delta$ .

- As indicated in *Chapter 3*, under the swelling cell conditions, the admissibility condition leads to the following relation between the absolute values of the normal fluid and solid phase velocities  $v_n^{fp}$ ,  $v_n^{sp}$  of the poroelastic Biot domain:

$$|v_n^{fp}| \approx |v_n^{sp}|. \quad (4.117)$$

**Porosity**  $\gamma^f$ 

Porosity of a porous medium defines the relative volume of fluid contained in the medium. Thus as follows from (4.108), for given fixed intracellular and extracellular amounts of substance  $a^{fp}$ ,  $a^b$  and ICS volume  $V^p$ , the transmembrane osmotic pressure difference is inversely proportional to the porosity. As suggested by (4.115), (4.115)&(4.117) and (4.115)&(4.116), the fluid flux  $j^p$ , normal solid phase velocity  $v_n^{sp}$ , ICS deformation  $u^{sp}$  (and thus the ICS volume  $V^p$ ) can also be expected to be inversely proportional to the porosity. It should be noted, that due to the non-trivial dependence of the OTPD on the porosity and intracellular fluid volume, the rates of change of the above mentioned quantities should not be expected to coincide with the rates of change in the porosity.

The simulation results for the variation of the porosity by 20% shown in Table 4.3 and Fig. 4.9a, 4.9b agree with the expected response in the values of deformation  $u^{sp}$ , ICS volume  $V^p$ , volumetric transmembrane flux  $j^\Sigma$  and solid phase velocity  $v^{sp}$ . Thus as shown in Table 4.3 and Fig. 4.9a, 4.9b, for the 20% increase/decrease of the porosity, the ICS deformation  $u^{sp}$  decreases by  $\approx 86.3\%$ /increases by 95.6% respectively ( $d = 3$ ).

**Elasticity coefficients**  $\lambda^s, \mu^s$ 

Since the shear modulus and Lamé's first coefficient are related (through the linear elasticity formula (3.2)), the elasticity coefficients are varied simultaneously. The effect of the ICS elasticity on the equilibrium displacement (volume) of the domain is reflected through the conditions (4.115)&(4.116):

$$j_T^p = 0 \quad \Rightarrow \quad \pi_T^\Delta = p_T^\Delta \quad \Rightarrow \quad \pi_T^\Delta = \mathcal{M} \frac{u_T^{sp}}{l_T^p}. \quad (4.118)$$

Condition (4.118) however does not suggest an immediate estimate for the elasticity effect on the displacement due to the dependence of the osmotic pressure difference  $\pi^\Delta$  on the domain volume (and thus the displacement).

The variation of the elasticity coefficients results in a very dampened and non-symmetric response of the measured quantities, see Table 4.3 and Fig. 4.9c, 4.9d. Increasing the coefficients by an order of magnitude results in a decrease of the final deformation by less than 15% percent; at the same time, the corresponding decrease of the elasticity has no noticeable influence on any of the measured quantities. These observations are particularly noteworthy, since (as indicated in Section 3.1) the experiments aimed at estimating the characteristic elastic properties of the cellular structures are difficult to perform and thus the available results may entail large measurement errors. However the obtained simulation results indicate, that the overall impact of such errors is partially compensated by a correspondingly low system sensitivity.

**Membrane permeability**  $L^p$ 

Since the ICS deformation (and consequently the ICS volume) depend on the elastic properties of the ICS skeleton and transmembrane pressure difference, but not on the membrane permeability, their equilibrium values should not be affected by the variations in  $L^p$ . As follows from the flux condition (4.115), the membrane permeability coefficient  $L^p$  is the proportionality coefficient relating the total transmembrane pressure difference to the transmembrane fluid flux. Thus for the fixed pressure difference and deformation, the change in  $L^p$  should result in the proportional change of the fluid flux, thus (as follows from condition (4.117)) solid phase velocity, thus the equilibration times.

The simulation results for the variation of the membrane permeability by 50% shown in Table 4.3 and Fig. 4.9e, 4.9f agree with the expected response of the above mentioned quantities.

***ICS Permeability  $k$*** 

Sensitivity tests for the ICS permeability  $k$  lead to ambiguous results. For the 2D simulation, the variation of the parameter by up to 5 orders of magnitude shows no influence on the solution of the Biot problem, up to what could be caused by numerical errors. In order to obtain results for the strong permeability reduction, the time step size has to be reduced dramatically, as the numerical computation becomes unstable for lowered values of  $k$ . For the reduction of more than 5 orders of magnitude, numerical oscillations can no longer be controlled by the time step size.

Such low sensitivity indicates that the flow of intracellular fluid relative to the cell solid structure is negligible with regard to the overall system dynamics.

**Table 4.3 Pure Biot problem simulations: parameter sensitivity.**

The data below shows sensitivity of the Biot domain  $\Omega^p$  simulations (with the *estimated* parameters) to the variations of the porosity (solidity)  $\gamma^f$  ( $\gamma^s$ ), elasticity coefficients  $\{\mu^s, \lambda^s\}$ , membrane permeability  $L^p$ . The simulation data is available for dimensions  $d = 3$ ,  $d = 2$ ; the membrane is assumed to be *strictly* semipermeable. The following quantities are evaluated:  $u_{max}^{sp}$  – maximum value (over mesh cells) of the ICS deformation  $u^{sp}$ ,  $V_T^p$  – final volume of the ICS,  $j_{max}^\Sigma$  – max. value of the volumetric transmembrane fluid flux,  $v_{max}^{sp}$  – max. value of the ICS solid phase velocity ( $v^{sp}(t) := \partial_t u^{sp}(t)$ ),  $t_{gc}$  – time by which approximately  $(1 - 1/e) \cdot 100\%$  of the total growth of the ICS is reached; the total time  $T$  is chosen as  $T := 30$  min. The values are first found for the Biot domain simulations with reference parameters, then one of the tested parameters is varied, while all other ones preserve their reference values. Reference parameter values and parameter units are given in (4.111), (4.113).

**d=3**

		$u_{max}^{sp}$ , [ $\mu\text{m}$ ]	$V_T^p$ [ $\mu\text{m}^3$ ]	$j_{max}^\Sigma$ [ $\mu\text{m}^3/\text{min}$ ]	$v_{max}^{sp}$ [ $\mu\text{m}/\text{min}$ ]	$t_{gc}$ [min]
Reference parameter set		4.627	647.145e3	49.18e3	1.604	2.4 - 2.8
Varied*	Value					
$\gamma^f$	0.4	8.620	800.939e3	102.34e3	3.253	2.4 - 2.8
	0.6	0.202	501.289e3	15.23e3	0.506	2.4 - 2.8
$L^p$	0.835e-9	4.593	645.955e3	24.31e3	0.802	5.6 - 6.0
	3.340e-9	4.627	647.148e3	100.64e3	3.209	0.8 - 1.2
$\{\lambda^s, \mu^s\}$	{51.0e5, 13.0e5}	4.708	650.077e3	49.291e3	1.604	2.4 - 2.8
	{51.0e7, 13.0e7}	3.950	623.194e3	48.091e3	1.604	2.0 - 2.4

**d=2**

		$u_{max}^{sp}$ , [ $\mu\text{m}$ ]	$V_T^p$ [ $\mu\text{m}^2$ ]	$j_{max}^\Sigma$ [ $\mu\text{m}^2/\text{min}$ ]	$v_{max}^{sp}$ [ $\mu\text{m}/\text{min}$ ]	$t_{gc}$ [min]
Reference parameter set		5.476	9.544e3	392.11	1.241	4.0 - 4.4
Varied*	Value					
$\gamma^f$	0.4	11.050	11.581e3	848.72	2.707	4.0 - 4.4
	0.6	1.231	8.124e3	82.40	0.263	4.0 - 4.4
$L^p$	0.835e-15	5.268	9.471e3	194.46	0.620	8.0 - 8.4
	3.340e-15	5.481	9.545e3	777.82	2.481	1.6 - 2.0
$\{\lambda^s, \mu^s\}$	{51.0e11, 13.0e11}	5.574	9.578e3	392.72	1.241	4.0 - 4.4
	{51.0e13, 13.0e13}	4.654	9.260e3	388.91	1.241	3.2 - 3.6



**Figure 4.9 Pure Biot problem simulations: parameter sensitivity.**

The plots below demonstrate the sensitivity of the ICS  $\Omega^p$  simulations to the variations of the porosity  $\gamma^f$ , elasticity coefficients  $\{\lambda^s, \mu^s\}$ , membrane permeability  $L^p$  and ICS permeability  $k$  over time  $t \in (0, T)$ , where following the arguments given in *Section 4.6.2*, the simulations are terminated at  $T = 30$  min. The simulation data is available for dimensions  $d = 3$ ,  $d = 2$ , the membrane is assumed to be *strictly* semipermeable. More detailed descriptions of the plotted quantities are given in *Table 4.3*. Results corresponding to the simulations with reference parameters are plotted in red.

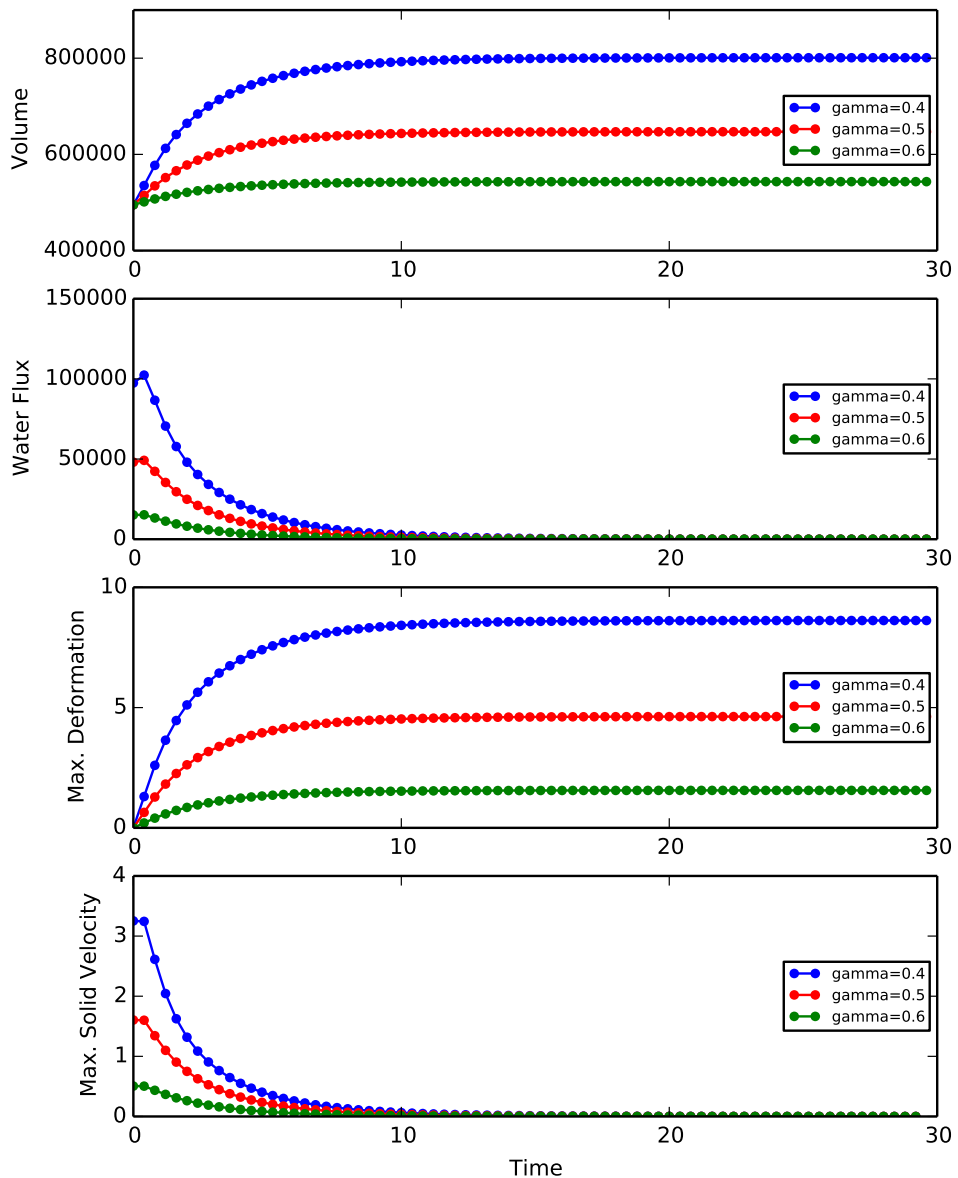
(a) Porosity  $\gamma^f$ ,  $\mathbf{d} = \mathbf{3}$ :

Figure 4.9

(b) Porosity  $\gamma^f$ ,  $d = 2$ :

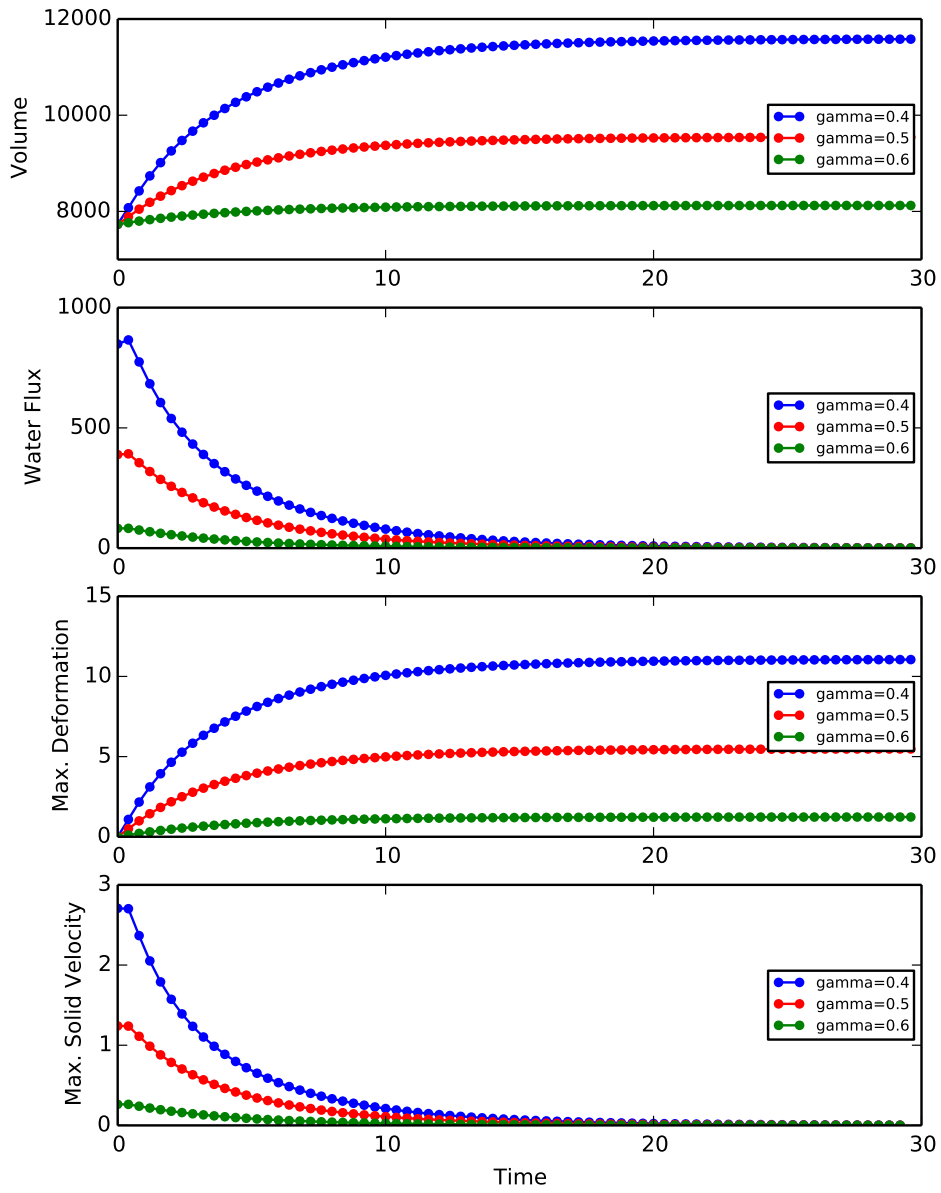


Figure 4.9

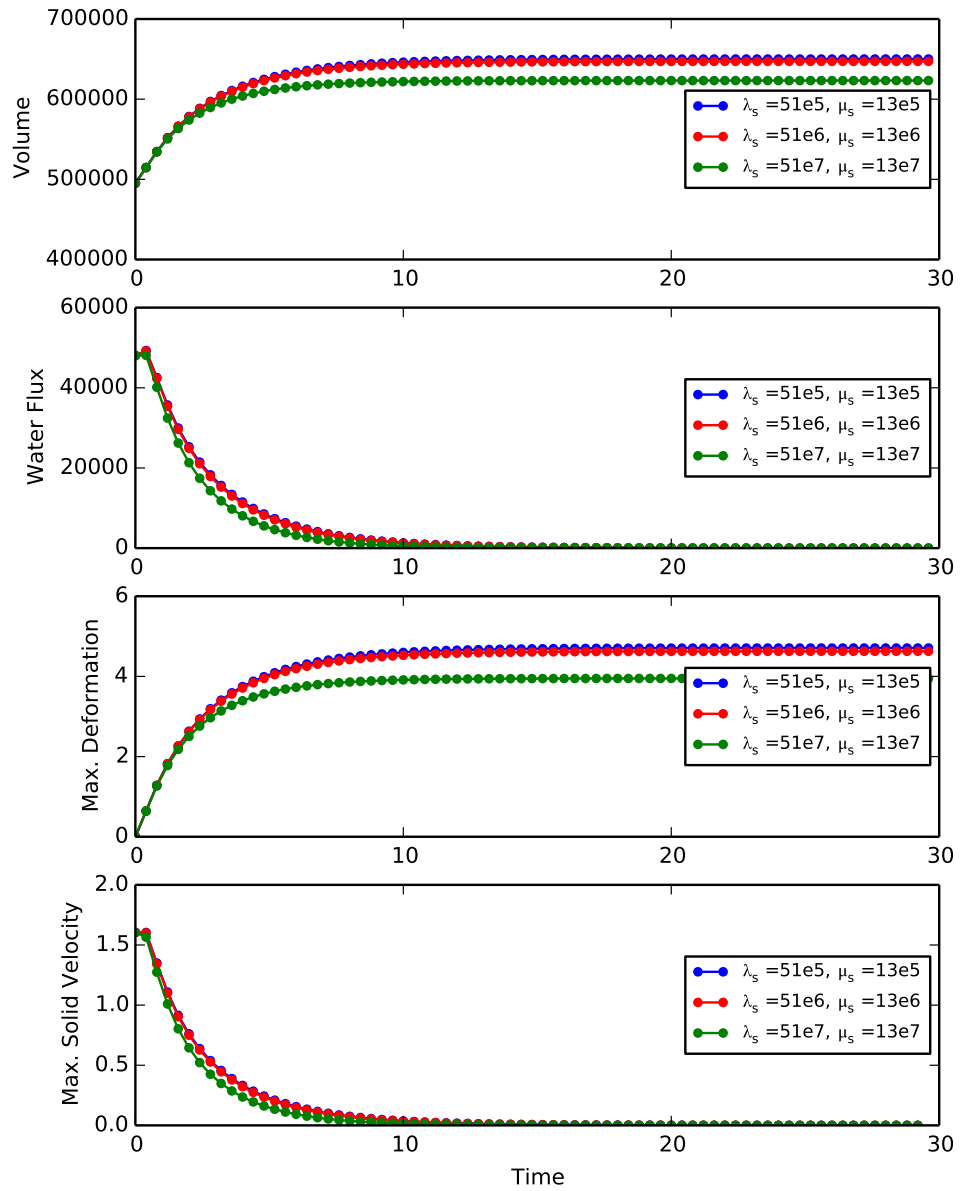
(c) Elasticity coefficients  $\lambda^s, \mu^s, \mathbf{d} = \mathbf{3}$ :

Figure 4.9

(d) Elasticity coefficients  $\lambda^s, \mu^s, \mathbf{d} = \mathbf{2}$ :

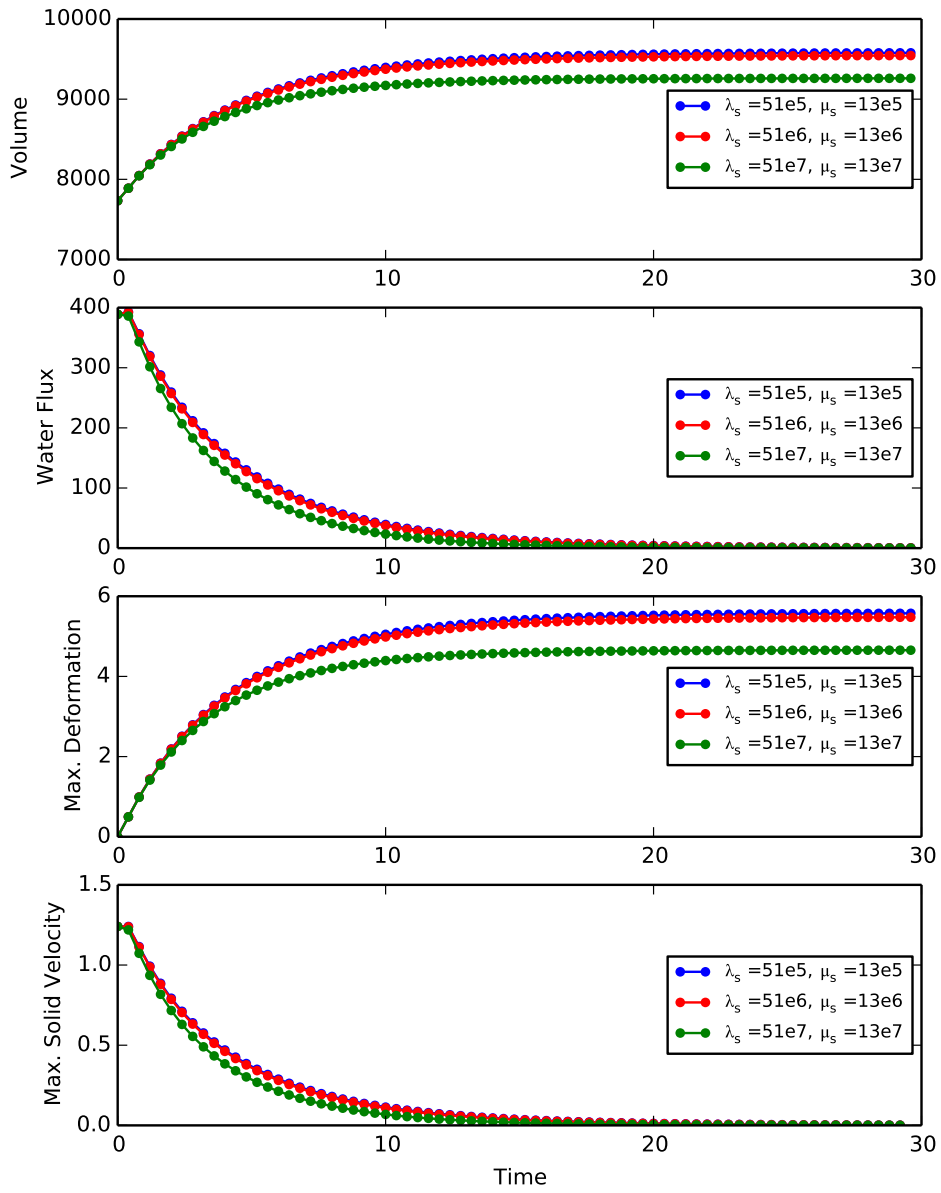


Figure 4.9

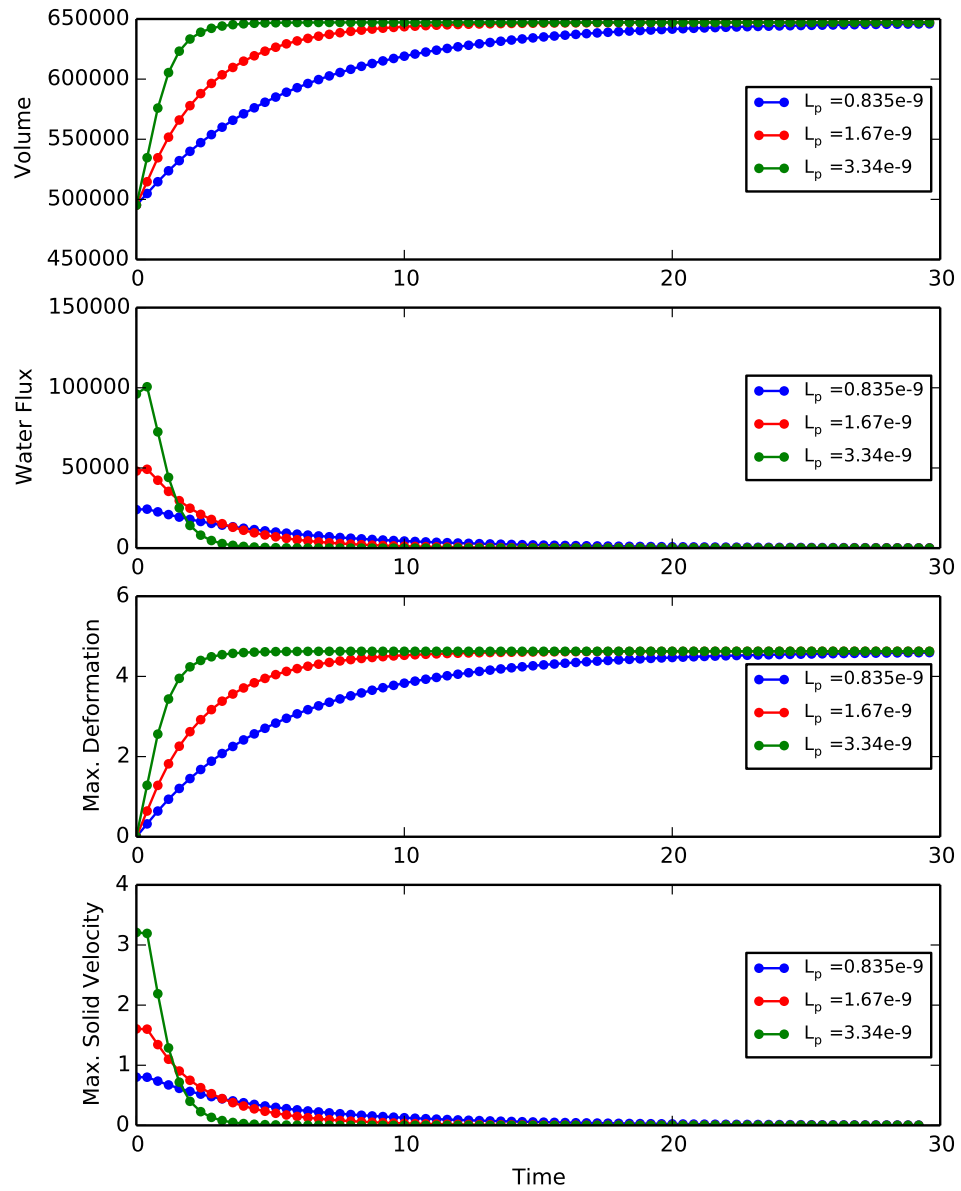
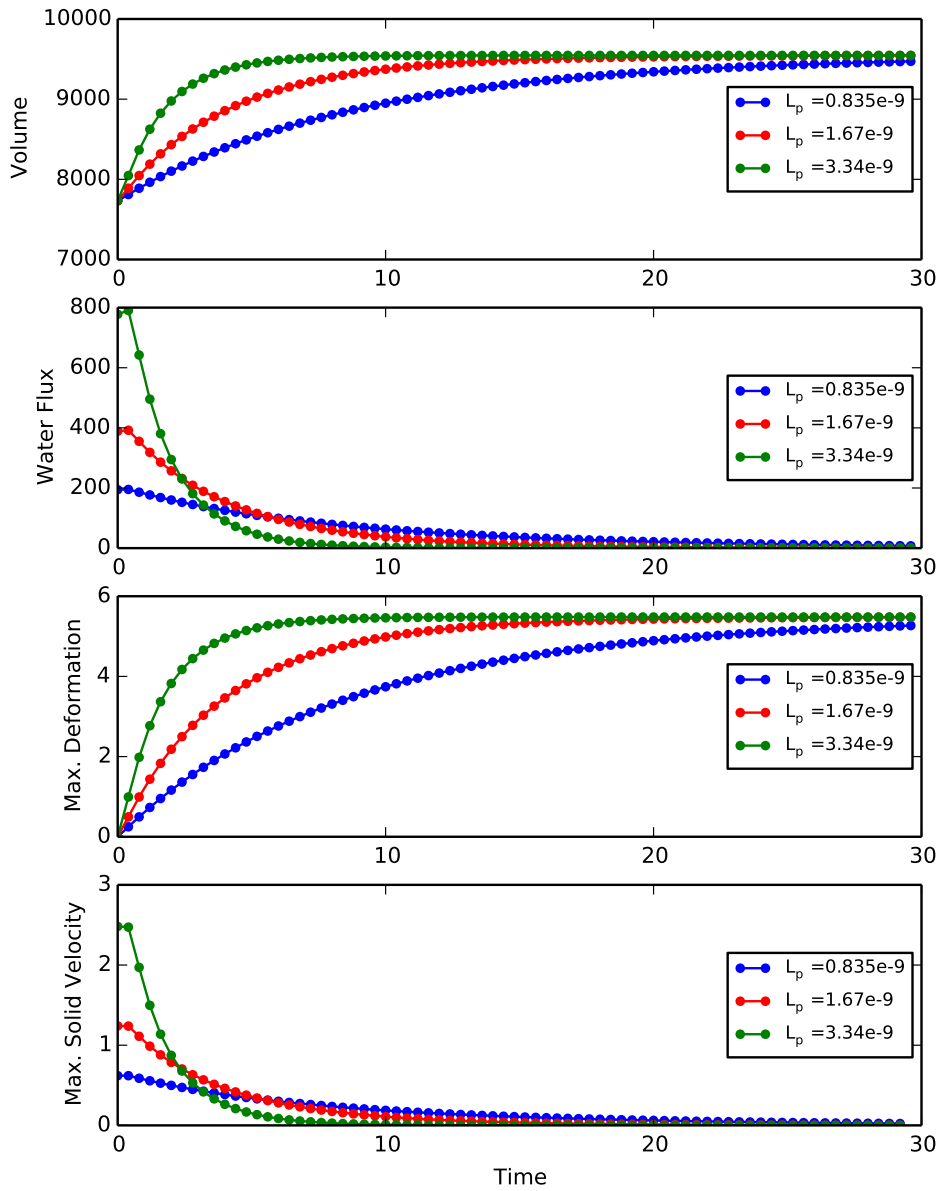
(e) Membrane permeability  $L^p$ ,  $d = 3$ :

Figure 4.9

(f) Membrane permeability  $L_p$ ,  $d = 2$ :



### 4.6.3 Coupled Biot-Stokes problem with circular Biot domain

*Problem:* coupled Biot-Stokes problem (4.59), (4.60) for the solid phase displacement  $u^{sp}$ , pore pressure  $p^p$ , solid phase velocity  $v^{sp}$ , bulk fluid velocity  $v^b$ , bulk fluid pressure  $p^b$  and fluid domain displacement  $u^b$ . The parameters, initial, interface and boundary values correspond to the *estimated* data values from Tables 3.5, 3.6. The coupled problem is solved following the operator splitting scheme (4.87)-(4.104). Boundary, initial and interface conditions are as described in Section 4.4.

*Domain:*  $\Omega := \Omega^b(t) \cup \Omega^p(t) \in \mathbb{R}^d$ ,  $d = \{2, 3\}$ , where the Biot domain  $\Omega^p(t)$  is rotationally symmetric with the inner radius  $r = a$  at  $\Gamma^{pin}$  and outer radius  $r = b$  at  $\Gamma^i(t)$ ,  $\partial\Omega^p(t) := \Gamma^{pin} \cup \Gamma^i(t)$ , located centrally within  $\Omega$  and completely surrounded by the Stokes fluid  $\Omega^b(t)$ ,  $\partial\Omega^b(t) := \Gamma^{bw} \cup \Gamma^i(t)$ . The geometry of the coupled problem is as shown in Fig. 4.12a.

Here it is shown, that for the coupled Biot-Stokes problem where the Biot domain is rotationally symmetric (circular), the Stokes fluid velocity is essentially zero and so the Stokes hydraulic pressure is essentially constant up to numerical fluctuations. Thus the solution of the *Pure* Biot problem with *appropriate* boundary conditions (as described in the beginning of Section 4.6.2) is almost identical to the solution of the *Coupled* Biot problem, i.e. the Biot problem solved as a part of the coupled Biot-Stokes problem.

In Table 4.4, the values of a (one-dimensional) quantity  $q$  obtained from the *Pure* and *Coupled* Biot problem solutions (denoted as  $q_p$ ,  $q_c$  respectively) are compared through the computation of the  $L^2$  and  $L^\infty$  errors (denoted as  $Err_2$  and  $Err_{max}$  respectively), such that:

$$\begin{aligned} Err_2(q) &:= \left( \int_0^T (q_p(t) - q_c(t))^2 dt \right)^{1/2}, \\ Err_{max}(q) &:= \max_t \{ |q_p(t) - q_c(t)| : t \in (0, T) \}. \end{aligned} \quad (4.119)$$

Relative errors  $Err_2^\Delta$ ,  $Err_{max}^\Delta$  are defined as a ratio between the errors  $Err_2$ ,  $Err_{max}$  and the maximum value of the quantity, i.e. for the quantity  $q$ :

$$Err_2^\Delta(q) := \frac{Err_2(q)}{q_{max}}, \quad Err_{max}^\Delta(q) := \frac{Err_{max}(q)}{q_{max}}. \quad (4.120)$$

The plots of the *Pure* and *Coupled* Biot problem simulation results for certain quantities are compared in Fig. 4.10a. In Fig. 4.10b, 4.10c, the difference between the *Coupled* Biot problem simulation results obtained on mesh refinement levels 0, 1 and *Pure* Biot problem simulation results on level 1 is plotted.

The magnitudes of the numerical solutions for the hydraulic pressures, Biot solid phase velocity and Stokes bulk fluid velocity at several time steps are shown in Fig. 4.11. As expected, the hydraulic pressure difference between the domains increases in time and the Stokes fluid velocity is (close to) zero.

Further results for the simulations of the *Coupled* Biot problem with circular Biot domain can be found in Section 4.6.4.

**Table 4.4 Coupled Biot-Stokes vs Pure Biot problem: *circular* Biot domain geometry.**

Below, the simulation results for the 2-dimensional Pure Biot problem (as described in *Section 4.6.2*) and Coupled Biot problem (i.e. the Biot problem solved as a part of the coupled Biot-Stokes problem), where the Biot domains have *circular* (as shown in *Fig. 4.12a*) geometry, are compared on mesh refinement levels 0, 1. In particular,  $L^2$  and  $L^\infty$  errors  $Err_2$ ,  $Err_{max}$ , as well as the relative errors  $Err_2^\Delta$ ,  $Err_{max}^\Delta$  (defined in (4.119), (4.120)) are computed between the Pure Biot and Coupled Biot simulation results for the terminal ICS volume ( $V_T^p$ , [ $\mu\text{m}^2$ ]), maximum value of the volumetric transmembrane fluid flux ( $j_{max}^\Sigma$ , [ $\mu\text{m}^2/\text{min}$ ]), max. ICS deformation ( $u_{max}^{sp}$ , [ $\mu\text{m}$ ]) and max. ICS deformation velocity ( $v_{max}^{sp}$ , [ $\mu\text{m}/\text{min}$ ]). In the implementation of the pure and coupled problems, the *estimated* parameters and initial values (from *Table 3.6*) for the strictly semipermeable membrane assumption were used.

	Level 0				Level 1			
	$Err_2$	$Err_2^\Delta$	$Err_{max}$	$Err_{max}^\Delta$	$Err_2$	$Err_2^\Delta$	$Err_{max}$	$Err_{max}^\Delta$
$V_T^p$	3.000e+01	3.14e-3	4.487e+01	4.70e-3	6.538e+00	6.82e-4	7.120e+00	7.42e-4
$j_{max}^\Sigma$	5.226e+00	1.33e-2	2.049e+01	5.23e-2	1.168e-01	2.98e-4	2.200e-01	5.66e-4
$u_{max}^{sp}$	7.807e-02	1.43e-3	1.599e-01	2.92e-3	1.413e-03	2.57e-4	2.020e-03	3.68e-4
$v_{max}^{sp}$	2.677e-02	2.16e-2	1.306e-01	1.05e-1	2.748e-04	2.22e-4	1.250e-03	1.01e-3



**Figure 4.10 Coupled Biot-Stokes vs Pure Biot problem: *circular* Biot domain geometry.**

Below, the simulation results for the 2-dimensional Pure Biot problem (as described in *Section 4.6.2*) and Coupled Biot problem (i.e. the Biot problem solved as a part of the coupled Biot-Stokes problem), where the Biot domains have *circular* (as shown in *Fig. 4.12a*) geometry, are compared on mesh refinement levels 0, 1. In particular, the following quantities are plotted: the ICS volume  $V^p$  (*Volume*, [ $\mu\text{m}^2$ ]), volumetric transmembrane fluid flux  $j^\Sigma$  (*Water flux*, [ $\mu\text{m}^2/\text{min}$ ]), maximum value (over mesh cells) of the ICS deformation  $u^{sp}$  (*Max. Deformation*, [ $\mu\text{m}$ ]), max. value of the ICS deformation velocity  $v^{sp}(t) := \partial_t u^{sp}(t)$  (*Max. Solid velocity*, [ $\mu\text{m}/\text{min}$ ]). In the implementation of the pure and coupled problems, the *estimated* parameters and initial values (from *Table 3.6*) for the strictly semipermeable membrane assumption were used. All quantities are shown to develop over time  $t \in (0, T)$ , [ $\text{min}$ ], where  $T := 30 \text{ min}$ .

(a) Coupled and Pure Biot problem simulations.

The reference plot (in green) corresponds to the pure Biot problem simulations; the results of the Coupled Biot problem simulations on mesh refinement levels 0, 1 are plotted in blue and red respectively.

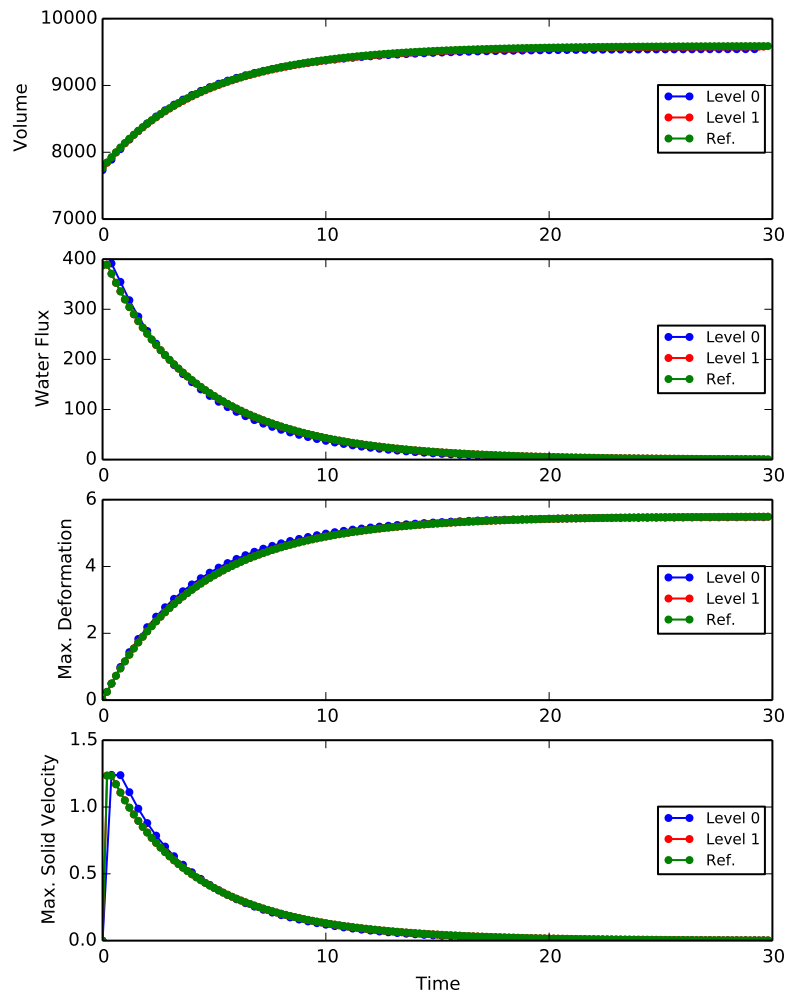


Figure 4.10

(b) Difference between the Pure and Coupled Biot problem simulation results. The difference between the simulation results for the Pure Biot problem on mesh refinement level 1 and Coupled Biot problem on level 0 is plotted in blue; between the Pure and Coupled Biot problems on level 1 – in red.

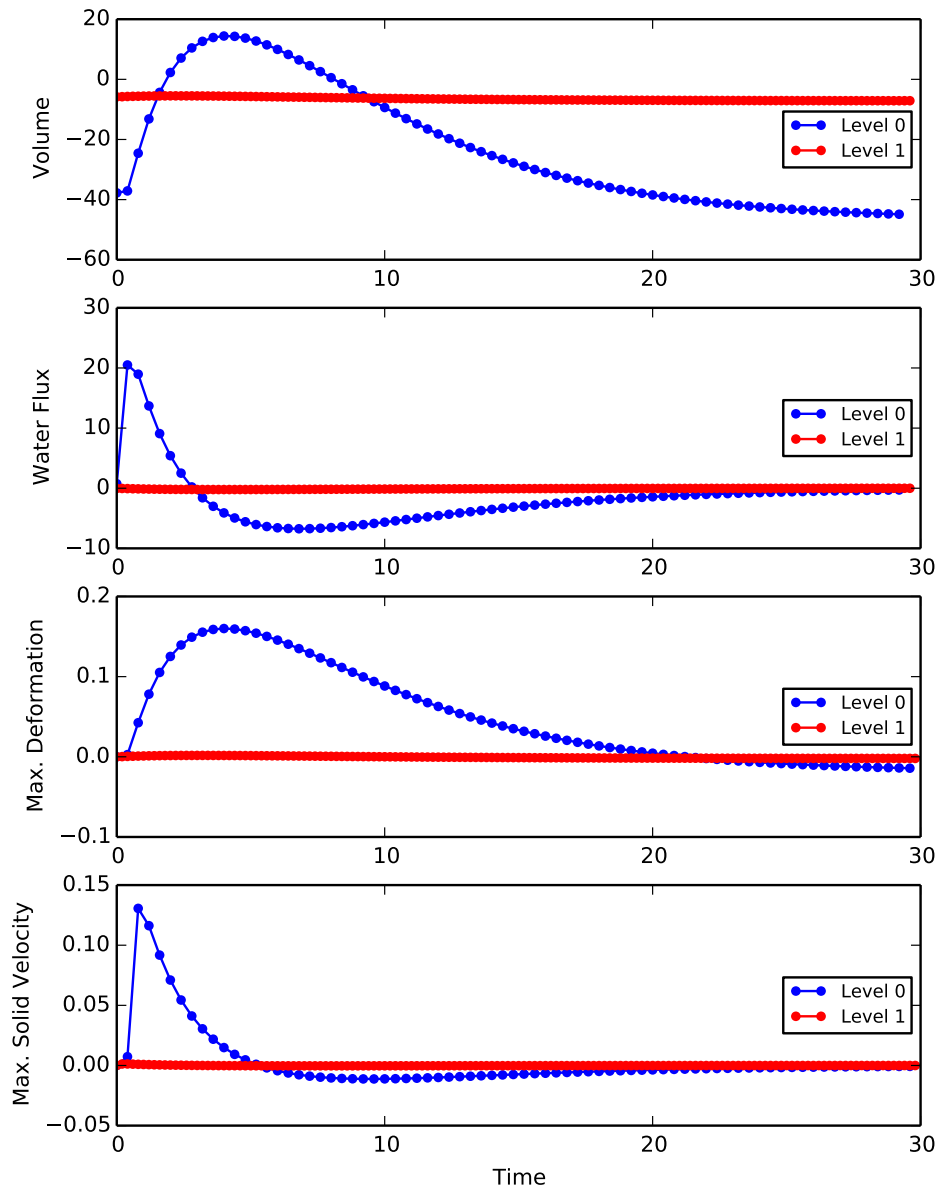
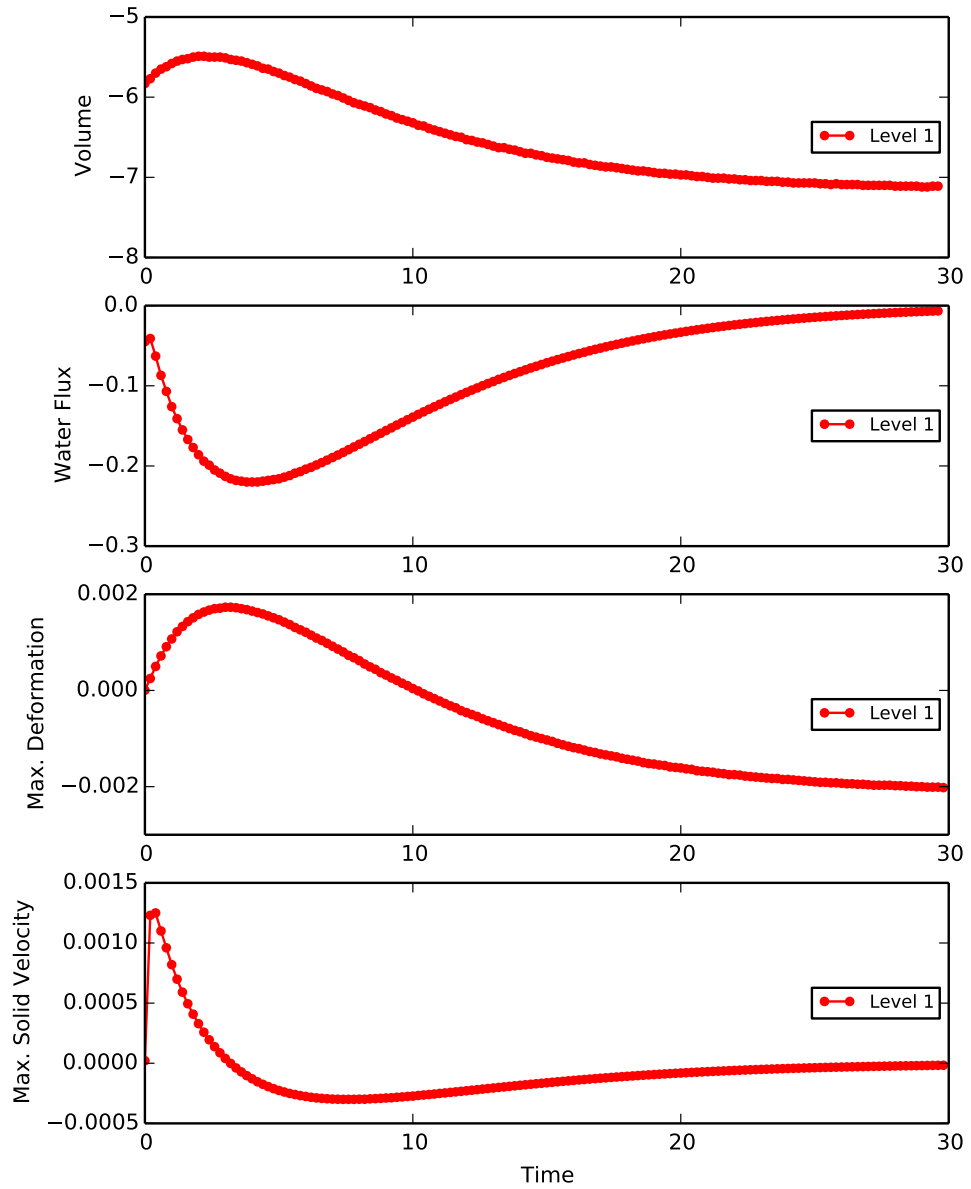


Figure 4.10

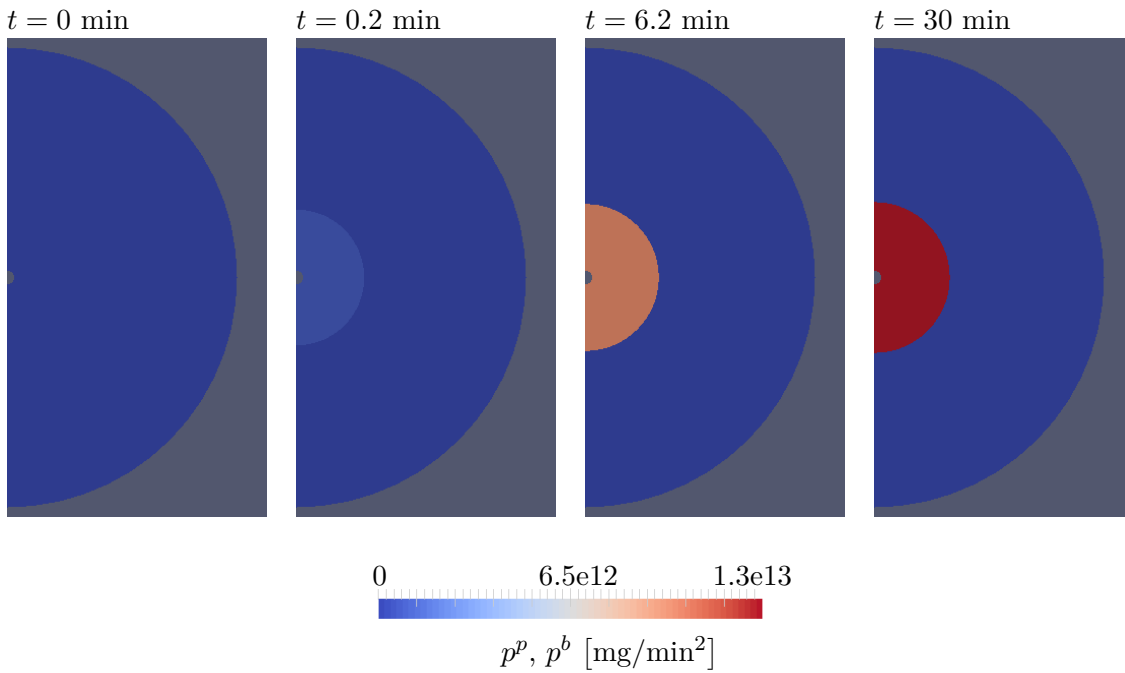
(c) Difference between the Pure and Coupled Biot problem simulation results on level 1.



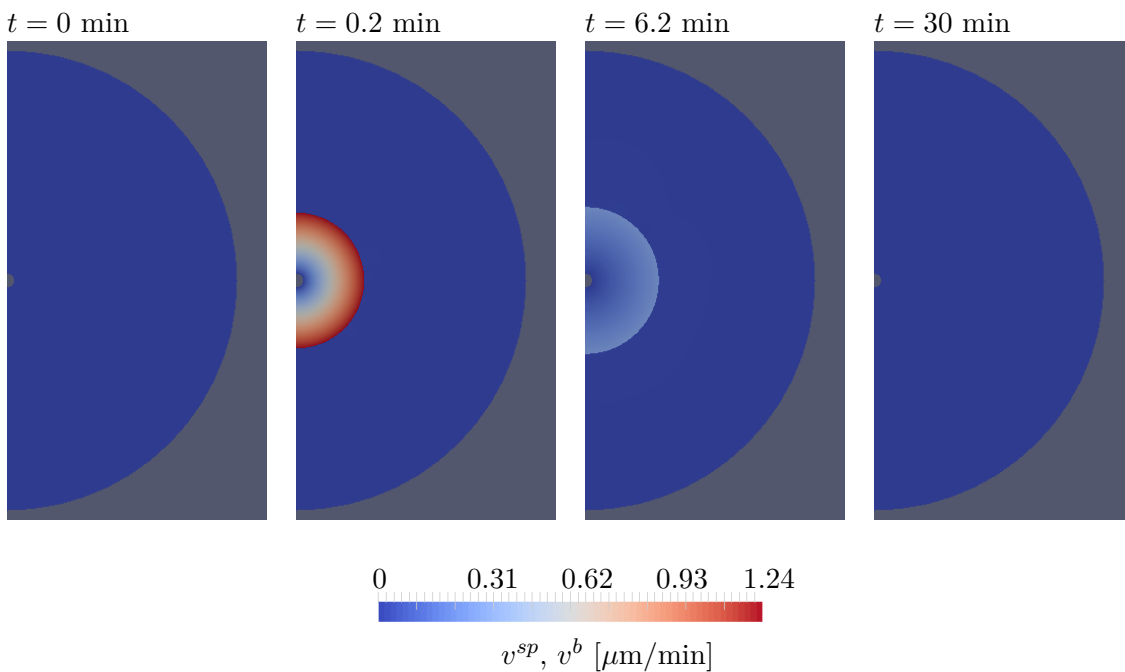
**Figure 4.11 Coupled Biot-Stokes problem: *circular* Biot domain geometry.**

On the pictures below, the magnitudes of the hydraulic pressures  $p^p$ ,  $p^b$ , Biot solid phase velocity  $v^{sp}$  and Stokes fluid flow velocity  $v^b$  defined on the ICS  $\Omega^p$  and ECS  $\Omega^b$  respectively are shown at several time steps  $t \in (0, T)$ ,  $T := 30$  min, for the simulations of the 2-dimensional coupled Biot-Stokes problem (described in the beginning of the section) with the *estimated* parameters (strict membrane assumption) on mesh refinement level 1.

(a) Hydraulic pressures  $p^p \in \Omega^p$ ,  $p^b \in \Omega^b$ :



(b) Biot deformation velocity  $v^{sp} \in \Omega^p$  and Stokes fluid flow velocity  $v^b \in \Omega^b$ :



#### 4.6.4 Coupled Biot-Stokes problem with non-trivial Biot domain geometry

*Problem:* coupled Biot-Stokes problem (4.59), (4.60) for the solid phase displacement  $u^{sp}$ , pore pressure  $p^p$ , solid phase velocity  $v^{sp}$ , bulk fluid velocity  $v^{fp}$ , bulk fluid pressure  $p^b$  and fluid domain displacement  $u^b$ ; boundary and interface conditions are as given in Section 4.4. The parameters, initial, interface and boundary values correspond to the *estimated* data values from Tables 3.5, 3.6. The coupled problem is solved following the operator splitting scheme (4.87)-(4.104).

*Domain:*  $\Omega := \Omega^b(t) \cup \Omega^p(t) \in \mathbb{R}^d$ ,  $d = \{2, 3\}$ , where the Biot domain  $\Omega^p(t)$ ,  $\partial\Omega^p(t) := \Gamma^{pin} \cup \Gamma^i(t)$ , is completely surrounded by the Stokes fluid  $\Omega^b(t)$ ,  $\partial\Omega^b(t) := \Gamma^{bw} \cup \Gamma^i(t)$ . The considered Biot domain is topologically equivalent to the circular Biot domain described in Section 4.6.3, but has a non-trivial geometry. In particular, the following two geometry types are considered:

- **Variant 0** geometry: four-pointed star with short, wide, smooth (rounded) edges, where the bounding radius is  $51.89 \mu\text{m}$ , inner radius of the outer boundary –  $42.85 \mu\text{m}$ , and from the center of which a circle of radius  $5 \mu\text{m}$  is cut out, see Fig. 4.12b.
- **Variant 1** geometry: four-pointed star with elongated smooth (rounded) edges, where the bounding radius is  $76.12 \mu\text{m}$ , inner radius of the outer boundary –  $32.95 \mu\text{m}$ , and from the center of which a circle of radius  $5 \mu\text{m}$  is cut out, see Fig. 4.12c.

Simulation results for the coupled Biot-Stokes problem for three different geometry types Biot domain, i.e. *Circular*, *Variant 1*, *Variant 2* as shown in Fig. 4.12, are compared in Table 4.5 and Fig. 4.13.

In Fig. 4.14a, 4.15a, 4.15b, the magnitudes of the Biot and Stokes domain displacements  $u^{sp}$ ,  $u^b$ , and Stokes fluid flow velocity  $v^b$  are shown at several time steps  $t \in (0, T)$  for different geometries. It can be observed, that while the Stokes velocity appears to reach higher values with the increase of the Biot domain anisotropy, the observed difference is in fact small. The chaotic behaviour of the Stokes velocity field at  $t = 0.01$  in Fig. 4.15a is caused by numerical oscillations, which are rapidly (i.e. max. three time steps) resolved.

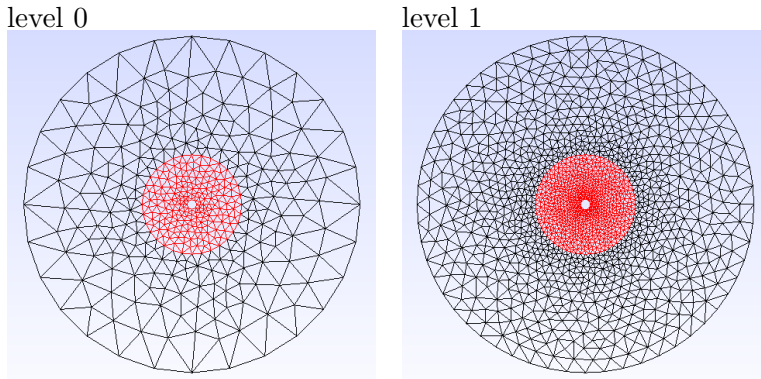
*Pure* and *Coupled* Biot problem simulation results for the *Variant 0*, *Variant 1* Biot domain geometries are compared in Table 4.6 and Fig. 4.16. Thus in Table 4.6, the errors  $Err_2$ ,  $Err_{max}$  and relative errors  $Err_2^\Delta$ ,  $Err_{max}^\Delta$  defined in (4.119), (4.120) are computed. In 4.16, several quantities are plotted.

From these comparisons it follows, that also for the considered less trivial geometries, the simulation results obtained for the *Pure* and *Coupled* Biot problems are almost identical.

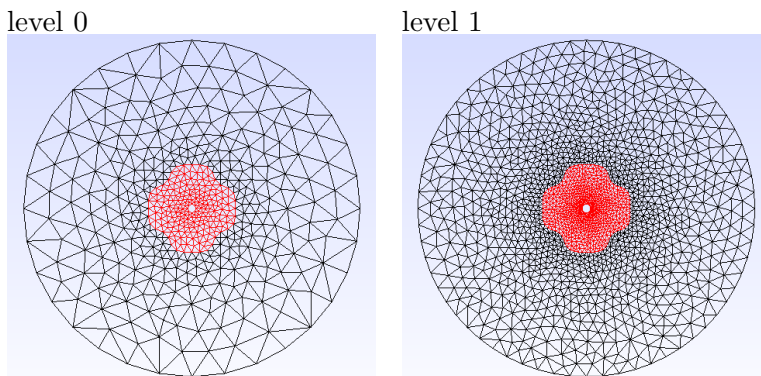
**Figure 4.12 Biot-Stokes problem meshes.**

On the pictures below, computation meshes for the Biot-Stokes problem with different geometry types of the Biot and Stokes domains are shown. The Biot domain mesh  $\Omega_h^p$  is depicted in red, and the Stokes domain mesh  $\Omega_h^b$  – in black.

(a) Circular Biot domain:



(b) Variant 0 geometry:



(c) Variant 1 geometry:

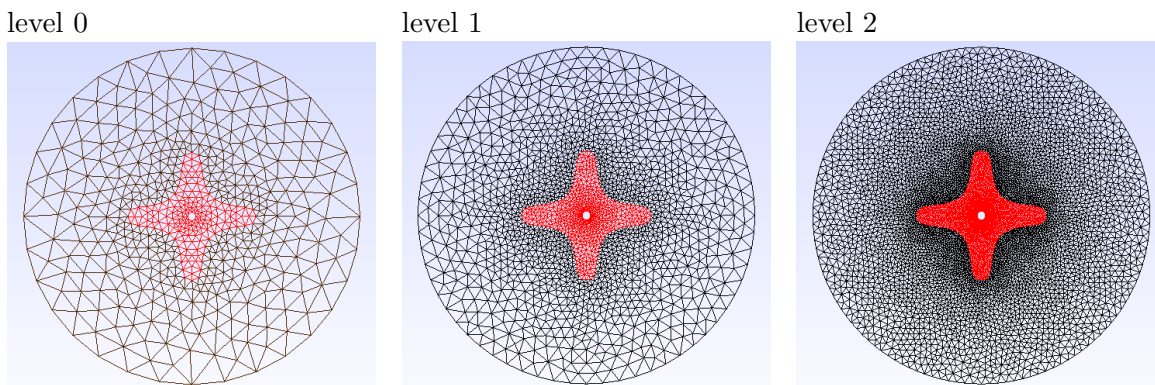


**Table 4.5 Coupled Biot-Stokes problem simulations: comparison between different cell geometries.**

The data given below was obtained for the 2-dimensional coupled Biot-Stokes problem simulations with physical (*estimated*) parameters and initial values (given in *Table 3.5, 3.6*, strict membrane assumption) on mesh refinement levels 0, 1, 2 (denoted as L0, L1, L2). The results are compared for three different geometry types of the ICS (Biot domain): *Circular, Variant 1, Variant 2*, as shown in *Fig. 4.12*. The following quantities are evaluated:  $u_T$  – final (terminal) displacement,  $V_0^p$  – initial volume of the ICS  $\Omega^p$ ,  $V_T^p$  – final volume of the ICS  $\Omega^p$ ,  $V_\Delta^p := V_T^p - V_0^p$  – increase (growth) of the ICS volume,  $V_{err}^p$  – numerical volume growth error (defined in (4.110)),  $A_0^p$  – initial surface area of the ICS  $\Omega^p$ ,  $A_T^p$  – final surface area of the ICS  $\Omega^p$ ,  $\pi_0^\Delta$  – initial transmembrane osmotic pressure difference,  $\pi_T^\Delta$  – final transmembrane osmotic pressure difference. As discussed in *Section 4.6.2*, the simulations are terminated at  $T := 30$ . The total number of the mesh cells (in both  $\Omega_h^p, \Omega_h^b$ ) is denoted by  $N$ .

		Circular		Variant 0		Variant 1		
Unit		L0	L1	L0	L1	L0	L1	L2
$N$	–	788	3224	972	3706	1074	3888	14644
$u_T$	$\mu\text{m}$	5.47	5.49	5.79	5.82	7.71	8.35	8.38
$V_0^p$	$\mu\text{m}^2$	7732.9	7764.8	7744.0	7770.7	7735.6	7770.6	7778.1
$V_T^p$	$\mu\text{m}^2$	9543.6	9581.7	9558.1	9590.1	9549.1	9592.2	9601.4
$V_\Delta^p$	$\mu\text{m}^2$	1810.7	1816.9	1814.1	1819.4	1813.6	1821.6	1823.3
$V_{err}^p$	–	8.19e-2	4.08e-2	8.67e-2	4.35e-2	12.69e-2	6.37e-2	3.19e-2
$A_0^p$	$\mu\text{m}$	313.6	314.0	333.4	335.9	489.2	493.9	494.8
$A_T^p$	$\mu\text{m}$	348.1	348.5	370.2	372.9	543.3	548.5	549.
$\pi_0^\Delta$	$\text{mg}/\text{min}^2$	7.42e14	7.34e14	7.41e14	7.39e14	7.42e14	7.39e14	7.38e14
$\pi_T^\Delta$	$\text{mg}/\text{min}^2$	1.36e13	1.40e13	1.33e13	1.36e13	1.28e13	1.28e13	1.28e13

**Figure 4.13 Coupled Biot-Stokes problem simulations: comparison between different cell geometries.**

The plots below show results for the 2-dimensional coupled Biot-Stokes problem simulations with the *estimated* parameters and initial values (given in *Tables 3.5, 3.6*, strict membrane assumption) on mesh refinement level 1. The results are compared for three different geometry types of the ICS (Biot domain): *Circular, Variant 1, Variant 2* as shown in *Fig. 4.12*. The compared quantities are the ICS volume  $V^p$  (*Volume,  $[\mu\text{m}^2]$* ), volumetric transmembrane fluid flux  $j^\Sigma$  (*Water flux,  $[\mu\text{m}^2/\text{min}]$* ), maximum value (over the mesh cells) of the ICS deformation  $u^{sp}$  (*Max. Deformation,  $[\mu\text{m}]$* ), max. value of the ICS deformation velocity  $v^{sp}(t) := \partial_t u^{sp}(t)$  (*Max. Solid velocity,  $[\mu\text{m}/\text{min}]$* ). All quantities are shown to develop over time  $t \in (0, T)$ ,  $[\text{min}]$ , where  $T := 30$  min.

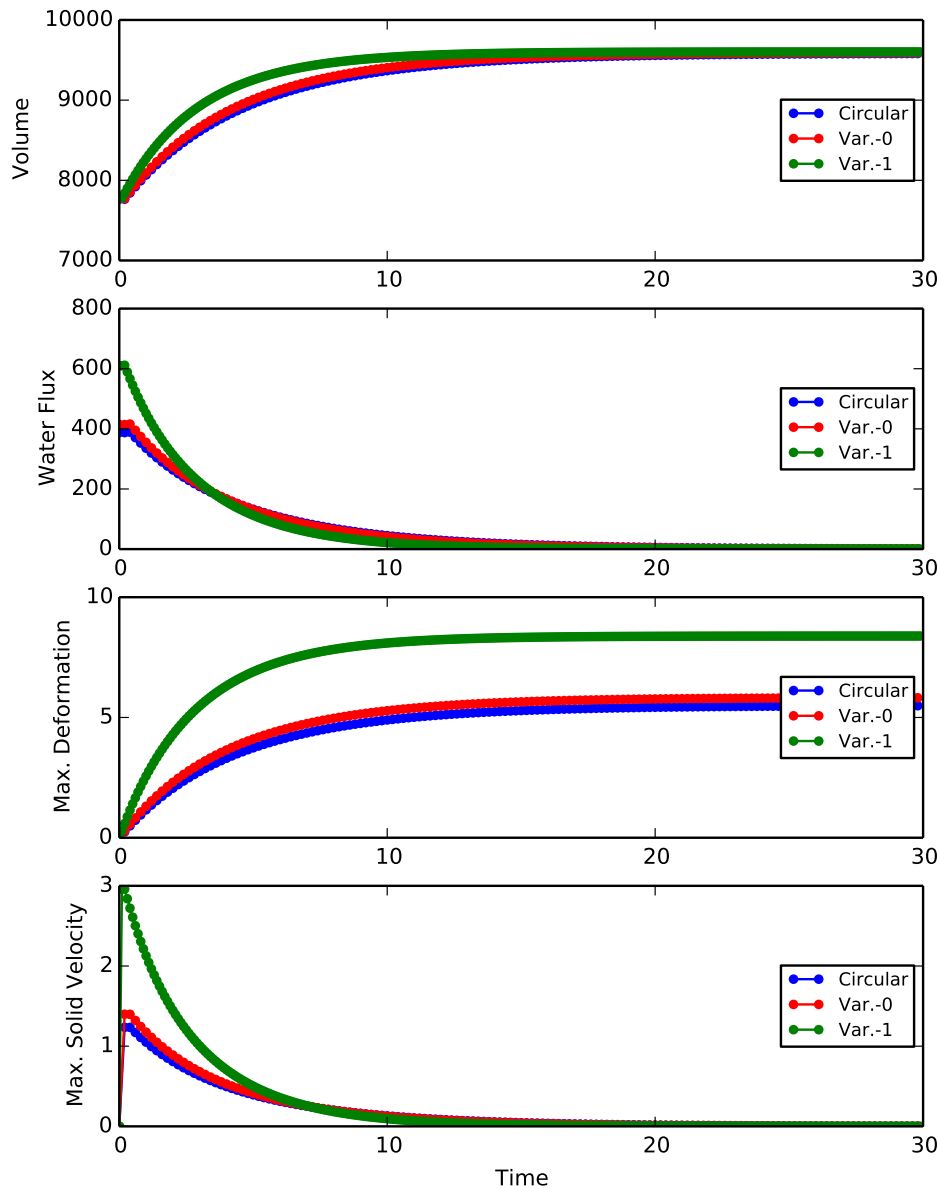




**Figure 4.14 Coupled Biot-Stokes problem: *Circular, Variant 0, Variant 1* geometries.**

On the pictures below, the magnitudes of the Biot and Stokes domain displacements  $u^{sp}$ ,  $u^b$  and Stokes fluid flow velocity  $v^b$  are shown at several time steps  $t \in (0, T)$ ,  $T := 30$  min, for the simulations of the 2-dimensional Biot-Stokes problem (described in the beginning of the section) with the *estimated* parameters (strict membrane assumption) on mesh refinement level 1.

(a) Deformations  $u^{sp} \in \Omega^p$ ,  $u^b \in \Omega^b$ :

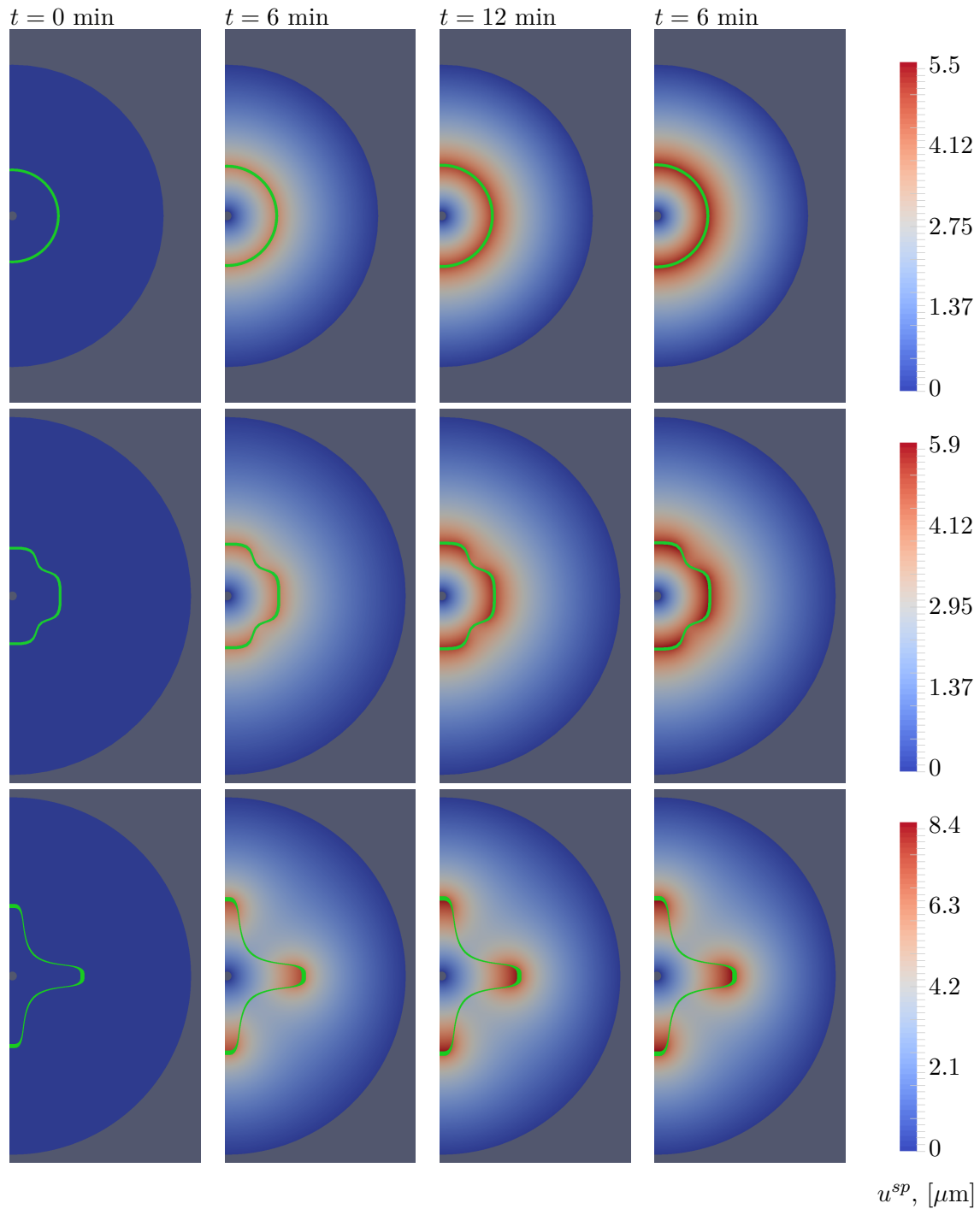


Figure 4.15

(a) Stokes fluid flow velocity  $v^b \in \Omega^b$ :

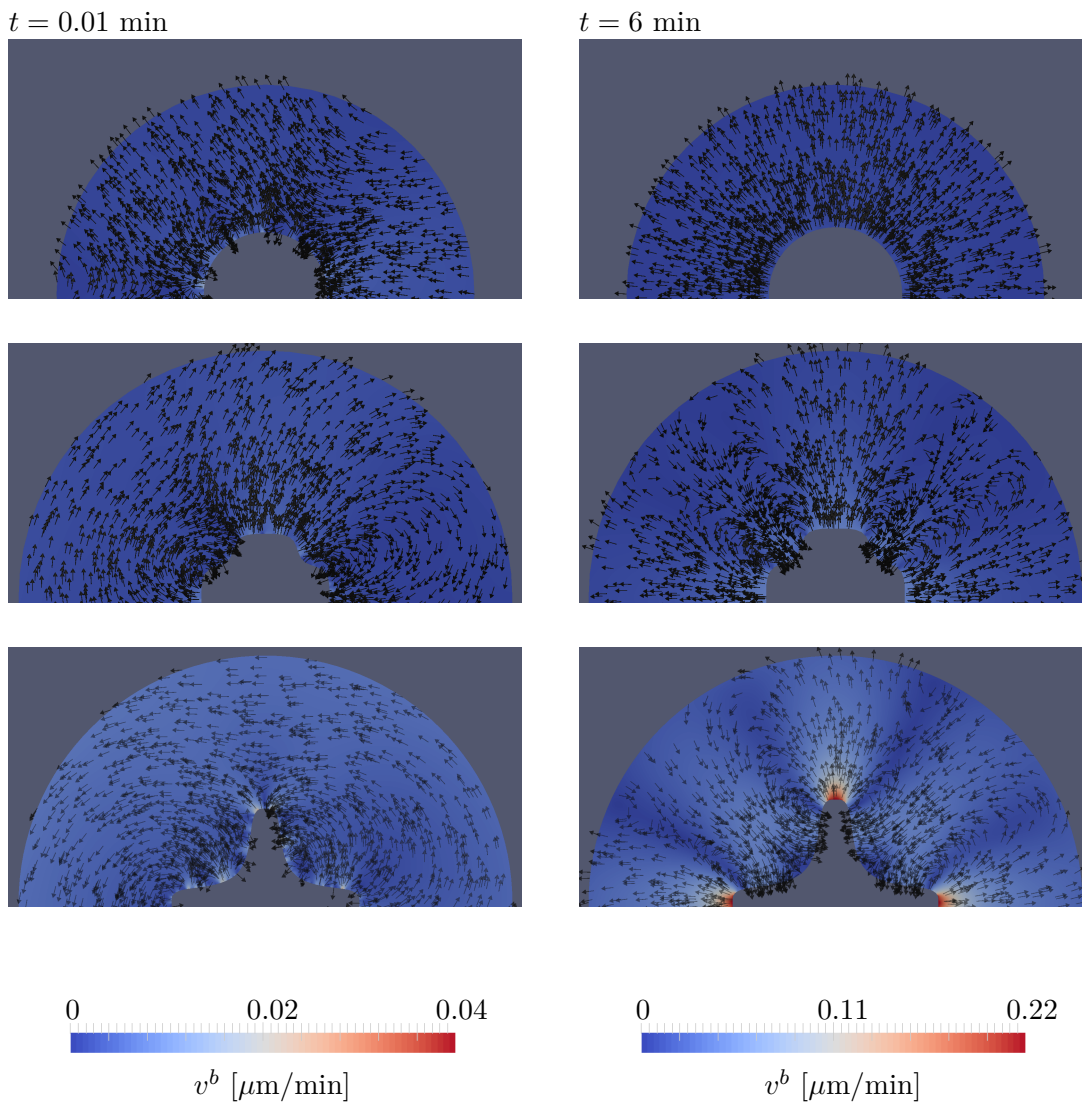
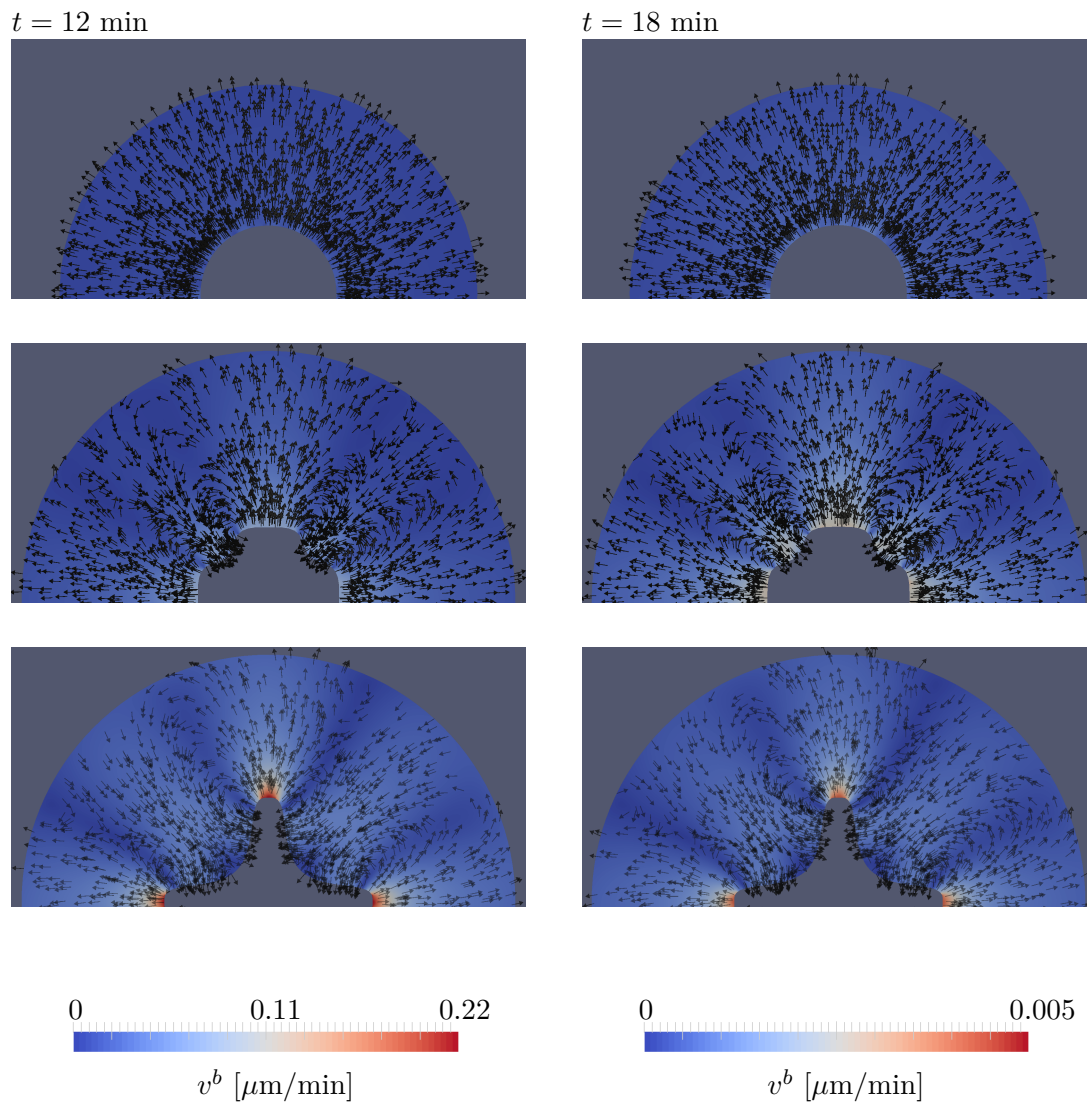


Figure 4.15

(b) Stokes fluid flow velocity  $v^b \in \Omega^b$ :

**Table 4.6 Coupled Biot-Stokes vs Pure Biot problem: *non-trivial* Biot domain geometries.**

Below, the simulation results for the 2-dimensional Pure Biot problem (as described in *Section 4.6.2*) and Coupled Biot problem (i.e. the Biot problem solved as a part of the coupled Biot-Stokes problem), where the Biot domains have non-trivial (*variant 0* and *variant 1* as shown in *Fig. 4.12b, 4.12c*) geometries, are compared on mesh refinement levels 0, 1, 2. In particular,  $L^2$  and  $L^\infty$  errors  $Err_2$ ,  $Err_{max}$  as well as the relative errors  $Err_2^\Delta$ ,  $Err_{max}^\Delta$  (defined in (4.120)) are computed between the Pure Biot and Coupled Biot simulation results for the terminal ICS volume ( $V_T^p$ , [ $\mu\text{m}^2$ ]), maximum value of the volumetric transmembrane fluid flux ( $j_{max}^\Sigma$ , [ $\mu\text{m}^2/\text{min}$ ]), max. ICS deformation ( $u_{max}^{sp}$ , [ $\mu\text{m}$ ]) and max. ICS deformation velocity ( $v_{max}^{sp}$ , [ $\mu\text{m}/\text{min}$ ]). In the implementation of the pure and coupled problems, the *estimated* parameters and initial values (from *Table 3.6*) for the strictly semipermeable membrane assumption were used.

**Variant 0 geometry**

		Level 0				Level 1			
	Value	$Err_2$	$Err_2^\Delta$	$Err_{max}$	$Err_{max}^\Delta$	$Err_2$	$Err_2^\Delta$	$Err_{max}$	$Err_{max}^\Delta$
$V_T^p$	9590.2	4.635e1	4.83e-3	7.787e1	8.12e-3	1.296e1	1.35e-3	3.067e1	3.20e-3
$j_{max}^\Sigma$	416.28	1.392e1	3.34e-2	6.878e1	1.65e-1	4.436e0	1.07e-2	2.423e1	5.82e-2
$u_{max}^{sp}$	5.820	5.535e-1	9.51e-2	6.760e-1	1.16e-1	6.316e-2	1.09e-2	1.580e-1	2.71e-2
$v_{max}^{sp}$	1.399	7.478e-2	5.34e-2	1.940e-1	1.39e-1	2.624e-2	1.88e-2	6.558e-2	4.69e-2

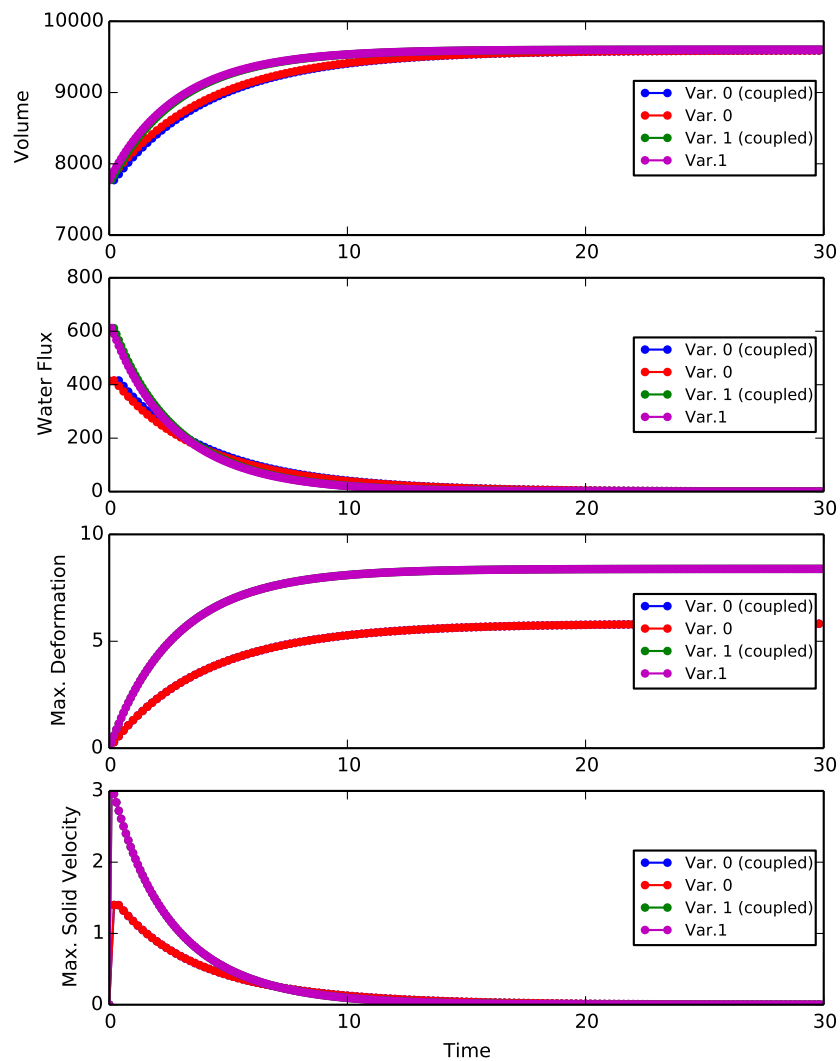
**Variant 1 geometry**

		Level 0				Level 1			
	Value	$Err_2$	$Err_2^\Delta$	$Err_{max}$	$Err_{max}^\Delta$	$Err_2$	$Err_2^\Delta$	$Err_{max}$	$Err_{max}^\Delta$
$V_T^p$	9601.4	4.635e1	4.83e-3	7.787e1	8.11e-3	1.296e1	1.35e-3	3.067e1	3.19e-3
$j_{max}^\Sigma$	611.973	1.392e1	2.27e-2	6.878e1	1.12e-1	4.436e0	7.25e-3	2.423e1	3.96e-2
$u_{max}^{sp}$	8.386	5.535e-1	6.60e-2	6.760e-1	8.06e-2	6.316e-2	7.53e-3	1.580e-1	1.88e-2
$v_{max}^{sp}$	2.961	7.478e-2	2.53e-2	1.940e-1	6.55e-2	2.624e-2	8.86e-3	6.558e-2	2.21e-2

		Level 2			
	Value	$Err_2$	$Err_2^\Delta$	$Err_{max}$	$Err_{max}^\Delta$
$V_T^p$	9601.4	< 1e-2	< 1.04e-6	< 1e-2	< 1.04e-6
$j_{max}^\Sigma$	611.973	8.780e-2	1.43e-4	4.160e-1	6.80e-4
$u_{max}^{sp}$	8.386	8.535e-5	1.02e-5	4.115e-4	4.91e-5
$v_{max}^{sp}$	2.961	5.700e-6	1.93e-6	< 2.0e-5	< 6.75e-6

**Figure 4.16 Coupled Biot-Stokes vs Pure Biot problem: *non-trivial* Biot domain geometries.**

Below, the simulation results for the 2-dimensional *Pure* Biot problem (as described in *Section 4.6.2*) and *Coupled* Biot problem (i.e. the Biot problem solved as a part of the coupled Biot-Stokes problem), where the Biot domains have non-trivial (*Variant 0* and *Variant 1* as shown in *Fig. 4.12b, 4.12c*) geometries, are compared for mesh refinement levels 1 (*Variant 0*) and 2 (*Variant 1*) respectively. In particular, the following quantities are plotted: the ICS volume  $V^P$  (*Volume*, [ $\mu\text{m}^2$ ]), volumetric transmembrane fluid flux  $j^\Sigma$  (*Water flux*, [ $\mu\text{m}^2/\text{min}$ ]), maximum value (over the mesh cells) of the ICS deformation  $u^{sp}$  (*Max. Deformation*, [ $\mu\text{m}$ ]), max. value of the ICS deformation velocity  $v^{sp}(t) := \partial_t u^{sp}(t)$  (*Max. Solid velocity*, [ $\mu\text{m}/\text{min}$ ]). In the implementation of the pure and coupled problems, the *estimated* parameters and initial values (from *Table 3.6*) for the strictly semipermeable membrane assumption were used. All quantities develop over time  $t \in (0, T)$ , [ $\text{min}$ ], where  $T := 30 \text{ min}$ . The plots corresponding to the *Pure* Biot simulation results are shown in red and purple, the *Coupled* problem results are plotted in blue and green.





# Summary and outlook

## Summary of the work

This work is devoted to the description of the osmotic swelling of a brain cell due to the absorption of the extracellular fluid during the formation of the cytotoxic oedema. The description of the considered problem involves:

- development of a physically motivated mathematical model;
- analysis of the relevant experimental data and its integration into the developed model;
- numerical implementation and simulations of the resulting system.

The dynamics of a system comprising of a single swelling cell and surrounding extracellular fluid is approximated by the coupled Biot-Stokes equations. It is shown, that for the considered data range, the temporal pressure derivative term of the Biot equations derived from the microscale is negligible. A set of coupling interface conditions is suggested. The driving force of the transmembrane osmotic pressure difference and the filtering effects of the cell membrane are reflected in a coupling condition relating the normal fluid flux to the total pressure difference across the membrane. The general osmotic pressure model implies the use of the transport equations for the molar concentrations of the osmotically active substances diluted in the bulk extracellular fluid and in the fluid phase of the poroelastic intracellular space.

The data characterising the properties of the considered media and the conditions of the experimental settings is analysed. It then follows, that certain effects and processes included into the developed general coupled model can be neglected, leading to the formulation of a simpler (*reduced*) mathematical model.

The *reduced* coupled interaction problem is discretized using the FEMs (in space) and the implicit Euler scheme (in time) and solved following an operator-splitting approach, that results in apparently stable numerical solutions. The numerical implementations of the two and three dimensional (pure) Biot problem are verified by comparing the analytic and numerical solutions. The sensitivity of the Biot problem solution to the variations of (a) the key parameters and (b) the domain geometry is tested and analysed. The results obtained for the coupled Biot-Stokes problem indicate, that under the assumptions of the developed model, the influence of the Stokes domain over the Biot domain solution is small.

## Further challenges

In this work, the mechanical properties of the membrane are considered to be a sub-scale effect and are therefore not explicitly modelled, but incorporated into the elasticity model and its parametrisation. For certain types of living cell however, the mechanical effects that may influence the character of cell deformation, such as the ability of the bilipid membrane to preserve its surface area, may have a significant impact on the dynamics of the cell, and would need to be considered explicitly.

The works devoted to the modelling and numerical treatment of the bilipid membranes and their interaction with the surrounding fluids are briefly discussed in the *Introduction*. However the modelling approximations of the effects of the membrane and their numerical treatment described in [7] indicate, that such approach may introduce a new level of complexity into the already sophisticated model developed in this thesis. Therefore finding a simpler way of incorporating the effect of the membrane incompressibility into the poroelasticity model may be greatly advantageous.

The results obtained in this thesis for a single cell can naturally be viewed as a step in the direction of approximating the processes that occur on a larger scale – namely, for the description of the brain tissue. Swelling of the cells influences the overall characteristics of the affected tissue and contributes to the advancement of the (cerebral) oedema formation. Thus cytotoxic oedema largely contributes to the creation of the necessary conditions for the development of a volume-occupying brain tissue oedema, when the extracellular constituents are joint by the substances from the intravascular space.

Possible approaches to approximating the behaviour of a swelling tissue include homogenization or averaging techniques, where the equations describing the processes occurring on a microscale are used as a basis for the development of the macroscale equations. The analysis of the data and numerical results for the cell swelling model derived in this thesis allows to determine the dominant effects of the cytotoxic swelling, giving an idea about the key characteristics that need to be included when developing a tissue model.

Owing to the great complexity of the coupled Biot-Stokes free boundary interaction problem, its mathematical analysis remains an open and challenging problem.



# A Appendix

## A.1 Reynolds transport theorem and its applications

The derivation of balance laws describing the motion of fluid or an elastic object is based on the Reynolds transport theorem (or General transport theorem), [176]. Thus consider the following general problem: an arbitrary domain  $\Omega$  is moving from its initial configuration  $\hat{\Omega} := \Omega(0)$  into a deformed (or current) configuration  $\Omega(t)$  over time interval  $(0, T)$  under a deformation  $X_t$ ,  $t \in (0, T)$ , such that:

$$\begin{aligned} X_t : \hat{\Omega} &\rightarrow \Omega(t) \quad \forall t \in (0, T), \\ x(\hat{x}, t) &= X_t(\hat{x}) \quad \forall x \in \Omega(t) \times (0, T), \end{aligned}$$

where the variables defined on the reference domain and with respect to the reference coordinates are denoted by "hats":  $\hat{\Omega} := \{\hat{x}\}$ ,  $\hat{f} := \hat{f}(\hat{x})$ . For all  $t \in (0, T)$  the motion is considered to be isothermal, and during the observed processes, the mass is neither created nor destroyed.

In the domain  $\Omega(t)$  consider an arbitrary volume  $\Omega^a(t) \subset \Omega(t)$ , such that its boundary  $\partial_t \Omega^a(t)$  is moving with velocity  $w^a(x, t)$ . In case the deformations are such, that no mass is transported across the boundary of the element  $\Omega^a(t)$ , and the surface velocity  $w^a$  coincides with the particle (or flow) velocity  $v(x, t)$  of the domain  $\Omega(t)$ , such volume is referred to as a *material volume* (or material element) and will be denoted as  $\Omega^m(t)$ .

**Reynolds transport theorem** states, that for a function  $f(x, t)$  integrated over an (in general changing in time) arbitrary volume  $\Omega^a(t)$ , the following derivation rule applies:

$$\frac{d}{dt} \int_{\Omega^a(t)} f(x, t) dV = \int_{\Omega^a(t)} \partial_t f dV + \int_{\partial_t \Omega^a(t)} w^a \cdot n f dA.$$

Ostrogradsky divergence theorem applied to the boundary integral in the RHS of the equation allows to rewrite the statement of the Transport theorem in a more familiar (commonly used) form:

$$\frac{d}{dt} \int_{\Omega^a(t)} f(x, t) dV = \int_{\Omega^a(t)} \partial_t f dV + \int_{\Omega^a(t)} \nabla \cdot (w^a f) dV. \quad (\text{A.1})$$

Physical balance laws are commonly derived on the volume conserving domains using the concept of the *material volume*. Yet as the problems considered in this thesis involve exchange of mass (volume) between the domains, the derivations of the balance equations for the problems defined on in general moving, growing or shrinking domains are described below. It is thus important to note, that the Reynolds' theorem is applicable to any arbitrary volume  $\Omega^a(t)$  and is not restricted to material volumes only. In particular, for a material volume  $\Omega^m(t)$ , equation (A.1) reads:

$$\frac{d}{dt} \int_{\Omega^m(t)} f(x, t) dV = \int_{\Omega^m(t)} \partial_t f dV + \int_{\Omega^m(t)} \nabla \cdot (v f) dV. \quad (\text{A.2})$$

Then for *all* arbitrary domains  $\Omega^a(t)$  that coincide with the material element  $\Omega^m(t)$  at time  $t \in (0, T)$ , one has:

$$\int_{\Omega^m(t)} \partial_t f dV = \int_{\Omega^a(t)} \partial_t f dV,$$

and the following relationship between the material derivatives over the material and arbitrary domains can be derived, [177]:

$$\frac{d}{dt} \int_{\Omega^a(t)} f(x, t) dV := \frac{d}{dt} \int_{\Omega^m(t)} f(x, t) dV + \int_{\Omega^a(t)} \nabla \cdot [f(x, t)(w_a(x, t) - v(x, t))] dV. \quad (\text{A.3})$$

The applications of the Reynolds theorem are described in multiple works, see e.g. [178], [179], [82]. Below, the derivations of the conservation equations that are used in this work are given. It should be noted, that the Transport theorem equations are written with respect to the deformed configuration  $\Omega(t)$ , and so the balance laws are originally obtained in the ***Eulerian*** coordinates (formulation).

### ***Volume of the domain***

The transport theorem can be used to find the domain volume change  $V^\Delta(t)$  over time  $(0, t)$ . In particular, taking  $\Omega^a(t) := \Omega(t)$  and setting  $f(x, t) := 1$  in (A.1) results in:

$$V^\Delta(t) \triangleq \frac{d}{dt} \int_{\Omega(t)} dV \stackrel{(\text{A.1})}{=} \int_{\Omega(t)} \nabla \cdot w(x, t) dV, \quad (\text{A.4})$$

where  $w$  is the velocity of the boundary of  $\Omega$ . Then at each  $t \in (0, T)$  the volume of the domain  $\Omega(t)$  can be found as:

$$V(t) \triangleq \int_{\Omega(t)} dV := V(0) + V^\Delta(t),$$

where  $V(0)$  is the initial volume of  $\Omega$ .

### ***Mass balance law***

The conservation of mass equation is obtained by taking the material derivative of mass  $m^a(t)$  enclosed in an arbitrary control volume  $\Omega^a(t) \subset \Omega(t)$  and then applying the Reynolds' theorem (A.3):

$$\frac{dm^a(t)}{dt} \triangleq \frac{d}{dt} \int_{\Omega^a(t)} \rho(x, t) dV \stackrel{(\text{A.3})}{=} \frac{d}{dt} \int_{\Omega^m(t)} \rho(x, t) dV + \int_{\Omega^a(t)} \nabla \cdot (\rho(x, t)(w^a(x, t) - v(x, t))) dV,$$

where  $\rho(x, t)$  is the mass density of the enclosed substance. Since there exists no flow through the boundary of the material volume, mass  $m^m$  contained in  $\Omega^m(t)$  must remain constant,

$$\frac{dm^m(t)}{dt} \triangleq \frac{d}{dt} \int_{\Omega^m(t)} \rho(x, t) dV = 0,$$

therefore the mass balance equation reads:

$$\frac{d}{dt} \int_{\Omega^a(t)} \rho(x, t) dV \stackrel{(\text{A.3})}{=} \int_{\Omega^a(t)} \nabla \cdot (\rho(x, t)(w^a(x, t) - v(x, t))) dV. \quad (\text{A.5})$$

The definition of a *homogeneous* material implies that the density  $\rho(x, t)$  does not depend on the spatial variable  $x$ , thus:

$$\rho(x, t) = \rho(t) \quad \forall x \in \Omega(t), t \in (0, T).$$

A homogeneous material is said to be *incompressible*, if and only if its density  $\rho(t)$  is constant throughout the observed process:

$$\rho(t) = \rho(0) = \text{const} \quad \forall t \in (0, T).$$

Then for a homogeneous incompressible material the mass balance (A.5) can be simplified as:

$$\frac{d}{dt} \int_{\Omega^a(t)} dV = \int_{\Omega^a(t)} \nabla \cdot [w^a(x, t) - v(x, t)] dV. \quad (\text{A.6})$$

Since the above equations are assumed to hold on any arbitrary domain  $\Omega^a(t) \subset \Omega(t)$ , combining (A.6) and the volume change relation (A.4), the classical mass conservation law for an *incompressible flow* is obtained:

$$\begin{aligned} \nabla \cdot v(x, t) &= 0 \\ \rho(x, t) &= \text{const} \end{aligned} \quad \forall x \in \Omega(t), t \in (0, T). \quad (\text{A.7})$$

### **Momentum balance laws**

Forces applied to volume  $\Omega(t)$  can be categorized as either volume forces  $f$  that act on each point of the domain, or boundary forces  $\sigma \cdot n$  applied at the boundary of the domain, such that  $\sigma$  is a **stress tensor** and  $n$  is an outward pointing vector normal to the boundary of  $\Omega(t)$ . From the First Newton's law it follows, that the acting forces result in the change of linear momentum  $LM$ , and therefore for each material volume:

$$\begin{aligned} LM &\triangleq \int_{\Omega(t)} \rho v dV, \\ \frac{d}{dt} LM &:= \frac{d}{dt} \int_{\Omega^m(t)} \rho v dV = \int_{\Omega^m(t)} \rho f dV + \int_{\partial_t \Omega^m(t)} \sigma \cdot n dA, \end{aligned} \quad (\text{A.8})$$

where  $A$  is the area element,  $\rho$  is the mass density of the material and  $n$  is an outward pointing vector normal to the boundary of  $\Omega(t)$ . Reynolds' theorem applied to each scalar component of vector  $\rho v := \{\rho v^i\}$  gives:

$$\frac{d}{dt} \int_{\Omega^m(t)} \rho v dV \stackrel{(\text{A.2})}{=} \int_{\Omega^m(t)} \partial_t(\rho v) dV + \int_{\Omega^m(t)} \nabla \cdot [\rho v \otimes v] dV. \quad (\text{A.9})$$

Transforming the last term of (A.8) into the volume integral and combining equations (A.8) and (A.9), the following relation is obtained:

$$\int_{\Omega^m(t)} \partial_t(\rho v) dV + \int_{\Omega^m(t)} \nabla \cdot [\rho v \otimes v] dV = \int_{\Omega^m(t)} \rho f dV + \int_{\Omega^m(t)} \nabla \cdot \sigma dV.$$

The equation above is valid for any  $\Omega^m(t) \subset \Omega(t)$ ; then for a homogeneous and incompressible

material ( $\rho = \text{const}$ ), the linear momentum conservation law reads:

$$\rho \partial_t v(x, t) + \rho \nabla \cdot (v \otimes v) = \rho f + \nabla \cdot \sigma \quad \forall x \in \Omega(t) \times (0, T). \quad (\text{A.10})$$

The angular momentum conservation together with the above law implies the symmetry of the stress tensor  $\sigma$ :

$$\sigma = \sigma^T. \quad (\text{A.11})$$

## A.2 Structure dynamics: elasticity equations

### Conservation Laws

Derivation of the equations describing the motion of an elastic body  $\Omega^s(t) \in \mathbb{R}^n \times (0, T)$  deforming from its reference configuration  $\hat{\Omega}^s$  into the current frame  $\Omega^s(t)$  is based on the conservation principles described above, and consequently the elasticity equations are initially written in the Eulerian coordinates on the deformed domain  $\Omega^s(t)$ . Thus for the deformation mapping  $T_t^s$ , displacement  $u^s(x, t)$  and deformation velocity  $v^s(x, t)$  defined as:

$$\begin{aligned} \hat{T}_t^s : \hat{\Omega}^s &\rightarrow \Omega^s(t), & u^s &:= x - \hat{x} = \hat{u}^s \\ \hat{T}_t^s(\hat{x}) &= x(\hat{x}, t), & v^s &:= d_t u^s = \partial_t \hat{u}^s = \hat{v}^s, \end{aligned} \quad x \in \Omega^s(t), \quad \hat{x} \in \hat{\Omega}^s,$$

the body motion equations for an incompressible material, corresponding to the momentum and mass conservation laws (A.10), (A.11), (A.7), read:

$$\begin{cases} \nabla \cdot \sigma^s + \rho^s g = \rho^s \partial_t v^s \\ \rho^s = \text{const} \end{cases} \quad \text{in } \Omega^s(t) \times (0, T), \quad (\text{A.12})$$

where the volume forces  $\rho^s g$  are assumed to be produced by gravitation  $g$  only,  $\rho^s$  is the density of the material and  $\sigma^s$  is the (symmetric) Eulerian stress tensor representing the surface forces acting on  $\Omega^s(t)$ .

As the domain is moving, the coordinates of the current configuration  $\Omega^s(t)$  are not known, and so system (A.12) is incomplete. Moreover, the principle variable of the system is the deformation  $u^s$  that determines the movement of the domain, and so the coordinates of  $\Omega^s(t)$  depend on the unknowns of the system. The most intuitive solution to this problem is to rewrite equations (A.12) with respect to *some* fixed configuration  $\tilde{\Omega}^s$ . Since the domain is actually moved by the deformation  $u^s$ , the arbitrary domain  $\tilde{\Omega}^s$  can be chosen to coincide with the reference undeformed configuration  $\hat{\Omega}^s$ :

$$\tilde{\Omega}^s \equiv \hat{\Omega}^s,$$

such that the mapping  $\hat{T}_t^s$  defines a *Lagrangian* transformation of the domain.

In order to rewrite equations (A.12) with respect to the reference coordinates, deformation gradient tensor  $\hat{F}^s$  and its determinant  $\hat{J}^s$  are introduced:

$$\begin{aligned} \hat{F}^s &:= \hat{\nabla} \hat{T}_t^s = I + \hat{\nabla} \hat{u}^s, \\ \hat{J}^s &:= \det(\hat{F}^s). \end{aligned}$$

It can be shown, that the conservation equations (A.12) transformed into the Lagrangian coordinates take the following form:

$$\hat{\nabla} \cdot (\hat{J}^s \hat{\sigma}^s (\hat{F}^s)^{-T}) + \hat{J}^s \rho^s g = \hat{J}^s \rho^s \partial_t \hat{v}^s \quad \text{in } \hat{\Omega}^s \times (0, T). \quad (\text{A.13})$$

The derivation of the relations between the Lagrangian and Eulerian systems is purely technical; an interested reader can find further details in e.g. [82], [102], and references therein.

### **Stress Modelling. Hooke's Law**

In case the solid material can be assumed to be elastic, a symmetric Lagrangian stress tensor  $\hat{\sigma}^s$  is found via an elasticity law  $M^s$ , that relates  $\hat{\sigma}^s$  to the non-linear strain tensor  $\hat{E}^s$ :

$$\hat{\sigma}^s = M^s(\hat{E}^s),$$

where  $\hat{E}^s$  is defines as

$$\hat{E}^s = \frac{1}{2}((\hat{F}^s)^T \hat{F}^s - 1) = \frac{1}{2} \left( \hat{\nabla} \hat{u}^s + (\hat{\nabla} \hat{u}^s)^T + \hat{\nabla} \hat{u}^s (\hat{\nabla} \hat{u}^s)^T \right).$$

Assuming further, that the stress of the considered elastic material can be approximated by a *linear material law*, and that the material is also homogeneous and isotropic, the stress-strain relation takes the form of the **Hooke's law**:

$$\hat{\sigma}^s = 2\mu^s \hat{E}^s + \lambda^s \text{tr}(\hat{E}^s) I,$$

where the shear modulus  $\mu^s$  and Lamé's first coefficient  $\lambda^s$  are the material parameters of the medium, that are related to the Poisson's ratio  $\nu$  and Young's modulus E as:

$$\mu^s := \frac{E}{2(1+\nu)}, \quad \lambda^s := \frac{E\nu}{(1+\nu)(1-2\nu)}.$$

*St. Venant Kirchhoff materials* must also satisfy

$$3\lambda^s + 2\mu^s > 0, \quad \mu^s > 0, \quad \nu > 0, \quad E > 0.$$

### **Small deformations: linear strain tensor**

From the definitions of deformation gradient  $\hat{F}^s$  and determinant  $\hat{J}^s$ , it follows that in case for all  $t \in (0, T)$  the deformations are small compared to the size of the domain, the deformation gradient is expected to be small, such that  $\hat{F}^s$  can be approximated by the identity matrix, such that  $\hat{J}^s \approx 1$ :

$$\|\hat{u}^s\| \ll \|\hat{x}\| \quad \forall t \in (0, T) \quad \Rightarrow \quad \|\hat{\nabla} \hat{u}^s\| \ll 1 \quad \Rightarrow \quad \hat{F}^s := I + \hat{\nabla} \hat{u}^s \approx I, \quad \hat{J}^s \approx 1. \quad (\text{A.14})$$

Therefore the strain and stress elasticity tensors reduce to:

$$\begin{aligned} \hat{E}^s &= \hat{\epsilon} := \frac{1}{2} \left( \hat{\nabla} \hat{u}^s + (\hat{\nabla} \hat{u}^s)^T \right), \\ \hat{\sigma}^s &= \mu^s \left( \hat{\nabla} \hat{u}^s + (\hat{\nabla} \hat{u}^s)^T \right) + \lambda^s \hat{\nabla} \cdot \hat{u}^s I, \end{aligned} \quad (\text{A.15})$$

and so the motion equations formulated on the reference domain for a linear homogeneous isotropic elastic material undergoing small deformations can be written as:

$$\hat{\nabla} \cdot \left( \mu^s \left( \hat{\nabla} \hat{u}^s + (\hat{\nabla} \hat{u}^s)^T \right) + \lambda^s \hat{\nabla} \cdot \hat{u}^s I \right) + \hat{\rho}^s g = \hat{\rho}^s \partial_{tt} \hat{u}^s \quad \text{in } \hat{\Omega}^s. \quad (\text{A.16})$$

Further details on the derivation and applicability of the linear elasticity equations can be found in e.g. [131], [180], [82].

## A.3 Fluid Dynamics

### *Conservation Laws*

Assume that some amount of incompressible fluid is moving within (flowing through) a volume  $\Omega^f(t)$  with velocity  $v^f(x, t)$ , where  $\Omega^f(t)$  is an in general deforming domain. The conservation laws (A.7), (A.10) written for an incompressible homogeneous fluid flow through  $\Omega^f(t)$  read:

$$\rho^f \partial_t v^f + \rho^f (v^f \cdot \nabla) v^f = \rho^f g + \nabla \cdot \sigma^f \quad \text{in } \Omega^f(t) \times (0, T), \quad (\text{A.17})$$

$$\nabla \cdot v^f = 0 \quad \text{in } \Omega^f(t) \times (0, T), \quad (\text{A.18})$$

where  $g$  is the volume force density corresponding to gravity, mass density  $\rho^f$  is constant, and stress tensor  $\sigma^f$  is symmetric.

### *Stress Modelling. Stokes Equations*

Assuming that the material filling  $\Omega^f(t)$  can be modelled as a **Stokes fluid**, the stress tensor  $\sigma^f$  can be represented as the sum of a spherically symmetric tensor  $\sigma_{sph}^f$  and a shear tensor  $\sigma_{sh}^f$ :

$$\sigma^f := \sigma_{sph}^f + \sigma_{sh}^f,$$

such that the spherical part of the tensor  $\sigma^f$  is proportional to the hydraulic fluid pressure  $p^f$  and the shear stress is linked to the *strain rate* tensor  $E^f$  via a material law  $M^f$ :

$$\begin{aligned} \sigma_{sph}^f &:= -p^f I, \\ \sigma_{sh}^f &:= \sigma_{sh}^{fT} = M^f(E^f), \end{aligned}$$

where the strain rate tensor is proportional to the velocity gradient:

$$E^f := \frac{1}{2} \left( \nabla v^f + (\nabla v^f)^T \right).$$

Assuming that the *material law* of the isotropic fluid is *linear*, i.e.

$$\sigma_{sh}^f = 2\mu^f E^f + \lambda^f \text{tr}(E^f) I \quad (\text{A.19})$$

for the material constants  $\mu^f$ ,  $\lambda^f$  ( $\mu^f$  is the dynamic fluid viscosity,  $\lambda^f$  is the bulk viscosity), and noticing that the last term in (A.19) cancels due to the incompressibility condition (A.18):

$$\text{tr}(E^f) = \nabla \cdot v^f = 0,$$

a law for the *Newtonian* fluid stress tensor is obtained:

$$\sigma^f = -p^f I + 2\mu^f (\nabla v^f + \nabla v^{fT}).$$

Incompressibility condition can also be used when applying the divergence operator to the stress tensor in (A.17):

$$\nabla \cdot \sigma^f = -\nabla p^f + \mu^f (\Delta v^f + \nabla(\nabla \cdot v^f)) = -\nabla p^f + \mu^f \Delta v^f,$$

and so the conservation equations for the flow of an isothermal incompressible Newtonian fluid take the form of the **Navier-Stokes** equations:

$$\begin{cases} -\nabla p^f + \mu^f \Delta v^f + \rho^f g = \rho^f (\partial_t v^f + (v^f \cdot \nabla)v^f) \\ \nabla \cdot v^f = 0 \end{cases} \quad \text{in } \Omega^f(t) \times (0, T). \quad (\text{A.20})$$

### **Deforming domain: ALE formulation**

The above formulated equations are written in the Eulerian coordinates on the current domain  $\Omega^f(t)$ . Fluid flow problems are often formulated on *fixed* domains, such that the coordinates of the deformed configuration  $\Omega^f(t)$  coincide with the reference frame, i.e.  $\Omega^f(t) \equiv \hat{\Omega}^f$  for all  $t \in (0, T)$ , and are therefore known. However in case the domain is deforming, the position of  $\Omega^f(t)$  and therefore the Eulerian coordinates  $\{x\}$  are unknown. Therefore a law (mapping) describing the evolution of the domain  $\Omega^f(t)$  must be provided:

$$\hat{T}_t^f : \hat{\Omega}^f \rightarrow \Omega^f(t) \quad \forall t \in (0, T),$$

such that  $\hat{T}_t^f$  maps each point  $\hat{x}$  of the reference domain into the deformed domain, and the domain displacement function  $\hat{u}^f(\hat{x}, t)$  as well as the domain deformation velocity  $\hat{w}^f(\hat{x}, t)$  can be defined for all  $\hat{x} \in \hat{\Omega}^f$  as:

$$\begin{aligned} \hat{T}_t^f(\hat{x}) &= x(\hat{x}, t), & \hat{u}^f(\hat{x}, t) &= u^f(x, t) = x(\hat{x}, t) - \hat{x}, & x &\in \Omega^f(t), \quad \hat{x} \in \hat{\Omega}^f. \\ & & \hat{w}^f &:= \partial_t \hat{T}_t^f = \partial_t \hat{u}^f, & & \end{aligned}$$

It should be noted, that the domain deformation velocity  $w^f$  is in general not related to the flow velocity  $v$ , and so  $v(x, t) \neq w(x, t)$ .

Unless  $\hat{T}_t^f$  or  $\hat{u}^f$  are explicitly given, they need to be constructed. Apart from being sufficiently regular, domain displacement  $\hat{u}^f$  must satisfy the conditions at the moving boundaries:

$$\hat{u}^f = \hat{u} \quad \text{at } \hat{\Gamma}^f \times (0, T), \quad (\text{A.21})$$

where  $\hat{u}$  is the displacement of the domain boundaries. In other regards  $\hat{T}_t^f$  can be chosen arbitrarily. A mapping that fulfils the above requirements is called an **Arbitrary Lagrangian-Eulerian** transformation.

In case the domain boundaries are smooth enough (i.e. there are no sharp edges), mapping  $\hat{T}_t^f$  can be chosen such that the displacement  $\hat{u}^f$  satisfies Laplace's equation:

$$\hat{\Delta} \hat{u}^f(\hat{x}(x, t)) = 0 \quad \text{in } \hat{\Omega}^f \times (0, T). \quad (\text{A.22})$$

If the boundary deformation  $\hat{u}$  is known for all  $t \in (0, T)$ , Laplace's equation (A.22) with the boundary conditions (A.21) can be solved for the displacement  $\hat{u}^f$  independently of the fluid

problem. Then the deformed configuration is found through the solution of (A.22), (A.21):

$$x(\hat{x}, t) = \hat{x} + \hat{u}^f \quad \forall x \in \Omega^f(t).$$

The settings of the interaction problems considered in this work are however such, that  $\hat{u}(\hat{x}, t)$  is a solution of the equations describing the movement of a domain  $\Omega^i(t)$  that borders  $\Omega^f(t)$ , and the equations on  $\Omega^f(t)$  and  $\Omega^i(t)$  can not be solved independently due to the coupling conditions at the common interface. Deformation  $\hat{u}$  *does* depend on the solution of the fluid flow equations as a result of interaction between  $\Omega^f(t)$  and  $\Omega^i(t)$  exerting stresses on each other.

As noted in *Section A.2*, the equations including the domain deformation function as an unknown must be solved on a fixed (reference) domain, therefore the fluid flow equations (being a part of an interaction problem) must be written with respect to fixed coordinates. It can be shown (see e.g. [82]), that the conservation equations (A.12) take the following form in ALE coordinates:

$$\left\{ \begin{array}{l} \hat{\nabla} \cdot (\hat{J}^f \hat{\sigma}^f (\hat{F}^f)^{-T}) + \hat{J}^f \rho^f g = \\ \rho^f \hat{J}^f \left( \partial_t \hat{v}^f + [(\hat{F}^f)^{-1}(\hat{v}^f - \hat{w}^f) \cdot \hat{\nabla}] \hat{v}^f \right) \quad \text{in } \hat{\Omega}^f \times (0, T), \\ \hat{\nabla} \cdot (\hat{J}^f (\hat{F}^f)^{-1} \hat{v}^f) = 0 \\ \hat{\sigma}^f := \mu^f \left( \hat{\nabla} \hat{v}^f (\hat{F}^f)^{-1} + (\hat{F}^f)^{-T} (\hat{\nabla} v^f)^T \right) - \hat{p}^f I \end{array} \right. \quad (\text{A.23})$$

where  $\hat{F}^f$  is the ALE deformation gradient tensor and  $\hat{J}^f$  – its determinant:

$$\begin{aligned} \hat{F}^f &:= \hat{\nabla} \hat{T}^f = I + \hat{\nabla} \hat{u}^f, \\ \hat{J}^f &:= \det(\hat{F}^f). \end{aligned}$$

### Small deformations

The Navier-Stokes equations (A.23) formulated in an ALE configuration are highly non-linear and are thus a challenge to solve. However as noted before in *Section A.2* (A.14), if during the time of observation the displacements remain small compared to the size of the domain, the gradient of the displacement is also expected to be small, and thus the ALE transformation terms can be significantly simplified:

$$\|\hat{u}^f\| \ll \|\hat{x}\| \quad \forall t \in (0, T) \quad \Rightarrow \quad \|\hat{\nabla} \hat{u}^f\| \ll 1 \quad \Rightarrow \quad \hat{F}^f := I + \hat{\nabla} \hat{u}^f \approx I, \quad \hat{J}^f \approx 1.$$

such that the Navier-Stokes equations formulated in ALE coordinates on the reference domain can be significantly simplified, such that:

$$\left\{ \begin{array}{l} \hat{\nabla} \cdot \hat{\sigma}^f + \rho^f g = \rho^f \left( \partial_t \hat{v}^f + [(\hat{v}^f - \hat{w}^f) \cdot \hat{\nabla}] \hat{v}^f \right) \\ \hat{\nabla} \cdot \hat{v}^f = 0 \end{array} \right. \quad \text{in } \hat{\Omega}^f \times (0, T).$$

$$\hat{\sigma}^f := \mu^f \left( \hat{\nabla} \hat{v}^f + (\hat{\nabla} v^f)^T \right) - \hat{p}^f I$$

## A.4 Poroelasticity equations: Mixture Theory approach

Porous medium  $\Omega^p$  is defined as a *superposition* of two distinct continuous media: solid skeleton  $\Omega^{sp}$  and pore fluid  $\Omega^{fp}$ . This means that each point  $x \in \Omega^p$  of the porous domain contains both



solid and fluid parts and traces the evolution of both phases.

Treating a porous medium as a continuum, it is in general possible to derive the governing equations for  $\Omega^p(t)$  using the conservation laws in the spirit of the fluid flow or elasticity equations. Thus as described above, for a homogeneous, incompressible medium, the mass and momentum balance laws can be written as:

$$\begin{aligned}\nabla \cdot \sigma^p + \rho^p f &= \rho^p \partial_t v^p(x, t) + \rho^p \nabla \cdot (v^p \otimes v^p) \\ \nabla \cdot v^p &= 0\end{aligned}\quad \forall x \in \Omega^p(t) \times (0, T),$$

where  $f$  are the body forces,  $\sigma^p$  is the stress tensor,  $v^p$  is the velocity and  $\rho^p$  is the density of the porous medium. However unlike in case of fluid flow or solid deformation problems, the meanings or definitions of  $\sigma^p$ ,  $v^p$ ,  $\rho^p$  are not clear. In addition, the material parameters for an arbitrary porous medium are not in general known, since even very moderate changes of the fluid content may influence the physical characteristics of the medium significantly.

A rigorous derivation of the Biot poroelasticity equations is described in *Section 2.1.2*. Here a simpler, but possibly more intuitive derivation of the poroelasticity equations based on a more straightforward combining of the effects the fluid and solid phases is outlined.

In the derivation of the conservation laws for a poroelastic material outlined below, the notion of a *representative elementary volume* (REV)  $\Phi(t)$ , which is defined as the smallest volume in  $\Omega^p(t)$  on which the poroelasticity equations for the overall medium hold, is used. On the microscale level,  $\Phi(t)$  can be split into solid and fluid parts, such that  $\Phi(t) = \Phi^f(t) \cup \Phi^s(t)$ , and on the macro scale, it reduces to a point  $x \in \Omega^p(t)$  that carries information from the microscale.

### ***Porosity and Solidity***

Porosity  $\gamma^f(x, t)$  is defined as a relation between the local volume of the fluid content  $dV^{fp}(x, t)$  and the overall volume  $dV^p(x, t)$  in a REV  $\Phi(t)(x)$ :

$$\gamma^f(x, t) = \frac{dV^{fp}(x, t)}{dV^p(x, t)}.$$

Analogously, solidity  $\gamma^s(x, t)$  is defined as

$$\gamma^s(x, t) = \frac{dV^{sp}(x, t)}{dV^p(x, t)} \quad \forall (x, t) \in \Omega^p(t) \times (0, T),$$

where  $dV^{sp}(x, t)$  is the local volume of solid grains. In case the porous medium does not contain other phases, the saturation condition reads:

$$\gamma^f(x, t) + \gamma^s(x, t) = 1 \quad \forall (x, t) \in \Omega^p(t) \times (0, T), \quad (\text{A.24})$$

and therefore for each  $\Phi(t) \subset \Omega^p(t)$ , the following volume integral transformations can be written:

$$\int_{\Phi(t)} dV^p = \int_{\Phi^f(t)} dV^f + \int_{\Phi^s(t)} dV^s = \int_{\Phi(t)} \gamma^f dV^p + \int_{\Phi(t)} \gamma^s dV^p. \quad (\text{A.25})$$

Porous material is said to be *homogeneous*, if the volume fractions of the fluid and solid phases are

the same in each elementary volume, and so the local and global phase volumes are proportional:

$$\begin{aligned} \frac{dV^{fp}(x, t)}{dV^p(x, t)} &= \frac{V^{fp}(t)}{V^p(t)} \\ \frac{dV^{sp}(x, t)}{dV^p(x, t)} &= \frac{V^{sp}(t)}{V^p(t)} \end{aligned} \quad \forall (x, t) \in \Omega^p(t) \times (0, T),$$

where  $V^{fp}(t)$ ,  $V^{sp}(t)$ ,  $V^p(t)$  are respectively the fluid phase, solid phase and total porous medium volumes at time  $t \in (0, T)$ .

Thus in a homogeneous porous medium, porosity  $\gamma^f(x, t)$  does not depend on the spatial variable:

$$\begin{aligned} \gamma^s(x, t) &:= \gamma^s(t), \\ \gamma^f(x, t) &:= \gamma^f(t), \end{aligned} \quad \forall (x, t) \in \Omega^p(t) \times (0, T).$$

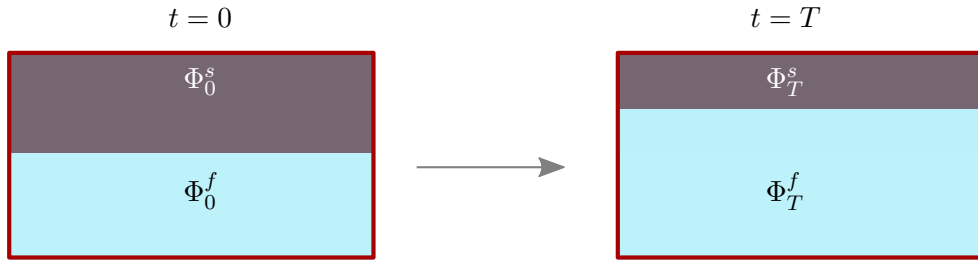
### ***Incompressibility Constraint***

In case the considered porous medium is growing (swelling) due to the inflow of fluid only, the porosity and solidity must change in time. Assuming that the medium remains homogeneous during the swelling, it can be concluded that the proportions of the solid and fluid parts in any *fixed* elementary volume  $\Phi$  would change in time:

$$\begin{aligned} 0 &= \frac{d}{dt} \int_{\Phi} dV = \frac{d}{dt} \int_{\Phi^s(t)} dV^s + \frac{d}{dt} \int_{\Phi^f(t)} dV^f, \\ \frac{d}{dt} \int_{\Phi^s(t)} dV^s &\neq 0, \quad \frac{d}{dt} \int_{\Phi^f(t)} dV^f \neq 0. \end{aligned} \quad (\text{A.26})$$

This means that the volume of solid "pressed out" of  $\Phi$  is equal to the volume of fluid flowing into the element, see *Fig. A.1*.

**Figure A.1 Change of fluid and solid phase proportions in a representative volume.**



Following (A.25), the fluid and solid domain integrals in (A.26) are transformed into integrals over  $\Phi$ , then the Reynolds' theorem is applied to each of the terms, resulting in:

$$\int_{\Phi} \left( \partial_t \gamma^f + \gamma^f \nabla \cdot v^{fp} \right) dV + \int_{\Phi} \left( \partial_t \gamma^s + \gamma^s \nabla \cdot v^{sp} \right) dV = 0. \quad (\text{A.27})$$

The considered porous medium is assumed to be fully saturated, (A.24), thus the sum of the porosity and solidity time derivatives in (A.27) reduces to zero:

$$\partial_t (\gamma^f + \gamma^s) = \partial_t 1 = 0,$$

and since (A.27) holds on any  $\Phi \subset \Omega^p(t)$ , the following equation is obtained:

$$\nabla \cdot (\gamma^f v^{fp} + \gamma^s v^{sp}) = 0 \quad \text{in } \Omega^p(t) \quad (\text{A.28})$$

Equation (A.28) corresponds to the *incompressibility* condition for the porous media, where the velocity  $v^p$  of  $\Omega^p(t)$  is defined as

$$v^p := \gamma^f v^{fp} + \gamma^s v^{sp}.$$

It can be observed, that while the volume of  $\Phi$  is fixed, the *mass* within it is not conserved if the densities of the fluid and solid phases are not equal, since the proportions of the volume fractions change:

$$\frac{d}{dt} \int_{\Phi^f(t)} \rho^f dV + \frac{d}{dt} \int_{\Phi^s(t)} \rho^s dV = \frac{d}{dt} \int_{\Phi} (\gamma^f \rho^f + \gamma^s \rho^s) dV \neq 0.$$

This effect reflects the change of material properties of the medium due to swelling or shrinking.

### **Momentum conservation**

The conservation of the linear momentum equation (or *equilibrium relation*) is obtained in a way that is similar to the derivation of the incompressibility constraint (A.28). Linear momentum of the porous medium  $LM^p$  is created by the momenta of its phases, thus the temporal variation of  $LM^p$  reads:

$$\begin{aligned} \frac{d}{dt} LM^p &:= \frac{d}{dt} \int_{\Phi^f(t)} \rho^f v^{fp} dV^f + \frac{d}{dt} \int_{\Phi^s(t)} \rho^s v^{sp} dV^s = \frac{d}{dt} \int_{\Phi(t)} (\rho^f \gamma^f v^{fp} + \rho^s \gamma^s v^{sp}) dV \\ &= \int_{\Phi(t)} \left\{ \rho^f \partial_t (\gamma^f v^{fp}) + \rho^f \gamma^f \nabla \cdot (v^{fp} \otimes v^{fp}) + \rho^s \partial_t (\gamma^s v^{sp}) + \rho^s \gamma^s \nabla \cdot (v^{sp} \otimes v^{sp}) \right\} dV. \end{aligned}$$

Assuming that the *deformations are small* (as in (A.14), (A.14)), such that the porosity and solidity can be considered to remain constant and the non-linear inertial terms can be neglected, the expression for the variation of the linear momentum reduces to:

$$\frac{d}{dt} LM^p = \int_{\Phi(t)} (\gamma^f \rho^f \partial_t v^{fp} + \gamma^s \rho^s \partial_t v^{sp}) dV.$$

As stated in (A.8), the change of linear momentum results from the volume ( $g$ ) and surface ( $\sigma^p$ ) forces acting on the media:

$$\int_{\Phi(t)} (\rho^f \partial_t v^{fp} + \rho^s \partial_t v^{sp}) dV = \int_{\Phi(t)} \rho^p g dV + \int_{\partial_t \Phi(t)} \sigma^p \cdot n dS, \quad (\text{A.29})$$

and since (A.29) holds on any  $\Phi(t) \subset \Omega^p(t)$ , applying the Ostrogradsky divergence theorem to the boundary term, an equilibrium relation on  $\Omega^p(t)$  undergoing small deformations is obtained:

$$\nabla \cdot \sigma^p + \rho^p g = \gamma^f \rho^f \partial_t v^{fp} + \gamma^s \rho^s \partial_t v^{sp}. \quad (\text{A.30})$$

### **Stress Modelling**

In a porous medium, the phases interact exerting stresses on each other, such that some of the effects dominate the other ones. Thus according to the *Terzaghi's principle*, the total stress  $\sigma^p$  in a porous medium is equal to the sum of the effective stress  $\sigma^{eff}$  and pore fluid pressure

tensor  $-p^p I$ , [181]:

$$\sigma^p := \sigma^{eff} - p^p I.$$

It is assumed that the effective stress is supported by the solid skeleton only. Since the material composing the skeleton  $\Omega^{sp}$  satisfies the equations of linear elasticity, the effective stresses in the porous medium written in the *Eulerian* and *Lagrangian* coordinates are defined as:

$$\begin{aligned}\sigma^{eff} &:= \sigma^{sp} = J^s (F^s)^{-1} \left( \mu^s \left( \nabla u^{sp} + (\nabla u^{sp})^T \right) + \lambda^s \nabla \cdot u^{sp} I \right) (F^s)^{-T}, \\ \hat{\sigma}^{eff} &:= \hat{\sigma}^{sp} = (\hat{J}^s)^{-1} \hat{F}^s \left( \mu^s \left( \hat{\nabla} \hat{u}^{sp} + (\hat{\nabla} \hat{u}^{sp})^T \right) + \lambda^s \hat{\nabla} \cdot \hat{u}^{sp} I \right) (\hat{F}^s)^T,\end{aligned}$$

such that if the medium is undergoing *small deformations*, the coordinate transformation terms  $J^s (F^s)^{-1}$ ,  $(F^s)^{-T}$ ,  $(\hat{J}^s)^{-1} \hat{F}^s$ ,  $(\hat{F}^s)^T$  can be neglected as in (A.16). Then the total stress tensor of the poroelastic medium can be approximated as:

$$\begin{aligned}\sigma^p &= \mu^s \left( \nabla u^{sp} + (\nabla u^{sp})^T \right) + \lambda^s \nabla \cdot u^{sp} I - p^p I && \text{in } \Omega^p(t) \times (0, T), \\ \hat{\sigma}^p &= \mu^s \left( \hat{\nabla} \hat{u}^{sp} + (\hat{\nabla} \hat{u}^{sp})^T \right) + \lambda^s \hat{\nabla} \cdot \hat{u}^{sp} I - \hat{p}^p I && \text{in } \hat{\Omega}^p \times (0, T).\end{aligned}$$

The derivation of the poroelasticity equations outlined above follows the ideas of the Consolidation (or Mixture Theory) models considered or developed in [182], [183], [184], [22], [24], [23], [185], [26], [107], [97], [28] and further works.

### **Modified Darcy's Law**

The balance laws derived above contain the pore fluid velocity  $v^{fp}$  as an unknown. Therefore in order to complete the system of poroelasticity equations, an additional equation describing the evolution of  $v^{fp}$  is needed.

Stokes equations written for the fluid phase of the medium on the pore scale and then homogenized over the domain, transform into **Darcy's filtration law** that relates the rate of flux (or *seepage velocity*)  $q$  to the pressure gradient across the domain:

$$\mu^f q = -K \nabla p^p,$$

where  $\mu^f$  is the dynamic viscosity of the fluid and  $K$  is the *permeability* tensor. In a deforming medium, the rate of flux  $q$  is defined through the *relative* (with respect to the solid phase velocity) fluid phase velocity  $v^{fp} - v^{sp}$  as:

$$q := \gamma^f (v^{fp} - v^{sp}).$$

Thus the filtration law for a deforming isotropic porous medium allows to express the pore fluid velocity  $v^{fp}$  through the principle unknowns of the Biot equation, i.e. the displacement  $u^{sp}$  and pore pressure  $p^p$ :

$$v^{fp} = \partial_t u^{sp} - \frac{k}{\gamma^f \mu^f} \nabla p^p. \tag{A.31}$$

Equations (A.28) and (A.30), where the fluid velocity  $v^{fp}$  is substituted using expression (A.31), constitute the **Biot poroelasticity equations** for an incompressible, homogeneous, isotropic

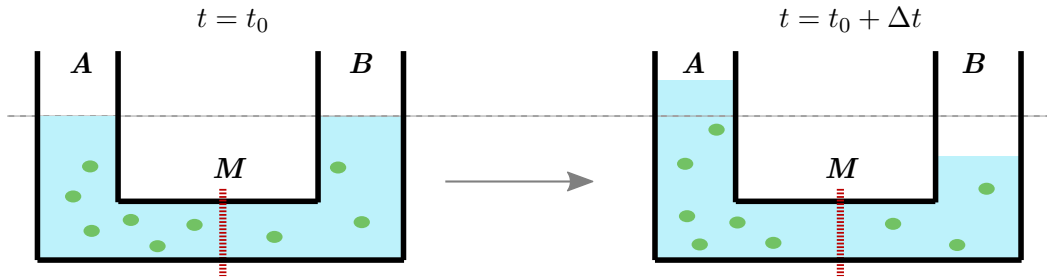
medium undergoing small deformations:

$$\begin{cases} \nabla \cdot \sigma^p + \rho^p g - (\gamma^s \rho^s + \gamma^f \rho^f) \partial_{tt} u^{sp} + \frac{\rho^f k}{\mu^f} \partial_t (\nabla p^p) = 0 \\ \nabla \cdot \left( \partial_t u^{sp} - \frac{k}{\mu^f} \nabla p^p \right) = 0 \end{cases} \quad \text{in } \Omega^p(t) \times (0, T). \quad (\text{A.32})$$

## A.5 Osmosis and osmotic pressure

Assume that initially (at time  $t_0$ ) solutions  $A$  and  $B$  of concentrations  $c_A$  and  $c_B$  respectively, are separated by a *strictly semipermeable membrane*  $M$  (a membrane that is permeable to the solvent only). If the concentrations are such that  $c_A > c_B$ , and the hydrostatic pressures acting on both solutions are equal, then after some time  $\Delta t$  an increase of volume  $V_A(t)$  due to the inflow of solvent from  $B$  is observed, see *Fig. A.2*. This process is known as *osmosis* and the force that drives the flow of solvent is referred to as *osmotic pressure*.

Figure A.2 Osmosis in communication vessels.



### Osmosis in brain tissue

The ionic exchange processes of a *healthy brain cell* can be roughly described in the following way:

- The macromolecules can not leave the cell unless it ruptures (the molecules are said to be *fixed* within the cell), and their concentration is much higher within the cell than in the ECS.
- Potassium ions are pumped into the cell through the ATP-dependent exchanger  $Na^+/K^+$ , and so sodium ions get concentrated in the extracellular space in order to counter-balance the concentration of the fixed negative charges.
- The outflow of cations creates a negative membrane potential ( $60 - 80 \text{ mV}$ ), also called *transmembrane voltage*, since the diffusion of ions occurs only in the vicinity of the membrane.

Thus although the chemical compositions of the intra- and extracellular fluids are different and there exist individual ionic concentration gradients, the healthy cell mechanisms ensure osmotic balance across the membrane in order to keep the volume of the cell *constant*.

*Note:* Depending on multiple factors, cells can in general change their volume at different moments of their healthy activity. However the healthy variations of the cell volume are not significant compared to the swelling rates of ischaemic cells.

One of the major causes of the *ischaemic cell swelling* is the increase of membrane permeability to  $Na^+$ , [41]. The ions of sodium diffuse into the cell along their concentration gradients, and since during ischaemia the energy is not available, sodium ions accumulate within the cell due to the failure of  $Na^+/K^+$  pump. Membrane failure allows the flow of potassium ions out of the cell, but the total inflow of  $Na^+$  dominates the outflow of  $K^+$ . The membrane depolarizes, the accumulation of sodium within the cell leads to the *jump* in the total intracellular and extracellular concentrations across the membrane and the consequent (osmosis-driven) swelling of the cell.

Further details on the healthy and ischaemic distributions of the chemicals diluted in the intracellular and extracellular spaces can be found in e.g. [69], [52], [51], [10], [43].

### A.5.1 Virial theorem (osmotic pressure model)

There exist multiple ways of explaining osmosis. On the macroscopic level, the flow of water through the membrane is observed, but in order to give an accurate description (and so to write an accurate model) the process needs to be understood on the molecular level. Following [186], [187], the derivation of the osmotic pressure model (van 't Hoff formula) based on the virial theorem is described below.

Assume that the solution is *diluted*, and so the solute molecules do not interact with each other; the temperature and concentration are constant. The connection between fluid pressure  $p_w$  enclosed in a volume  $V$  and molecular interactions is demonstrated by the *virial theorem*, which for pure solvent (water) reads:

$$p_w V = \frac{2}{3} [E_w^k] + \frac{1}{3} \left[ \sum_{i,j=1}^{N^w} F(w_i, w_j) \right],$$

where  $F(w_i, w_j)$  is the interaction force between molecules  $w_i, w_j$ ,  $N^w$  is the number of water molecules,  $E^k$  is the kinetic energy of the molecules, and square brackets "[ ]" denote the time average. Note that if the particles are far away from each other, the interaction forces become negligible, since they depend on the distance between molecules, and therefore the formula reduces to the ideal gas law.

In a diluted solution, apart from the "water-water" molecular type of interaction, the interaction of water molecules with the solute must also be considered. As the solute molecules  $s_i$  are assumed to not interact with each other, the following relations for solute pressure  $p_{ss}$  and solvent pressure  $p_{sw}$  contained in the solution  $V$  are obtained:

$$p_{ss} V = \frac{2}{3} [E_{ss}^k] + \frac{1}{3} \left[ \sum_{i,j=1}^{i=N^s, j=N^w} F(s_i, w_j) \right],$$

$$p_{sw} V = \frac{2}{3} [E_{sw}^k] + \frac{1}{3} \left[ \sum_{i,j} F(w_j, s_i) \right], + \frac{1}{3} \left[ \sum_{i,j} F(w_i, w_j) \right],$$

where  $N^s$  is the number of the solute molecules and the solute-solvent interaction forces are related such that:

$$\left[ \sum_{i,j} F(s_i, w_j) \right] \equiv - \left[ \sum_{i,j} F(w_j, s_i) \right].$$

Considering that the kinetic energies of pure water and water in the solution are equal, it can be deduced that the difference in the pressures of pure solvent and diluted solution occupying the same volume can be found as:

$$(p_w - p_{sw} - p_{ss})V = \frac{2}{3} \left( [E_w^k] - [E_{sw}^k] - [E_{ss}^k] \right) = -\frac{2}{3} [E_{ss}^k]. \quad (\text{A.33})$$

The average kinetic energy of the solute molecules diluted in a much larger amount of solvent can be found through the ideal gas law written for the pressure  $p_{si}$  that the solute would exert in the volume  $V$  in the absence of solvent:

$$N^s kT = p_{si} V = \frac{2}{3} [E_{ss}^k], \quad (\text{A.34})$$

where  $k$  is the Boltzmann constant and  $T$  is the temperature.

Combining (A.33) and (A.34), the following relation for the *fluid pressure of the solution*  $p_s$  is obtained:

$$p_s := p_{ss} + p_{sw} = p_w + p_{si}.$$

The fluid pressure of a solution is thus equal to the sum of the pressure of a pure solvent,  $p_w$ , and osmotic pressure  $\pi$ :

$$p_s = p_w + \pi,$$

such that the osmotic pressure  $\pi$  can be seen as a measure of the deviation of  $p_s$  from  $p_w$ , that corresponds to the pressure  $p_{si}$  of an ideal gas, that the molecules of the solute would exert within the volume  $V$  in the absence of solvent:

$$\pi := p_{si} \stackrel{(\text{A.34})}{=} \frac{N^s kT}{V}. \quad (\text{A.35})$$

Passing from the molecular to the continuum scale in (A.35), the following osmotic pressure model is obtained:

$$\pi = \frac{N^s kT}{V} = \frac{N^s N_A kT}{V} = \frac{nRT}{V} = cRT,$$

where  $n := N^s/N_A$  is the amount of substance of the solute,  $N_A$  is Avogadro's constant,  $R$  is the gas constant and  $c$  is the molar concentration (or the *molarity*) of the solute diluted in the volume  $V$ :

$$c := \frac{n}{V}.$$

Note, that the volumes of the solution and of the solvent can be considered equal, since the

solute volume is negligible:

$$V = V_{sw} + V_{ss} \approx V_{sw}.$$



# List of Figures

1.1	Localization of the problem. . . . .	12
1.2	Evolution of the cell representation. . . . .	15
1.3	Microscopic membrane deformation types: unfolding and stretching. . . . .	16
1.4	Cell swelling with respect to the surface area conservation. . . . .	17
1.5	Leaky and strictly semipermeable membranes. . . . .	20
1.6	Environment of the OCD depending on the experiment type. . . . .	22
1.7	Overall domain $\Omega = \Omega^b(t) \cup \Omega^p(t) \in \mathbb{R}^d, d \in \{2, 3\}$ . . . . .	23
2.1	Deformation and fluid flux on the microscopic level. . . . .	36
2.2	Displacement of the cell surface. . . . .	38
2.3	Overall domain $\Omega = \Omega^b(t) \cup \Omega^p(t) \in \mathbb{R}^d, d \in \{2, 3\}$ . . . . .	46
3.1	Lengths of the domains . . . . .	58
4.1	Overall domain $\Omega = \Omega^b(t) \cup \Omega^p(t) \in \mathbb{R}^d, d \in \{2, 3\}$ . . . . .	90
4.2	Pure Biot domain $\Omega^p(t) \in \mathbb{R}^d, d \in \{2, 3\}, t \in (0, T)$ . . . . .	91
4.3	Nodal points of $P_1, P_2$ simplex elements in dimensions $d = \{2, 3\}$ . . . . .	96
4.4	Rotationally symmetric Biot domain $\Omega^p$ . . . . .	101
4.5	Pure Biot problem meshes. . . . .	110
4.6	Numerical vs analytic Biot problem solution. . . . .	111
4.7	Pure Biot problem simulations with the <i>estimated</i> data. . . . .	116
4.8	Pure Biot problem simulations with the <i>estimated</i> data: deformation solution. . . . .	120
4.9	Pure Biot problem simulations: parameter sensitivity. . . . .	125
4.10	Coupled Biot-Stokes vs Pure Biot problem: <i>circular</i> Biot domain geometry. . . . .	133
4.11	Coupled Biot-Stokes problem: <i>circular</i> Biot domain geometry. . . . .	136
4.12	Biot-Stokes problem meshes. . . . .	138
4.13	Coupled Biot-Stokes problem simulations: comparison between different cell geometries. . . . .	140
4.14	Coupled Biot-Stokes problem: <i>Circular, Variant 0, Variant 1</i> geometries. . . . .	141
4.16	Coupled Biot-Stokes vs Pure Biot problem: <i>non-trivial</i> Biot domain geometries. . . . .	145
A.1	Change of fluid and solid phase proportions in a representative volume. . . . .	158
A.2	Osmosis in communication vessels. . . . .	161



# List of Tables

3.1	Parameters (in SI units). . . . .	82
3.2	Domain dimensions (in SI units). . . . .	82
3.3	Description of further symbols. . . . .	83
3.4	Times, velocities and pressures (in SI units). . . . .	83
3.5	Volumes, amounts of substance and concentrations (in SI units). . . . .	84
3.6	Data in the units of the numerical implementation. . . . .	85
4.1	Comparison between numerical and analytic Biot problem solutions. . . . .	110
4.2	Pure Biot problem simulations with the <i>estimated</i> data. . . . .	115
4.3	Pure Biot problem simulations: parameter sensitivity. . . . .	124
4.4	Coupled Biot-Stokes vs Pure Biot problem: <i>circular</i> Biot domain geometry. . . . .	132
4.5	Coupled Biot-Stokes problem simulations: comparison between different cell geometries. . . . .	139
4.6	Coupled Biot-Stokes vs Pure Biot problem: <i>non-trivial</i> Biot domain geometries. . . . .	144



# Bibliography

- [1] Capovilla R, Guven J. Stresses in lipid membranes. *Journal of Physics A: Mathematical and General* 2002; **35**:6233–6247.
- [2] Capovilla R, Guven J. Stress and geometry of lipid vesicles. *Journal of Physics: Condensed Matter* Jun 2004; **16**(22):2187–2191.
- [3] Tu ZC. Elastic theory of membranes. *AAPPS Bulletin* 2006; **16**(3):30–33.
- [4] Tu ZC, Ou-Yang ZC. A geometric theory on the elasticity of bio-membranes. *Journal of Physics A: Mathematical and General* Nov 2004; **37**:11 407–11 429.
- [5] Janmey Pa, Kinnunen PKJ. Biophysical properties of lipids and dynamic membranes. *Trends in cell biology* Oct 2006; **16**(10):538–546.
- [6] Carin M, Barthès-Biesel D, Edwards-Lévy F, Postel C, Andrei DC. Compression of bio-compatible liquid-filled HSA-alginate capsules: determination of the membrane mechanical properties. *Biotechnology and bioengineering* Apr 2003; **82**:207–212.
- [7] Boedec G, Leonetti M, Jaeger M. 3D vesicle dynamics simulations with a linearly triangulated surface. *Journal of Computational Physics* Feb 2011; **230**(4):1020–1034.
- [8] Canham P. The minimum energy of bending as a possible explanation of the biconcave shape of the human red blood cell. *Journal of Theoretical Biology* 1970; **26**:61– 81.
- [9] Helfrich W. Elastic properties of lipid bilayers: theory and possible experiments. *Zeitschrift fur Naturforschung. Teil C: Biochemie, Biophysik, Biologie, Virologie* 1973; **28**:693–703.
- [10] Elkin BS, Shaik MA, Morrison B. Fixed negative charge and the Donnan effect: a description of the driving forces associated with brain tissue swelling and oedema. *Philosophical transactions. Series A, Mathematical, physical, and engineering sciences* Feb 2010; **368**:585–603.
- [11] Albro MB, Chahine NO, Caligaris M, Wei VI, Likhitpanichkul M, Ng KW, Hung CT, Ateshian GA. Osmotic loading of spherical gels: a biomimetic study of hindered transport in the cell protoplasm. *Journal of Biomechanical Engineering* 2007; **129**(4):503–510.
- [12] Ateshian GA, Likhitpanichkul M, Hung CT. A mixture theory analysis for passive transport in osmotic loading of cells. *Journal of biomechanics* Jan 2006; **39**:464–475.
- [13] Mauck RL, Hung CT, Ateshian GA. Modeling of neutral solute transport in a dynamically loaded porous permeable gel: implications for articular cartilage biosynthesis and tissue engineering. *Journal of Biomechanical Engineering* 2003; **125**(5):602–614.
- [14] Bausch AR, Ziemann F, Boulbitch AA, Jacobson K, Sackmann E. Local measurements of viscoelastic parameters of adherent cell surfaces by magnetic bead microrheometry. *Biophysical Journal* 1998; **75**:2038–2049.

- [15] Bausch AR, Möller W, Sackmann E. Measurement of local viscoelasticity and forces in living cells by magnetic tweezers. *Biophysical journal* Jan 1999; **76**:573–579.
- [16] Tinevez JY, Schulze U, Salbreux G, Roensch J, Joanny JF, Paluch E. Role of cortical tension in bleb growth. *Proceedings of the National Academy of Sciences of the United States of America* Nov 2009; **106**(44):18 581–18 586.
- [17] Wakatsuki T, Kolodney MS, Zahalak GI, Elson EL. Cell mechanics studied by a reconstituted model tissue. *Biophysical journal* 2000; **79**(5):2353–2368.
- [18] Ngwa W, Chen K, Sahgal A, Stepanov EV, Luo W. Nanoscale mechanics of solid-supported multilayered lipid films by force measurement. *Thin Solid Films* Jun 2008; **516**:5039–5045.
- [19] Safran S, Gov N, Nicolas A, Schwarz U, Thlsty T. Physics of cell elasticity, shape and adhesion. *Physica A* Jul 2005; **352**:171–201.
- [20] Gardel ML, Kasza KE, Brangwynne CP, Liu J, Weitz DA. Chapter 19: Mechanical response of cytoskeletal networks. *Methods in cell biology* Jan 2008; **89**:487–519.
- [21] Xu J, Schwarz WH, Käs JA, Stossel TP, Janmey PA, Pollard TD. Mechanical properties of actin filament networks depend on preparation, polymerization conditions, and storage of actin monomers. *Biophysical journal* May 1998; **74**:2731–2740.
- [22] Barry SI, Aldis GK. Comparison of models for flow induced deformation of soft biological tissue. *Journal of Biomechanics* 1990; **23**(7):647–654.
- [23] Barry SI, Aldis GK. Flow-induced deformation from pressurized cavities in absorbing porous tissues. *Bulletin of mathematical biology* 1992; **54**(6):977–997.
- [24] Barry SI, Aldis GK. Unsteady flow induced deformation of porous materials. *International Journal of Non-Linear Mechanics* 1991; **26**(5):687–699.
- [25] Canic S, Lamponi D, Mikelić A, Tambaca J. Self-consistent effective equations modeling blood flow in medium-to-large compliant arteries. *Multiscale Modeling & Simulation* 2005; **3**(3):559–596.
- [26] Holmes MH, Mow VC. The nonlinear characteristics of soft gels and hydrated connective tissues in ultrafiltration. *Journal of biomechanics* Jan 1990; **23**(11):1145–1156.
- [27] Holmes MH. A theoretical analysis for determining the nonlinear hydraulic permeability of a soft tissue from a permeation experiment. *Bulletin of mathematical biology* 1985; **47**(5):669–683.
- [28] Kwan MK, Lai WM, Mow VC. A finite deformation theory for cartilage and other soft hydrated connective tissues–I. Equilibrium results. *Journal of biomechanics* Jan 1990; **23**(2):145–155.
- [29] Jäger W, Mikelić A, Neuss-Radu M. Analysis of differential equation modelling the reactive flow through a deformable system of cells. *Archive for Rational Mechanics and Analysis* 2009; **192**(2):331–374.
- [30] Jäger W, Mikelić A, Neuss-Radu M. Homogenization-limit of a model system for interaction of flow, chemical reactions and mechanics in cell tissues. *SIAM Journal on Mathematical Analysis* 2011; **43**(3):1390–1435.

- 
- [31] Mikelić A, Wheeler M. On the interface law between a deformable porous medium containing a viscous fluid and an elastic body. *Mathematical Models and Methods in Applied Sciences* 2012; **22**.
- [32] Zenisek A. The existence and uniqueness theorem in Biot's consolidation theory. *Aplikace matematiky* 1984; **29**(3):194–211.
- [33] Showalter RE. Diffusion in poro-elastic media. *Journal of Mathematical Analysis and Applications* 2000; **251**:310–340.
- [34] Marciniak-Czochra A, Mikelić A. A rigorous derivation of the equations for the clamped Biot-Kirchhoff-Love poroelastic plate. *Archive for Rational Mechanics and Analysis* 2015; **215**(3):1035–1062.
- [35] Tavakoli A, Ferronato M. On existence-uniqueness of the solution in a nonlinear Biot's model. *Applied Mathematics and Information Sciences* 2013; **7**(1):333–341.
- [36] Badia S, Quaini A, Quarteroni A. Coupling Biot and Navier–Stokes equations for modelling fluid–poroelastic media interaction. *Journal of Computational Physics* Nov 2009; **228**:7986–8014.
- [37] Muntz S. Fluid structure interaction for fluid flow normal to deformable porous media. PhD Thesis, Technische Universität Kaiserslautern, Kaiserslautern 2008.
- [38] Barzó P, Marmarou A, Fatouros P, Hayasaki K, Corwin F. Contribution of vasogenic and cellular edema to traumatic brain swelling measured by diffusion-weighted imaging. *Journal of Neurosurgery* 1997; **87**(6):900–907.
- [39] Brillault J, Lam TI, Rutkowsky JM, Foroutan S, O'Donnell ME. Hypoxia effects on cell volume and ion uptake of cerebral microvascular endothelial cells. *American Journal of Physiology-Cell Physiology* 2008; **294**(1):88–96.
- [40] Karaszewski B, Wardlaw JM, Marshall I, Cvorov V, Wartolowska K, Haga K, Armitage Pa, Bastin ME, Dennis MS. Early brain temperature elevation and anaerobic metabolism in human acute ischaemic stroke. *Brain: a journal of neurology* Apr 2009; **132**:955–964.
- [41] Kempfski O, Zimmer M, Neu A, von Rosen F, Jansen M, Baethmann A. Control of glial cell volume in anoxia. In vitro studies on ischemic cell swelling. *Stroke* May 1987; **18**:623–628.
- [42] Li XG, Holst HV, Ho J, Kleiven S. Three dimensional poroelastic simulation of brain edema: initial studies on intracranial pressure. *World Congress on Medical Physics and Biomedical Engineering, IFMBE Proceedings Volume 25/4*, 2010: Munich, Germany, 2009; 1478–1481.
- [43] Liang D, Bhatta S, Gerzanich V, Simard JM. Cytotoxic edema: mechanisms of pathological cell swelling. *Neurosurgical Focus*. Jan 2007; **22**(5).
- [44] Lipton P. Ischemic cell death in brain neurons. *Physiological reviews* Oct 1999; **79**:1431–1568.
- [45] Mortazavi MM, Romeo AK, Deep A, Griessenauer CJ, Shoja MM, Tubbs RS, Fisher W. Hypertonic saline for treating raised intracranial pressure: literature review with meta-analysis. *Journal of neurosurgery* Jan 2012; **116**:210–221.

- [46] Loubinoux I, Volk A, Borredon J, Guirimand S, Tiffon B, Seylaz J, Méric P. Spreading of vasogenic edema and cytotoxic edema assessed by quantitative diffusion and T2 magnetic resonance imaging. *Stroke* 1997; **28**:419–427.
- [47] Rohl L, Gyldensted C, Sakoh M, Simonsen CZ, Vestergaard-Poulsen P, Sorensen JC, Ostergaard L. Time evolution of cytotoxic and vasogenic edema measured by DWI and T2 in a porcine stroke model. *Proceedings of the International Society for Magnetic Resonance in Medicine* 2001; **9**:1456.
- [48] Rosenberg GA. Ischemic brain edema. *Progress in Cardiovascular Diseases* 1999; **42**(3):209–216.
- [49] Schaefer PW, Grant PE, Gonzalez RG. Diffusion-weighted MR Imaging of the brain. *Radiology* 2000; **217**(2):331–345.
- [50] Sen S, Al E. Acute stroke: Diffusion-Weighted Imaging. <http://emedicine.medscape.com/article/1155506-overview#aw2aab6b5>, 2013.
- [51] Simard JM, Kent TA, Chen M, Tarasov KV, Gerzanich V. Brain oedema in focal ischaemia: molecular pathophysiology and theoretical implications. *Lancet neurology* Mar 2007; **6**:258–68.
- [52] Somjen GG. Ion regulation in the brain: implications for pathophysiology. *The Neuroscientist* 2002; **8**:254–267.
- [53] Steiner LA, Andrews PJD. Monitoring the injured brain: ICP and CBF. *British journal of anaesthesia* 2006; **97**(1):26–38.
- [54] Wintermark M, Fiebach J. Imaging of brain parenchyma in stroke. *Applied Radiology* 2007; **July**:10–18.
- [55] Zador Z. Mechanisms of cytotoxic brain edema. PhD Thesis, University of Szeged, Szeged 2009.
- [56] Fung YC. Mechanical properties of living tissues. Second edn., Springer-Verlag, 1993.
- [57] Reinis S. Physiology Lectures: The distribution of body fluids and ionic control. *Technical Report*, Third Faculty of Medicine, Charles University, Prague 2003.
- [58] D'Sa DJ, de Juan Pardo EM, de las Rivas Astiz R, Sen S, Kumar S. High-throughput indentational elasticity measurements of hydrogel extracellular matrix substrates. *Applied Physics Letters* 2009; **95**.
- [59] Damask A. Synapse, Neuron, Brain. Elsevier, 2012.
- [60] Rintoul GL, Filiano AJ, Brocard JB, Kress GJ, Reynolds IJ. Glutamate decreases mitochondrial size and movement in primary forebrain neurons. *The Journal of neuroscience* Aug 2003; **23**(21):7881–7888.
- [61] Liu KF, Li F, Tatlisumak T, Garcia JH, Sotak CH, Fisher M, Fenstermacher JD. Regional variations in the apparent diffusion coefficient and the intracellular distribution of water in rat brain during acute focal ischemia. *Stroke* 2001; **32**:1897–1905.



- 
- [62] Chudler EH. Brain facts and figures: Neuron. <http://faculty.washington.edu/chudler/facts.html#neuron>: University of Washington, 2015.
- [63] Chan YHM, Marshall WF. Scaling properties of cell and organelle size. *Organogenesis* 2010; **6**(2):88–96.
- [64] Howard C, Jolleys G, Stacey D, Fowler A, Wallen P, Browne MA. Measurement of total neuronal volume, surface area, and dendritic length following intracellular physiological recording. *NeuroProtocols: A Companion to Methods in Neurosciences* 1993; **2**:113–120.
- [65] Levental I, Georges PC, Janmey PA. Soft biological materials and their impact on cell function. *Soft Matter* 2006; **2**:1–9.
- [66] Freitas Jr RA. 8.5.3.3 Cytosol. *Nanomedicine, Volume I: Basic Capabilities*. Landes Bioscience, 1999.
- [67] Austin G, Sato M, Yai H. Osmolality effects in Aplysia neurons: I. Permeability coefficient and a model of water. *Mathematical Biosciences* 1967; **1**:493–513.
- [68] Shapiro BE. Osmotic forces and gap junctions in spreading depression: a computational model. *Journal of computational neuroscience* 2001; **10**:99–120.
- [69] Jakobsson E. Interactions of cell volume, membrane and membrane transport parameters. *American Journal of Physiology* 1980; **238**(5):196–206.
- [70] Kapoor KL. A textbook of physical chemistry, Vol. 3. Applications of thermodynamics. 3rd edn., Macmillan India Ltd.: New Delhi, 2011.
- [71] Haynie DT. Biological thermodynamics. Cambridge University Press, 2001.
- [72] Diamond JM, Wright EM. Biological membranes: the physical basis of ion and nonelectrolyte selectivity. *Annual review of physiology* Jan 1969; **31**:581–646.
- [73] Kozono D, Yasui M, King LS, Agre P. Aquaporin water channels: atomic structure and molecular dynamics meet clinical medicine. *Journal of Clinical Investigation* 2002; **109**:1395–1399.
- [74] Agre P, King LS, al E. Aquaporin water channels: from atomic structure to clinical medicine. *Journal of Physiology* 2002; **542**:3–16.
- [75] Ishibashi K, Sasaki S, Fushimi K, Uchida S, Kuwahara M, Saito H, Furukawa T, Nakajima K, Yamaguchi Y, Gojobori T. Molecular cloning and expression of a member of the aquaporin family with permeability to glycerol and urea in addition to water expressed at the basolateral membrane of kidney collecting duct cells. *Proceedings of the National Academy of Sciences of the United States of America* Jul 1994; **91**:6269–6273.
- [76] Wolff M, Vogel W, Safronov BV. Uneven distribution of K<sup>+</sup> channels in soma, axon and dendrites of rat spinal neurones: functional role of the soma in generation of action potentials. *Journal of Physiology* 1998; **509**(Pt 3):767–776.
- [77] Batchelor GK. An introduction to fluid dynamics. Cambridge University Press, 2000.
- [78] Galdi GP. An introduction to the Navier-Stokes initial-boundary value problem. *Fundamental Directions in Mathematical Fluid Mechanics Advances in Mathematical Fluid Mechanics* 2000; :1–70.

- [79] Landau LD, Lifshitz EM. Lehrbuch der Theoretischen Physik. Akademie Verlag GmbH: Berlin, 1991.
- [80] Meschede D. Gerthsen Physik. Springer-Verlag Berlin Heidelberg, 2004.
- [81] Temam R. Navier-Stokes equations: theory and numerical analysis. North-Holland Publishing Company, 1977.
- [82] Richter T. Numerical methods for fluid-structure interaction problems. Heidelberg, Vorlesungsskriptum, 2010.
- [83] Tolstoy Ie. Acoustics, elasticity, and thermodynamics of porous media: Twenty-one papers by M. A. Biot. Acoustical Society of America: New York, 1992.
- [84] R E Showalter. Poroelastic filtration coupled to Stokes flow. Published in O. Imanuvilov, G. Leugering, R. Triggiani, and B.-Y. Zhang (Editors). *Control Theory of Partial Differential Equations, Lecture Notes in Pure and Applied Mathematics, Chapman & Hall, Boca Raton* 2005; **242**:229–241.
- [85] Garikipati K, Arruda EM, Grosh K, Narayanan H, Calve S. A continuum treatment of growth in biological tissue: the coupling of mass transport and mechanics. *Journal of the Mechanics and Physics of Solids* Jul 2004; **52**:1595–1625.
- [86] Alt HW. Lineare Funktional-analysis. 5., überar edn., Springer-Verlag Berlin Heidelberg, 2006.
- [87] de Boer R. Theory and applications of transport in porous media. Trends in continuum mechanics of porous media. Springer-Verlag, 2005.
- [88] Markert B. A constitutive approach to 3-d nonlinear fluid flow through finite deformable porous continua. *Transport in Porous Media* Mar 2007; **70**:427–450.
- [89] Preziosi I, Farina A. On Darcy’s law for growing porous media. *International Journal of Non-Linear Mechanics* 2002; **37**:485–491.
- [90] Spiegelman BM. Flow in deformable porous media. Part 1 Simple analysis. *Journal of Fluid Mechanics* 1993; **247**:17–38.
- [91] Saffman A. On the boundary condition at the surface of a porous medium. *Studies in Applied Mathematics* 1971; **1**:93–101.
- [92] Jäger W, Mikelić A. On the interface boundary condition of Beavers, Joseph, and Saffman. *SIAM Journal on Applied Mathematics* 2000; **60**(4):1111–1127.
- [93] Jäger W, Mikelić A. On the boundary conditions at the contact interface between a porous medium and a free fluid. *Annali della Scuola Normale Superiore di Pisa - Classe di Scienze (4)* 1996; **23**(3):403–465.
- [94] Jäger W, Mikelić A. On the effective equations of a viscous incompressible fluid flow through a filter of finite thickness. *Communications on Pure and Applied Mathematics* 1998; **51**(9-10):1073–1121.
- [95] Jäger W, Mikelić A, Neuss N. Asymptotic analysis of the laminar viscous flow over a porous bed. *SIAM Journal on Scientific Computing* 2006; **22**(6):2006–2028.

- 
- [96] Marusic-Paloka E, Mikelić A. The derivation of a nonlinear filtration law including the inertia effects via homogenization. *Nonlinear Analysis* 2000; **42**:97–137.
- [97] Kumar V. Coupling of free flow and flow in porous media – a dimensional analysis. PhD Thesis, Universität Stuttgart - Institut für Wasserbau, Stuttgart 2011.
- [98] Lankveld IMAMV. Validation of boundary conditions between a porous medium and a viscous fluid. August, Technische Universiteit Eindhoven: Eindhoven, 1991.
- [99] Morse HN. The osmotic pressure of aqueous solutions, report on investigations made in the Chemical Laboratory of the Johns Hopkins University during the years 1899-1913. Washington, Carnegie Inst., 1914.
- [100] Boiarkine O, Kuzmin D, Čanić S, Guidoboni G, Mikelić A. A positivity-preserving ALE finite element scheme for convection–diffusion equations in moving domains. *Journal of Computational Physics* Apr 2011; **230**:2896–2914.
- [101] Formaggia L, Nobile F. A stability analysis for the arbitrary Lagrangian Eulerian formulation with finite elements. *East-West Journal of Numerical Mathematics* 1999; **7**(2):105–131.
- [102] Yang Y. Mathematical modeling and simulation of the evolution of plaques in blood vessels. PhD Thesis, Heidelberg University, Heidelberg 2014.
- [103] Plumb Oa, Whitaker S. Dispersion in heterogeneous porous media: 1. Local volume averaging and large-scale averaging. *Water Resources Research* 1988; **24**(7):913–926.
- [104] LaBolle EM, Quastel J, Fogg GE. Diffusion theory for transport in porous media: Transition-probability densities of diffusion processes corresponding to advection-dispersion equations. *Water Resources Research* 1998; **34**(7):1685–1693.
- [105] Roth K. Soil physics. Lecture notes. Institute of Environmental Physics, Heidelberg University, 2012.
- [106] Donnan F. The theory of membrane equilibria. *Chemical Reviews* 1924; **1**:73–90.
- [107] Huyghe J M, Janssen JD. Quadriphasic mechanics of swelling incompressible porous media. *International Journal of Engineering Science* 1997; **35**(8):793–802.
- [108] Moyne C, Murad Ma. Electro-chemo-mechanical couplings in swelling clays derived from a micro/macro-homogenization procedure. *International Journal of Solids and Structures* Dec 2002; **39**:6159–6190.
- [109] Ehlers W, Karajan N, Markert B. An extended biphasic model for charged hydrated tissues with application to the intervertebral disc. *Biomechanics and Modeling in Mechanobiology* 2009; **8**(3):233–251.
- [110] Kargol A. Modified Kedem-Katchalsky equations and their applications. *Journal of Membrane Science* 2000; **174**:43–53.
- [111] Slezak A, Jarzynska M. Developing Kedem-Katchalsky equations of the transmembrane transport for binary nonhomogeneous non-electrolyte solutions. *Polimery w Medycynie* 2005; **35**(1):15–20.

- [112] Hron J, Neuss-Radu M, Pustejovska P. Mathematical modeling and simulation of flow in domains separated by a leaky semipermeable membrane including osmotic effects. *Applications of Mathematics* 2011; **56**(1):51–68.
- [113] Kleinhans FW. Membrane permeability modelling: Kedem-Katchalsky vs a Two-Parameter formalism. *Cryobiology* 1998; **37**:271–289.
- [114] Woods EJ, Liu J, Gilmore JA, Reid TJ, Gau DY, Critser JK. Determination of human platelet membrane permeability coefficients using the Kedem–Katchalsky formalism: estimates from two- vs three-parameter fits. *Cryobiology* 1999; **38**:200–208.
- [115] Behmanesh S, Kempinski O. Mechanisms of endothelial cell swelling from lactic acidosis studied in vitro. *American journal of physiology. Heart and circulatory physiology* Oct 2000; **279**:H1512–H1517.
- [116] Karaszewski B, Wardlaw J, Marshall I, Cvorovic V, Wartolowska K, Haga K, Armitage P, Bastin M, Dennis M. Measurement of brain temperature with magnetic resonance spectroscopy in acute ischemic stroke. *Annals of Neurology* 2006; **60**(4):438–446.
- [117] Busto R, Dietrich WD, Globus MY, Ginsberg MD. The importance of brain temperature in cerebral ischemic injury. *Stroke* Aug 1989; **20**(8):1113–1114.
- [118] Gunnarson E, Axehult G, Baturina G, Zelenin S, Zelenina M, Aperia A. Lead induces increased water permeability in astrocytes expressing aquaporin 4. *Neuroscience* Jan 2005; **136**(1):105–114.
- [119] Zelenina M, Brismar H. Osmotic water permeability measurements using confocal laser scanning microscopy. *European biophysics journal* Jan 2000; **29**:165–171.
- [120] Levin E, Muravchick S, Gold MI. Density of normal human cerebrospinal fluid and tetra-caine solutions. *Anesthesia and analgesia* Nov 1981; **60**(11):814–817.
- [121] Pastor RW, Venable RM, Karplus M. Model for the structure of the lipid bilayer. *Proceedings of the National Academy of Sciences of the United States of America* Feb 1991; **88**:892–896.
- [122] Sengupta K, Limozin L, Tristl M, Haase I, Fischer M, Sackmann E. Coupling artificial actin cortices to biofunctionalized lipid monolayers. *Langmuir* Jun 2006; **22**:5776–5785.
- [123] Brydon HL, Hayward R, Harkness W, Bayston R. Physical properties of cerebrospinal fluid of relevance to shunt function. 1: The effect of protein upon CSF viscosity. *British journal of neurosurgery* Jan 1995; **9**:639–644.
- [124] Luby-Phelps K. Cytoarchitecture and physical properties of cytoplasm: volume, viscosity, diffusion, intracellular surface area. *International review of cytology* Jan 2000; **192**:189–221.
- [125] Verkman A S. Solute and macromolecule diffusion in cellular aqueous compartments. *Trends in Biochemical Sciences* 2002; **27**(1):27–33.
- [126] Kestin J, Sokolov M, Wakeham WA. Viscosity of liquid water in the range -8C to 150C. *Journal of Physical and Chemical Reference Data* 1978; **7**(3):941–948.

- 
- [127] Valentine MT. Mechanical and microstructural properties of biological materials. PhD Thesis, Harvard University, Cambridge, Massachusetts 2003.
- [128] Cussler E. Diffusion: mass transfer in fluid systems. Cambridge University Press, 1997.
- [129] Goodman JA, Kroenke CD, Bretthorst GL, Ackerman JJH, Neil JJ. Sodium ion apparent diffusion coefficient in living rat brain. *Magnetic resonance in medicine* May 2005; **53**:1040–1045.
- [130] Moritani T, Ekholm S, Westesson PLA. Diffusion-weighted MR Imaging of the brain. Springer Science & Business Media, 2009.
- [131] Ciarlet PG. Three-dimensional elasticity. Elsevier, 1988.
- [132] Yoon J, Cai S, Suo Z, Hayward RC. Poroelastic swelling kinetics of thin hydrogel layers: comparison of theory and experiment. *Soft Matter* 2010; **6**:6004–6012.
- [133] Hopkinson D, De Vita R, Leo D. Failure pressure of bilayer lipid membranes. *SPIE Conference for Smart Structures & Materials/NDE*, 2006.
- [134] Fettiplace R, Haydon D. Water permeability of lipid membranes. *Physiological reviews* Apr 1980; **60**(2):510–550.
- [135] Rosenberg PA, Finkelstein A. Water permeability of gramicidin A-treated lipid bilayer membranes. *The Journal of general physiology* Sep 1978; **72**:341–350.
- [136] Fushimi K, Uchida S, Hara Y, Hirata Y, Marumo F, Sasaki S. Cloning and expression of apical membrane water channel of rat kidney collecting tubule. *Nature* 1993; **361**:549–552.
- [137] Tseng HY, Sun S, Shu Z, Ding W, Reems JA, Gao D. A Microfluidic study of megakaryocytes membrane transport properties to water and dimethyl sulfoxide at suprazero and subzero temperatures. *Biopreservation and Biobanking* 2011; **9**:355–362.
- [138] Scherer JR. The partial molar volume of water in biological membranes. *Proc. Natl. Acad. Sci. USA* 1987; **84**:7938–7942.
- [139] Kedem O, Katchalsky A. A physical interpretation of the phenomenological coefficients of membrane permeability. *The Journal of general physiology* Sep 1961; **45**:143–179.
- [140] Kettenmann H, Ransom BR. Neuroglia. Oxford University Press, 2013.
- [141] Kettenmann H, Verkhratsky A. Neuroglia, der lebende Nervenkit. *Fortschritte der Neurologie-Psychiatrie* 2011; **79**(10):588–597.
- [142] Ignácio AR, Müller YMR, Carvalho MSL, Nazari EM. Distribution of microglial cells in the cerebral hemispheres of embryonic and neonatal chicks. *Brazilian journal of medical and biological research* Nov 2005; **38**:1615–1622.
- [143] Swamydas M. Role of hormones in the sexual dimorphism of oligodendrocytes. ProQuest, 2007.
- [144] Taxy JB, Husain AN, Montag AG. Biopsy interpretation: the frozen section. Lippincott Williams & Wilkins, 2012.

- [145] Luisi PL, Stano P. The minimal cell: the biophysics of cell compartment and the origin of cell functionality. Springer Science & Business Media, 2010.
- [146] Mishra S R. Biomolecules. Discovery Publishing House, 2003.
- [147] Brooker R, Widmaier EP, Graham LE, Stiling PD. Biology. Second edn., McGraw-Hill, 2011.
- [148] Sherwood L. Human physiology: from cells to systems. Cengage Learning, 2008.
- [149] Saar MO. The relationship between permeability, porosity and microstructure in vesicular basalts. PhD Thesis, University of Oregon 1998.
- [150] Detournay E, Cheng AHD. Fundamentals of poroelasticity. *Comprehensive Rock Engineering: Principles, Practices and Projects, Vol. 2*, Hudson J (ed.). Pergamon Press: Oxford, UK, 1993; 113–171.
- [151] Torquato S. Random heterogeneous media: Microstructure and improved bounds on effective properties. *Applied Mechanics Reviews* 1991; **44**:37–76.
- [152] Carman PC. Fluid flow through a granular bed. *Transactions of the Institution of Chemical Engineers* 1937; **15**:150–156.
- [153] Scheidegger AE. The physics of flow through porous media. 3rd edn., University of Toronto Press: Toronto, 1974.
- [154] Teng H, Zhao TS. An extension of Darcy 's law to non-Stokes flow in porous media. *Chemical Engineering Science* 2000; **55**:2727–2735.
- [155] Carrier WD. Goodbye, Hazen; Hello, Kozeny-Carman. *Journal of Geotechnical and Geoenvironmental Engineering* 2003; **129**(11):1054–1056.
- [156] Saucier R. Shape factor of a randomly oriented cylinder. Army Research Laboratory ARL-TR-2269, 2000.
- [157] Ingham DB, Pop I. Transport phenomena in porous media II. Elsevier, 2002.
- [158] Millington RJ, Quirk JP. Permeability of porous solids. *Transactions of the Faraday Society* 1961; **57**:1200–1207.
- [159] Czosnyka M, Pickard JD. Monitoring and interpretation of intracranial pressure. *Journal of Neurology, Neurosurgery & Psychiatry* Jun 2004; **75**:813–821.
- [160] Kelly G. Appearances observed in the dissection of two individuals; death from cold and congestion of the brain. *Trans Med Chir Sci Edinb* 1824; **1**:84–169.
- [161] Mokri B. The Monro-Kellie hypothesis: applications in CSF volume depletion. *Neurology* 2001; **56**(12):1746–1748.
- [162] Maugis B, Brugués J, Nassoy P, Guillen N, Sens P, Amblard F. Dynamic instability of the intracellular pressure drives bleb-based motility. *Journal of cell science* Nov 2010; **123**:3884–3892.
- [163] Kelly S, Macklem P. Direct measurement of intracellular pressure. *American Journal of Physiology* 1991; **260**(3 Pt 1):652–657.

- 
- [164] Caspi A, Benninger F, Yaari Y. KV7/M channels mediate osmotic modulation of intrinsic neuronal excitability. *The Journal of Neuroscience* Oct 2009; **29**(36):11 098–11 111.
- [165] Paula S, Volkov AG, Hoek ANV, Haines TH, Deamer DW. Permeation of protons, potassium ions, and small polar molecules through phospholipid bilayers as a function of membrane thickness. *Biophysical journal* 1996; **70**:339–348.
- [166] Atwell BJ, Kriedemann PE, Turnbull CGN. Transport of molecules across cell membranes. *Plants in Action: Adaptation in Nature, Performance in Cultivation*. Macmillan Education Australia Pty Ltd: Melbourne, Australia, 1999.
- [167] Atanasov AT. Method for tentative evaluation of membrane permeability coefficients for sodium and potassium ions in unicellular organisms. *Open Journal of Biophysics* 2013; **3**:91–98.
- [168] Schilling WP, Schuil DW, Bagwell EE, Lindenmayer GE. Sodium and potassium permeability of membrane vesicles in a sarcolemma-enriched preparation from canine ventricle. *The Journal of Membrane Biology* 1983; **77**(2):101–114.
- [169] Yarin L. Chapter 2: Basics of the dimensional analysis. *The Pi-Theorem: Applications to Fluid Mechanics and Heat and Mass Transfer*. Springer Science & Business Media, 2012; 3–39.
- [170] Szirtes T, Rozsa P. Applied dimensional analysis and modeling. December, Elsevier Butterworth-Heinemann, 2007.
- [171] Basser PJ. Interstitial pressure, volume and flow during infusion into brain tissue. *Microvascular Research* 1992; **44**:143–165.
- [172] Bastian P, Droske M, Engwer C, Klöfkorn R, Neubauer T, Ohlberger M, Rumpf M. Towards a unified framework for scientific computing. *Proceedings of the 15th Conference on Domain Decomposition Methods*, 2005.
- [173] Bastian P, Heimann F, Marnach S. Generic implementation of finite element methods in the distributed and unified numerics environment (DUNE). *Kybernetika* 2010; **46**(2):294–315.
- [174] Müthing S. A flexible framework for multi physics and multi domain PDE simulations. PhD Thesis, University of Stuttgart 2015.
- [175] Li XS, Demmel JW, Gilbert JR, Grigori L, Shao M, Yamazaki I. SuperLU Users' Guide. [http://crd-legacy.lbl.gov/~xiaoye/SuperLU/superlu\\_ug.pdf](http://crd-legacy.lbl.gov/~xiaoye/SuperLU/superlu_ug.pdf), 2011.
- [176] Reynolds O. Papers on mechanical and physical subjects. The sub-mechanics of the universe. *Cambridge University Press* 1903; **3**.
- [177] Lemonnier H. Two-phase flows balance equations. Lecture notes. CEA Grenoble: Grenoble, 2012.
- [178] Quarteroni A, Formaggia L. Mathematical modelling and numerical simulation of the cardiovascular system. *Handbook of Numerical Analysis* 2004; **12**:3–127.
- [179] Rannacher R. Numerische Mathematik 3 (Numerik von Problemen der Kontinuumsmechanik), vol. 3. Heidelberg, Vorlesungsskriptum WS 2004/2005, 2008.

- [180] Landau LD, Lifshitz EM. Theory of elasticity. Elsevier, 1986.
- [181] Bennethum LS, Murad MA, Cushman JH. Modified Darcy's law, Fick's law, and Terzaghi's effective stress principle for swelling clay soils. *Computers and Geotechnics* 1997; **20**(3-4):245–266.
- [182] Biot MA. Theory of propagation of elastic waves in a fluid-saturated porous solid. I. Low-frequency range. *The Journal of the Acoustical Society of America* 1956; **28**(2):168–178.
- [183] Biot MA. General theory of three-dimensional consolidation. *Journal of Applied Physics* 1941; **12**:155–164.
- [184] Lemon G, King JR, Byrne HM, Jensen OE, Shakesheff KM. Mathematical modelling of engineered tissue growth using a multiphase porous flow mixture theory. *Journal of Mathematical Biology* 2006; **52**:571–594.
- [185] Barry SI, Mercer GN. Deformation and fluid flow due to a source in a poro-elastic layer. *Applied Mathematical Modelling* 1997; **21**:681–689.
- [186] Clausius R. On a mechanical theorem applicable to heat. *Philosophical Magazine, Ser. 4* 1870; **40**(265):122–127.
- [187] Lorentz HA. Sur la théorie moléculaire des dissolutions diluées. *Archives Néerlandaises de Sciences Exactes Et Naturelles*, 1892.